Left-right asymmetry in *Xenopus laevis*: Functional dissection of leftward flow

Dissertation zur Erlangung des Doktorgrades
der Naturwissenschaften (Dr. rer. nat.)

Fakultät Naturwissenschaften
Universität Hohenheim

Institut für Zoologie

vorgelegt von
Philipp Vick

aus Stuttgart
2009

Dekan:	Prof. Dr. Heinz Breer
1. berichtende Person:	Prof. Dr. Martin Blum
2. berichtende Person:	Prof. Dr. Heinz Breer
Eingereicht am:	13.10.2009
Mündliche Prüfung am:	09.12.2009

Die vorliegende Arbeit wurde am 13.11.2009 von der Fakultät Naturwissenschaften der Universität Hohenheim als „Dissertation zur Erlangung des Doktorgrades der Naturwissenschaften“ angenommen.

Danksagung

Herrn Prof. Dr. Martin Blum möchte ich vielmals danken für das Wecken meines Interesses an der Embryologie, das Überlassen dieses spannenden Themas und vor allem auch für die dabei gewährten „Forscher-Freiheiten“. Weiter danke ich ihm für sein Vertrauen in meine Fähigkeiten und deren Förderung. Ich hoffe, ich konnte mir etwas von seiner positiven und zuversichtlichen Art aneignen.

Herrn Prof. Dr. Heinz Breer danke ich vielmals für das Interesse an meiner Arbeit und für die Hilfe zur unkomplizierten Abwicklung der Endphase meiner Dissertation.

Herrn Dr. Axel Schweickert möchte ich für alles danken, was er mir beigebracht hat – und das war echt viel. Dafür dass er immer ein offenes Ohr und eine gute Antwort parat hat („K-N“) und vor allem für die super angenehm lockere und inspirierende Art, mit der bei uns im Labor gearbeitet wurde. Mach ab und zu ein paar Minis und realisier Deine besten Ideen auch mal selber – SNAFU!

Bei Thomas möchte ich mich für die viele Hilfe bei den Abbildungen bedanken – und bei der Statistik – und bei den Flow-Sachen – und dafür, dass er mir Photoshop und Illustrator beigebracht hat – und vor allem für die extrem lustige Zeit und die rockigen „Freitage“. Du weißt ja, wir treffen uns Back-to-Back und so – IDLTDBTDLM.

Philipp danke ich für die lange Zeit der geistig und trophologisch bereichernden Bench- und PC-Nachbarschaft. Ich hoffe wir sehen uns für so manche Barbecues.

Bei Tina möchte ich mich für die Unterstützung mit den Rasteraufnahmen und für die kompetenten Diskussionen bedanken, aus denen ich immer mit einer Portion Erkenntnis oder gar Erleuchtung mehr gekommen bin.

Bei all den Kollegen der Embryologie möchte ich mich vielmals für die unbeschreiblich angenehme Arbeitsatmosphäre bedanken; sie hat so ziemlich alles angenehmer gemacht (selbst den Bako-Müll) und wird sicherlich immer ein Maßstab sein. Außerdem noch vielen Dank für die vielen geistig bereichernden Diskussionen zur Entwicklungsbiologie und anderem „Besenkram“ und an Susanne und Verena noch eine Extraportion „Danke“ für die tausend Kleinigkeiten (und Großigkeiten) die mir im Laufe der Jahre die Arbeit erleichtert haben. Auch meinen 4 Diplomanden und zukünftigen Lehrern möchte ich sage: Vielen Dank, habt Ihr gut gemacht, viel Erfolg.

Auch bei den restlichen Angestellten der Zoologie möchte ich mich bedanken für die vielen netten Gespräche, Feste, Exkursionen, Smalltalks (die ich allerdings oft zu vermeiden suche), Witze und so weiter und natürlich bei den Jungs vom Tierhaus. Herrn Schmid danke ich für seine professionellen Zeichnungen.

Ein spezieller Dank gilt den 13695 *Xenopus*-Embryonen, die sich für die hier präsentierten Daten uneigennützig geopfert haben und all ihren Kollegen, die leider nicht zum Zuge kamen.

Der letzte, aber sicher nicht kleinste Dank gilt meiner wunderbaren Frau Anja für ihre bedingungslose Unterstützung und Aufopferung in den letzten Jahren, meinen Eltern und meinem Bruder für das tolle Verhältnis und den jahrelangen Rückhalt während meines langen Bildungsweges, und ich danke Schnitzel – er weiß wofür.

Abstract

Despite their external bilateral symmetry, vertebrates have a conserved left right (LR) asymmetry of their inner organs. For all vertebrates, it is well-known that the asymmetric organogenesis is preceded by the left-sided nodal signaling cascade during embryonic development. A question which has not been settled in detail is how the first asymmetrically directed signal arises, which activates nodal only on the left side. In mice and fish embryos an extracellular leftward fluid flow – generated by rotating cilia – was shown to be functionally necessary for gene activation. Recently, this process has also been demonstrated in frog embryos and its mechanic inhibition caused laterality defects. This raised the question if this process is also conserved among vertebrates.

The aim of this study was to analyze the mechanism of flow in the frog in the context of the known models. Thereby, its prerequisites and the exact mode of activation of the left-sided genes should be assessed. Finally, general conclusions on the symmetry breakage of vertebrates were to be drawn.

Loss of function of axonemal dynein heavy chains inhibited ciliary movement, fluid flow and laterality development of the embryos. By showing that flow was only necessary on the left half of the ciliated epithelium (GRP), definite statements could be made concerning origin, identity and possibility of a transported substance. Moreover, a function for GRP morphogenesis and thus for the generation of flow were proven for the serotonin receptor 3 and the calcium channel Pkd2. These results did not confirm the hypothesis that Pkd2 causes a flow-dependent left-sided calcium signal. Consequently, this contradicted the so-called "2-cilia model" in favor of an early morphogenetic function in frog.

In the course of a collaboration it could be shown, that the RNA-binding protein xBic-C has a conserved function for cilia polarization and thus for the flow in both *Xenopus* and mice. Additionally, up to now, a right-sided nodal inhibitory function has been assigned to the protein coco. However, the exact mechanism was unknown. By specific, combined left- and right-sided loss of function experiments with coco, nodal and the above mentioned components, it could be demonstrated that coco but not nodal is directly dependent on leftward flow. With the flow, coco was downregulated

on the left side only and could thus no longer inhibit nodal there. Loss of flow or xBic-C function – but not that of Pkd2 – could be rescued by coco inhibition; this revealed a clear hierarchy.

Taken together a sequence of conditions could be formulated: Pkd2 and the serotonin receptor 3 are obligatory for the formation of the GRP and correct flow before neurulation. xBic-C also precedes the flow and is required for cilia polarization but seemed also to have a further function. coco is downstream of the fluid flow and is downregulated as its direct consequence on the left side. nodal, in turn, is downstream of this order and is only released on the left side where it can thus act as a putative mediator to transfer the generated signal into the lateral plate mesoderm. These results are discussed in terms of evolutionary origin and conservation.

Zusammenfassung

Trotz ihrer äußeren Bilateralsymmetrie weisen Wirbeltiere eine konservierte Links-Rechts (LR)-Asymmetrie der inneren Organe auf. Es ist bekannt, dass bei allen Vertebraten der embryonalen, asymmetrischen Organogenese die linksseitig aktive nodal-Signalkaskade vorangeht. Eine im Detail noch nicht geklärte Frage ist, wie das erste asymmetrisch gerichtete Signal entsteht, welches nodal nur links aktiviert. In Maus- und Fischembryonen wurde ein durch rotierende Cilien erzeugter, linksgerichteter extrazellulärer Flüssigkeitsstrom für die Genaktivierung als funktionell notwendig nachgewiesen. Vor kurzem wurde gezeigt, dass solch ein Prozess auch im Froschembryo stattfindet und dessen mechanische Inhibition Lateralitätsdefekte zur Folge hat. Dadurch stellte sich die Frage, ob dieser Vorgang ebenfalls konserviert ist.

Das Ziel dieser Arbeit war es, vor dem Hintergrund bekannter Modelle den genauen Mechanismus des Flüssigkeitsstroms, seine Voraussetzungen und den Modus der genauen Aktivierung der linksseitigen Gene am Froschmodell zu untersuchen. Damit sollten letztlich allgemeine Schlussfolgerungen zum Symmetriebruch der Wirbeltiere gezogen werde.

Der Funktionsverlust von axonemalen schweren Dyneinketten führte zur Störung der Cilienbewegung, des Flüssigkeitsstroms und damit zu Lateralitätsproblemen der Embryonen. Es konnte gezeigt werden, dass der Flüssigkeitsstrom nur auf der linken Hälfte des cilierten Epithels (GRP) nötig war, wodurch klare Aussagen über Herkunft, Identität und Möglichkeit einer transportierten Substanz gemacht werden konnten. Weiter wurden für den Serotonin-Rezeptor 3 und den Calciumkanal Pkd2 eine Funktion für die Morphogenese der GRP und damit für die Entstehung des Flüssigkeitsstromes nachgewiesen. Diese Resultate bestätigten nicht die Hypothese, dass Pkd2 ein stromabhängiges linksseitiges Calcium-Signal erzeugt und somit auch nicht das so genannte „2-Cilien Modell“, sondern favorisiert eine frühe morphogenetische Funktion im Frosch. Für das RNA-Bindeprotein xBic-C konnte im Rahmen einer Kollaboration eine konservierte Funktion für korrekte Cilienpolarität und damit für den Flüssigkeitsstrom in *Xenopus* und Maus gezeigt werden.

Dem nodal-Inhibitor coco wurde bisher eine rechtsseitige Funktion zugeschrieben, der genaue Mechanismus war jedoch unbekannt. Durch gezielte, kombinierte links- und rechtsseitige Funktionsverlust-Experimente mit coco, nodal und den oben genannten Komponenten, konnte gezeigt werden, dass coco aber nicht nodal vom linksgerichteten Flüssigkeitsstrom direkt abhängig ist. Es wird von diesem linksseitig runterreguliert und hemmt dadurch nodal dort nicht mehr. Der Verlust der Flüssigkeitsströmung oder der Funktion von xBic-C, nicht aber von Pkd2 konnten durch *coco*-Inhibition gerettet werden; dies zeigte eine klare Hierarchie.

Zusammengefasst kann damit eine Abfolge von Bedingungen formuliert werden: Pkd2 und der Serotonin-Rezeptor 3 sind zwingend nötig für die Bildung der GRP und einen funktionellen Flüssigkeitsstrom. xBic-C ist diesem ebenfalls vorangestellt und für die Cilienpolarisierung nötig, scheint aber auch noch eine weitere Funktion zu haben. Coco ist dem Flüssigkeitsstrom nachgeschaltet und wird als dessen direkte Konsequenz links herunterreguliert. nodal wiederum ist dieser Rangfolge nachgeschaltet und wird als Vermittler des Signals linksseitig von der Hemmung freigesetzt und kann so als Vermittler für die Weiterleitung des generierten Signals ins Seitenplattenmesoderm fungieren. Die Ergebnisse werden im Kontext des evolutionäre Ursprungs und der Konservierung diskutiert.

Table of contents

Introduction

Discussion

Introduction

1. Metazoan embryonic development

In all eumetazoan animals, embryogenesis - the process by which the fertilized oocyte (zygote) divides and reorganizes itself to finally end up in a juvenile or larval organism – is characterized by very similar basic processes. For most embryos, the first axis (animal-vegetal) is already maternally established in the unfertilized egg and would represent the future anterior-posterior (AP) axis of the embryo. Some diploblastic animals keep this axis as a single adult one and are therefore radial symmetric. All other phyla, however, belong to the Bilateria and are thus characterized by a second, post-fertilization established dorso-ventral (DV) axis and a bilateral symmetric appearance (Brusca and Brusca, 2003). According to the ecological strategy, egg cells possess a taxon-specific amount of yolk as an energy supply for the first non-feeding period of development, typically deposited at one (the vegetal) pole of the cell. This also correlates with the mode of how cleavages occur - the first rapid embryonic cell divisions without any growth (Gilbert, 2006; Pflugfelder, 1970). This first step in embryogenesis comprises fast cell cycles without G phases that result in a clump of cells, the blastula, in most cases with a fluid-filled cavity inside – the blastocoele. In yolk-rich egg cells, these cleavages are mostly meroblastic (i.e. partial) at the yolk-free pole (animal pole) while in yolk-poor cells they are often holoblastic (i.e. total) – along the whole animal-vegetal axis. The resulting blastula stage represents the starting point for the formation of the basal body plan with its further axes and relations. For vertebrates the further development begins with gastrulation, followed by neurulation and finally ends with completed organogenesis (Wolpert et al., 1997). These vertebrate-typical developmental phases are used to generalize embryogenesis below.

1.1 Gastrulation – generation of germ layers and axes

For all metazoan animals gastrulation exhibits an exceedingly important developmental process as it translates earlier obtained axial information into true embryonic axes.
After blastula stages cells begin to rearrange by changing their shape and adhesion properties and, most important, start to migrate either as single cells or as groups. This marks the beginning of the gastrulation, by which the three (or two for non-bilaterian animals) germ layers ectoderm, mesoderm and endoderm are formed. Gastrulation starts with the migration of mesodermal and endodermal cells into the embryo. By this event, those germ layers get inside and as most cells migrate as groups or epithelia, they generate a new cavity, the primitive gut or archenteron. This archaic process constitutes an important part of gastrulation as the archenteron will give rise to the later digestive tract. In those species that posses a blastocoele (like most amphibians), this is displaced by the expanding capacity of the primitive gut. The ectoderm remains outside, spreads and finally covers the whole embryo. At the end of gastrulation the germ layers are properly arranged with endodermal tissue inside, ectoderm covering the embryo and mesoderm in between (Stern, 2004; Wolpert et al., 1997).

1.2 Neurulation process

During this process the neuroectodermal tissue becomes more concentrated either dorsally or ventrally (dorsally for vertebrates, ventrally for protostomes). In vertebrates, the neural plate thickens, neural folds elevate, the edges move from lateral positions more medially towards each other and finally fuse to form the neural tube (Gilbert, 2006). In parallel – already started during gastrulation – dorsal neuroectoderm and the underlying notochord perform axial elongation via so-called convergent and extension (CE) cell movements, by which the cells intercalate medially in the plane of their epithelial sheet and thus the epithelium and thereby the whole embryo is stretched along the AP axis (Keller, 2002; Wallingford et al., 2002). Simultaneously, somitogenesis occurs on both sides of the notochord. At the end of this phase a vertebrate tailbud stage emerges (often referred to as phylotypic stage; Slack et al., 1993; Wolpert et al., 1997).

1.3 Organogenesis and post-embryonic development

After neurulation, an embryo already possesses organ fields or anlagen, the precursors of later organs. These primordia then further develop into the respective organ by proliferation, tissue-rearrangement, change of cell morphology, cell migrations, differentiation or apoptosis. At the end of organogenesis, embryonic development is finished per definition and post-embryonic development starts (Gilbert, 2006). This phase is mainly characterized by growth of the organism. For many animal groups, post-embryonic development is represented in the form of a larva that finally either hatches or passes through a metamorphosis (like a frog tadpole or an insect holometabolous larva). In other groups embryogenesis ends up in a specimen with an appearance very similar to the adult that only changes in proportions and dimensions (like a mammalian fetus or an insect hemimetabolous nymph; Brusca and Brusca, 2003).

2. Embryonic development of *Xenopus laevis*

In the last decades several model organisms have been established to analyze the special embryonic processes from different points of view and with different questionings. Among them are invertebrate species from the primitive radial symmetric cnidarian *Nematostella vectensis* up to the nematode *Caenorhabditis elegans* or the dipteran *Drosophila melanogaster*, as well as classical vertebrates like the house mouse *Mus musculus*, the chicken *Gallus gallus*, the zebrafish *Danio rerio* or the African clawed frog *Xenopus laevis*, which was used in this study.
The genus *Xenopus* comprises 18 fully aquatic species that live in muddy lakes in sub-Saharan Africa. As it will lay 1.000-2.000 eggs a day, ~12h upon subcutaneous injection of human chorionic gonadotropin all through the year, *Xenopus* has become a favorite model system to study the basal development of vertebrates (Sive et al., 2000).

In contrast to many mammalian and sauropsid families, amphibians (and fish) do not develop via a blastodisc but display a spherical blastula and gastrula embryo (Hamburger and Hamilton, 1992; Hassoun et al., 2009; Nieuwkoop and Faber, 1994;

Pflugfelder, 1970). Their eggs are mostly quite large (~1mm) and relative easily to manipulate by microinjections and microsurgery like ablation or transplantation experiments.

2.1 Gastrulation movements in *Xenopus*

The *Xenopus* zygote performs several total cleavages and so finally ends as a typical blastula. As the mesolecithal yolk accumulates more vegetally, those cells cleave more slowly resulting in a blastula with larger vegetal cells (Gilbert, 2006; Nieuwkoop and Faber, 1994). The amphibian blastula is composed of three main regions, the animal cap around the blastocoele is destined to become epidermis ventrally and neuroectoderm dorsally, the yolky vegetal subblastoporal endoderm will be incorporated into the forming endodermal digestive tract, and finally the marginal zone in between. The marginal zone consists of a two-layered (superficial and deep layer) ring around the equatorial region of the embryo, separating endoderm and ectoderm. The mesodermal deep layer gives rise to – from dorsal to ventral – notochord, somites, heart and lateral plate mesoderm (LPM). The superficial layer is composed ventrally and laterally of endodermal future cells of the digestive tract and dorsally (and partial laterally) of superficial mesoderm (to be described in detail below; Dale and Slack, 1987; Moody, 1987; Stern, 2004).

Gastrulation starts with the formation of the blastopore lip at a dorso-vegetal position of the embryo. This slit-like structure is visible by an up-concentration of cortical pigment due to apical constriction of the cells. The process is started by the invagination of the so-called bottle cells. They migrate inside the deeper layer and dorsally towards the animal pole and so initiate the gastrulation movement. The deep and superficial layers of the marginal zone thereby involute in the same direction (Stern, 2004). In parallel, this axial mesoderm and the overlying non-involuting ectoderm undergo convergent and extension movements and thus elongate the dorsal AP axis. With ongoing dorsal involution movements the lip extends laterally and ventrally until the whole marginal zone starts to involute and thereby the ectoderm closes over the remaining vegetal yolk cells (yolk plug) by constriction towards the vegetal center. At the end of gastrulation in *Xenopus*, the marginal

endodermal cells line the newly generated gut and the yolky endodermal cells are incorporated inside (Keller and Danilchik, 1988; Keller et al., 1985; Stern, 2004).

2.2 The patterning of the blastula and the Spemann-Organizer

As mentioned, dorsal lip formation marks the beginning of gastrulation and finally the dorsal side of the developing embryo. Yet this occurrence does not constitute the de-novo establishment of the second bilaterian axis (the dorso-ventral one) but only its consequence. Its formation is initiated by the entry of the sperm into the animal part of the egg cell. By this, sperm centriole-induced massive cytoskeletal rearrangements are started that result in a process called cortical rotation. Cortical rotation is a microtubule-dependent rotational movement of the outer layers of the zygote of about 30° relative to the core towards the sperm entry point. In this process, maternally deposited vegetal cortex Wnt (wingless-related mouse mammary tumor virus integration site) pathway components (e.g. Dishevelled (Dsh) protein or *wnt11* mRNA) are transported to the future dorso-vegetal side of the embryo (Tao et al., 2005). In this region a dorsal signaling center is formed, the Nieuwkoop center (Nieuwkoop, 1973; Smith and Harland, 1991). The sperm entry point therefore marks the future ventral side and indirectly induces the dorsal side by translocating Dsh to this part of the embryo.

Dsh is a component of the canonical Wnt pathway. Wnt ligands bind to transmembrane Frizzled receptors and thus Dsh is activated in the cytoplasm. Activated Dsh inhibits a complex of the serine/threonine protein kinase Glycogen synthase kinase 3 (GSK-3), the tumor suppressor gene APC (adenomatosis polyposis coli) and Axin. When Wnt signaling is inactive, this complex inhibits β-catenin by promoting its degradation. β-catenin is normally known to be involved in cell adhesion by interacting with cadherins. But in the case of Wnt signaling it is known to act as a transcription factor (TF). Therefore, when Dsh interacts with its inhibition, β-catenin is released from the complex, stabilized, enters the nucleus and influences gene activity in interaction with other TFs (Croce and McClay, 2006; MacDonald et al., 2009). Consequently, after cortical rotation, β-catenin is active only on the dorsal side and activates specific gene expression there.

In addition, the above mentioned regionalization of vegetal endoderm, equatorial mesoderm and animal ectoderm in blastula stages is induced by maternal deposited

mRNAs (*VegT*, *wnt11*, *Vg1*) at the vegetal pole that are important for endoderm formation (Heasman et al., 2001; Tao et al., 2005). The product of the TGF-β (transforming growth factor-beta) superfamily member *Vg1* diffuses towards the animal pole and thus forms a vegetal to animal gradient. It has been shown that it is able to induce mesoderm and to activate *Xenopus nodal-related* genes (*Xnr*) – also TGF-β members that are important for mesoderm and endoderm formation. The Nieuwkoop center is established where the vegetal and dorsal signals overlap, namely dorsal Wnt and vegetal TGF-β signals (Agius et al., 2000; Crease et al., 1998; De Robertis et al., 2000).

The most important signaling center in the *Xenopus* embryo is the dorsal organizer region that is induced by and develops directly animal to the Nieuwkoop center, the Spemann organizer.
In 1924 Hans Spemann and Hilde Mangold discovered by elegant grafting experiments that this region had an inductive ability. When this dorsal part of an unpigmented newt (*Triton cristatus*, today *Triturus cristatus*) was transplanted into the corresponding ventral region of a pigmented species (*Triton taeniatus*, today *Triturus vulgaris*), a Siamese twin embryo developed that had an unpigmented notochord but all other axial structures (neural tube, somites) were pigmented and thus derived from the host and induced by the graft tissue (Spemann and Mangold, 1924).
Today it is known that this organizing tissue expresses a range of different TFs like *goosecoid* (*Gsc*), *Siamois* (*Sia*), *notochord homeobox* (*Xnot*), *LIM homeobox protein 1* (*Lhx1* or *Xlim-1*) or *forkhead box A2* (*FoxA2* or *HNF3-beta*) and secreted growth factor (GF) antagonists like *chordin*, *noggin*, *follistatin*, *frizbee* and different *Xenopus nodal-related* genes (*Xnr*) and thereby dictates dorso-ventral development. The secreted inhibitors restrict the function of the ventrally produced GFs like BMP 4 or BMP 2 (bone morphogenetic factor 4 and 2); thus the organizer prevents ventral fates on the dorsal side. By secretion of such ventral inhibitors, a gradient of ventral GFs is established from ventral to dorsal and thus also patterns the mesoderm and ectoderm (De Robertis, 2006; De Robertis, 2009).

2.3 Neurulation process in *Xenopus*

After DV axis establishment and finished gastrulation, the frog embryo resembles an archetypical vertebrate neurula with a large archenteron lined by endoderm and ventrally concentrated yolk cells. Axial structures are the notochord and the overlying neural plate that both still undergo convergent extension movements, and the somites that are generated from anterior to posterior lateral of the notochord. At the posterior pole around the blastopore, the circumblastoporal collar (cbc) is located, the remnant of the early organizer (Gont et al., 1993; Hausen and Riebesell, 1991).
With ongoing neurulation and during the following tailbud stages, the axial tissues further elongate and thus the embryo lengthens considerably. These processes take place until outgrowth of the tail. Then the tail organizer, the chordoneural hinge (cnh), still produces axial tissue in the posterior part of the tail but the anterior part of the embryo stops elongating (Beck and Slack, 1999; Gont et al., 1993).

3. The left-right body axis in vertebrates

The Bilateria are characterized by having a bilateral symmetric body plan with mirror-imaged structures on left and right side. Generally, this is valid for the outside and the inside. For many phyla this is originally true but in contrast to that, the deuterostomes display differences in left and right body halves (Boorman and Shimeld, 2002a; Palmer, 2004; Speder et al., 2007).
Vertebrates show a highly conserved arrangement of their inner organs. In mammals, the heart points to the left side and more important, there is a functional asymmetry due to the separated systemic and pulmonary circulatory system. The other visceral organs (except the bilateral kidney) are all asymmetrically arranged inside the thorax or abdomen; the lungs are bi-lobed on the left and tri-lobed on the right side (for *Homo sapiens*), liver and gallbladder are situated on the right, spleen and stomach on the left and the gut also coils asymmetrically. This normal arrangement is called *situs solitus*; in about one of 10.000 of human births (very variable between different populations) all organs are mirror-imaged – the left and right side are thus inverted – an often undetected cause non-pathogenic situation referred to as *situs inversus* (Cooke, 2004). If the organs are randomly arranged

within the body or if one side is duplicated and therefore the other one is missing dramatic pathological effects are caused, called heterotaxia or isomerism, respectively (Storm van's Gravesande and Omran, 2005). In principle, these positional relationships apply for all vertebrates.

Such asymmetries are already specified during organogenesis in embryonic development. This suggests the specification of a third axis, the vertebrate left-right (LR) axis before organogenesis directing asymmetric organ development.

Already in 1990 Brown and Wolpert proposed that there should be (1) “a process termed *conversion,* in which a molecular handedness is converted into handedness at the cellular level,” (2) “a mechanism for *random generation of asymmetry,* which could involve a reaction-diffusion process, so that the concentration of a molecule is higher on one side than the other” and (3) “a tissue-specific interpretation process which responds to the difference between the two sides, and results in the development of different structures on the left and right” (Brown and Wolpert, 1990). This prediction has been validated for most of its characteristics as described below.

4. The conserved left-sided nodal signaling cascade

Indeed there is a directing signal that leads asymmetric organogenesis and represents point (3) of the predicted model – namely during neurulation and the following tailbud stages. In 1995, an asymmetric gene cascade was described for the first time in developing chick embryos, involving the chick *nodal-related*, *sonic hedgehog* and *activin receptor IIa* genes (Levin et al., 1995).

Today it is well known that the nodal signaling cascade is only activated in the lateral plate mesoderm on the left side of the vertebrate embryo. This gene cascade involves the TGF-β members *nodal* (*Xenopus nodal-related 1*, *Xnr1* in frog; *southpaw*, *spaw* in zebrafish; Long et al., 2003; Lowe et al., 1996) and the *left-right determination factor* (*lefty* or *antivin*; Meno et al., 1996; Thisse and Thisse, 1999) and the *paired-like homeodomain transcription factor 2* (*Pitx2*; Campione et al., 1999; Ryan et al., 1998). *nodal* is activated in late neurula stages and its product activates

its own expression in a positive feedback loop, as well as that of its antagonist *lefty* and of *Pitx2c*. nodal, as other TGF-β members, signals through the tetrameric serine-threonine kinase activin receptor complex consisting of two type I receptor ALK4 (ActRIB) units and two type II receptor ActRII (ActRIIA or ActRIIB) units. nodal receptor activation needs a co-factor of the EGF-CFC (epidermal growth factor-like-cripto/FRL-1/cryptic family 1) class (Shen, 2007). The intracellular signal is further mediated to the nucleus via SMAD TF signals. *Lefty* has a second domain of activity in the midline where it is thought to function as a midline barrier to prevent left nodal from diffusing into the right LPM, as nodal is a very potent morphogen (Bisgrove et al., 1999; Cheng et al., 2000; Ohi and Wright, 2007). The LPM expression of *lefty* is thought to be important to restrict nodal activity temporally. The asymmetric organogenesis itself is thought to be mediated by Pitx2c, although these processes are not completely understood (Davis et al., 2008; Simard et al., 2009).

Interestingly, this left-sided nodal cascade is not only conserved in all vertebrate species investigated so far but it has also recently been shown to be conserved in the basal chordate clades, the Urochordata and the Cephalochordata. Surprisingly, it is also expressed in developing sea urchin gastrula/neurula stages – but on the right and not on the left side (Boorman and Shimeld, 2002a; Boorman and Shimeld, 2002b; Duboc and Lepage, 2008; Duboc et al., 2005; Yu et al., 2002).

5. Symmetry breakage and unilateral signal generation

In contrast to the now well-studied LPM nodal signaling, the inductive signal that activates this cascade only on the left side – and thus points (1) and (2) of Brown and Wolpert's model – is not understood very well.

5.1 Ciliopathies and laterality

First indications were brought forward by the description of a human syndrome called Kartagener or immotile ciliary syndrome in 1976 (Afzelius, 1976). Although correlation between *situs inversus* and bronchiectasis had been known since the beginning of the 20th century, it was Afzelius in 1976 who realized that the affected

patients suffered from immotile cilia due to structural defects in cilia (Afzelius, 1976; Karthagener, 1933; Zivert, 1904). The symptoms of the Kartagener syndrome are typically *situs inversus*, chronic inflammations of the upper and lower respiratory tract (sinusitis, bronchitis, pneumonia, and otitis media) and infertility. If patients display *situs solitus*, meaning they have no LR defects, then this syndrome is called primary ciliary dyskinesia (PCD; Storm van's Gravesande and Omran, 2005; Zariwala et al., 2007).

5.2 Ciliogenesis and cilia function

Cilia constitute ancestral organelles and are found throughout the animal kingdom. In vertebrates, cells of virtually all tissues possess cilia, which grow out of basal bodies in non-dividing cells. Now it is known that cilia serve a plethora of functions; immotile cilia, for example, are involved in mechanosensation (hearing, balance, excretion), vision (ciliary photoreceptors) and signaling pathways (Bisgrove and Yost, 2006). Motile cilia propel cells and organisms (protists, larvae and sperm); they are involved in airway clearance, the transport of early embryos along the female reproductive tract and direct organ laterality (see below; Fliegauf et al., 2007; Ginger et al., 2008; Satir and Christensen, 2007).

Cilia are membrane-sheathed cellular protrusions with an internal microtubular skeleton (axoneme). The archetypical cilium consists of nine peripheral microtubule doublets and a central apparatus of a single doublet (9x2+2 axoneme). Variants lacking the central apparatus (9+0) are frequently found, and recently 9+4 axonemes, representing an apparent duplication of the central apparatus, have been described in rabbit and mouse (Caspary et al., 2007; Feistel and Blum, 2006; Satir and Christensen, 2007). The ciliary proteome comprises several hundred proteins, many of these are involved in intraflagellar transport (IFT), a process that manages the construction, maintenance and destruction of cilia (Pedersen et al., 2008; Scholey and Anderson, 2006). They can roughly be classified as motile or immotile and additionally, according to their axoneme structure and their function, although overlaps are common (Fliegauf et al., 2007).

5.3 Dynein motor proteins

Ciliary motility is governed by dynein motor proteins, i.e. inner and outer arm dynein complexes attached to the outer microtubule doublets. Dynein complexes consist of several proteins including two or three dynein heavy chains, representing the central part which conducts the motor function. Additionally, there are several intermediate and light chain dyneins important for cargo interaction and motor regulation (Asai and Koonce, 2001; Hook and Vallee, 2006). Dynein heavy chains are large proteins (~4500 amino acids) classified according to their function and intracellular localization (Asai and Wilkes, 2004). Mutations in dynein genes result in impaired ciliary motility or even complete loss of motility due to structural defects in inner or outer arm complexes (Afzelius, 2004; Fliegauf et al., 2007; Hornef et al., 2006; Schwabe et al., 2008).

Axonemes of Kartagener patient cilia often display structural defects and lack outer or inner dynein arms. Until today, dynein-related mutations have been assigned to dynein axonemal heavy chain (dnah) genes *dnah5* and *dnah11*, and the intermediate chain gene *dnai1* (Bartoloni et al., 2002; Guichard et al., 2001; Olbrich et al., 2002; Omran et al., 2000; Schwabe et al., 2008). In the long known mouse *iv* mutant (*inversus viscerum*), characteristically 50% of specimens displays inversed placement of their inner organs (Hummel and Chapman, 1959). The mutation has been linked to an outer arm dynein heavy chain gene, namely in *left right dynein* (*lrd*), a gene homologous to human *dnah11*, and further more, *dnah5* mutant mice show laterality defects (Ibanez-Tallon et al., 2002; Supp et al., 1999; Supp et al., 1997).

5.4 Extracellular leftward fluid-flow

In the context of vertebrate left-right axis formation, the connection to ciliary motility was revealed in 1998. Then Nonaka et al. showed that an extracellular leftward fluid-flow (then called “nodal flow”) was the symmetry breaking event upstream of the left-sided nodal cascade in the LPM and thus the claimed mechanism of number (2) of Brown and Wolpert’s model, the biased signal (Nonaka et al., 1998). This flow was shown to be generated by a ciliated epithelium which is located at the most distal part, anterior of the primitive streak and posterior of the notochord of the 8 day old

mouse embryo (Sulik et al., 1994). Very convincingly, this flow and the resulting laterality could be inverted or even rescued in *iv*-mutant mice by generation of an artificial flow (Nonaka et al., 2002).

Despite irritations in nomenclature (Beddington et al., 1992), it has become clear now, that this ciliated epithelium is not the homologous structure to the Hensen's node but actually represents the posterior part of the notochordal plate. Therefore it was proposed to be named "posterior notochord" (PNC; see above and Blum et al., 2007; Hensen, 1876).

Cilia on the PNC are motile, mostly of type 9+0 (although it is not clear how many different types there are indeed) and are anchored at the posterior end of the cell. Importantly, as they all only rotate in a clockwise manner and as the cells are slightly convex, cilia are posteriorly tilted and the rotational movement can be separated into two different phases (Fig. 01). The first phase comprises the half-rotational movement near the surface of the epithelium which, due to friction of the fluid, is not able to drive any current. The second phase – the left half of the rotational movement – strives through the extracellular fluid, able to drive it leftwards (Fig. 1; Nonaka et al., 2005).

Up to now, several knockout mice have been reported that show LR defects due to loss of leftward flow – most of them in genes important for proper function or structure of ciliated cells. Correspondingly, genes important for ciliary motility are also active in the PNC (Beckers et al., 2007; Murcia et al., 2000; Nonaka et al., 1998; Okada et al., 1999; Supp et al., 1999; Zhang et al., 2004).

With the description of leftward flow and its loss in *iv*-mutant mouse embryos it became clear that this dynein-dependent mechanism was the symmetry breaking event in mice and humans. As cilia bear an intrinsic chirality due to their structure, they mostly and preferably rotate in one direction (clockwise in ventral view) and thus they represent the proposed part that performs the "*conversion*" of a molecular to a cellular handedness, meaning number (1) as postulated by Brown and Wolpert (Brown and Wolpert, 1990).

Supporting flow as a symmetry breaking mechanism, further studies have also revealed a similar process in rabbit (*Oryctolagus* cuniculus; Fig. 03), zebrafish and medaka (*Oryzias latipes*) embryos, generated by a similar ciliated epithelium, the

rabbit PNC and the long known Kupffer's vesicle (KV) in teleost fish (Kupffer, 1868). Additionally, flow in medaka and zebrafish was proven to be upstream of the left nodal cascade, underlining functional conservation of this process (Essner et al., 2005; Kramer-Zucker et al., 2005; Okada et al., 2005). In this context, the requirement of another axonemal dynein heavy chain, *dnah9*, was demonstrated for fish.

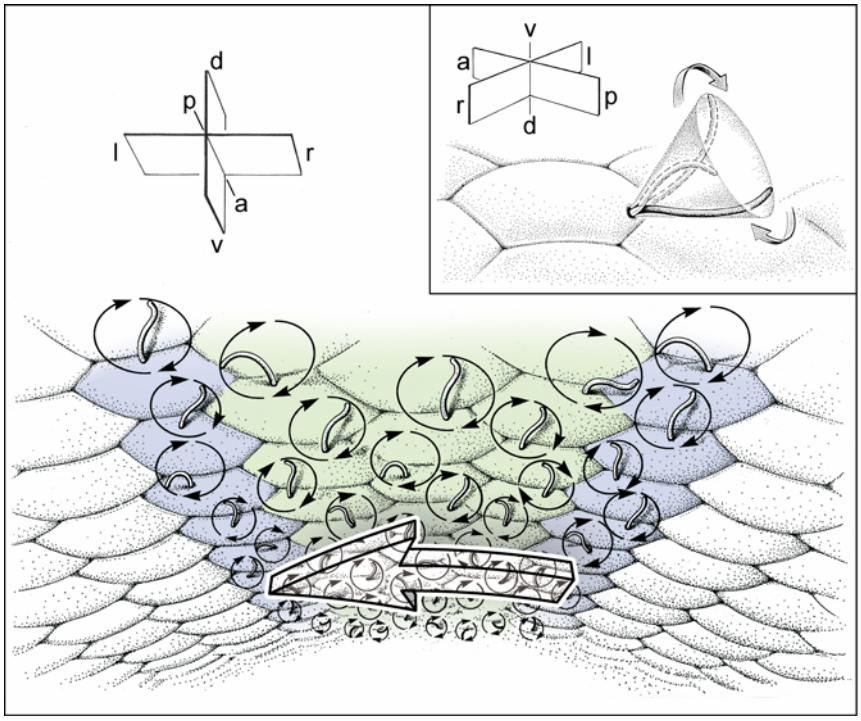

Fig. 01 The ciliated LR field Schematic representation of the monociliated field of the vertebrates (green), bordered by a bilateral expression domain of *nodal* (blue). Cilia are all rotating in a clockwise manner at the posterior pole of the cells (inset). Thus they produce an extracellular fluid flow towards the left side. Figure adapted from (Blum et al., 2009a).

After it had been shown that flow is upstream of the *nodal* expression in the LPM, two models were proposed for flow-mediated activation of *nodal*: the transport of a morphogen across the field of ciliated cells (Hirokawa et al., 2006; Nonaka et al., 1998; Okada et al., 1999), and the two-cilia model, in which one population of ciliated cells produces the flow and another perceives it via sensory cilia (see below; McGrath et al., 2003; Tabin and Vogan, 2003) – up to now, both are still under debate.

With the description of the flow as the symmetry breaking event, today the establishment of LR asymmetry in the vertebrate embryo can be subdivided into four phases:

(A) Breakage of the early bilateral symmetry by the leftward fluid-flow,

(B) transfer of a left-sided signal to the lateral plate mesoderm,

(C) asymmetric activity of the *nodal* gene cascade in the left LPM, and

(D) left marker gene mediated asymmetric organ morphogenesis.

5.5 Early determinants and the ion flux model

As mentioned, the mechanism of symmetry breakage has been quite well investigated in mammals so far and was also shown to be conserved in teleost fish. But for the other vertebrate groups – namely amphibians and sauropsids (i.e. birds and reptiles) – a completely different (temporal, spatial and mechanistical) mode of breaking the symmetry was proposed.

In *Xenopus* (and quite similarly in chicken), it was claimed that gap junctional communication is important in dorsal and not in ventral blastomeres and gap junctions were shown to be necessary for correct laterality development upstream of *nodal* expression in the LPM (Levin and Mercola, 1998). Additionally, asymmetries in mRNA distribution of a *H/K-ATPase* α-subunit (enriched on the right side) and its importance for correct LR development upstream of *nodal* were published (Levin et al., 2002).

On the basis of these findings, the so-called ion flux model has been proposed by the author of all of these studies: in the first place, mRNAs coding for ion transporters, which are randomly distributed in the zygote would be directionally transported to the right side during 2cell stage to finally end in the right ventral blastomere in 4cell stage. This should be achieved by the ordered arrangement (from right to left with one pole) of microtubule tracks on which the mRNA would be unilaterally transported via dynein or kinesin motor proteins. The resulting asymmetric distribution – and function – of ion transporters (mainly H^+/K^+-ATPase) would then result in differential membrane voltage and pH among cells on either side of the midline. Gap junctional connections were claimed to be located only on the dorsal side. Thus, the existing voltage gradient would drive asymmetric electrophoresis of unknown small charged signaling molecules through the gap junctions towards the right (or left according to Levin, 2003) ventral side (Zhang and Levin, 2009).

As the basis of this model was the asymmetric expression of *H/K-ATPase* α-subunit, it had also been looked for an asymmetrically located small molecule. As a candidate for the transport through gap junctions the neurotransmitter serotonin (5HT) was identified. It was shown to be putatively localized asymmetrically on the right side of 32cell stage embryos. It was demonstrated that serotonin receptor 3 (Htr3) and 4

(Htr4) mediated signaling as well as serotonin transporter functions (vesicular monoamine transporter, VMAT and plasma membrane serotonin transporter, SERT) were necessary for correct laterality (Fukumoto et al., 2005a; Fukumoto et al., 2005b). Drug-mediated inhibition of the receptors resulted in a randomization of LPM *nodal* expression and laterality defects.

As the components of the ion flux model were largely analyzed by pharmacological treatments and such drugs are difficult to wash out of the embryonic tissue and cavities, the temporal aspect – when these components are exactly important for LR axis development – was not clearly demonstrated.

With the apparently extremely different modes of symmetry breakage in amphibians and birds, as compared to mammals and fish, a possible conserved mechanism for all vertebrates was hardly expected.

5.6 Leftward flow and the superficial mesoderm in *Xenopus laevis*

Although there were accumulating publications dealing with the details of the ion flux hypothesis and thus more and more rejecting a unifying model for symmetry breakage in vertebrates, there were also some indications that there could be a PNC-homologous structure and flow-process in *Xenopus* as well. Though vaguely, gene expression analysis in early neurula stages showed that the *dnah9* gene displayed a distinct region of activity in the dorsal posterior part of the archenteron (Essner et al., 2002). Additionally, a detailed descriptive work done by Shook et al. on the fates of special dorsal superficial mesoderm (SM) in the blastulae of two *Xenopus* species (*X. laevis* and *X. tropicalis*) uncovered that this superficial layer transiently reaches the posterior-most roof of the archenteron after gastrulation, superficially embedded in gut lining endoderm (Shook et al., 2004). This mesoderm-derived tissue was named gastrocoel roof plate (GRP) and comprises an epithelium of smaller cells (as compared to the lining endoderm cells) that is transiently present during neurulation (Fig. 02). Very remarkably, they described that each of these cells carried a single cilium on its surface and speculated about a possible homology with the “notochordal plate of the mouse” (PNC) and a possible function for LR asymmetry (Shook et al., 2004; Sulik et al., 1994).

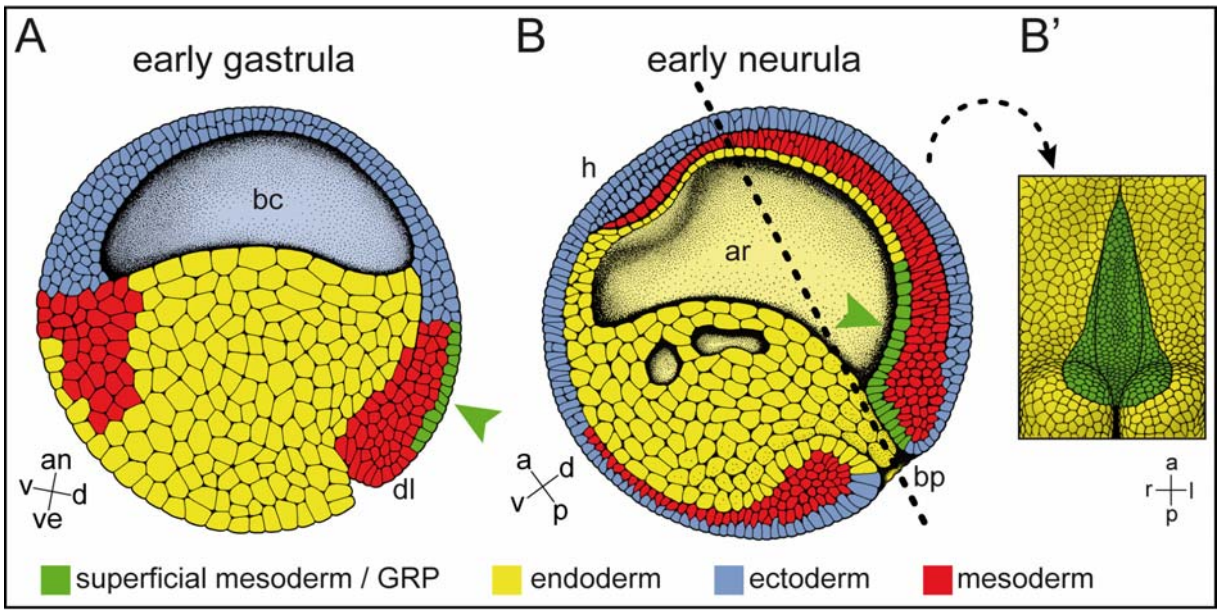

Fig. 02 Origin of the GRP in neurula stages from superficial mesoderm of the gastrula.
(A) Sagittally sectioned early gastrula embryo with animal ectoderm, vegetal endoderm and deep marginal mesoderm. Superficial mesoderm – the precursor of the GRP – is located on the dorsal side above the embryonic organizer (dorsal lip). **(B)** Sagittal section of an early neurula embryo after finished gastrulation. Ectoderm covers the exterior, endoderm most of the formed archenteron and mesoderm is in between. The GRP is transiently found at the posterior archenteron roof, embedded in the endoderm. Dashed line indicates plane of section for explant preparation in B'. **(B')** Prepared neurula stage dorsal explant in ventral view with GRP and endodermal archenteron lining. a, anterior; an, animal; ar, archenteron; bc, blastocoele; bp, blastopore; d, dorsal; dl, dorsal lip; h, head; p, posterior; v, ventral; ve, vegetal. Green arrowhead highlights SM or GRP.

Shortly thereafter, we performed detailed analyses of the GRP, its function and temporal appearance. We demonstrated its homology to the PNC and KV and, moreover, its relevance for the left-right axis. These recently published results argue for the possible existence of a conserved LR mechanism. We have shown that the GRP indeed has the same properties as KV and PNC – a single rotating posterior polarized cilium per cell, the expression of *dnah9* in this epithelium and an extracellular fluid-flow over the GRP, always directed from the right to the left side (cf. Figs. 01-03). More importantly the injection of highly viscous methyl cellulose solution (MC; e.g. the main component of wallpaper paste) directly upon the GRP inhibited cilia-generated flow and resulted in a loss of left marker gene induction and laterality defects in those tadpoles (Schweickert et al., 2007).

These findings clearly showed the importance of a flow mechanism for LR asymmetry but of course raised more specialized questions which needed additional approaches with different methods – like the exact properties of the frog leftward flow and the nature of the signal generated (see also below).

However, very crucially, these findings questioned the disparity of symmetry breakage in different vertebrate classes and opened up the possibility to find a unifying model for symmetry breakage. In other words, with this revelation, the long existing “thorn in the side of the cilia model that just won’t go way” was finally open to be evaluated again – namely the early asymmetries in *Xenopus* (Tabin, 2005).

5.7 The ciliated posterior notochord and its homologs

In order to underpin the conserved state of the PNC and its homologs and to differentiate those from organizer tissue, a detailed descriptive analysis was performed. It clearly demonstrated that the PNC and the mouse organizer are distinct structures, distinguishable by gene expression (*nodal* bilaterally flanking and *lrd* in the PNC – *Gsc* in the organizer) and morphology (Fig. 3 and Blum et al., 2007). The same properties applied to the rabbit PNC and the frog GRP. Therefore the symmetry breaking tissue of vertebrates – the LR coordinator – can be clearly defined. It constitutes a ciliated mesodermal epithelium directly anterior of the embryonic organizer (node, dorsal lip, embryonic shield and Hensen’s node), displays clear germ layer distinction in contrast to the latter and represents the posterior-most roof of the archenteron (Blum et al., 2007; Blum et al., 2009a).

One mentionable exception is the chicken – as the only analyzed representative of the sauropsids, which seems to have lost a ciliated epithelium and leftward flow but kept asymmetric nodal signaling via asymmetric node morphology (Blum et al., 2009b; Levin et al., 1995; Manner, 2001). Very recently, it could be shown that the chick node cells perform an asymmetric cell movement which was demonstrated to be upstream of node and marker gene asymmetry (Gros et al., 2009).

5.8 Serotonin signaling in left-right asymmetry

As mentioned above, receptor type 3 and 4 mediated serotonin signaling seems to be involved in LR axis development upstream of the nodal cascade, although the exact role remained elusive (Levin, 2003; Zhang and Levin, 2009).

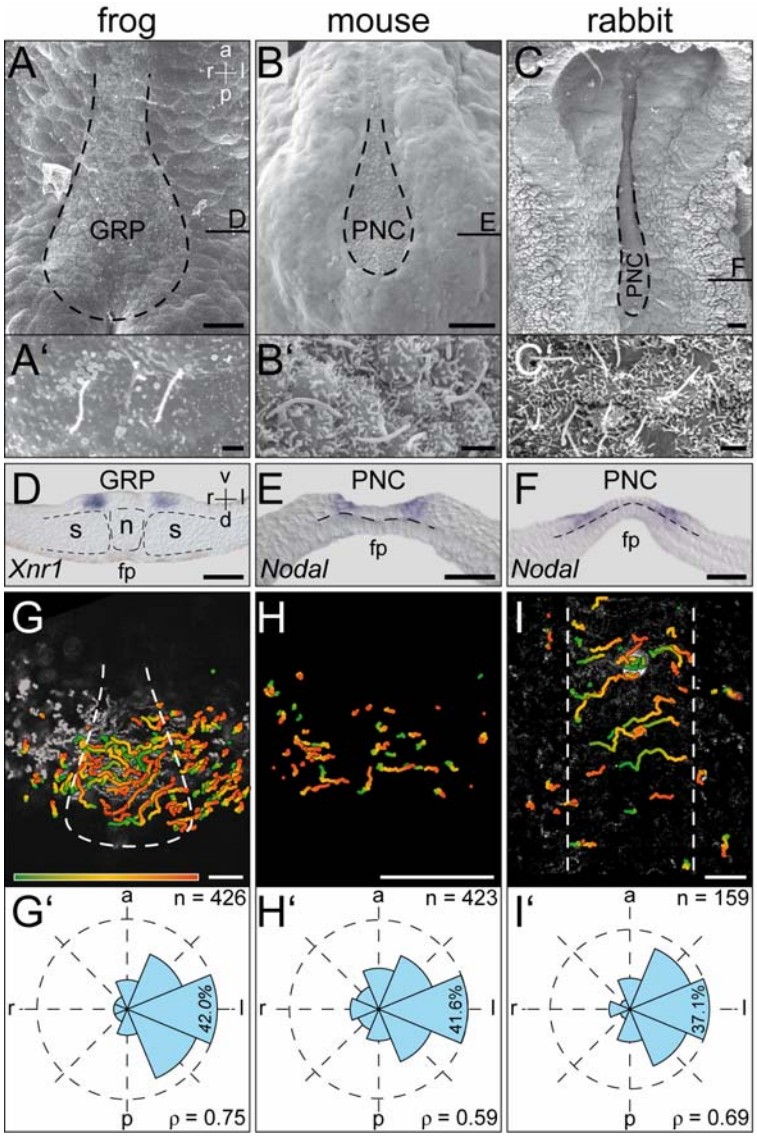

Fig. 03 Comparison of ciliated epithelia and leftward flow in frog, mouse, and rabbit.

(A-C) Scanning electron microscope pictures of monociliated epithelia (dashed lines) at the GRP (A), and PNC in mouse (B) and rabbit (C). A'–C': High magnifications of cilia. Note that the dimensions of the respective structures vary considerably.

(D-F) Topology of GRP/PNC shown in transverse sections (levels of sections indicated in A–C) of embryos after WMISH for the expression of the *nodal* gene, flanking the epithelium.

(G-I) Comparison of leftward flow shown as GTTs (G–I) and as statistical analysis of direction (G'–I').
a, anterior; d, dorsal; fp, floor plate; GRP, gastrocoel roof plate; l, left; n, notochord; p, posterior; PNC, posterior notochord; r, right; s, somite; v, ventral.
Bar graphs = 50µm in A–C and D–I, 2µm in A'–C'. Color gradient bar in G and I =25 sec, and 4.3 sec in H. Figure adapted from (Blum et al., 2009a).

Furthermore, up to now, it was not shown how these early processes could finally result in a left (and not right) asymmetric nodal cascade one day later and what mechanisms or components might be involved in transmission of the primary signal.

In the light of the recently discovered leftward flow in *Xenopus*, a different possibility surfaced: for different organisms and tissues, it was published that serotonin signaling may alter ciliary beat frequency (Christopher et al., 1996; Christopher et al., 1999; Konig et al., 2009; Nguyen et al., 2001; Sanderson et al., 1985; Schor, 1965; Wada et al., 1997). As stated above, pharmacological inhibitory experiments are difficult to interpret in their temporal component, thus one might envision that these drugs could have accumulated in the gastrocoel/archenteron and finally affected ciliary beating and thus leftward flow. Therefore it would be very insightful to analyze the components of the ion flux model in context of the leftward flow mechanism in *Xenopus* and, if possible, to identify the mode of symmetry breakage in amphibians.

6. Signal perception at the margin of the LR coordinator

Although the flow as the symmetry breaking mechanism is studied in detail, the signal the flow transports or generates is less well understood and currently under debate. Especially for the mouse system some theories have been raised which will be described below.

6.1 The morphogen model

When the leftward fluid-flow was originally published, the authors also postulated a possible mechanism how the flow could finally generate a left signal; with the so-called “morphogen model” (Nonaka et al., 1998; Okada et al., 2005). According to this, the flow transports a secreted morphogen which accumulates on the left side, binds the receptor and thus activates an unknown signal that finally results in *nodal* activation in the left LPM only (Fig. 04A). Concerning a possible source, it has also been suggested that the morphogen might either be released from the PNC itself or its margin (Okada et al., 1999). In the context of this model, several candidates have been proposed to be transported. The most attractive has always been nodal itself (Cartwright et al., 2008; Hamada, 2008; Saijoh et al., 2003; Tabin, 2006), as it is expressed bilaterally, flanking the PNC (and all other homolog structures) during flow stages and was reported to increase on the left side in mouse (Blum et al., 2007; Long et al., 2003; Lowe et al., 1996). After this concept, nodal produced at the right margin of the PNC would be transported by the flow to the left side, where it enriched and induced a signal. But up to now, the true nature of a possible morphogen is still uncovered.

As the mouse and fish model systems do not provide a possibility to dissect the flow and flow-sensing mechanism and the nature of a morphogen in more detail, it would be very informative to address this issue in the frog. To be more specific, *Xenopus* offers the opportunity to inhibit single processes (e.g. flow, nodal production) side- and region-specific and thus to reveal the requirement of the flow in respect to side or component.

As a variation of the morphogen model the transport of so-called NVPs (nodal vesicular parcels) has been proposed. According to this model not a single morphogen but the NVPs – membrane-sheathed vesicles – should be released from the PNC cells in a FGF- and microvilli-dependent process (Hirokawa et al., 2006; Tanaka et al., 2005). It was presented that these vesicles contained sonic hedgehog (shh) protein and retinoic acid (RA). Further, these vesicles should be transported by the leftward flow and then be fragmented at the left margin of the PNC to release their content. Though this model attractively unifies several LR components implicated earlier, there have not been any follow-up experiments that might clarify this model in more detail.

6.2 *Polycystic kidney disease* genes and the LR axis

Besides the Kartagener Syndrome, another group of human disorders has linked the requirement of cilia function to laterality – hereditary polycystic kidney diseases. There are two main types of such genetic diseases, the autosomal recessive (ARPKD) and the dominant polycystic kidney disease (ADPKD), with the latter being more prevalent (Wilson, 2004). The two genes *polycystic kidney disease 1* and *2* (*Pkd1* and *Pkd2*) have been shown to be mutated in 85% and 15% of ADPKD patients, respectively. *Pkd1* codes for the eleven transmembrane protein PC1 and *Pkd2* for the six transmembrane calcium channel PC2 (Harris and Torres, 2009; Vassilev et al., 2001).
In the current view, both interact in a complex in the membrane of renal cilia as a sensor of the velocity of the urinary fluid. PC1 is thought to represent the sensor that measures bending of the cilium, thereby the speed of the fluid and, consequently, indirectly the diameter of the nephric tubule. By this mechanosensation, and via their connection, PC2 is assumed to be activated and to release a calcium signal. With this “measuring device” the proliferation of the tubule epithelial cells is supposed to be regulated (Praetorius and Spring, 2003; Witzgall, 2005). Loss of either of these genes therefore causes dramatic kidney phenotypes with large fluid-filled cysts inside the kidney that consequently ceases function more and more.

The two genes are widely conserved from mammals to nematodes, as well as the ciliary location of their products (Barr and Sternberg, 1999; McGrath et al., 2003; Sun

et al., 2004; Venglarik et al., 2004). Generated knockout (KO) mice display a comparable kidney phenotype and homozygotic specimens die before birth (Pennekamp et al., 2002). More interestingly, when these mice were analyzed in detail, it was shown that homozygous embryos displayed laterality defects in a high percentage of cases. Accordingly, left marker genes *nodal* and *lefty* were mostly (>80%) not expressed but, remarkably, *Pitx2* expression was bilaterally with a more posterior retracted anterior border. Therefore this displays one of the very rare examples where the nodal cascade genes are not coupled (Pennekamp et al., 2002). These results provided the first direct link between kidney development and laterality; however, due to the ubiquitous expression pattern and the disparity of left markers, functional categorization was difficult in mice and further studies in other organisms were needed.
Remarkably, a similar analysis revealed that the knockout of *Pkd1* did not cause any LR axis defects, strongly suggesting an individual role for *Pkd2* for LR asymmetry. Additionally, PC2 and not PC1 was located on mouse PNC cilia (Karcher et al., 2005).

Another intriguing, though much less understood gene important for kidney development is the mammalian homolog of the *Drosophila bicaudal C homolog 1* gene (*Bicc1*). In *Drosophila* Bicc was originally described as a RNA-binding protein involved in the translational repression of *oskar* mRNA during AP development in oocytes (Mahone et al., 1995; Saffman et al., 1998). Its *Xenopus* homolog (*xBic-C*) is strongly expressed in the vegetal part of the early embryonic stages and was shown to induce dorsal endoderm in dependence of its K homology (KH) RNA-binding domain. Remarkably, in later stages transcripts were found on the dorsal lip and in the tadpole developing pronephric system (amphibian tadpole primitive kidney system; Wessely and De Robertis, 2000). In accordance with this expression pattern, knockdown of the transcript caused massive edema formation in tadpoles, characterized by multiple cysts in different organs and cavities (Tran et al., 2007).
Additional information came with the positional cloning of the genes mutated in two common mouse models for a ADPKD- and a ARPKD-like disease – *jcpk* and *bpk* respectively – which where shown to bear both a mutation in the mouse *Bicc1* gene (Cogswell et al., 2003). Interestingly, the two distinct mutations in the same gene cause two forms of PKD.

A first connection of *Bicc1* to the LR axis was established when a knockout mouse was generated and analyzed for laterality. It could be demonstrated that these mice indeed display laterality defects with a randomization of left marker genes (Maisonneuve et al., 2009). Furthermore, this phenotype was obviously due to missing polarization of the PNC cilia caused by impaired PNC formation. These results raised the question whether this phenotype was conserved among vertebrates.

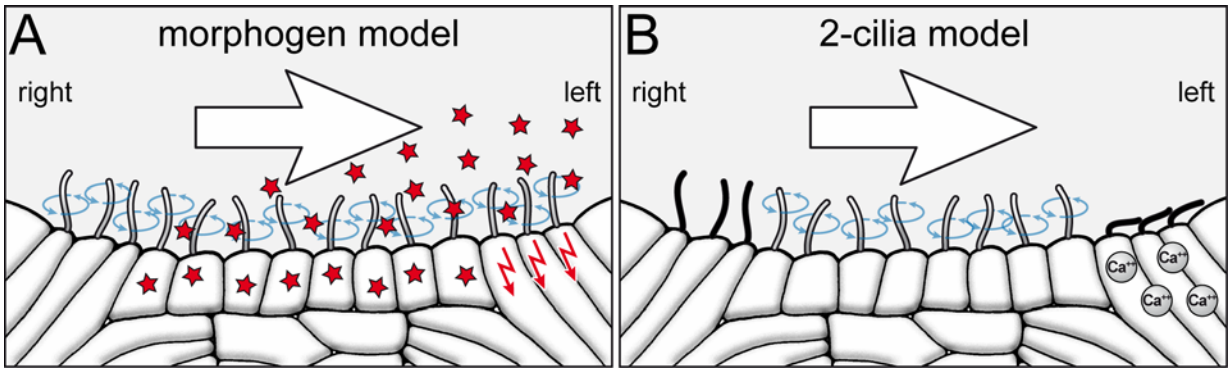

Fig. 04 Comparison of two leftward flow models.
(A) Morphogen model. In this illustration the molecule (red stars) is secreted from the ciliated epithelium. **(B)** Two-cilia model with motile cilia in the center and immotile sensory cilia at the margin of the ciliated epithelium. These would initiate a Ca^{2+}-signal. See text for details. Illustration kindly provided by Thomas Weber.

6.3 *Pkd2* and the two-cilia model

After the description of LR axis impairment in the *Pkd2* knockout mouse, it was intended to figure out the role PC2. Analysis of leftward flow in knockout mice was not yet published and transcription analysis was not informative. Nevertheless, with the background of LR requirement and the proposed sensory function of the PC1-PC2 complex in the mammalian kidney, a second model for flow sensation was postulated – the “two-cilia model” (Fig. 04B; Tabin and Vogan, 2003).

By generating a GFP-“knockin”-mouse that expressed GFP (green fluorescent protein) coupled N-terminally to the lrd (dnah11) protein, it was demonstrated that this dynein heavy chain localized to PNC-cilia. Ciliary localization was verified by additionally performing an immunohistochemistry (IHC) with an antibody against the acetylated alpha-tubulin that specifically detects ciliary microtubules (Chu and Klymkowsky, 1989). Furthermore, an antibody against PC2 was used to show colocalization with lrdGFP and thus with PNC cilia. For this colocalization, the authors highlighted cilia peripheral at the GRP that apparently showed a red PC2 but no

green lrdGFP signal (McGrath et al., 2003). To connect this phenomenon to the known function of polycystin-2 as a Ca^{2+}-permeable ion channel, Ca^{2+} measurements were performed. In wildtype specimens, a strong calcium signal could be detected on the left peripheral side of the PNC while in *Pkd2*- as well as *lrd*-mutant embryos this sided Ca^{2+} detection was lost.

Based on these results the authors thus suggested that – according to their model – all PNC cilia would bear the PC2 channel but lrd would only be located on the central ones. So the motile cilia located in the middle were thought to drive leftward flow, whereas the lateral, presumed immotile population of mechanosensory cilia would be bent (in analogy to kidney cilia) on the left side and generate the calcium-signal (McGrath et al., 2003; Tabin and Vogan, 2003).

Although very attractive in theory, the immunostaining pattern was not reported to be similar in any other species. Nevertheless, a sided calcium-signal could be found in chicken, zebrafish and was reproduced in mouse (Hadjantonakis et al., 2008; Raya et al., 2004; Sarmah et al., 2005). The advantage of this model is that it might explain the different phenotypes of left marker gene expression in mutant mice. Those harboring immotile cilia due to a mutation in the dynein heavy chain gene (*lrd*) show a randomization of marker gene activation. In contrast, mice lacking cilia due to loss of ciliary proteins required for IFT (e.g. polaris or kinesins) either fail to activate the cascade or display bilateral expression (Lowe et al., 1996; Murcia et al., 2000; Nonaka et al., 1998).

As already mentioned, flow had also not been measured in *Pkd2* mutant embryos during this study, so the observed lack of calcium-signal might as well be attributed to a possible loss of cilia motility. Therefore, the present available techniques to dissect the mechanism of leftward flow in *Xenopus* offers an interesting chance to test this model in detail and to identify PC2 as a component of LR axis establishment in the frog.

6.4 The bilateral *Xnr1* expression at the border of the LR coordinator

As referred to earlier, a bilaterally active *nodal* expression domain can be found at the margin of the ciliated epithelium in all vertebrates during neurula stages (Fig. 03D-F; Blum et al., 2007; Levin et al., 1995; Long et al., 2003; Lowe et al., 1996). In more detail, this domain varies between different vertebrate species. While in chicken

it is first initialized only on the left and subsequently becomes activated also on the right side, it is bilaterally symmetrically initiated in all other vertebrates analyzed to date. In mouse, expression starts in a horseshoe-like pattern posteriorly around the PNC (thus also partially in the organizer; for details see Blum et al., 2007), then posterior and right expression diminishes and the left part increases (Lowe et al., 1996). As this correlates with leftward flow it was not only suggested that nodal could be the transported factor (see 6.1) but alternatively (or additionally), it might also be increased only on the left margin and be directly transported to the left LPM (Oki et al., 2007).

Independent of its exact function, it has been convincingly demonstrated that the bilateral domain is necessary for left LPM *nodal* expression by generating transgenic mouse lines that fail to express this domain. Both expressions of *nodal* in the LPM and at the PNC were shown to be controlled by distinct enhancer elements – the ASE (asymmetric enhancer) and the NDE (node-specific enhancer) and specific inhibition of the latter resulted in loss of expression at the PNC and the LPM (Brennan et al., 2002; Saijoh et al., 2003).

To account for the slight left raise in bilateral *nodal* expression occurring in parallel to leftward flow, a long-known theoretical model has been incorporated that accounts for the discrepancy between this effect and the strong, sudden expression of *nodal* only in the left LPM. This “reaction-diffusion model” (or more specifically a “self-enhancement and lateral-inhibition system”) comprises the diffusible activator nodal and the faster diffusible inhibitor lefty, which both coexist and diffuse in parallel, finally resulting in a stable pattern on the induced side. Thus the flow-generated small difference at the edge of the PNC is thought to be translated into a robust asymmetry resulting in the activation of the nodal cascade (Hirokawa et al., 2006; Meinhardt and Gierer, 2000; Nakamura et al., 2006; Ohi and Wright, 2007; Oki et al., 2007; Turing, 1952).

This is an interesting model, accounting for the robust asymmetry. Yet as there are no transcriptional asymmetries reported for the *Xenopus* or teleost fish bilateral nodal domain it is not evident if this mechanism is conserved in other classes. More important, it is unclear how the flow would initially establish the small biased difference between the left and right sides and what factors are important for this scenario.

6.5 The cerberus/Dan/Gremlin family of TGF-β inhibitors

Besides the TGF-β member lefty, that binds nodal protein or blocks its co-receptor cryptic (Chen and Shen, 2004; Cheng et al., 2004; Sakuma et al., 2002), another potent group of inhibitors of nodal signaling has been described, the cerberus/Dan/Gremlin family (Belo et al., 2008; Bouwmeester et al., 1996; Stanley et al., 1998). These are secreted inhibitors that bind Wnt, Bmp and TGF-β ligands in the extracellular space and therefore inhibit signaling (Bell et al., 2003; Piccolo et al., 1999).

One group of cerberus-like members of this family has been shown to be necessary for the establishment of the LR axis in all vertebrates. Again, as an exception for vertebrates, the chick *caronte* gene is expressed in the left LPM and paraxial mesoderm adjacent to the node and promotes left *nodal* expression by inhibiting a nodal-repressive function of Bmp on this side (Rodriguez Esteban et al., 1999). In contrast, the mouse *cerberus-like2* (*Cerl-2* or *Dand5*) gene shows a similar expression as *nodal* at the PNC but after bilateral induction, the left-sided domain decreases – reciprocally to *nodal*. The knockout caused mostly bilateral expression of the left marker genes in the LPM (Belo et al., 2000; Marques et al., 2004). The teleost homolog of *cerberus-like2* is *charon*, which has been analyzed in zebrafish, medaka, Fugu (*Fugu rubripes*) and in the bastard halibut (*Paralichthys olivaceus*) and the spotted halibut (*Verasper variegates*; (Hashimoto et al., 2007; Hashimoto et al., 2004; Hojo et al., 2007). Remarkably, only in medaka a right-elevated expression pattern at the KV – as in mouse – has been described, in the other species this domain remains bilaterally equal-sized. Nevertheless, similar to mouse, knockdown caused mainly bilateral expression of markers in both medaka and zebrafish and could be blocked in zebrafish by combined knockdown of *charon* and *spaw*. Finally, the protein of the *Xenopus* homolog of these genes, *coco*, was also shown to inhibit Bmp, Wnt and TGF-β ligands and has recently been reported to be expressed bilaterally in the paraxial mesoderm flanking the GRP (Bell et al., 2003; Vonica and Brivanlou, 2007). In contrast to the analyzed fish species, *coco* clearly overlapped with the expression of *Xnr1* at the GRP. Although knockdown of *coco* mostly resulted in bilateral expression of the left nodal cascade, it apparently showed no bias in left or right expression preference (Vonica and Brivanlou, 2007). Further, epistatic knockdown experiments with *coco* and *Xnr1* in *Xenopus* resulted in a loss of

unilateral gene induction and it could be demonstrated that *Xnr1* was only necessary on the left and *coco* only on the right side.
There are still several questions to be resolved because there is an apparent discrepancy between the vertebrate species examined so far. Most importantly, tough the expression patterns fit well with the appearance of leftward flow in mammals, fish and frog, no correlation has been raised for most of them.

Thus, with the description of a leftward flow in *Xenopus* and its side-exclusive manipulability, it would be interesting to analyze both *Xnr1* and *coco* expression in dependence of flow. This would reveal a possible hierarchical relationship among those components and the flow. Thus information about the true conservational state of the underlying mechanism could be obtained.

7. Signal transfer from the midline to the lateral plate mesoderm

The second phase of the establishment of a stable LR axis during embryogenesis – the transfer of the left-sided signal into the lateral plate mesoderm – is probably the least well-known. As mentioned above, nodal produced at the PNC has been hypothesized to directly diffuse into the LPM to activate its own expression. As nodal has been shown to act as a long-range signal in mouse and fish, this represents an intriguing possibility (Chen and Schier, 2001; Constam, 2009). It was further shown that in mice, this diffusion needs the *growth differentiation factor 1* (*Gdf1*) as a co-factor, a TGF-β member that was already implicated in LR development. Although expressed in the LPM and at the PNC, for correct LR development, it is only important at the PNC (Rankin et al., 2000; Tanaka et al., 2007). Problematically, nodal protein itself is very hard to visualize. Theoretically, the published calcium-signal might also be part of the mechanism that activates nodal in the LPM but no direct evidence has been published so far.

Recently, another mechanism has been suggested, involving sulfated glycosaminoglycans (GAGs) in the above mentioned transfer process (Oki et al., 2007). The authors showed that externally applied nodal was not able to induce *nodal* in the LPM and thus indicating an internal route. Further, cryptic co-factor

activity was only important in the LPM, demonstrating that no receptor binding of nodal is needed between the PNC and the lateral plate. Finally, they showed that nodal interacts with GAGs and that their inhibition prevented activation of *nodal* in the LPM. Therefore, the authors suggested nodal to migrate via GAG-routes into the LPM where it activates its own expression. This attractive model still awaits confirmation in other model systems.

Aim of this study

The last decade shed light on the previously poorly known establishment of the vertebrate left-right axis. Especially the left-sided nodal signaling cascade in the lateral plate mesoderm is now well understood in most vertebrates. In contrast, the initial symmetry breaking event had only been comprehended poorly. If investigated at all, different modes of translating the first two established axes into a LR-axis have been proposed for the different species. With the very recent insight that there is also a cilia-generated extracellular leftward fluid flow in *Xenopus laevis*, which is necessary to initialize the left nodal cascade, this situation has changed. In addition, all investigated mammalian and fish species show this feature, too. Thus, as opposed to earlier views, it has become clear that there is actually a plausible possibility, that most vertebrates display an ancient mode of symmetry breakage resulting in a stable LR-axis that was inherited from a common ancestor.

Although well shown by functional and descriptive methods, the symmetry breaking leftward flow needed a lot more detailed investigation in context of prerequisites, conditions, functionality, required components, sensing and transfer of the signal to the LPM. These characteristics have been studied best in the mouse system. Especially, several components have been identified which are necessary for the formation or function of the flow-generating ciliated epithelium. Unfortunately, knockdown technology is very time-consuming and it takes a lot effort to specifically test different components in mice.
With the background of a leftward flow as the symmetry breaking event, some of the more or less well-know components were therefore tested for their role in frog symmetry breakage. Moreover, I took advantage of the opportunities in the frog – namely to be able to target specifically into left or right parts of the GRP or other regions. *Xenopus* further offers a way to manipulate several flow-required components very specifically in the same experiment.

In a first set of experiments the properties of *Xenopus* flow were analyzed by specific interference with ciliary motility:

I. One of the best known requirements for proper generation of a leftward flow is the correct function of axonemal dynein heavy chains, which are necessary for the motility of cilia. To prove the conserved requirement of these flow-components and to underline the role of the flow as the symmetry breaking event, I cloned the homologous frog genes, analyzed their expression patterns and performed a functional characterization by specific gene knockdown. Furthermore, to obtain more understanding about the exact properties of the flow and whether nodal itself is transported by the flow, I tested the possibility that single knockdown on the left or right side of the GRP would cause distinct effects.
II. Serotonin signaling is known for its ability to alter the frequency of ciliary beating in different organisms and its type 3 receptor mediated part was shown to be involved in LR asymmetry of *Xenopus* development. Therefore the consequences of subtype-specific inhibition of serotonin signaling in the GRP were assessed. Inhibition of the receptor was expected to alter ciliary motility, consequently leftward flow and thus cause LR defects. With this analysis the expected first link between the early asymmetries and flow would be made.

In a second approach, the connection between polycystic kidney disease genes and the left-right axis was investigated:

III. A mutation in the *Pkd2* gene coding for the calcium channel polycystin 2 was shown to cause polycystic kidney disease and to be essential for correct left-right development in zebrafish and mouse. It has been proposed that the flow induces a left-sided, PC2-dependent calcium wave which in turn would activate the left nodal cascade. Here, the defined manipulability of the frog was used to obtain a clear picture of the function of Pkd2 for LR development. After expression analysis, the homologous *Xenopus* gene was knocked down side-specifically to confirm the proposed function and dissect the mechanism of flow-dependent activation of a calcium-signal on the left side upstream of *nodal*.
IV. A further gene whose absence causes kidney malformations and that is also connected to mouse laterality establishment is the RNA-binding protein coding gene *bicaudal C 1*. In the course of a cooperation project aimed to understand a possible role for bicaudal C in LR development of mouse and frog, the *Xenopus* homolog *xBic-C* was analyzed for GRP expression and investigated by defined

knockdown to reveal a function for leftward flow and the expected interplay with Pkd2 at the GRP upstream of nodal.

In the third experiment, the perception of the leftward flow in dependence of the different components was surveyed by epistatic knockdowns:

V. Hierarchy of the components and the direct read-out and left-sided signal generation at the margin of the ciliated epithelium was examined. Both, nodal and its inhibitor coco had been shown to be expressed bilaterally at the GRP and were thus candidates for direct flow- or calcium-dependent perception. This was addressed first by careful expression analyses of *nodal* and *coco* at the margin of the epithelium and second by epistatic experiments via combined knockdown of several components. Nodal and coco were expected to be downstream of flow. Exact hierarchical interrelationships were determined.

The overall aim was thus to categorize the factors necessary for correct flow-based symmetry breakage at the midline of the *Xenopus* neurula stage embryo in more detail and therefore to reveal the framework involved in this process.

Results

1. Dynein heavy chain function in *Xenopus* LR development

Generally, ciliary motility has been shown to be dependent on many structural components associated with the ciliary axoneme. Among these, proteins of the inner and outer arm dynein complex have been shown to be most important. Most Kartagener syndrome patients bear mutations in genes coding for outer arm dynein heavy chain genes and, consequently, their cilia are immotile (Storm van's Gravesande and Omran, 2005). Furthermore, studies with *dnah* mutant or morphant in different model organisms have confirmed functional conservation of these genes (Ibanez-Tallon et al., 2002; Kramer-Zucker et al., 2005). However, in amphibians dynein genes have not been functionally studied in LR development so far. Therefore these ciliary components were chosen for a descriptive and functional study in *Xenopus laevis*. With this approach it should be possible to manipulate leftward flow in a defined way.

1.1 Cloning of outer arm dynein heavy chain genes *dnah5*, *9*, and *11*

dnah5, *dnah9* and *dnah11* have been identified in human, mouse and zebrafish left-right axis formation (Bartoloni et al., 2002; Essner et al., 2005; Ibanez-Tallon et al., 2002; Olbrich et al., 2002; Omran et al., 2000; Supp et al., 1997) and are thus interesting candidates for a functional study in *Xenopus*. As it is presumed that different dynein heavy chains may be expressed in a tissue-specific manner or even show a distinct distribution along the cilium and as there were nearly no information about expression patterns in *Xenopus*, it was interesting to clone all three of these (Fliegauf et al., 2005; Zariwala et al., 2007). Because the full-length cDNAs of such dynein heavy chain genes span about 14 kb, fragments were cloned for expression analysis (for details see Materials and Methods).

1.1.1 Evolutionary conservation of dnah5

The human *dnah5* gene is the homolog of the *Chlamydomonas* outer arm gamma chain and has been shown to be responsible for most human cases of PCD as well as to cause LR defects in mutant mice (Ibanez-Tallon et al., 2002; Olbrich et al., 2002; Omran et al., 2000). Hence, it constitutes a promising candidate to have a role in LR axis development in frog, too.

As there was an EST (expressed sequence tag; accession number BJ064436) in the NCBI database, this fragment was chosen to be cloned. The amino acid (AA) alignment of *Xenopus* dnah5 showed a high degree of conservation throughout the metazoan species analyzed (Fig. 05).

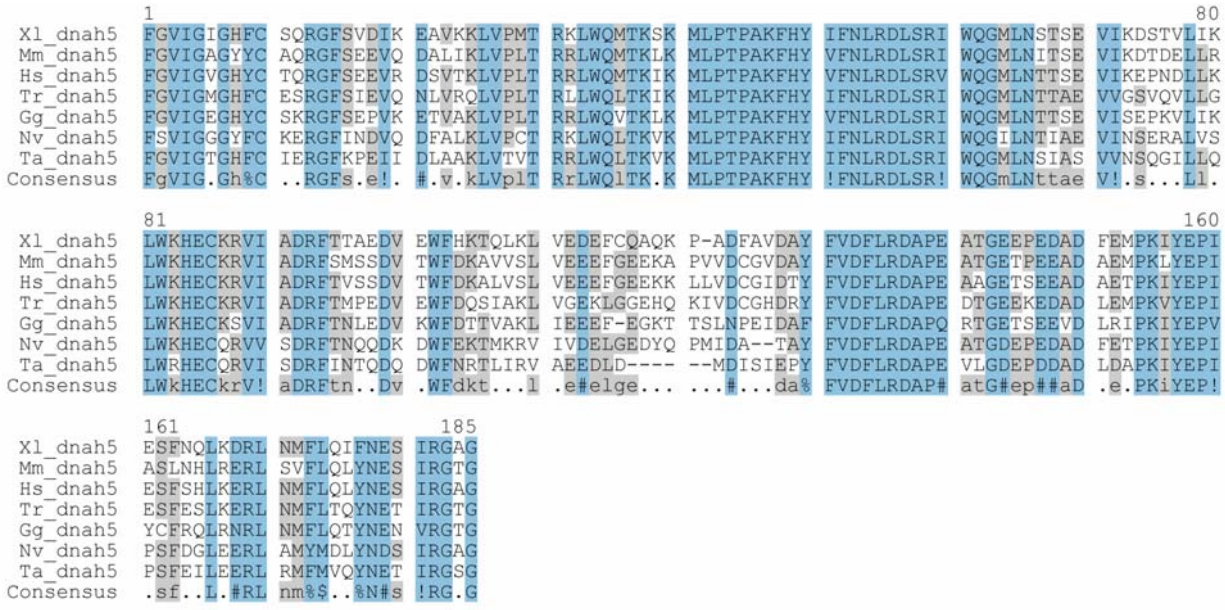

Fig. 05 Evolutionary conservation of dnah5. Alignment of partial amino acid sequences of dnah5 from *Xenopus laevis* (Xl_dnah5), mouse (Mm_dnah5), human (Hs_dnah5), *Takifugi rubripes* (Tr_dnah5), chick (Gg_dnah5), *Nematostella vectensis* (Nv_dnah5) and *Trichoplax adhaerens* (Ta_dnah5). Identical residues are highlighted in blue, similar amino acids are indicated in grey. ! is I or V; $ is L or M; % is F or Y; # is any residue of NDQEBZ

1.1.2 Conserved and distinct regions of dnah9 and dnah11

These two axonemal dynein heavy chain genes represent homologs of the *Chlamydomonas* outer arm beta chain genes which have been duplicated during vertebrate evolution (Asai and Wilkes, 2004). Therefore they might have tissue-specific functions as a result of slight changes in their encoded AA sequences and thus in their functional properties for ciliary motility. *dnah11* has been shown to be

involved in human PCD and is mutated in the *iv*-mouse, the embryos of which display a randomization of the inner organs and LR marker genes (Bartoloni et al., 2002; Schwabe et al., 2008; Supp et al., 1997). *dnah9*, in contrast, could not be linked to PCD or mammalian LR asymmetry up to now. Contrary to this, it has been clearly demonstrated that fish morphants show LR defects and that *dnah9* was probably expressed in the frog GRP (Essner et al., 2005; Essner et al., 2002).

A

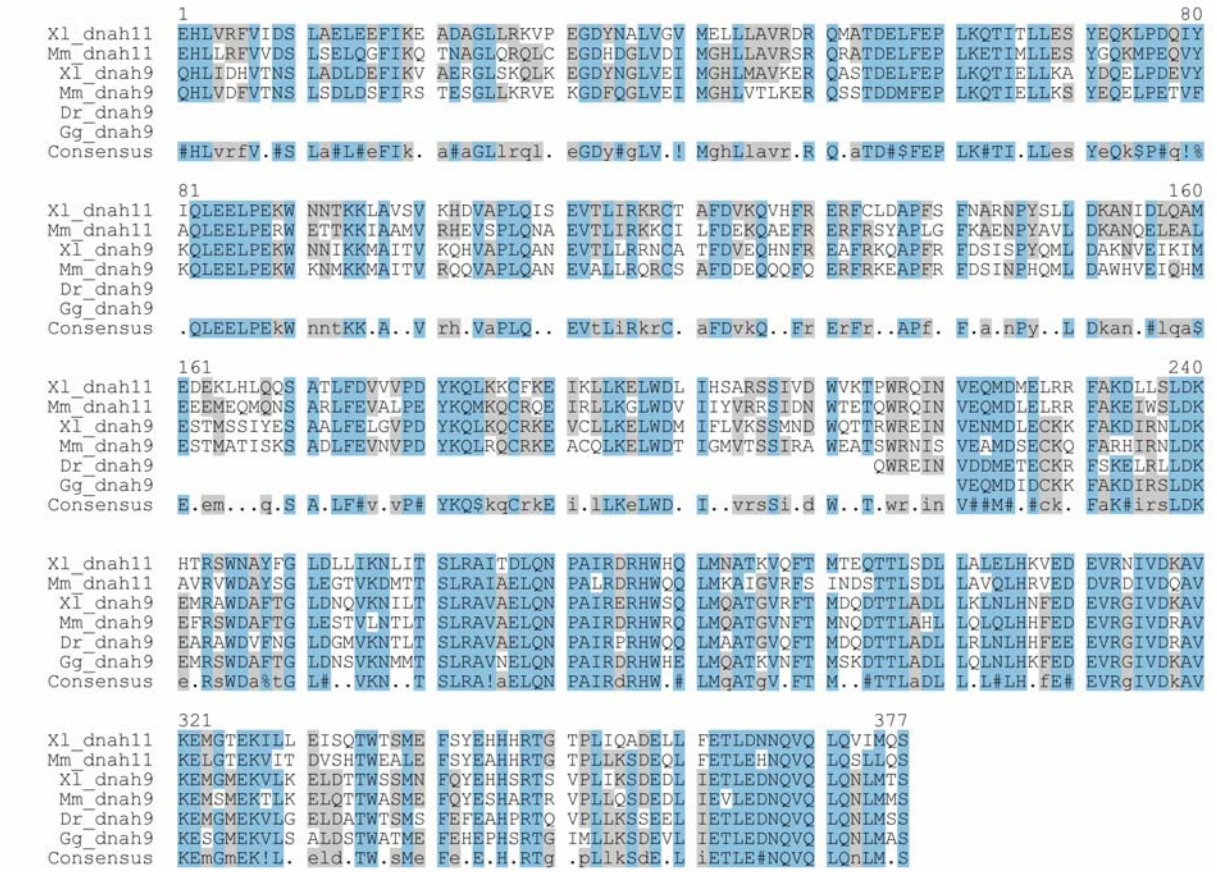

B

	Mus dnah11		*Mus* dnah9	
Xenopus dnah11	62%	(82%)	55%	(74%)
Xenopus dnah9	55%	(76%)	72%	(86%)
Mus dnah11		-	53%	(73%)
Gallus dnah9	59%	(78%)	72%	(84%)
Danio dnah9	58%	(77%)	71%	(83%)

Fig. 06 Conserved and distinct regions of dnah9 and dnah11. (A) Alignment of partial amino acid sequences of dnah9 and dnah11 from *Xenopus laevis* (Xl), mouse (Mm), zebrafish (Dr) and chick (Gg). Identical residues are highlighted in blue, similar amino acids are indicated in grey. ! is I or V; $ is L or M; % is F or Y; # is any residue of NDQEBZ (Corpet, 1988). (B) Degree of conservation of dnah9 and dnah11 in mouse and frog/chick/zebrafish. Note that *Xenopus* dnah9 shows the highest degree of conservation with mouse dnah9 (72% identity, 86% similarity), and *Xenopus* dnah11 likewise with mouse dnah11 (62% identity, 82% similarity; Tatusova and Madden, 1999).

Thus both genes were cloned for expression analysis in *Xenopus*. To clearly distinguish between these two beta chain genes, the same part of the N-terminal region 2 was cloned. The *dnah9* fragment corresponded to a published sequence (AY100020) and *dnah11* was cloned using a *Xenopus tropicalis* specific primer pair obtained by BLAST search with the mouse sequence in the genome of this frog species. The AA alignment with corresponding sequences from different vertebrate species showed AA positions conserved between all forms of these genes but also specific ones only conserved between the *dnah9* or *11* genes (Fig. 06A). More detailed analysis of the cloned fragments confirmed their identity, as the frog dnah9 and 11 clearly showed highest homology with the respective mouse orthologs (Fig. 06B).

1.2 Expression analysis of *dnah* genes during *Xenopus* embryogenesis

After the two cloned frog beta chains were shown to correspond to the different paralogous forms, a detailed expression analysis of all three genes was conducted by whole-mount *in situ* hybridization (WMISH) using digoxigenin-labeled antisense probes. During these studies only *dnah9* displayed a clear expression pattern during the entire *Xenopus* embryonic development (see also Fig. 07I), whereas the other two genes could not be found to be expressed before neurula (*dnah5*) and early tailbud stages (*dnah11*, not shown).

1.2.1 Maternal and zygotic expression pattern of *dnah9*

During early development maternal *dnah9* was strongly expressed in the animal region of cleavage stages; beginning in the zygote (Fig. 07A, C) it stayed active until blastula stages (Fig. 07D). No difference in blastomere staining was seen (Fig. 07C) and sense controls showed no signal in all cases (zygote in Fig. 07B and data not shown). During gastrulation, beginning at about stage 10, a weak, diffuse expression domain could be detected on the dorsal side (Fig. 07E). This domain condensed on the dorsal lip during gastrulation (Fig. 07F-H). Additionally, at stage 13, after mesodermal involution finished, a weak signal could be found in the posterior-most part of the archenteron roof, representing the developing GRP (Fig. 07H). This expression domain and the specificity of the signal could be confirmed by semi-

quantitative RT-PCR (Fig. 07I). The expression domain in the GRP got stronger with neurulation (Fig. 08A, B, D; cf. Schweickert et al., 2007) and stayed activate until about stage 20 (not shown). A further tissue that showed *dnah9* activity was the floor

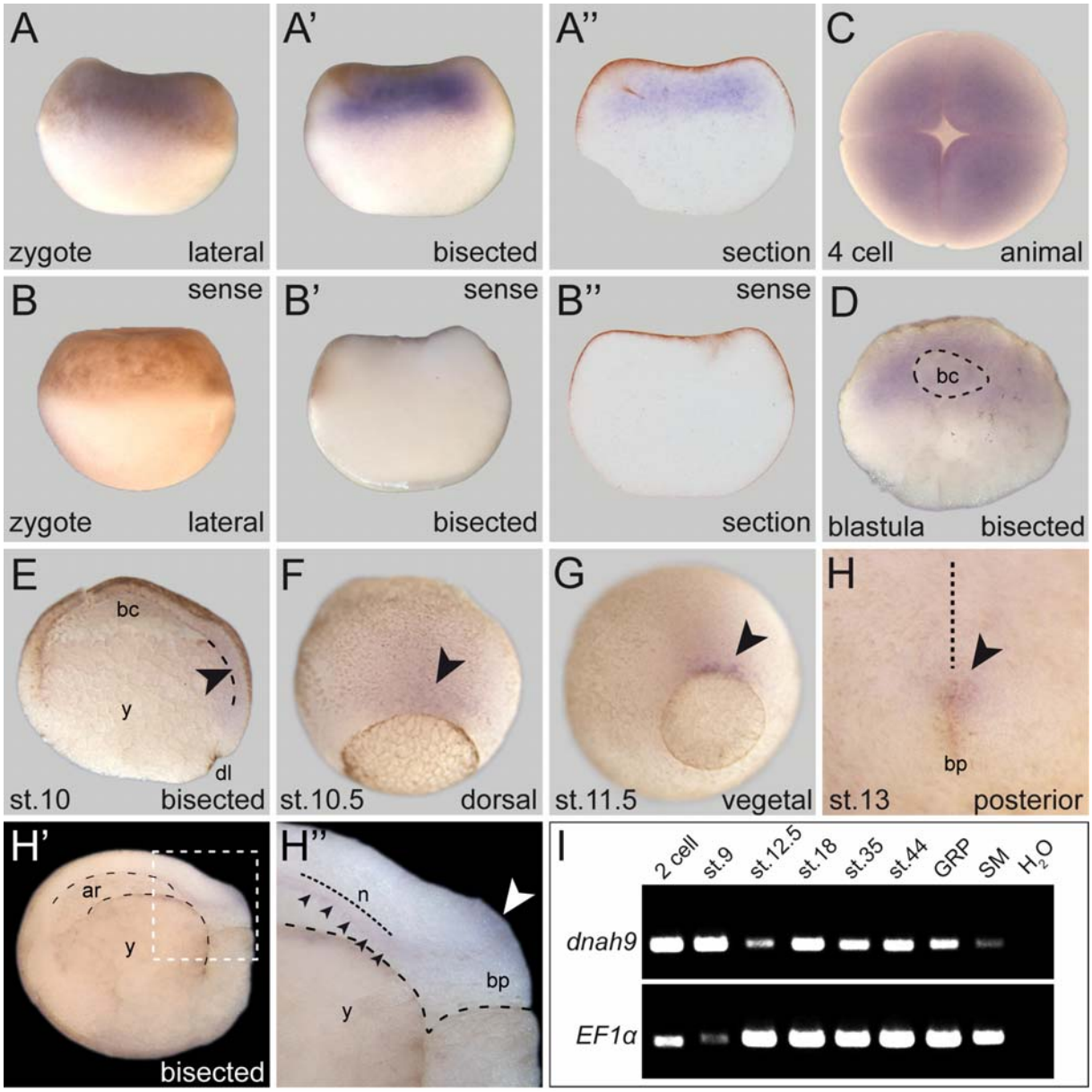

Fig. 07 Maternal and early zygotic expression of *dnah9*. Whole-mount in situ hybridization of staged embryos with a *dnah9*-specific antisense (A and C-H) or sense (B) probe. **(A-D)** Maternal mRNA localizes to the animal pole of the zygote (A), 4-cell embryo (C), and blastula stage embryo (D; blastocoel outlined by dashed line). Sense control revealed no staining (B). **(E–H)** Early zygotic expression in the dorsal region/lip of gastrula stage embryos (black arrowheads). st.10 (E; dorso-ventrally bisected; brachet's cleft indicated), st.10.5 (F), st.11.5 (G) and st.13 (white arrowhead in H'', midline indicated) showed increasing concentration of transcript in the lip region. Dorso-ventrally bisected st.13 embryo (H', H'') exposed beginning staining in the involuted GRP (black arrowheads in H''; archenteron indicated by dashed black, magnificated area by dashed white line and border between GRP and overlying notochord by dotted line). **(I)** Semi-quantitative RT-PCR from 2-cell to tadpole stages, and of isolated GRP and SM tissue. *Elongation factor 1 alpha* (bottom) served as control. A', B' and D animal-vegetally bisected and A'' and B'' 30 µm vibratome sections. Points of view are indicated. ar, archenteron; bc, blastocoel; bp, blastopore; dl, dorsal lip; GRP, gastrocoel roof plate; n, notochord; s, somite; SM, superficial mesoderm; y, yolk. Note the strong maternal expression of *dnah9* excluded from the cortex (A', A'' and D).

plate. Already indicated at st.13 (Fig. 07H) it became clearly visible at st.16 (Fig. 08C) and continued until late tailbud stages (Fig. 08E' and F). With neurulation, a spotty pattern was detected in epidermal cells, which came clearly visible in early (Fig. 8E)

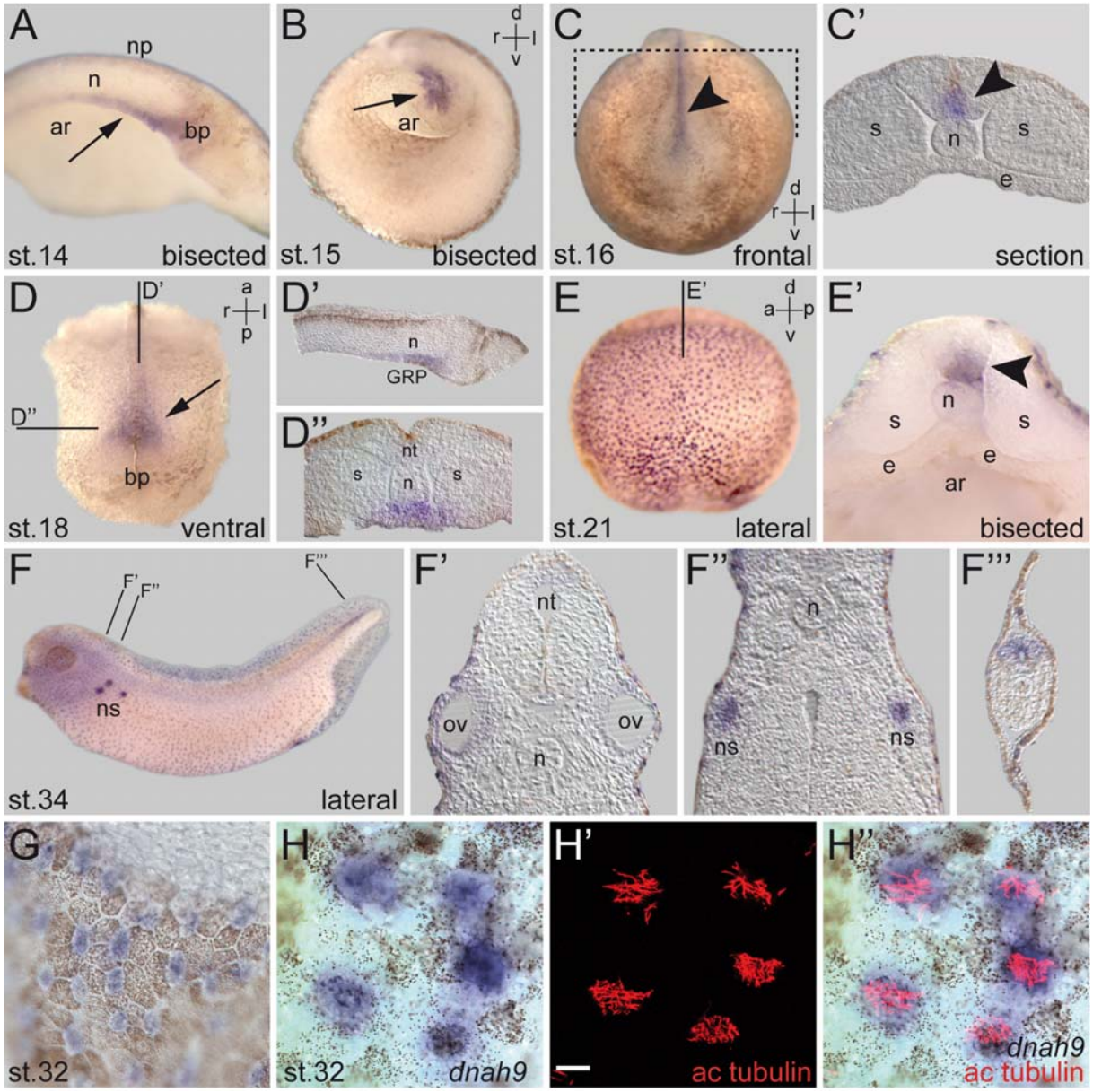

Fig. 08 Late *dnah9* expression patterns strongly correlate with ciliated tissues.
(A-D) Neurula stage embryos show expression in the GRP at stages 14, 15, and 18 (arrows in A, B, D) and floorplate (arrowhead in C', section at a level anterior to the gastrocoel roof plate as indicated). **(E, F)** Later localization of transcript in the floorplate of st. 21 (arrowhead in E'), epidermis of st.21 and st.34 (E, F) and in the otic vesicles, nephrostomes and the tailbud of stage 34 (F-F'''). **(G, H)** Localization of *dnah9* mRNA in multi-ciliated cells of the epidermis at stage 32 (section in G), demonstrated by sequential in situ hybridization (H') and immunohistochemistry using an antibody against acetylated tubulin (H''). Scale bar represents 15 µm. A sagittally bisected; B and E' dorso-ventrally bisected; D' and G sagittal and C', D'', and F'-F''' transversal 30 µm vibratome sections. In A-C' and D'-F''' is dorsal, in D anterior to the top. Points of view are indicated. ar, archenteron; bp, blastopore; dl, dorsal lip; e, endoderm; GRP, gastrocoel roof plate; n, notochord; np, ns, nephrostomes; neural plate; nt, neural tube; ov, otic vesicle; s, somite; y, yolk.

and late (Fig. 8F, G) tailbud stages and could be correlated with ciliated epidermal cells by subsequent whole-mount immunohistochemistry (WMIHC) with an antibody against acetylated α-tubulin, which specifically stains ciliary tubulin (Fig. 8H).

Further tissues with positive staining were the nephrostomes of the developing pronephric system (Fig. 08F, F''), the otic vesicles (Fig. 08F') and the tailbud region (Fig. 08F, F''').

1.2.2 Comparison of expression patterns of three *dynein heavy chain* genes

To further correlate the expression of all three *dnah* genes with ciliated tissue, the acetylated α-tubulin antibody was used to detect ciliation; parallel to this a comparative expression analysis was performed to detect cilia-correlative patterns. From neurulation onwards, expression of all three genes correlated with ciliated tissues, i.e. GRP (Fig. 09A), otic vesicle (Fig. 09B), nephrostomes (Fig. 09B, B'), epidermis (Fig. 09B, B'') and tailbud (Fig. 09B, B'''), as well as esophagus (not shown), stomach and small intestine (Fig. 09C). Common and distinct patterns were observed for the three genes. In the ciliated epithelium of the stage 17/18 GRP, signals for both *dnah5* and *dnah9* were detected, although to a much lesser extent in the former case (Fig. 09D, G), while *dnah11* was never seen in the GRP (Fig. 09J and data not shown). The multi-ciliated cells of the epidermis started to become positive for *dnah9* mRNA at stage 16 (data not shown), and persisted to about stage 43 (Figs. 08E-H, 09H, H'', I). Only very rarely a faint signal could be detected for *dnah5* (Fig. 09E, E''), and *dnah11* was negative throughout the epidermis in all experiments (Fig. 09K, K''). The nephrostomes were positive for both *dnah5* and *dnah9* (Fig. 09E, E', H, H' and Tran et al., 2007), again much stronger in the case of *dnah9*. As with the GRP and epidermis, *dnah11* was also absent from the nephrostomes (Fig. 09K, K'). This correlation held also for the otic vesicle, which was stained for *dnah5* and *dnah9* mRNA, but negative for *dnah11* (Fig. 08F', 09E', H', K', and data not shown). Co-expression of all three genes was found in the tailbud region (Fig. 08F, F''', 09E, E''', H, H''', K, K'''). *dnah5* and *dnah9* were seen in the posterior-most neural tube, i.e. chordoneural hinge derived floor plate and posterior wall-derived dorsal aspects of the neural tube (Fig. 09E''', H'''). In contrast, *dnah11* was additionally seen in the posterior wall itself (Fig. 09K''').

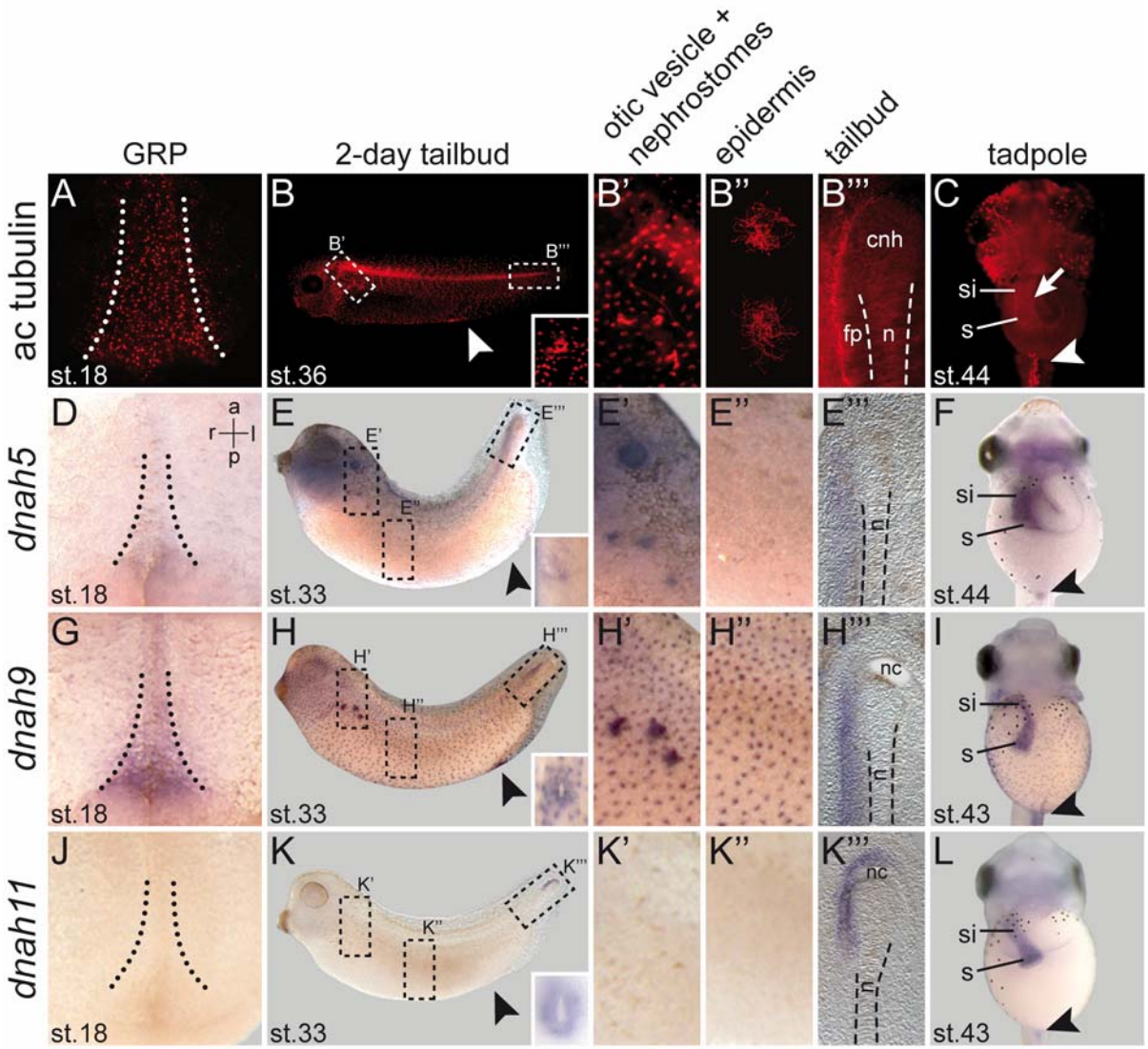

Fig. 09 Compared expressions of three *dynein heavy chain* genes.
Comparison of expression patterns of *dnah5*, *dnah9* and *dnah11* in ciliated embryonic tissues. **(A-C)** Immunohistochemistry using an antibody against acetylated alpha tubulin to highlight cilia. (A) Ciliated cells at the GRP, nephrostomes (B'), epidermis (B'') and tailbud (B''') of the 2-day tadpoles, and (C) in stomach and small intestine. **(D-L)** Whole-mount *in situ* hybridization of staged embryos with *dnah5* (D-F), *dnah9* (G-I) and *dnah11* (J-L) specific antisense probes. GRPs (A, D, G, J), outlined in dorsal explants by dotted lines, are shown in ventral view, anterior to the top. (B, E, H, K) 2-day tadpoles are oriented anterior to the left and dorsal up; blow-ups are indicated by dashed lines. Insets show frontal view of proctodeum (arrowhead). (C, F, I, L) Ventral views of stage 43/44 tadpoles. Proctodeum marked by arrowheads. Note that *dnah5* and *dnah9* are co-expressed in ciliated cells, with *dnah9* showing markedly stronger signals, whereas *dnah11* is only expressed in the proctodeum, tailbud and gastro-intestinal tract. Please note also, that *dnah5* and *dnah9* are restricted to the neural tube of the tailbud, whereas *dnah11* is additionally expressed in the posterior wall. cnh, chordoneural hinge; fp, floor plate; nc, neuroenteric canal; n, notochord; s, stomach; si, small intestine.

A further site where all three genes were transcribed was found in the gastro-intestinal tract of the stage 43/44 tadpole, namely the esophagus (not shown), the very anterior part of the small intestine and the stomach as well as the proctodeum (Fig. 09F, I, L, and insets in E, H, K).

In summary, the expression analysis of three of the >15 *dynein heavy chain* genes demonstrated that ciliated cells and tissues presented a strong common denominator of gene activity. Nevertheless, specific and distinct sites and expression levels were found in every single case.

1.3 Knockdown of *dnah9* caused multiple defects during development

As all three *Xenopus dnah* genes were active during development and their activity correlated with ciliated tissue, morpholino (MO)-mediated knockdown experiments were performed to investigate functional conservation. Morpholinos bind to the mRNA and specifically inhibit translation of the mRNA (see also Material and Methods). As *dnah11* showed no broad expression pattern and was obviously not active in the GRP, it was excluded from this functional approach. All in all, three different MOs were designed, one to inhibit the function of dnah5 and two to inhibit that of dnah9. Thereby, specificity of the obtain results should be underlined.
The first *dnah9*-MO (*dnah9*-AUG-MO) was designed to bind the region around the translational start site and thus to inhibit translation at all, of maternal and zygotic mRNA. To be able to clone the required sequence of the 5'-UTR (untranslated region) and the first part of the coding region, a primer pair was designed according to the corresponding *X. tropicalis* sequence, which in turn was obtained from a BLAST search with the mouse *dnah9* sequence. The other two MOs (*dnah5*-SB-MO and *dnah9*-SB-MO) were designed to interfere with splicing and therefore only to inhibit the zygotic mRNAs, as maternally deposited mRNA is already spliced.

1.3.1 Two *dnah* morpholinos specifically inhibited splicing of intron 2

A splice-blocking MO binds the pre-mRNA and therefore prevents correct intron-splicing. To design such a MO for the two *dynein* genes, a PCR using st.45 tadpole-derived genomic DNA was performed. For both genes the intron 2 donor site was chosen as the MO-attachment site and thus these MOs should inhibit splicing of intron 2. Primer pair sequences in exon 2 and 3 were designed after BLAST search of the *X. tropicalis* genome with the respective mouse sequences of the NCBI database. A rescue of the *dnah9*-MO phenotype was not tried, as the mRNA

comprises 14 kb, and a full-length cDNA clone was not available. For that reason inhibition of splicing was assessed by RT-PCR.

Fig. 10 Two *dnah* morpholinos specifically inhibit splicing of intron 2.

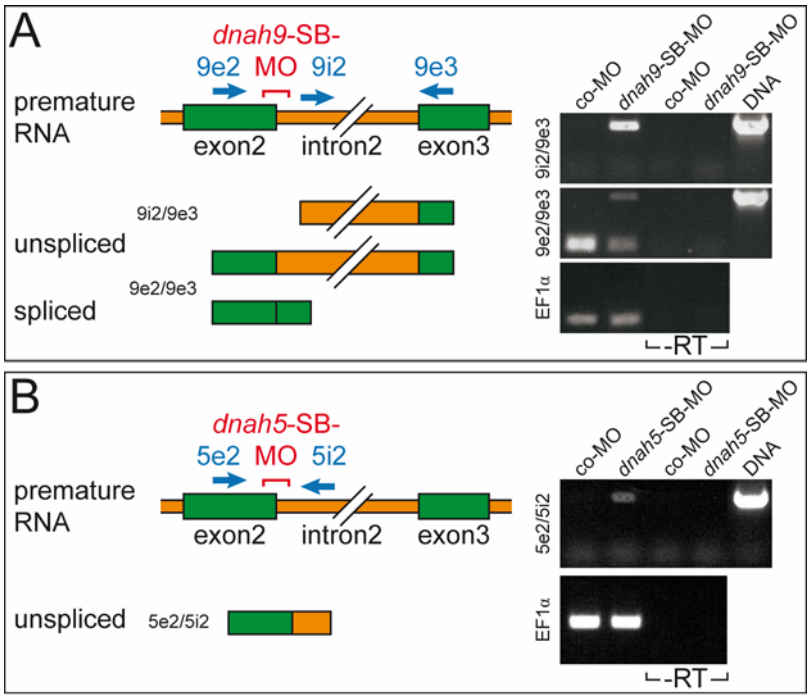

(A) Inhibition of intron2 splicing by *dnah9*-SB-MO. RT-PCR analysis of MO-injected embryos. Splicing was analyzed using forward primer 9e2 or forward primer 9i2, and reverse primer 9e3, schematically indicated by green (exons) and orange (intron) bars, and by blue arrows (primers). PCR of genomic DNA resulted in 1.5 kb (9e2-9e3) and 1.4 kb (9i2-9e3) bands. RT-PCR of co-MO in MO-injected specimens yielded no band with 9i2-9e3 and a strong band of 225 bp with 9e2-9e3, corresponding to the joined exons. In *dnah9*-MO-injected embryos, bands representing unspliced RNAs were observed with both 9e2-9e3 and 9i2-9e3, while the spliced band observed with 9e2-9e3 was much reduced compared to co-MO-injected samples (cf. EF1 alpha loading control). No products were amplified without prior RT reaction (-RT).
(B) Inhibition of intron 2 splicing by *dnah5*-SB-MO. RT-PCR analysis of MO-injected embryos. Splicing was analyzed using forward primer 5e2 and reverse primer 5i2, schematically indicated by green (exons) and orange (intron) bars, and by blue arrows (primers). PCR of genomic DNA resulted in 600bp (5e2-5i2) band. RT-PCR of co-MO in MO-injected specimens yielded no band with 5e2-5i2. In *dnah5*-SB-MO-injected embryos, a band representing unspliced RNA was observed with 5i2-5e3 (cf. EF1 alpha loading control). No products were amplified without prior RT reaction (-RT).

A control morpholino (co-MO) or *dnah9*-SB-MO was injected at the 4-cell stage into the animal region of all 4 blastomeres, embryos were grown to neurula stages (st.18) and total RNA was prepared. RT-PCR revealed that in co-MO injected embryos only spliced RNA species were found, corresponding to excision of intron 2, while in *dnah9*-SB-MO injected specimens this band was markedly reduced and unspliced bands were found (Fig. 10A). Thus, *dnah9*-SB-MO efficiently reduced the amount of spliced *dnah9* mRNA in the embryo. Similarly, RT-PCR with a reverse primer located inside intron 2 only resulted in a band with the cDNA of *dnah5*-MO but not of co-MO injected embryos (Fig. 10B). Consequently, both MOs specifically inhibited translation and could thus be used for knockdown of the respective gene.

1.3.2 Maternal knockdown of *dnah9* resulted in massive gastrulation defects

In a first loss of function approach, the *dnah9*-AUG-MO was used, and the phenotype of a knockdown of most transcripts (maternally deposited and zygotic) was analyzed. Embryos were injected in both dorsal blastomeres, as these are fated to become dorsal embryonic structures like GRP. Very surprisingly, embryos injected with 4pmol of MO in total, developed massive gastrulation defects (Fig. 11). When co-MO-injected embryos correctly reached stage 16/17, MO-injected specimens displayed posterior malformations represented by blastopore closure defects (Fig. 11B). In other cases, embryos showed even more severe phenotypes, represented by a total block of gastrulation (Fig. 11C). These embryos appeared as early

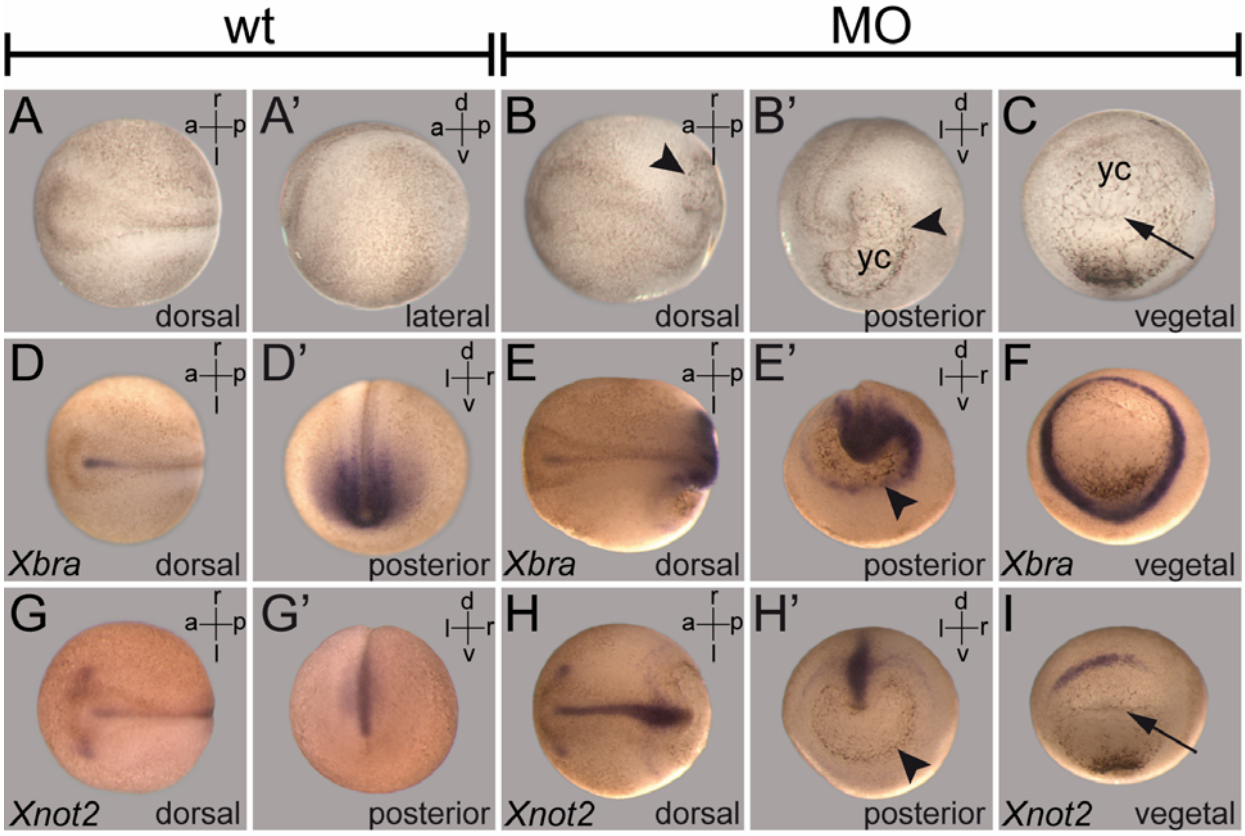

Fig. 11 Knockdown of maternal and zygotic *dnah9* result in massive gastrulation defects
Dorsal-marginal injections of 4pmol of a translation-blocking *dnah9*-AUG-MO at 4cell stage **(B, E, H)** caused massive gastrulation defects resulting in blastopore closure defects (arrowhead; B, B', E, E', H, H') or stop of gastrulation **(C, F, I)** whereas uninjected control embryos **(A, D, G)** appeared normal at stage 16. Subsequent WMISH with a *Xbra*- (D-F) or *Xnot2*-specific (G-I) probe either showed normal expression in the anterior part of the embryos and failure of blastopore closure (E, E', H, H') or expression normally exhibited at early gastrula stages (F and I). All embryos were fixed when controls reached stage 16. Please note unusual cleft in the center of the yolk of some embryos (arrow in C and I). Please also note normal anterior development in several embryos (E and H). a, anterior; d, dorsal; l, left; p, posterior; r, right; v, ventral; yc, yolk cells

gastrula stage when controls have reached st. 16 and some showed an unusual cleft in the center of the yolk (Fig. 11C and I). Although such embryos had pigmentation

reminiscent of a lip, it was not clear whether there was a dorso-ventral axis. To be able to better understand the described phenotype a WMISH with the two genes *brachyury* (*Xbra*) and *notochord homeobox 2* (*Xnot2*) was performed. *Xbra* is active in the presumptive mesoderm around the blastopore during gastrulation and in the posterior mesoderm and notochord during neurulation (Fig. 11D, D'; Smith et al., 1991). The expression of *Xnot2* is restricted to the dorsal lip mesoderm during gastrula and in the notochord during neurula stages (Fig. 11G, G'; Gont et al., 1993). Expression of both genes seemed to be normal anteriorly in those embryos having blastopore closure defects only posteriorly (Fig. 11E, H). In the posterior part of these embryos the cells (especially on the ventral side) did not fully involute as indicated by remaining *Xbra* expression (Fig. 11E', H'). In those embryos with severe phenotypes involution of the mesoderm did not occur as exemplified by the expression pattern of both genes (Fig. 11F, I).
As such morphological results had made a cilia-correlated analysis impossible the amount of morpholino had to be reduced.

1.3.3 Dose-dependent knockdown of *dnah9* resulted in cystic tadpoles and laterality defects

In a second approach with reduced MO concentrations (2-1pmol/embryo), embryos were to be grown until tadpole stages to evaluate LR defects. When the doses were reduced to 2 or 1pmol, embryos gastrulated and survived until tadpole stages 4 days later but displayed axial defects as represented by shortened AP axes and massive head defects, especially when injected with 2pmol (Fig. 12B-D). Embryos injected with 1pmol often showed nearly normal AP development but carried a ventrally bent tail (Fig. 12B). Additionally, 100% of those embryos injected with 2 and about 75% of those specimens injected with either 1 or 0.5 pmol became cystic, i.e. they started to develop fluid-filled edema in most body cavities, like the abdomen, pericardium, pronephros, and eyes, beginning at about stage 40 (Fig. 12B-E). Nevertheless, some of the embryos injected with the lower doses could be analyzed for their inner organ arrangement. Consequently, experiments were carried out in which laterality was assessed after injection of either *dnah9*-AUG-MO or *dnah9*-SB-MO. For the latter MO higher doses could be used (2 or 6pmol) as these morphants did not show a gastrulation or AP phenotype, although they did also develop cysts (data not shown).

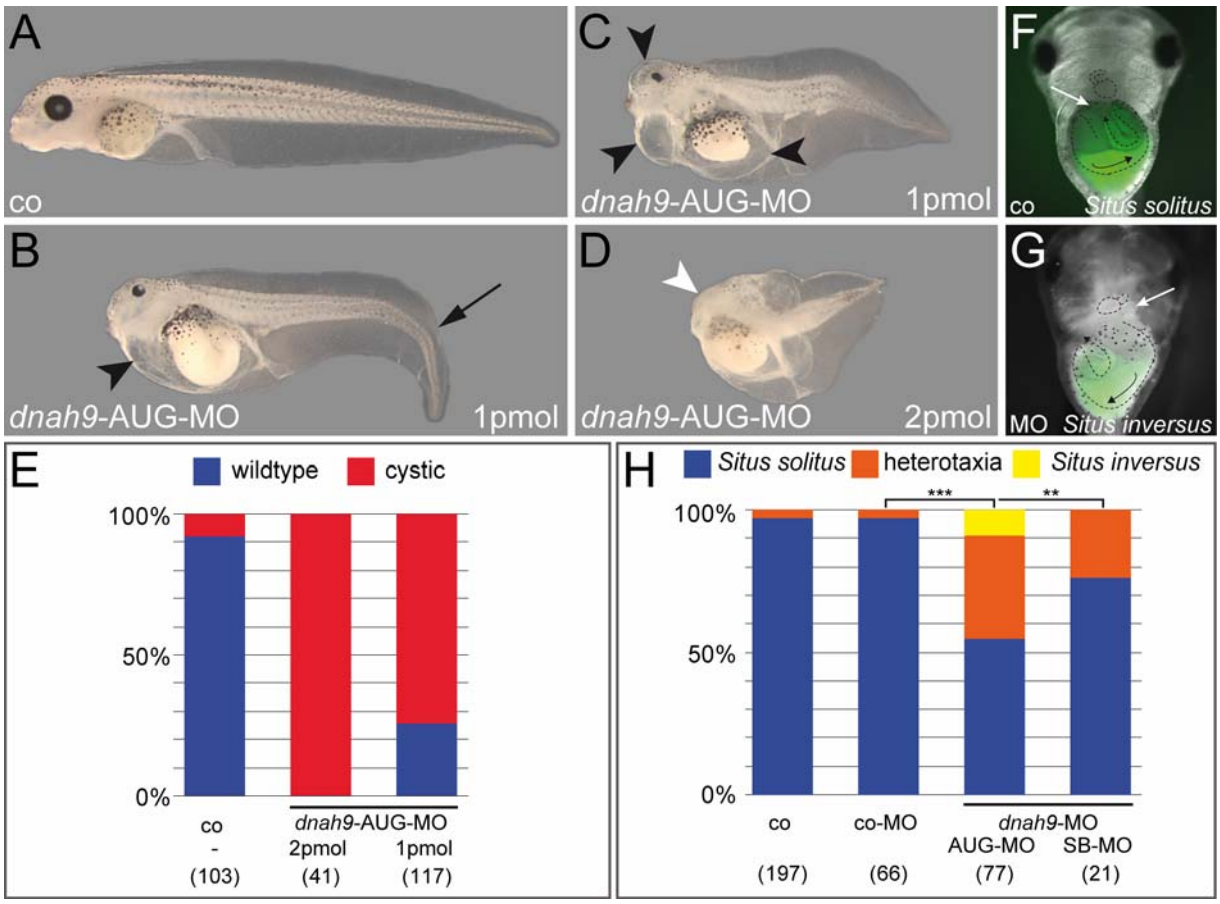

Fig. 12 Dose-dependent knockdown of *dnah9* results in cystic tadpoles and laterality defects
(A-E) Dorsal-marginal injections of 1pmol (B, C) or 2pmol (D) of a translation-blocking *dnah9*-AUG-MO caused massive cyst formation in multiple body cavities (black arrowheads in B and C), ventral bending of the tail (arrow in B), and general axial defects, while most control embryos showed normal development (A). Quantification showed that 100% of 2pmol injected and ~75% of 0.5 or 1pmol injected embryos showed a cystic phenotype, while less than 10% of controls showed malformations (E). Please note loss of head structures in some embryos injected with 2 pmol (white arrowhead in D).
(F-H) Remaining non-malformed embryos either injected with 1pmol of the *dnah9*-AUG-MO or 2-6 pmol of the *dnah9*-SB-MO (H) showed a high rate of s*itus inversus* (G) or heterotaxia (not shown), whereas uninjected controls or co-MO injected embryos displayed s*itus solitus* in over 95% (H). Position of the heart, *truncus arteriosus*, and direction of the gut coiling are outlined; position of the gall bladder is indicated with by white arrow (F, G).

For LR organ analysis of the tadpoles the incidence of normal arrangement, namely the *truncus arteriosus* pointing to the left, the gall bladder positioned on the right and the gut coiling clockwise (Fig. 12F; *situs solitus*) was compared to that of a complete mirror-image (Fig. 12G; *situs inversus*) or random arrangement (heterotaxia, not shown). While over 95% of control and co-MO injected specimens exhibited *situs solitus*, about 45% of *dnah9*-AUG-MO and ~25% of *dnah9*-SB-MO injected specimens displayed laterality defects (Fig. 12H). This was the first proof of conservation for dynein-function in correlation with laterality development in an amphibian species.

1.4 Impaired motility of epidermal cilia in *dnah9* morphant tadpoles

Having shown that the morpholinos efficiently knock down their targets and produce a specific phenotype, the next set of experiments was aimed to figure out if there was indeed a conserved function for ciliary motility of the frog *dnah9* gene.
The expression of *dnah9* in ciliated cells of the 2-day tadpole epidermis already indicated a function in epidermal ciliary motility and, consequently, tadpole motion. Because of its easier accessibility on the outside of the embryo and the large number of cilia, this tissue was chosen. Tadpoles become motile due to beating of epidermal cilia bundles at about stage 25, resulting in slow hovering movements of specimens when placed and observed on agarose dishes. In order to prove that *dnah9* was required for cilia-based tadpole motility, *dnah9*-MO was injected unilaterally into the right or left ventral blastomeres of the 4-8 cell embryo (1-2pmol/embryo). More specifically, MOs were targeted to the epidermis by injection into the marginal region of animal and vegetal blastomeres (Fig. 13A). Correct targeting was monitored by coinjection of DsRed or mRFP as a lineage tracer (Fig. 13A). Tadpoles were unaffected in their motion pattern when placed on their uninjected side, while being placed on the *dnah9*-MO injected sides specimens moved considerably slower (not shown; cf. Schweickert et al., 2007). To quantify the results, injected tadpoles were cultured to stage 32 and placed individually into six 5cm Petri dishes that were monitored simultaneously (for 10min), and the distance covered was calculated using a custom-made video-tracking software (Fig. 13B). No differences were recorded when uninjected tadpoles were placed on either side and analyzed for cilia-based motion (left: 7.17 mm/min ± 0.99; right: 6.65 mm/min ± 0.75; Fig. 13C). The analysis of *dnah9*-MO injected embryos, however, revealed drastic differences: displacement on the uninjected control side was 6.15 mm/min ± 0.89, while tadpoles were very highly significantly ($p<0.001$; $n=19$) slower on their knockdown side with an average of 2.47 mm/min ± 0.24 (Fig. 13C; see also M+M and Vick et al., 2009).

Either the *dnah9*-MO-mediated reduced tadpole motility could be due to a ciliation defect, or alternatively to impaired ciliary motility. Ciliation was analyzed by immunohistochemistry using the antibody against acetylated α-tubulin (Fig. 13D, E; green) and by scanning electron microscopy (SEM; Fig. 13F, G). Numbers of both ciliated cells and cilia per ciliated cell as well as cilia length appeared

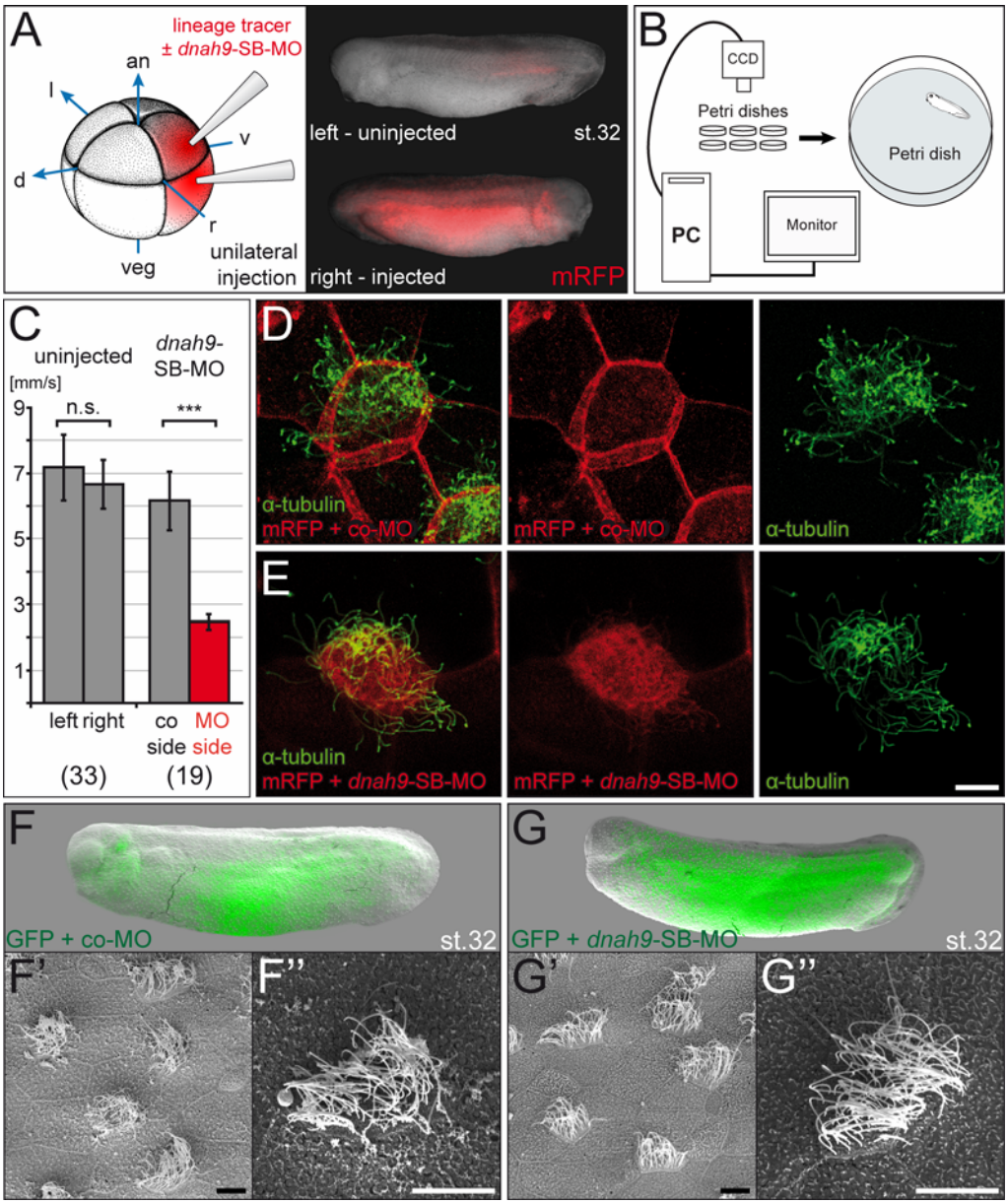

Fig. 13 Epidermis-specific knockdown of *dnah9* inhibits ciliary motility
(A) Ventral injection of lineage tracer mRFP into the marginal regions of vegetal and animal right blastomeres resulted in specific labeling of right but not left epidermis at stage 32. **(B)** Tadpole motion assay. Stage 32 tadpoles were placed individually into six Petri dishes and monitored by standard (CCD) digital camera at 25 fps. Movements were recorded via connected computers (PC) and calculated using a custom-made software. **(C)** Unilateral *dnah9*-MO injection resulted in a very highly significant decrease of tadpole velocity on the injected side. (D-G) Ciliation of epidermal cells was unaffected in *dnah9*-MO-injected tadpoles. **(D, E)** Immunohistochemistry of stage 32 tadpoles using an antibody against acetylated tubulin (green) and red fluorescence from co-injected lineage tracer mRFP (red). Overlays reveal equal ciliation in specimens injected with control MO (D) and in *dnah9* morphants (E). **(F, G)** Scanning electron micrographs of control MO (F) and *dnah9*-SB-MO injected tadpoles. Targeted regions of skin are highlighted in (F) and (G) by overlay with injected lineage tracer images (GFP) prior to SEM. Higher power magnifications of targeted regions in (F', F'', G', G'') demonstrate equal ciliation in control-injected and morphant embryos. an, animal; d, dorsal; l, left; r, right; v, ventral; veg, vegetal. Scale bars represent 10 µm. Quantitative analysis (B, C) performed by Stine Mencl (Mencl, 2008); SEM analysis (F, G) performed by Tina Beyer, University of Hohenheim (see Vick et al., 2009).

indistinguishable between co-MO (Fig. 13D, F) and *dnah9*-SB-MO (Fig. 13E, G) injected specimens, demonstrating that ciliation was unaffected in *dnah9*-morphants. Cilia movement was directly assessed by fluorescent video microscopy of MO injected embryos. This analysis showed that ciliary beating was unaffected in co-MO injected specimens. In contrast, *dnah9*-SB-MO-targeted cells displayed vibrating or frozen cilia, but never the normal fast beating pattern of wildtype or co-MO injected cells (not shown; cf. Vick et al., 2009).
These experiments showed that dnah9 is a necessary component of epidermal cilia to promote cilia beating and, consequently, muscle-independent tadpole motility (hovering).

1.5 Knockdown of *dnah9* or *dnah5* in the GRP caused laterality defects

Next, the GRP was targeted to assess *dnah5*/*9* function in LR axis formation. As the rates of lethality and even more that of cyst formation in the surviving embryos were very high after knockdown of *dnah9*, it was decided to use the left marker gene *Pitx2c* as readout for correct left-right development. As cyst formation and organ malformations mostly started at about stage 40, a much higher number of evaluable embryos was expected with this approach.

1.5.1 GRP-specific knockdown of *dnah9* and *5* caused loss of left marker genes

The ciliary role of *dnah9* for LR axis specification was assessed by MO-mediated gene knockdown specifically in the GRP. *dnah9*-SB-MO was injected into the marginal region of the dorsal left and right blastomeres at the 4-8 cell stage (Fig. 14A). Co-injected lineage tracer rhodamine-B-dextran revealed that the dorsal midline (GRP, notochord, floor plate) was efficiently targeted by this scheme (Fig. 14B, B'; cf. Blum et al., 2009)). co-MO and *dnah9*-SB-MO injected specimens were incubated until stage 31, and analyzed for expression of *Pitx2c* by WMISH. Control-injected tadpoles revealed normal left-asymmetric expression of *Pitx2c* in >95% of cases (Fig. 14C, E). In contrast, no *Pitx2c* signals were found in the left LPM of about 75% of *dnah9* morphant embryos injected with 8pmol/embryo (Fig. 14D, E). Statistically these differences in *Pitx2c* expression were very highly significant ($p<0.001$). When the MO dose was lowered to 4 and 2pmol/embryo, about 55% and

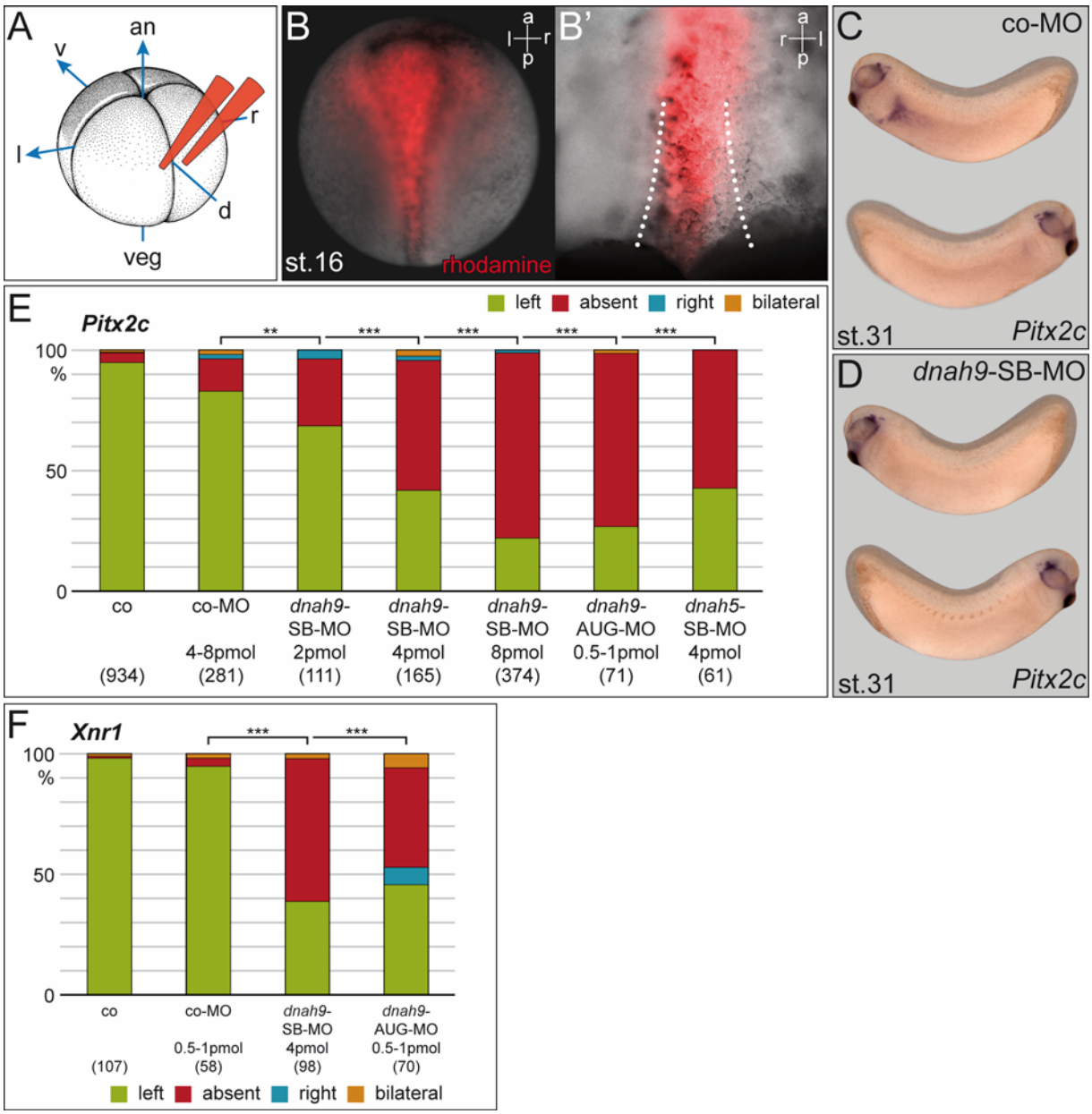

Fig. 14 GRP-specific knockdowns of *dnah9* and *5* cause loss of left marker genes
(A) Injection into the marginal region of left and right dorsal blastomeres specifically targets the floor plate (**B**; external view) and GRP (B'; ventral view of dorsal explant). **(C-F)** Laterality defects in morphants. Wildtype left-asymmetric expression of *Pitx2c* in co-MO-injected specimen (C) and absence of lateral plate expression in *dnah9*-MO-injected tadpole (D). (E) Quantification of *Pitx2c* results. Note that bilateral and right-asymmetric expression patterns were very rarely encountered, while absence of nodal cascade induction was found in up to 75% of cases. (F) *Xnr1* was not induced in the LPM in about 60% (*dnah9*-SB-MO) and 40% (*dnah9*-AUG-MO) of morphants. Please note that all three MOs resulted in similar effects as well as dose-dependency of *dnah9*-SB-MO. an, animal; d, dorsal; l, left; r, right; v, ventral; veg, vegetal. Parts of the injection experiments in (E) have been performed by Melanie Eberhardt (Eberhardt, 2008).

30% of embryos failed to induce *Pitx2c* transcription in the left LPM (Fig. 14E; $p<0.001$ and $p=0.0016$, respectively). Normal left-sided, right-asymmetric and bilateral expression patterns represented very small proportions of knockdown embryos with all three concentrations tested in these experiments (Fig. 14E). The observed dose-dependency underscore the specificity of the *dnah9*-SB-MO-effects.

To exclude *Pitx2c*-specific effects, *Xnr1* expression was analyzed as well and confirmed the results obtained for *Pitx2c* (Fig. 14F; p<0.001).

In order to investigate the specificity of the splice site MO, the *dnah9*-AUG-MO was targeted to the GRP as well. As high concentrations resulted in gastrulation and axis defects (Figs. 11 and 12), concentrations of injected *dnah9*-AUG-MO were carefully titrated; with the doses used (0.5-1pmol/embryo) early development was unaffected by *dnah9*-AUG-MO. Knockdown resulted in alterations of asymmetric *Pitx2c* and *Xnr1* expression at frequencies comparable to the splice site blocking MO (Fig. 14E, F; p<0.001). *dnah5* morphants were analyzed for LR defects as well, because of GRP co-expression with *dnah9* and absence of a maternal component (cf. Fig. 09D, G). Injection of the *dnah5*-SB-MO into the GRP resulted in about 55% of embryos without asymmetric *Pitx2c* mRNA expression (p<0.001; Fig. 14E).
Taken together, inhibition of either dnah5 or dnah9 functions specifically in the GRP resulted in a high number of laterality defects and thus confirmed functional conservation for LR axis development in amphibians.

1.5.2 *Dynein heavy chain* knockdown inhibited leftward flow

In *iv*-mouse mutants as well as in *dnah9* morphant zebrafish embryos immotile cilia cause an absence of leftward flow at the PNC and KV, respectively (Essner et al., 2005; Okada et al., 1999). Therefore flow was analyzed after *dnah9* and *dnah5* knockdown in the GRP of *Xenopus* tadpoles. Flow was investigated by adding fluorescent beads to the extracellular medium of dorsal explants of stage 17/18 embryos basically as described (Schweickert et al., 2007). In short, time-lapse videos of co-, *dnah9*- and *dnah5*-SB-MO injected specimens were processed to yield gradient time trails (GTTs), i.e. color-coded tracks of beads which reveal direction of transport and velocity of particles (from green to red; 25 sec). Undirected particle movement was eliminated from the analysis to filter out particles moved by Brownian motion (cf. Materials and Methods).

co-MO injected embryos revealed robust leftward flow at stage 17/18 (Fig. 15A; cf. Vick et al., 2009). Directionality of particle movement was quantified by calculating the percentages of GTTs projecting into one of 8 segments comprising 45° each (Fig.

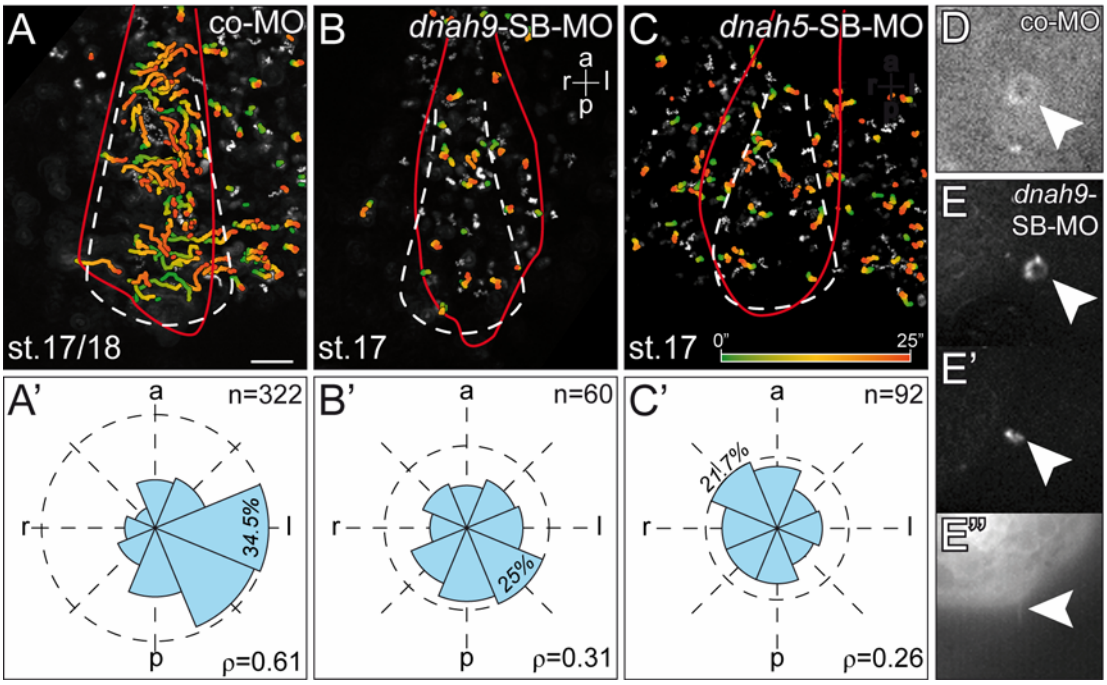

Fig. 15 Dynein heavy chain knockdown inhibited leftward flow and ciliary motion
Flow was analyzed by addition of fluorescent microbeads to dorsal explants and video microscopy. Representative examples of stage 17/18 dorsal explants of co-MO **(A)**, *dnah9*-SB-MO **(B)** and *dnah5*-SB-MO **(C)** injected embryos. Targeted areas indicated by red lines represent the limits of lineage tracer. Particle movements displayed as gradient time trails (GTTs), representing 25 sec from green to red (cf. bar in C). (A'-C') Quantitative analysis of GTT directionality over the area of the GRP demonstrating strong leftward flow in co-MO and absence of directed bead transport in *dnah9*-SB- and *dnah5*-SB-MO injected specimen. **(D, E)** Collapsed movies of *in vivo* imaged cilia movements by fluorescence microscopy using a PACRG::eGFP fusion construct. co-MO injection resulted in wildtype rotational pattern (D), whereas *dnah9*-SB-MO-injected GRPs displayed variant phenotypes, namely irregular circular movements (E), wiggling (E') or arrested motion (E''). Scale bar represents 50 µm. a, anterior; l, left; p, posterior; r, right. Analyses of flow and ciliary beating after dynein morpholino injections were conducted in collaboration with Thomas Weber (University of Hohenheim).

15A', B', C'). As a qualitative measure of flow, the mean resultant length of particle trails (Rayleigh's test of uniformity) was calculated and is indicated as a dimension-less number rho. A rho-value of 1 thus designates a situation in which all GTTs project uniformly into the same direction, whereas zero represents randomness of particle movements (GTTs projecting equally into all possible directions), i.e. no flow. The rho-value amounted to 0.61 in the co-MO injected explant (Fig. 15A'). Leftward flow was severely affected in *dnah9*- and *dnah5*-SB-MO injected embryos. The representative cases displayed in Fig. 15B', C'; for example; revealed rho-values of 0.31 and 0.26, i.e. no flow. Taken together, these data show that laterality defects in *dnah9* and *dnah5* morphants were caused by absence of leftward flow.

In order to analyze whether altered ciliary motility was the cause of absent flow, GRP cilia were imaged in co-MO and *dnah9*-SB-MO injected dorsal explants using a PACRG::eGFP fusion protein (Thomas Weber and Martin Blum, University of Hohenheim; unpublished). The parkin co-regulated gene *PACRG* encodes a protein

which – among other expression sites – is found on axonemes of ciliated cells (Dawe et al., 2005; Ikeda et al., 2007). GRP cilia beating was indeed disturbed in morphants. Cilia displayed rotational beating in wildtype (not shown) and co-MO injected explants (Fig. 15D). Cilia appeared normal in length but wildtype beating was not detected on cells targeted by *dnah9*-SB-MO. A range of ciliary movement defects were observed, namely cilia displaying uncoordinated rotations (Fig. 15E), wiggling cilia (Fig. 15E') or cilia frozen in their motility (Fig. 15E''; cf. Vick et al., 2009).
In summary, the analysis of laterality phenotypes in *dnah9* and *dnah5* morphants revealed that dnah9 and dnah5 were required for ciliary motility and that in morphants of both genes cilia beating and flow were severely impaired.

1.6 Flow is required at the left but not right side of the GRP

The efficient disruption of flow upon *dnah9*- and *dnah5*-SB-MO injection afforded the opportunity of testing whether flow was required throughout the GRP. *dnah9*- or *dnah5*-SB-MO were injected unilaterally into the dorsal margin of the left or right blastomere of 4-8 cell embryos, along with GFP or rhodamine-B dextran as lineage tracers (Fig. 16A, B). Flow was indistinguishable in untargeted and co-MO targeted halves (Fig. 16 C-E; cf. Vick et al., 2009). However, particle transport was selectively inhibited in *dnah9*- and *dnah5*-SB-MO injected GRP halves, while the respective uninjected sides displayed wildtype flow. GTTs projected normally in regions not hit by the *dnah9*- or *dnah5*-SB-MO, while in the targeted area GTTs did not progress (Fig. 16D, E). Quantitative analysis of flow revealed wildtype rho-values (>0.6) for co-MO and untargeted GRP areas, while *dnah9*-SB-MO resulted in absence of flow (rho-values of 0.26-0.49; Fig. 16C'-E'').
To assess the consequences of unilateral flow ablation, embryos were cultured to stage 33 and processed for *Pitx2c* mRNA expression. Surprisingly, ablation of flow on the right side of the GRP did not significantly alter marker gene expression (Fig. 16F). In >90% of injected embryos in which *dnah9*-SB-MO was targeted to the right side, *Pitx2c* was expressed in the left LPM as in co-MO injected and uninjected embryos (Fig. 16F). When the left side of the GRP was targeted by *dnah9*- or *dnah5*-SB-MOs, however, *Pitx2c* was not expressed in the left LPM in very highly significant percentages of cases compared to right-sided injections ($p<0.001$ throughout; Fig. 16F).

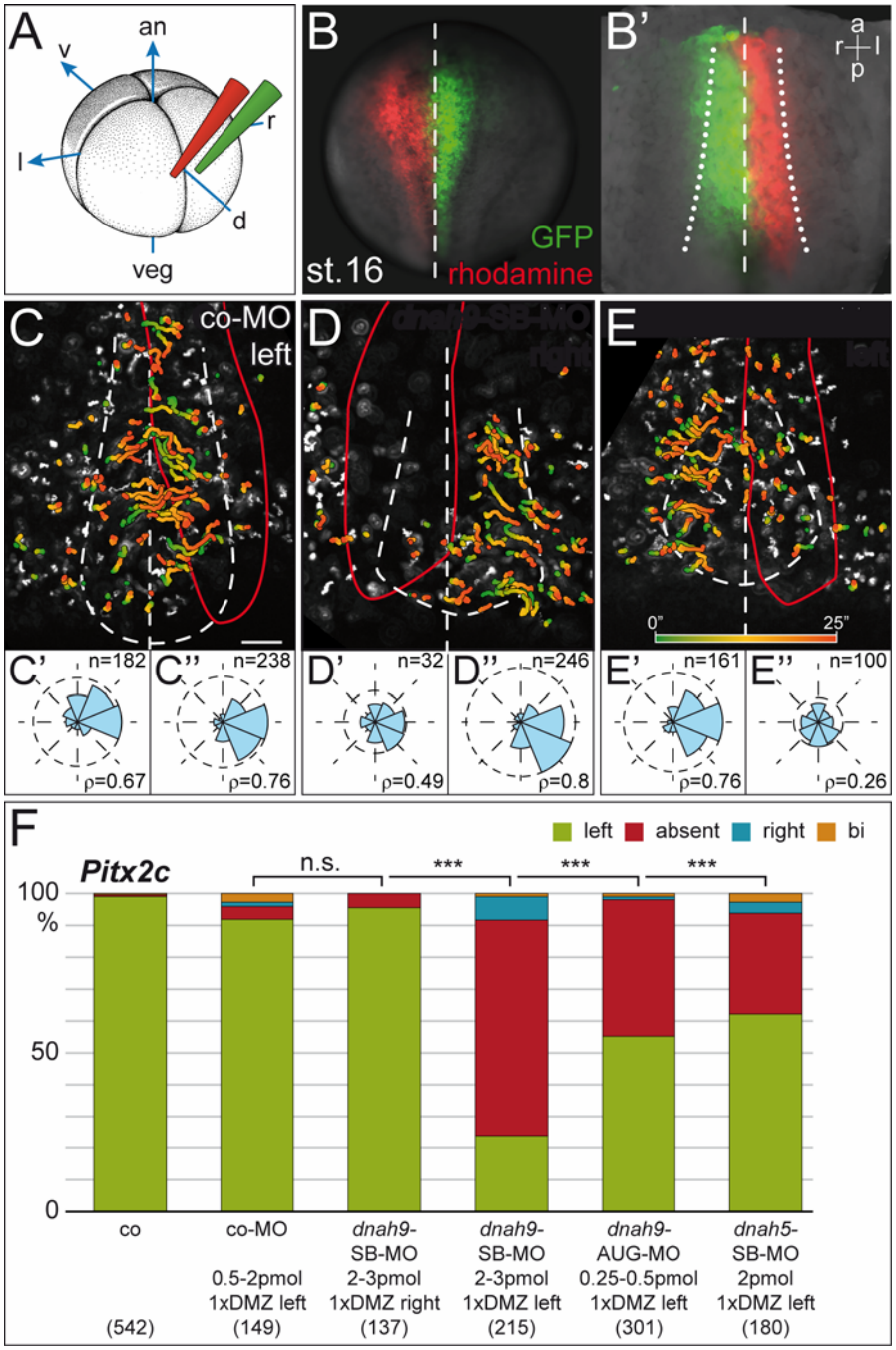

Fig. 16 Flow is dispensable on the right side of the GRP. **(A, B)** Injection scheme to specifically target left and right half of floor plate (B, external view) and GRP (B', ventral view of dorsal explant).

(C-E) Flow analysis of co-MO left (C), and *dnah9*-SB-MO right (D) and left (E) injected dorsal explants (ventral views, anterior up). Targeted areas indicated by red lines represent the limits of lineage tracer. Particle movements displayed as gradient time trails (GTTs), representing 25 sec from green to red (cf. bar in E). Note that flow was absent on *dnah9*-SB-targeted sides. (C'-E'') Quantitative analysis of GTT directionality over the respective left and right sides of the GRP.

(F) *Pitx2c* expression analysis. Wildtype left-asymmetric expression in co-MO and right *dnah9*-SB-MO injected tadpoles, and absence of signals in left *dnah9*-SB-MO, *dnah9*-AUG-MO and *dnah5*- SB-MO injected embryos.

a, anterior; an, animal; d, dorsal; DMZ, dorsal marginal zone; l, left; p, posterior; r, right; v, ventral; veg, vegetal. Scale bar in C represents 50 µm and applies to panels C-E.

The GRP-specificity of MO-targeting was further studied by injecting unilaterally into the dorsal-marginal (DMZ), dorso-lateral (D-LMZ) or ventral-marginal (VMZ) regions of the 4-cell embryo (Fig. 17A-C). Significant effects on *Pitx2c* gene expression were only observed when the GRP was hit upon dorsal marginal (75% of cases) and dorso-lateral (45% of cases) injections but not when injected into the left or right ventral blastomere (Fig. 17D). These very highly significant differences upon injection of the same dorsal blastomere suggest limited diffusion of MOs (Fig. 17A, B, D).

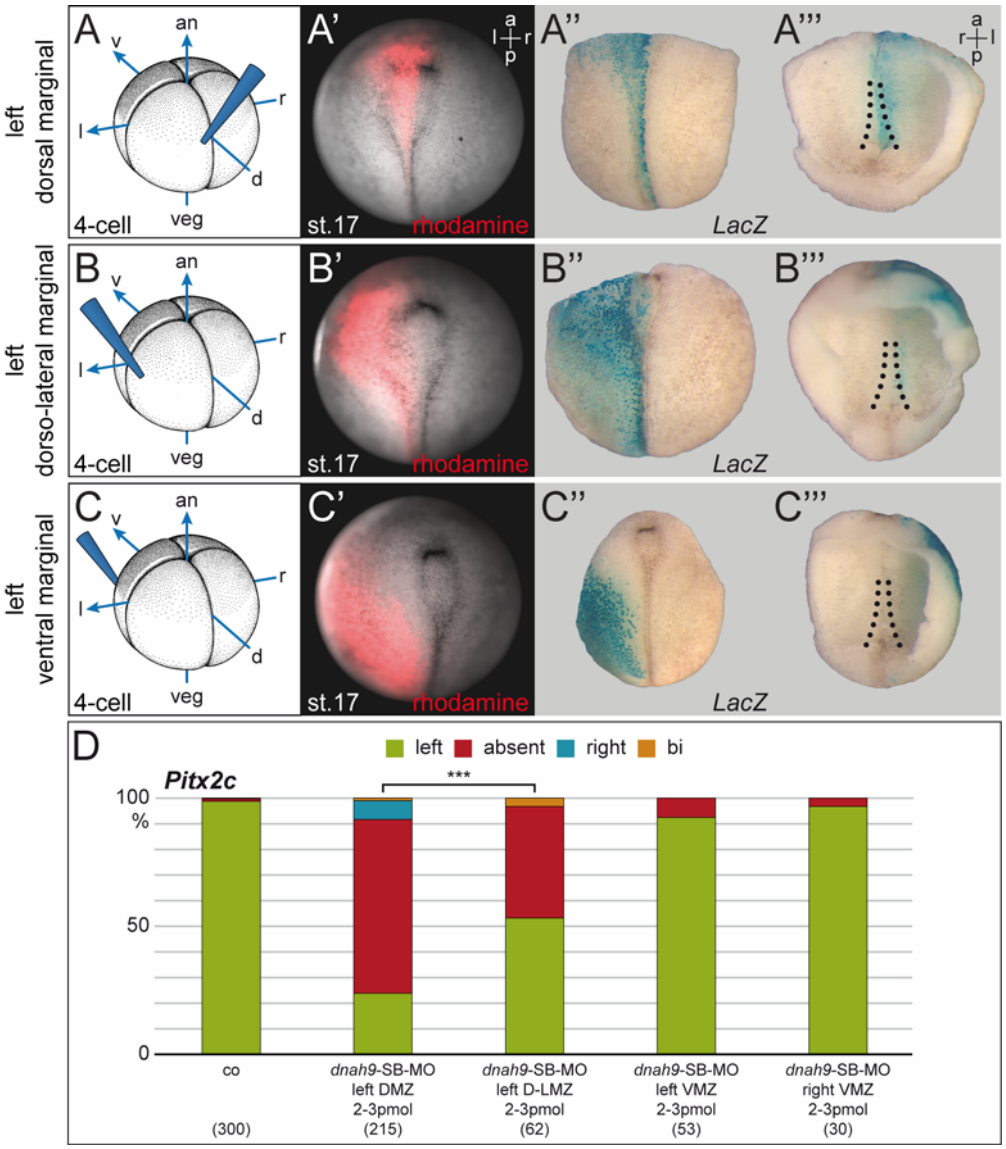

Fig. 17 Lineage-specific knockdown of *dnah9*.
Dorsal-marginal zone injections (DMZ; **A**) predominantly targeted GRP and floor plate (A'-A''') and resulted in >75% of altered *Pitx2c* gene expression **(D)**. Dorso-lateral marginal zone injections (D-LMZ; **B**) targeted lateral tissue (neural plate and somites) in addition to GRP and floor plate, which were hit less frequently (B'-B'''). Efficiency of laterality defects consequently dropped to about 45% (D). Ventral marginal injections (VMZ; **C**) resulted in lateral plate and skin targeting (C'-C''') and did not affect *Pitx2c* gene expression on either side (D). Please note that although identical blastomeres were injected in (A) and (B) effects varied very highly significantly ($p < 0.001$), suggesting limited diffusion.

In summary, these experiments show that flow was only required in the left half of the GRP for symmetry breakage to occur in a biased manner (Vick et al., 2009).

On a more general note, the experiments with the three *dynein heavy chain* genes of *Xenopus laevis* confirmed the conserved function of three motor proteins for ciliary motility, leftward flow and establishment of the LR axis. With the gained possibilities to manipulate leftward flow in *Xenopus*, flow as the symmetry breaking event should then further be explored. Therefore different components were chosen to be tested for their possible role in this process.

2. Receptor 3 type serotonin signaling and the LR axis

As a first candidate serotonin signaling was chosen for investigation, mainly for two reasons. On the one hand serotonin had already been implicated in *Xenopus* LR development earlier (Fukumoto et al., 2005). A pharmacological inhibition screen had shown that type 3 and 4 receptor mediated serotonin signaling was necessary for correct establishment of laterality. On the other hand it had been demonstrated in different tissues of several metazoan species that serotonin signaling might alter ciliary beat frequency (Christopher et al., 1999; Doran et al., 2004; Konig et al., 2009; Nguyen et al., 2001; Sanderson et al., 1985; Wada et al., 1997).
With the recently added insight that there also was a leftward flow in frog, these two parts could be logically connected. It was expected that inhibiting serotonin signaling would have an effect on ciliary beat frequency and thus on leftward flow. This would clearly explain why the inhibitor experiments had resulted in LR defects.
To address this issue from different angles, a joint project was started by our group in the Institute of Zoology. Within the frame of this subject, analysis was concentrated on receptor 3 mediated signaling. Database search for receptor 3 yielded two different ESTs, both containing cDNA sequences coding for a putative receptor 3 subunit homolog of human *Htr3a*; both were cloned and for distinction named XHtr3a and XHtr3c (short *3a* and *3c*) hereafter (Axel Schweickert, University of Hohenheim; unpublished). For both forms AUG-morpholinos were designed to perform knockdown experiments.
As a first approach (as done for *dnah9*; Fig. 13), expression analysis of *XHtr3c* had shown that this receptor was expressed in the ciliated cells of the epidermis; and concomitantly with this, morpholino-mediated knockdown specifically caused inhibition of cilia-based motion and cilia movement (Axel Schweickert, University of Hohenheim; Mencl, 2008).

2.1 GRP-specific loss of serotonin signaling resulted in LR defects

As it had been convincingly proven that XHtr3-mediated serotonin signaling modulated ciliary motility on the skin, it was to be tested if the knockdown of this receptor-subtype also led to impaired ciliary motility and thus leftward flow on the

GRP. After WMISH had not shown a positive signal for either *XHtr3a* or *3c* on the GRP, RT-PCR had been used and mRNA had been found in flow-stage neurula embryos and more importantly, also specifically in GRP-derived cDNA (Philipp Andre, University of Hohenheim, unpublished).

With this outcome, knockdown experiments were initiated for both subtypes. Injections were aimed directly to the GRP and experimental setup was as shown for *dnah*-MOs (Fig. 14). When 2-4pmol of *XHtr3a*-MO was injected into the DMZ of 4-8 cell embryos, two day later WMISH carried out for *Pitx2c* showed that, in contrast to controls and co-MO injected specimens, these embryos displayed LR defects in over 20%, which was highly significant (Fig. 18A; compared to co-MO with <5%; p=0.0031).

As there was no antibody available to prove efficient knockdown of the protein, specificity was aimed to be demonstrated by injecting two different MOs to knock down *XHtr3c* (*Htr3c1+2*-MO). The two MOs were designed to bind the same mRNA, one in the 5'UTR adjacent to the start codon and the other in the coding region and thus not overlapping with the first one (not shown). Low amounts (0.75-1pmol) of *Htr3c1*-MO caused only about 15% of altered *Pitx2c* expression (Fig. 18A; p=0.2059) which was not significant, whereas higher doses (2-3pmol) resulted in over 40%, which was very highly significant (Fig. 18A; p<0.001). These results could be confirmed with WMISH for the second left-sided gene *Xnr1* (not shown). Injecting the *XHtr3c2*-MO (short *3c2*-MO) concomitantly resulted in nearly 40% of absent *Pitx2c* expression (Fig. 18A; p<0.001). These experiments convincingly showed that GRP-specific loss of function of a *Xenopus* Htr3 receptor caused laterality defects.

Thus the cell should target the truncated receptor to the membrane but not to integrate it or to form the channel. Instead it was thought to be secreted because most of the lipophilic parts of the protein would not be present as analyzed by hydrophobicity analysis (not shown; see Bruss et al., 2000). As it possessed the binding domain it would be able to sequester serotonin in the extracellular space. Injection of 60ng/µl of this mRNA or the respective truncated version of subunit *3a* (*trHtr3a*) into the dorsal but not ventral marginal zone again caused about 40% of misexpressed left marker gene which was again very highly statistically significant (Fig. 18B; p<0.001).

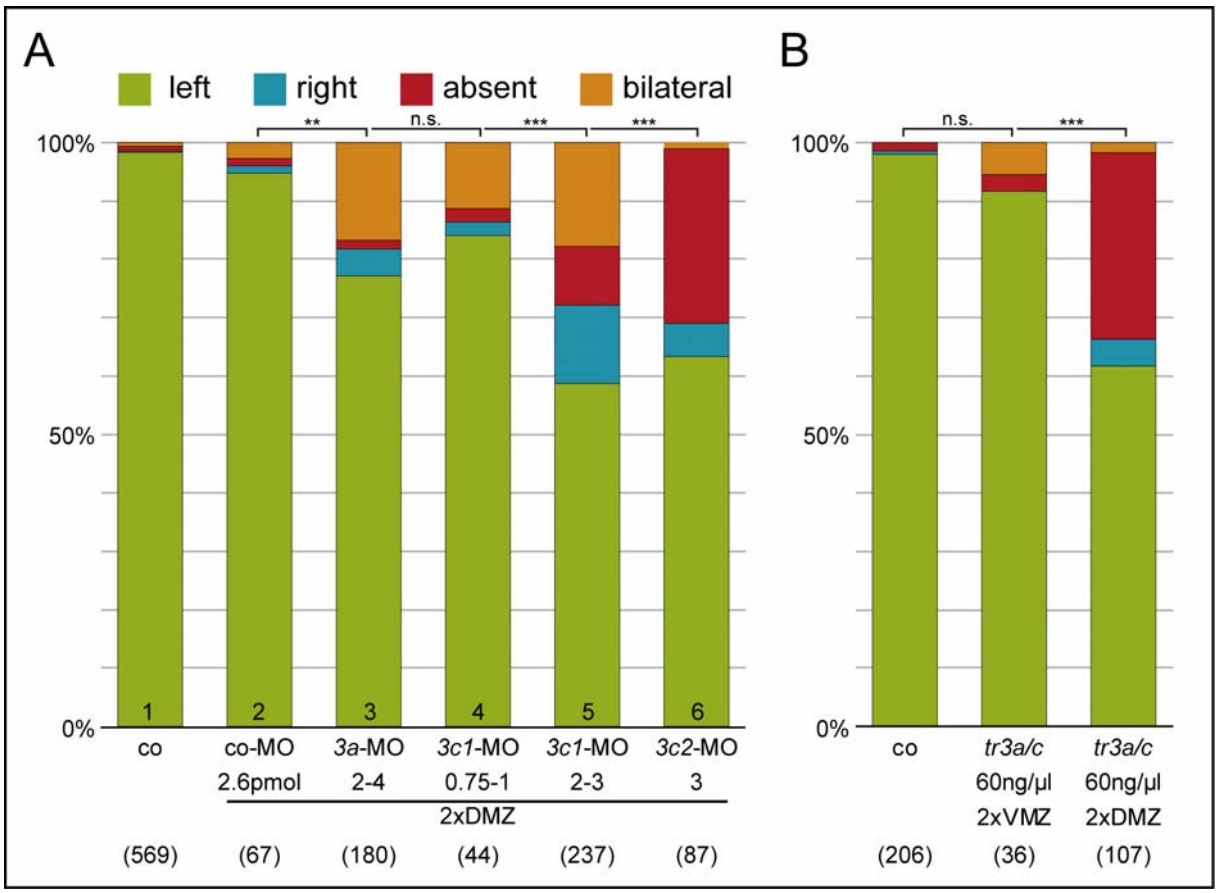

Fig. 18 GRP-specific loss of serotonin signaling results in LR defects
(A) Knockdown of two different subunits of a type 3 serotonin receptor caused left-right defects as detected by *Pitx2c* misexpression. While wildtype and co-MO injected specimens showed over 95% normal left-sided expressions, specimens injected with either a *3a*-specific or two *3c*-specific morpholinos displayed failure of correct *Pitx2c* activation in >20% (bar no. 3) or about 40% (bar no. 5 and 6), respectively. **(B)** Injection of 60ng/µl of mRNA of truncated version (*tr3a/c*) of either of these subunits which again yielded about 40% of LR defects when injected dorsally but not ventrally. Injections were performed as depicted in Fig. 17. DMZ, dorsal marginal zone; VMZ, ventral marginal zone

In summary, these knockdown experiments showed that the frog serotonin receptor 3 was needed for correct LR axis development at the GRP. Concomitantly with this results, analyses of leftward flows of *XHtr3c*-MO or *trHtr3* injected embryos revealed that these were severely impaired (Thomas Weber; unpublished). In more detail, most of the embryos showed no or only weak leftward flow. The outcome of the serotonin experiments thus clearly confirmed the insights obtained by the *dnah9* knockdown and its importance for LR asymmetry.

2.2 Knockdown of *XHtr3c* impairs GRP but not midline development

To be sure that the observed effects were due to impaired ciliary motility of the GRP cilia and not due to structural defects, the GRPs of such injected embryos were analyzed by scanning electron microscopy in parallel (Tina Beyer, University of

Hohenheim). Very surprisingly, it turned out that structural defects of the GRP epithelium were indeed found after the loss of serotonin receptor function. Embryos injected with the truncated versions, as well as those injected with the *XHtr3c*-MOs showed strong morphological changes specifically at the GRP (T. Beyer; unpublished). Cilia were mostly absent and cells displayed a changed morphology as represented by larger, partly stretched surfaces.

This strongly indicated an unexpected new role for serotonin signaling in the morphogenesis of the GRP and not necessarily in ciliary beat modulation. Therefore injected embryos were analyzed by WMISH for GRP marker gene expression. With this approach, more light should be shed on the type and extent of effects the knockdown induced. For these experiments, embryos were injected with the *XHtr3c1*-MO either unilaterally or bilaterally, one half fixed at the required neurula stages and the other half at later tailbud stages for *Xnr1* or *Pitx2c* expression as positive control. When bilaterally injected embryos were analyzed for expression of the *Xenopus sonic hedgehog* gene (*Shh*; Ekker et al., 1995) at either stage 17 (Fig. 19A-B) or stage 20 (Fig. 19C-D), no reduction of staining could be seen (Fig. 19B, D) compared to control embryos (Fig.19A, C). Similarly, no differences were detected for *Xnot2*, which as *Shh* represents a marker for correct midline development, which is expressed in the developing notochord (not shown). This demonstrated that in contrast to the GRP, general midline development was not impaired. To further dissect the extent of the GRP malformation; the GRP marker *dnah9* was analyzed. In *XHtr3c*-MO injected, but not in control embryos expression was either fully missing (~60%) or weakened (>30%) on the injected side(s) (Fig. 19E-H). The second GRP marker to be tested was the *hairy/enhancer-of-split* related gene *hey1* which is expressed in the hypochord precursor cells anterior to the GRP (Pichon et al., 2002). Its expression marked midline-positioned superficial hypochordal cells ventral to the notochord in the anterior half of the embryo which fused just anteriorly of the GRP and thus formed a reversed “Y” (Fig. 19I). These two arms of the “Y” only rarely reached into the GRP in wt but in injected embryos they mostly stretched far posterior inside the GRP reaching the circumblastoporal collar and partially fused at the blastopore (Fig. 19J, K). Further, the two branches stayed much more separated and only fused more anteriorly. This phenotype indicated a change in GRP patterning or in differentiation behavior of the cells when leaving the epithelium.

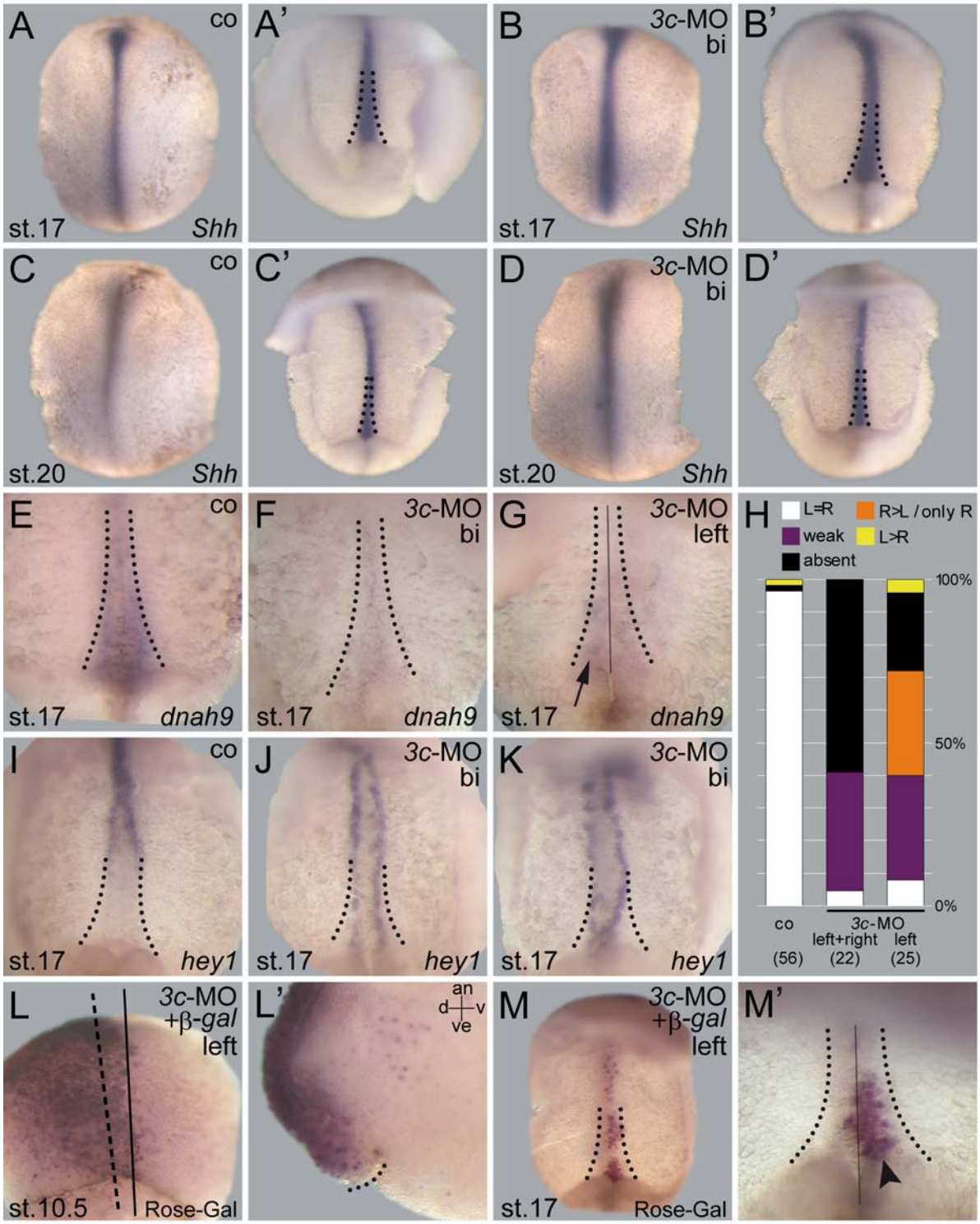

Fig. 19 Knockdown of serotonin receptor 3 impairs GRP but not midline development
(A-D) No difference of midline development as depicted by *Shh* gene expression between control (A and C) and *3c*-MO injected (B and D) specimens in both, stage 17 (A and B) and stage 20 (C and D). **(E-K)** Impaired GRP development as shown by expression of *dnah9* (E-H) and *hey1* (I-K). Bilateral or only left side *3c*-MO injected but not control embryos (normal expression in E) showed either bilateral (F) or bilateral and left-sided (G) loss of *dnah9* expression in the GRP in about 60% of cases (H). While control embryos (I) showed wt expression of *hey1*, *3c*-MO injected specimens (J and K) revealed altered expression. Please note greater distance between the two arms of the anterior expression part. **(L-M)** Coinjection of *3c*-MO and *β-gal* mRNA into the left DMZ showed correct left-sided Rose Gal staining of the SM at stage 10.5 (dorsal view in L and dorso-ventral section in L') and the GRP at stage 17 (M and higher magnification in M'). GRP outlined with dotted lines, midline indicated with solid lines and plane of section and dorsal lip in L with dashed or dotted line,

respectively. A, B, C and D are dorsal and A', B', C', D', E-G, I-K, M and M' are ventral views of dorsal explants. an, animal; bi, bilateral; d, dorsal; l, left; r, right; s, stage; v, ventral; ve, vegetal

To exclude the possibility that the cells containing the morpholino just died or did not reach their correct position in the GRP epithelium, the MO was injected unilaterally together with mRNA coding for the *lacZ* gene and embryos were fixed at stage 10.5 or stage 17 and stained with the β-galactosidase substrate Rose-Gal. At st.10.5, the injected side showed strong staining in the superficial and deeper layers of the dorsal marginal zone (Fig. 19L) and at st.17 of the corresponding side of the GRP (Fig.19M), strongly indicating that the cells stayed vital and took their position in the GRP correctly.

Finally, the bilateral *Xnr1* expression domain which borders the GRP was analyzed. As GRP morphogenesis was markedly disturbed, it was quite probable that this

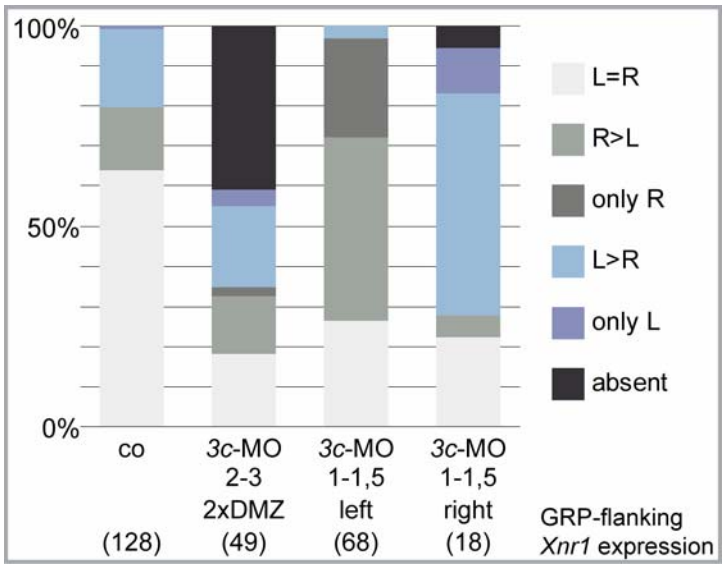

Fig. 20 Knockdown of serotonin receptor 3 inhibits the bilateral *Xnr1* domain
Control embryos showed wildtype-like expression of *Xnr1* with about 65% bilaterally equal-sized domains and about 35% with a larger left or right domain. In embryos bilaterally injected with the *3c*-MO about 40% had no expression of *Xnr1*. Embryos injected unilaterally on the left or right side showed reduction or absence of the corresponding side of the domain in about 70% of cases. DMZ, dorsal marginal zone; l, left; r, right

domain was also affected. Indeed, as compared to controls, expression was missing in about 40% of embryos injected bilaterally with the *XHtr3c*-MO (Fig. 20). Concomitantly with this, unilaterally injected specimens also showed either absent or markedly reduced activity on the injected side in about 60% of cases.

Taken together, the obtained results for serotonin signaling analysis revealed a novel, surprising role for serotonin receptor 3 mediated signaling for proper morphogenesis of the ciliated GRP-epithelium.

3. Polycystic kidney disease 2 gene in *Xenopus* development

Next, the *Pkd2* gene was investigated. Although it was known that mutations in the mouse and zebrafish gene caused LR defects, it was not clear which role a putative calcium signal exactly played (Pennekamp et al., 2002; Schottenfeld et al., 2007). As it had been proposed that PC2 generates the flow-dependent Ca^{2+}-wave on the left side and thus induces the nodal cascade in the LPM, it was planned to use the frog system and its advantage to be able to target different tissues side-specifically to be able to elaborate the role of *Pkd2* exactly. Therefore, gain and loss of function experiments and subsequent calcium measurements would be used to figure out the exact mechanism of flow perception.
The frog homolog had already been cloned in our lab and a translation-blocking AUG-MO (*Pkd2*-MO) was available (A. Schweickert, unpublished). This MO was used to work out the function of *Pkd2* in frog LR asymmetry.

3.1 Expression analysis of *Pkd2* during *Xenopus* embryogenesis

As a first step a detailed description of the mRNA expression pattern during embryogenesis of *Xenopus* was performed. *Pkd2* showed a strong maternal expression in the animal part as early as in the zygote (Fig. 21A). Interestingly, in most embryos the vegetal limit of transcript seemed to be different along the dorso-ventral axis. In the 4 cell stage no difference in staining between the single blastomeres could be detected (Fig. 21B). During gastrulation (st.10) mesodermal (and perhaps anterior endodermal) expression could be seen in the subepithelial layers of the involuting and non-involuting marginal zone (Fig. 21D). In later gastrula stages (st.11-13) expression was detected in the dorsal involuting mesoderm and in the deep mesenchymal cells of the circumblastoporal collar (Fig. 21E-F); and later during neurulation in the most posterior notochord (Fig. 21G). With the end of gastrulation an ectodermal signal could be found in the posterior neural plate, which expanded anteriorly, to be finally present in the whole neuroectoderm until early tailbud stages (Fig. 21F-I). No expression was detected in the epidermis, differentiated mesoderm or in the GRP. In later tailbud stages expression could be found in the intermediate mesoderm and later the pronephric system and ectodermal

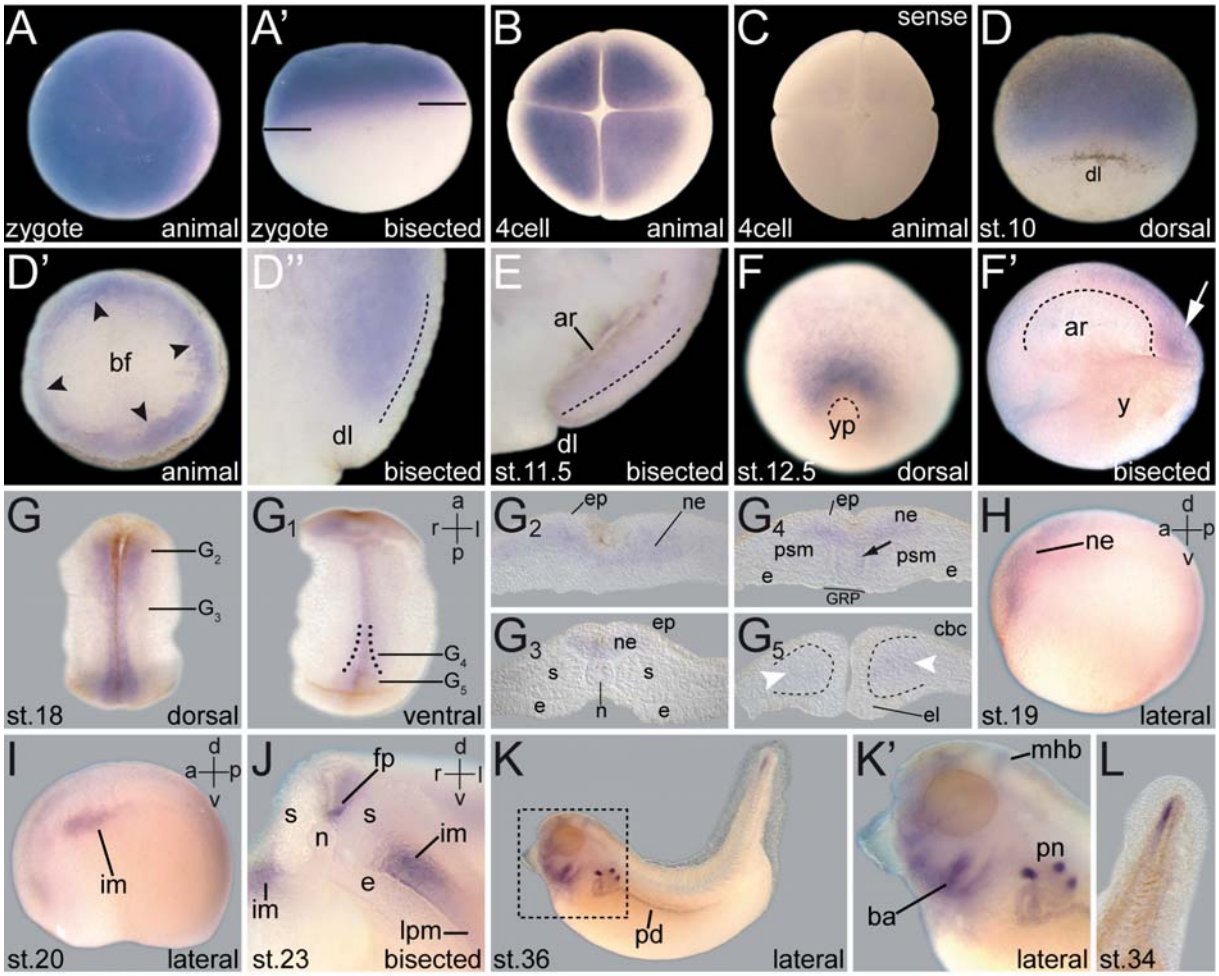

Fig. 21 Highly dynamic expression pattern of *Pkd2*
Expression analysis by whole-mount *in situ* hybridization of staged embryos with a *Pkd2*-specific antisense (A-B and D-L) or sense (C) probe. **(A-C)** Maternal transcript of *Pkd2* is highly enriched in the animal part of the zygote (A in animal view and A' animal-vegetally bisected) and the 4cell stage embryo (animal view in B) with equal distribution in the four blastomeres. No staining was obtained by a sense control (C). **(D-F)** Early zygotic expression was detected in the circumembryonic deeper marginal region of a st.10 embryo (D in dorsal, D' in animal and D'' in dorsal lip; dashed line indicates border between superficial epithelial and subepithelial deeper layers), in the involuting dorsal mesoderm in a stage 11.5 embryo (E; dashed line indicates border between superficial layer and involuting mesoderm) and in the posterior neuroectoderm (F) and circumblastoporal collar of stage 12.5 embryos (white arrow in F'; archenteron roof outlined by dashed line). **(G)** Neuroectodermal staining in dorsal explant in dorsal (G) and ventral view (G_1). Transversal sections (G_2-G_5; planes of sections indicated in G and G_1) additionally showed weak expression in the posterior part of the notochord (G_4) and the inner part of the circumblastoporal collar (cbc; G_5, white arrowheads). **(H-L)** Early (H-J; st.19, st.20, st.23) and late tailbud (K-L; st.34, st.36) analysis showed anterior neuroectodermal (H, I, K'), floorplate (J), intermediate mesodermal (I, J) pronephric (K, K'), branchial arch (K'), mid-hindbrain boundary, and tailbud (K, L) staining. Arrowheads in D' indicate equal amount of transcript dorsally, ventrally and laterally. Dashed box in K outlines area magnificated in K'. Please note unequal animal-vegetal distribution of transcript in the zygote (A'). Please note also missing expression in the superficial layer of gastrula stage embryos (D-E). D'', E and F' are embryos sagittally and J transversally bisected along the dorso-ventral axis. a, anterior; ar, archenteron; ba, branchial arch; bf, blastocoel floor; dl, dorsal lip; e, endoderm; el, epithelial layer (of the cbc); ep, epidermis; fp, floorplate; GRP gastrocoel roof plate; im, intermediate mesoderm; l, left; LPM, lateral plate mesoderm; mhb, mid-hindbrain boundary; n, notochord; ne, neuroectoderm; pd, pronephric duct; pn, pronephros; psm, presomitic mesoderm; s, somites; y, yolk; yp, yolk plug

staining was restricted posteriorly to the tailbud, anteriorly to the mid-hindbrain-boundary and diencephalon as well as to the floorplate (Fig. 21I-L).

Altogether, the expression pattern revealed to be very dynamic, being active in different germ layers and tissues during embryogenesis.

3.2 PC2 colocalized with serotonin on GRP cilia and epidermal cells

PC2 had been shown to be located on cilia of different tissue in different species (Bae et al., 2006; McGrath et al., 2003; Pazour et al., 2002; Schweickert et al., 2007). Furthermore, *serotonin receptor 3c* had been shown to be expressed in epidermal ciliated cells. Therefore, in a second approach, protein distribution was analyzed in comparison to serotonin. Firstly, to explore a possible localization of serotonin to the *Xenopus* developing skin, tadpoles of the stages 34 (Fig. 22A) and 44 (Fig. 22B) were processed for whole-mount immunohistochemistry (WMIHC) and treated with an antibody against serotonin. For both stages a spotty pattern could be detected covering most of the embryo (Fig. 22A' and B'). To test if the positive cells represented the subset of ciliated cells, a second staining with the antibody against acetylated α-tubulin was conducted and the exact localization analyzed by a confocal microscopy. The results clearly demonstrated that serotonin was not located in ciliated cells or on cilia (Fig. 22C). At higher magnification, serotonin staining was regularly distributed between the multiciliated cells and appeared to be concentrated in vesicular structures (Fig. 22C'). Interestingly, when stage 34 embryos were processed for anti-tubulin staining (Fig. 22D; red) and counter-staining was performed with an anti-Polycystin-2 antibody (Fig. 22D'; green), PC2 was again not localized to cilia (Fig. 22D''). Staining indicated a common localization for PC2 and serotonin. To address this question, a double staining with the antibodies against PC2 (Fig. 22E; red) and serotonin (Fig. 22E'; green) was performed, demonstrating that PC2 and serotonin indeed were co-localized (Fig. 22E''; red). As PC2 was not expressed on skin cilia, it was tested if it localized to GRP cilia, as staining of PNC cilia has been previously reported (McGrath et al., 2003). Indeed, staining with α-tubulin (Fig. 22F; red) and PC-2 (Fig. 22F'; green) revealed colocalization on those cilia (see also Schweickert et al., 2007). In contrast, up to know, serotonin could not been found to be located on GRP cilia (A. Schweickert, unpublished).

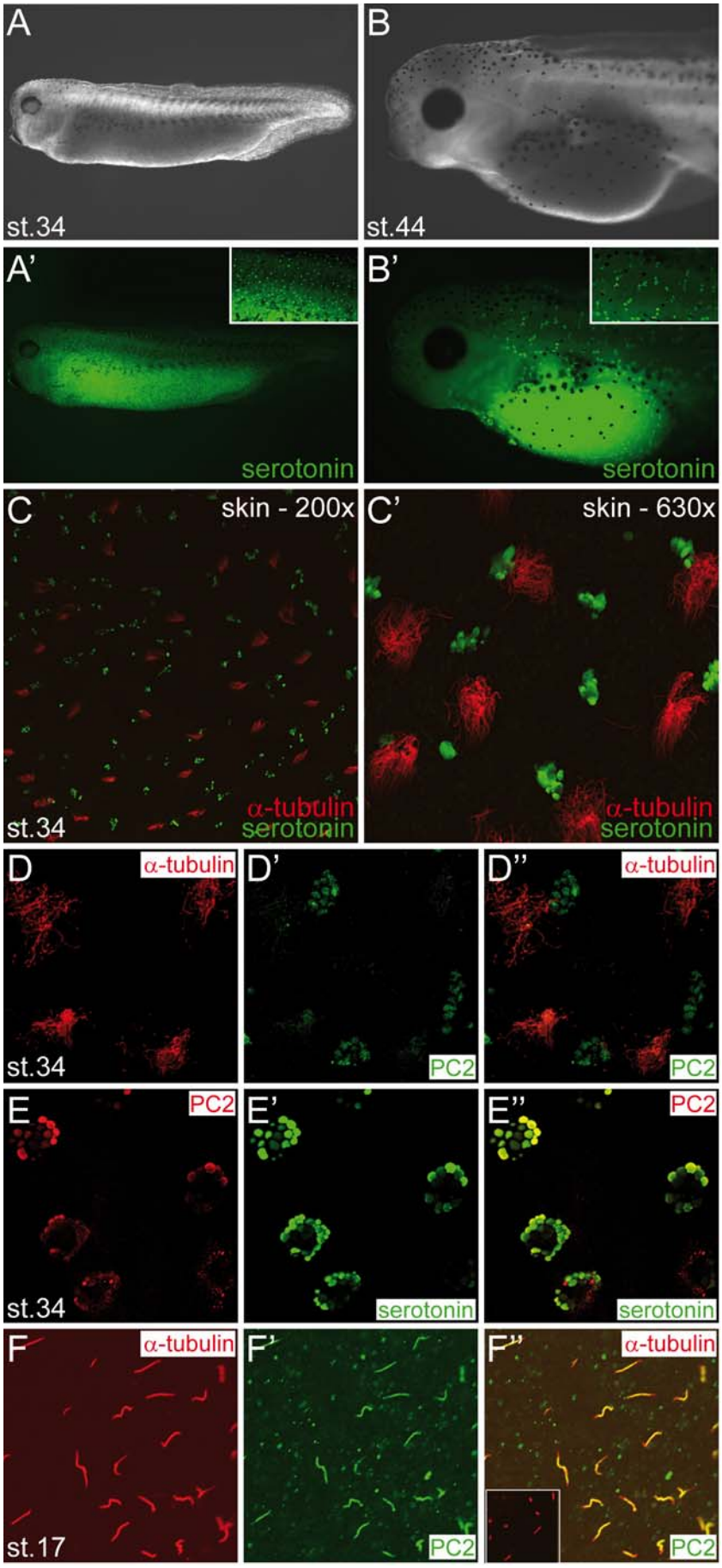

Fig. 22 PC2 colocalizes with serotonin on GRP cilia and epidermal cells
WMIHC with an anti-serotonin antibody (green) of stage 34 (**A**; in bright field) and stage 44 (**B**; in bright field) embryos. (A', B'). Higher magnification revealed a patchier pattern in st. 44 (cf. insets in A' and B'). Strong uniform signal in the ventral part reflects auto-fluorescence of the yolky endodermal cells. Higher-magnification analysis of st. 34 embryos counterstained with an anti-acetylated α-tubulin antibody (red) showed segregation of ciliated and serotonin-containing epidermal cells **(C, C')**.

(D) WMIHC of stage 34 with an anti-PC2 antibody (green; D') and counter staining with anti-acetylated α-tubulin antibody (red; D) showed non-ciliary spotty pattern on the epidermis (D'').

(E) WMIHC with an anti-PC2 antibody (red; E) and an anti-serotonin antibody (green; E') revealed colocalization in vesicular structures (E'').

(F) WMIHC of stage 17 dorsal explants with an anti-PC2 antibody (green channel; F') and with an anti-acetylated α-tubulin antibody (red; F) showed colocalization on GRP-cilia. Negative control missing the primary antibody showed no PC2 staining (inset in F''). PC2, Polycystin-2

3.3 Pkd2 loss of function caused cystic embryos and blastopore closure defects

After analysis of *Pkd2* mRNA localization, functional experiments were performed by using the *Pkd2*-MO. When a total amount of 8pmol (bilaterally) or of 4pmol (unilaterally) was injected into the dorsal marginal zone to target midline structures as the GRP, embryos developed in 97% of cases (30/31) blastopore closure defects at neurula (Fig. 23A) and tailbud stages (Fig. 23B). This phenotype made it impossible to analyze organ situs. After further decrease of the morpholino concentration,

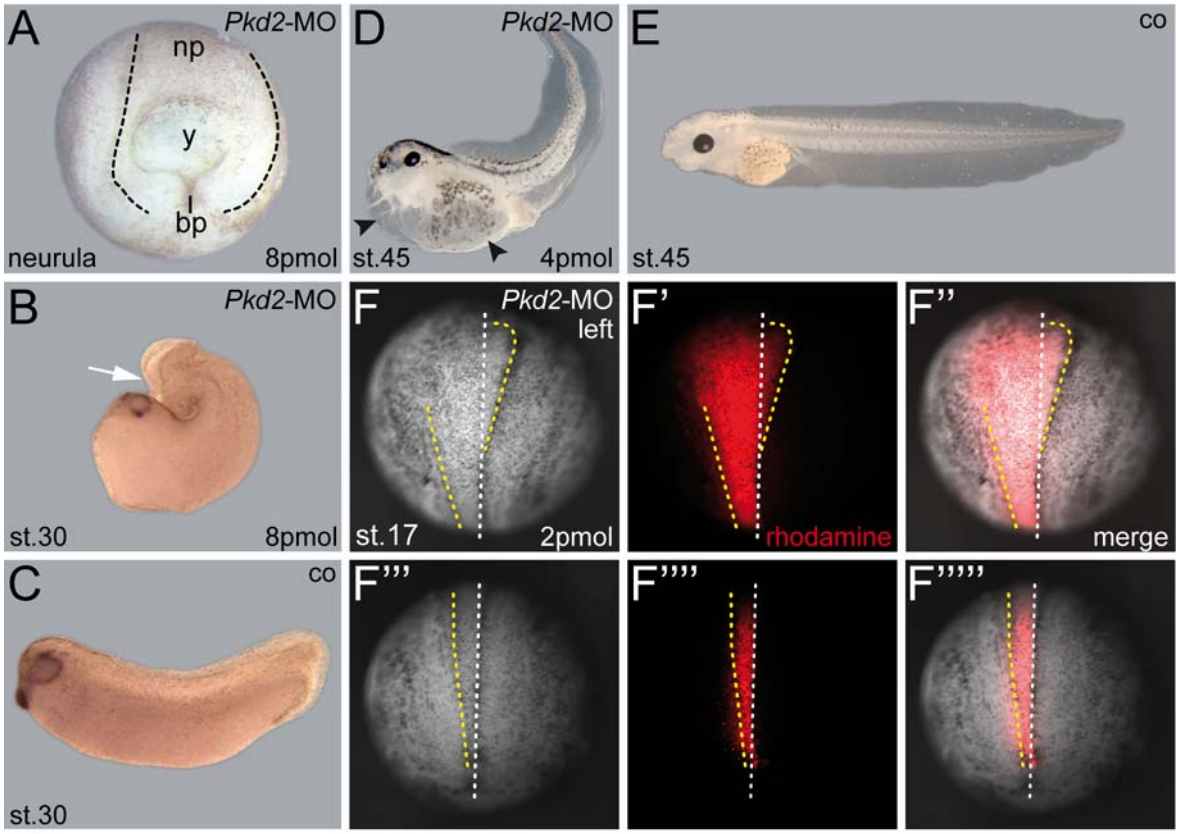

Fig. 23 Pkd2 loss of function causes cystic embryos and neural tube closure defects
(A-C) Injection of 8pmol of a *Pkd2*-specific translation-blocking AUG-morpholino caused blastopore and neural tube closure defects in neurula (A) and tailbud stages (B; white arrow), which could not be detected in control st. 30 embryos (C). **(D-E)** Reducing the morpholino amount to 4pmol caused cystic embryos with massive edema (arrowheads in D) only in *Pkd2*-MO-injected but not control embryos (E). **(F)** Unilateral left injection of 2pmol of *Pkd2*-MO revealed delay of anterior (F-F'') and posterior (F'''-F''''') neural tube closure only on the injected side as visualized via coinjection of red lineage tracer (F', F'', F''', F''''). Lineage-specific injections were performed as described in figure 14A (A-E) and 17 A (F). Neural folds are outlined by dashed line in A and by yellow dotted line in F and midline is indicated by dotted white line in F. bp, blastopore; np, neural plate; y, yolk

embryos proceeded through gastrulation but developed massive edema from about stage 40 on (Fig. 23D). The analysis of this particular phenotype was performed in

detail in the course of a collaboration (Tran et al., 2009). Additionally, during those experiments specificity of the *Pkd2*-MO had been demonstrated by Western blot analysis with a PC2-specific antibody.
When a dose of 2pmol was injected unilaterally together with a fluorescent lineage tracer, a delay in neural tube closure could be visualized (Fig. 23F). The uninjected side correctly closed neural folds as expected for stage 17, whereas the MO injected side was delayed and appeared like stage 15. This delay in closure could be traced until at least early tailbud stages when the anterior part of the neural tube stayed open representing a type of amphibian anencephaly (not shown).

3.4 Pkd2 loss of function caused LR defects and loss of leftward flow

Following the description of phenotypes and titration of the MO, analyses were focused on LR axis development. The aim of the experiment was to figure out a conservation of function for LR development between mammals and amphibians.

3.4.1 *Pkd2* was necessary for correct LR axis development

To circumvent cyst formation and the related problems with evaluation of a correct LR axis, injected embryos were fixed at late tailbud stages and processed for WMISH with a *Pitx2c* probe. After bilateral injection of a total of 2-4pmol of the *Pkd2*-MO into the DMZ a clear dose-dependent alteration of laterality was evident, with highest rates of over 65% misexpression (Fig. 24A; $p<0.001$ in all cases). This rate stayed below 10% in 1pmol *Pkd2*-MO or 2-4pmol co-MO injected specimens. It is mentionable that most embryos displayed loss of left marker activation (Fig. 24C-E) and that a range of axial impairments was observed. Although *Pitx2c* expression was consistently absent, some embryos had normal dorso-anterior index (DAI=5; Fig. 24C), some showed a slight ventralization (DAI=4-5; Fig. 24D) and some displayed antero-posterior shortenings (Fig. 24E).
As the dynein heavy chain experiments had revealed that lineage-specific unilateral injections might be very insightful, this was also carried out for *Pkd2* knockdown (Fig. 25). Again controls and co-MO injected on either side showed >90% normal LR development (Fig. 25, bar 1-3). Injections of *Pkd2*-MO between 0.25 and 2pmol into the left DMZ of 4-8 cell embryos to directly aim for the left GRP showed a dose-

dependent increase in *Pitx2c* misexpression from 10% (Fig. 25, bar 4; p=3.293) up to >75% (Fig. 25, bars 5-7; each p<0.001).

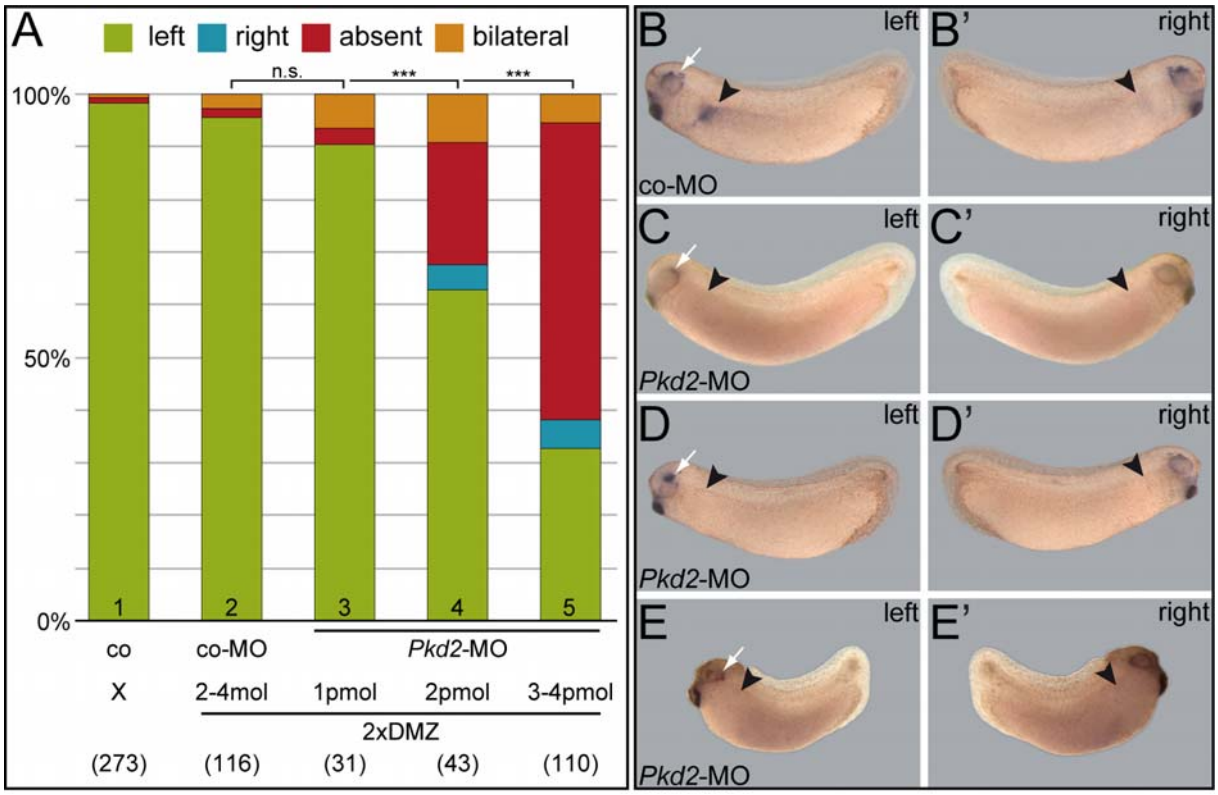

Fig. 24 Pkd2 loss of function causes LR defects
(A-E) Injection of the *Pkd2*-MO into both dorsal cells of the marginal zone of 4-8cell stage embryos (cf. Fig. 14A) caused dose-dependent perturbation of the LR axis in up to 65% as visualized by *Pitx2c* marker gene expression (A, bar 3-4). Control (A, bar 1) and co-MO (A, bar 2 and B) injected embryos exhibited normal left expression in over 95% of cases. Most of the *Pkd2*-MO injected embryos showed no expression on either side (A), but displayed different ranges of axial impairments, namely a normal axis development (C), slight ventralization (D), or shortening of the anterior-posterior axis (E). Black arrowhead indicates position of normal *Pitx2c* expressing tissue, white arrow expression of *Pitx2c* around the eye. DMZ, dorsal marginal zone

The higher, efficient concentrations were used to elucidate the regional requirements of *Pkd2* in the embryo by comparing dorsal and more ventral injections (cf. Fig. 17). The outcome of these was that the knockdown was most efficient when aimed at the most dorsal part (Fig. 25, bars 7-9). Injecting the dorsal blastomere laterally (cf. Fig. 17B), diminished efficiency to ~45% (Fig. 25, bar 8; p<0.001) and further ventral injections (cf. Fig. 17C) led to no significant effect (<5%, p=4.706; Fig. 25, bar 9).
This clearly showed that the function of *Pkd2* was required in the left epithelium of the GRP. In one last injection scheme it should be ruled out if there was also an effect when injecting into the right DMZ. Very surprisingly, this also resulted in about 35% of altered expression patterns which was highly significant (Fig. 25, bar 10; p=0.002).

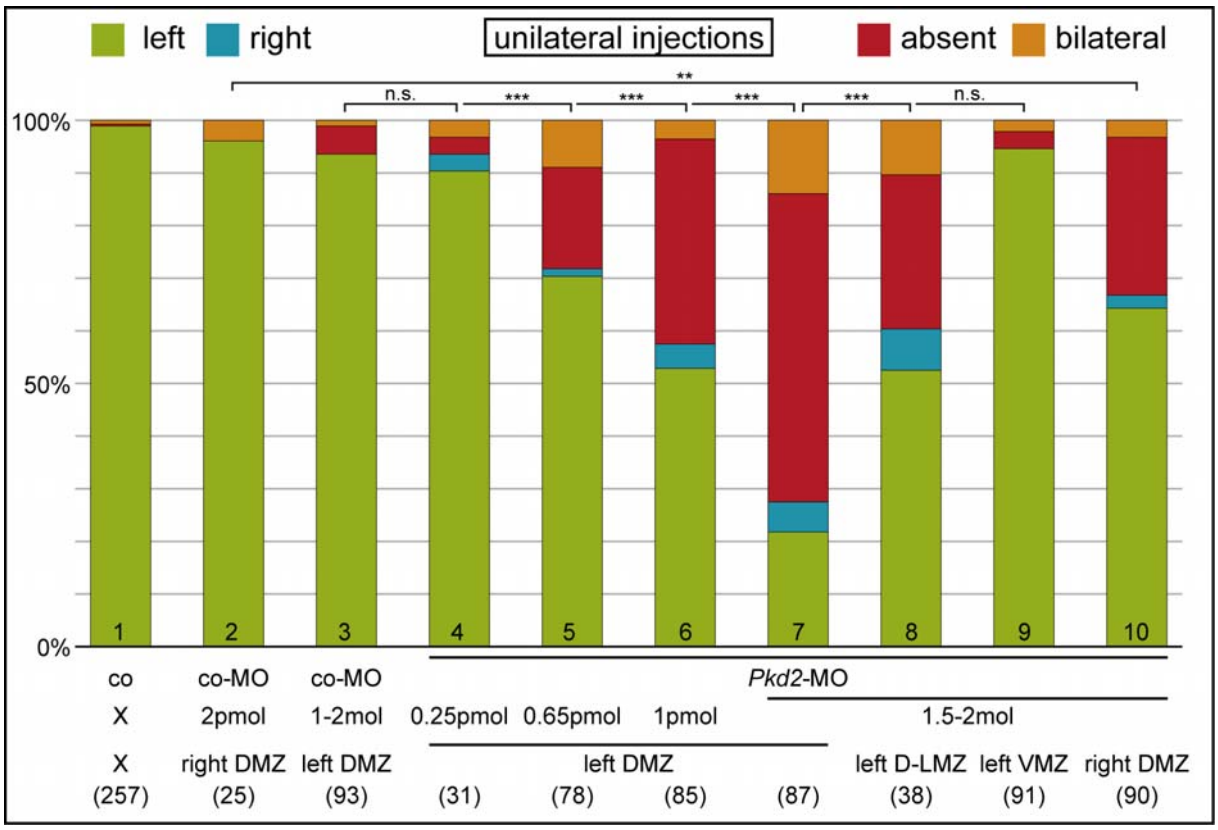

Fig. 25 Unilateral *Pkd2* knockdown
Unilateral injections as shown in Fig.17A showed increasing dose-dependency from 0.25 to 2pmol (bar 4-7) with up to 75% of misexpressed *Pitx2c*, while co (bar 1) and right (bar 2) or left side (bar 3) injections of co-MO in high concentrations showed no change of correct expression in over 90%. 1.5-2pmol injections performed as described in Fig. 17A-D for *dnah9* knockdown revealed highest efficiency of the morpholino when injected most dorsally (cf. bar 7 and 8) and no effect when injected ventrally (bar 9), but also a significant effect when injected in the right DMZ (bar 10). D-LMZ, dorso-lateral marginal zone; DMZ, dorsal marginal zone, VMZ, ventral marginal zone

In summary, these analyses confirmed the conserved role of *Pkd2* for establishment of the LR axis, but the exact function remained unknown.

3.4.2 Leftward flow was lost in *Pkd2* morphants

In the next step it was intended to test an effect of the knockdown on leftward flow. Although the knockout mouse had been analyzed for LR axis development, characterization of flow has not been reported (McGrath et al., 2003; Pennekamp et al., 2002). Therefore, unilateral and bilateral injections were performed in the same way as described in chapter 3.4.1 for highly efficient concentrations. Afterwards, leftward flow was analyzed in dorsal explants of stage 16-18 embryos as described in chapter 1.5.2. Unexpectedly, in most analyzed embryos leftward flow over the injected area was either massively inhibited or not detectable at all. To visualize the effect, unilateral injections were exemplary used.

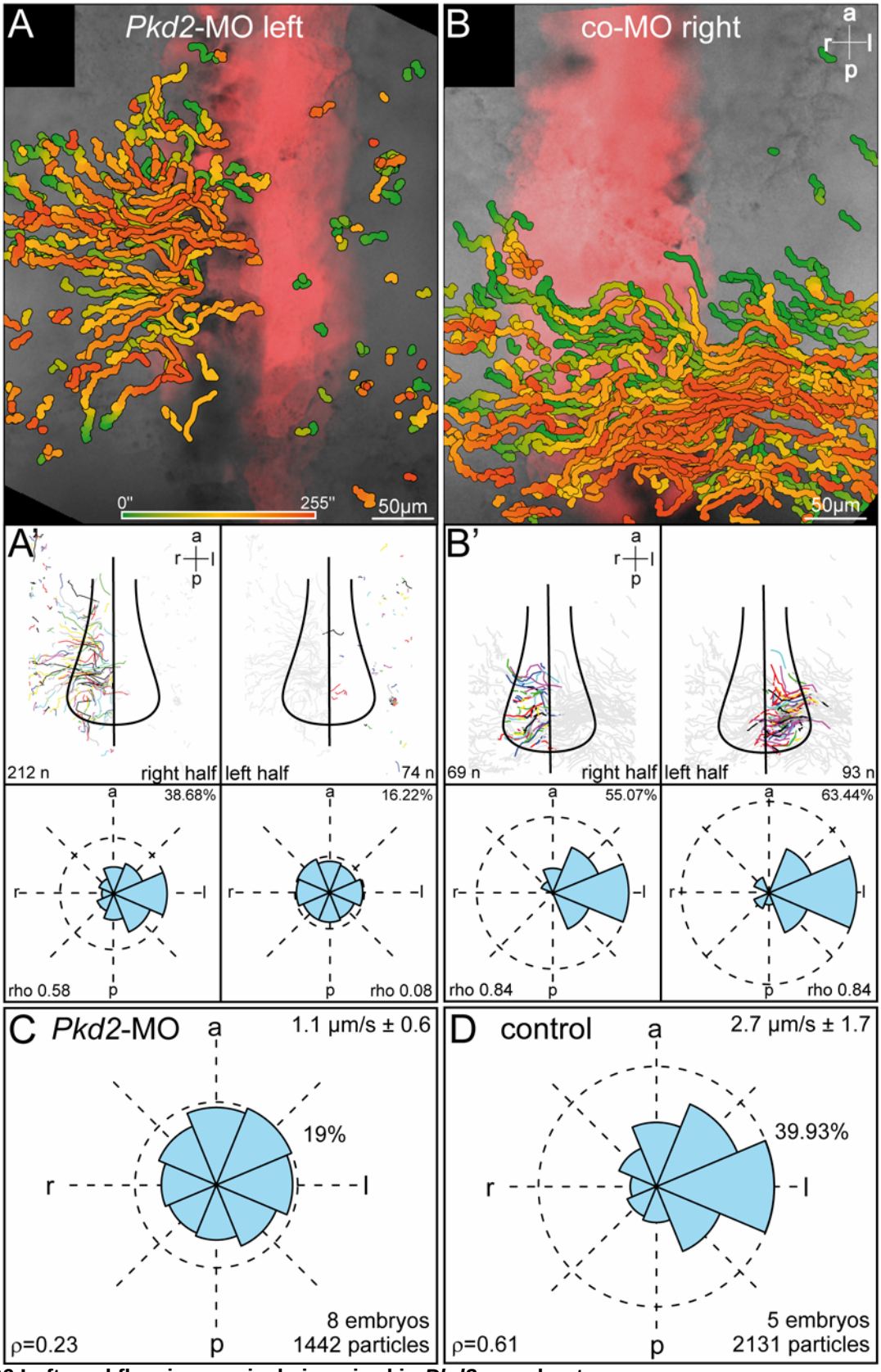

Fig. 26 Leftward flow is massively impaired in *Pkd2* morphants
Flow was analyzed by addition of fluorescent microbeads to dorsal explants and video microscopy. **(A, B)** Results of leftward fluid-flow analysis of exemplary embryos of stage 17/18 dorsal explants injected into the left DMZ either with 2pmol of *Pkd2*-MO (A) or co-MO (B). Targeted areas indicated by red fluorescence represent the limits of lineage tracer. Particle movements displayed as gradient time trails (GTTs), representing 25 sec from green to red (cf. bar in A) showed loss of flow only on the *Pkd2*-MO injected side but not on the co-MO injected or on either of the uninjected halves (A, B). (A',

B') Quantitative analysis of GTT directionality demonstrating strong leftward flow in co-MO and absence of directed bead transport in *Pkd2*-MO injected specimen as expressed by low rho number only for the *Pkd2*-MO hit side. **(C, D)** Summarized quantification of 8 embryos bilaterally injected with *Pkd2*-MO (C) and 5 embryos with co-MO (D) showed loss of flow with no directed transport and reduced particle speed in *Pkd2*-MO injected as compared to control specimens. a, anterior; l, left; p, posterior; r, right. This analysis was conducted with the kind help of Thomas Weber.

When the *Pkd2*-MO was delivered to the left side of the GRP (Fig. 26A), particles showed a robust flow over the right side but were abruptly stopped when reaching the MO-targeted area (indicated by lineage tracer DsRed) where no flow occurred at all. In contrast, a unilaterally-right injected co-MO displayed no inhibition of flow on either side (Fig. 26B).

To quantify this effect, both sides of the GRP were calculated independently for both embryos. For specimens injected with co-MO, no obvious differences could be detected in the robustness and directionality of leftward flow (Fig. 26B'), as indicated by the same rho value (0.84) for left and right sides. In contrast, the *Pkd2*-MO injected but not the uninjected internal control side showed a highly reduced rho number (Fig. 26A'; cf. 0.58 right half to 0.08 left half) and missed any directionality.

In order to quantify this phenomenon for several embryos, particles of 8 bilaterally with *Pkd2*-MO injected specimens and 4 bilaterally with co-MO injected plus one uninjected control specimen were merged to calculate a mean value for both groups. With a mean rho of 0.23 and nearly no directionality (Fig. 26C) as compared to the control group with 0.61 and a high directionality (Fig. 26D), morphant embryos were clearly strongly impaired. Additionally, the mean velocity of the particles was considerably reduced in contrast to control embryos (cf. 1.1µm/s and 2.7µm/s) which was further reflected by fewer particles left (cf. 1442 to 2131) as they were excluded by the program due to absent directionality (see methods for description; Schweickert et al., 2007).

The unexpected outcome of these studies indicated that *Pkd2* was not necessary for perception but for generation of the flow itself in *Xenopus*.

3.5 Morphogenesis and gene activity was disturbed in *Pkd2* morphants

The loss of flow in *Pkd2* morphants initiated a new perspective on how this molecule could be incorporated in the breakage of symmetry in frog. Therefore experiments

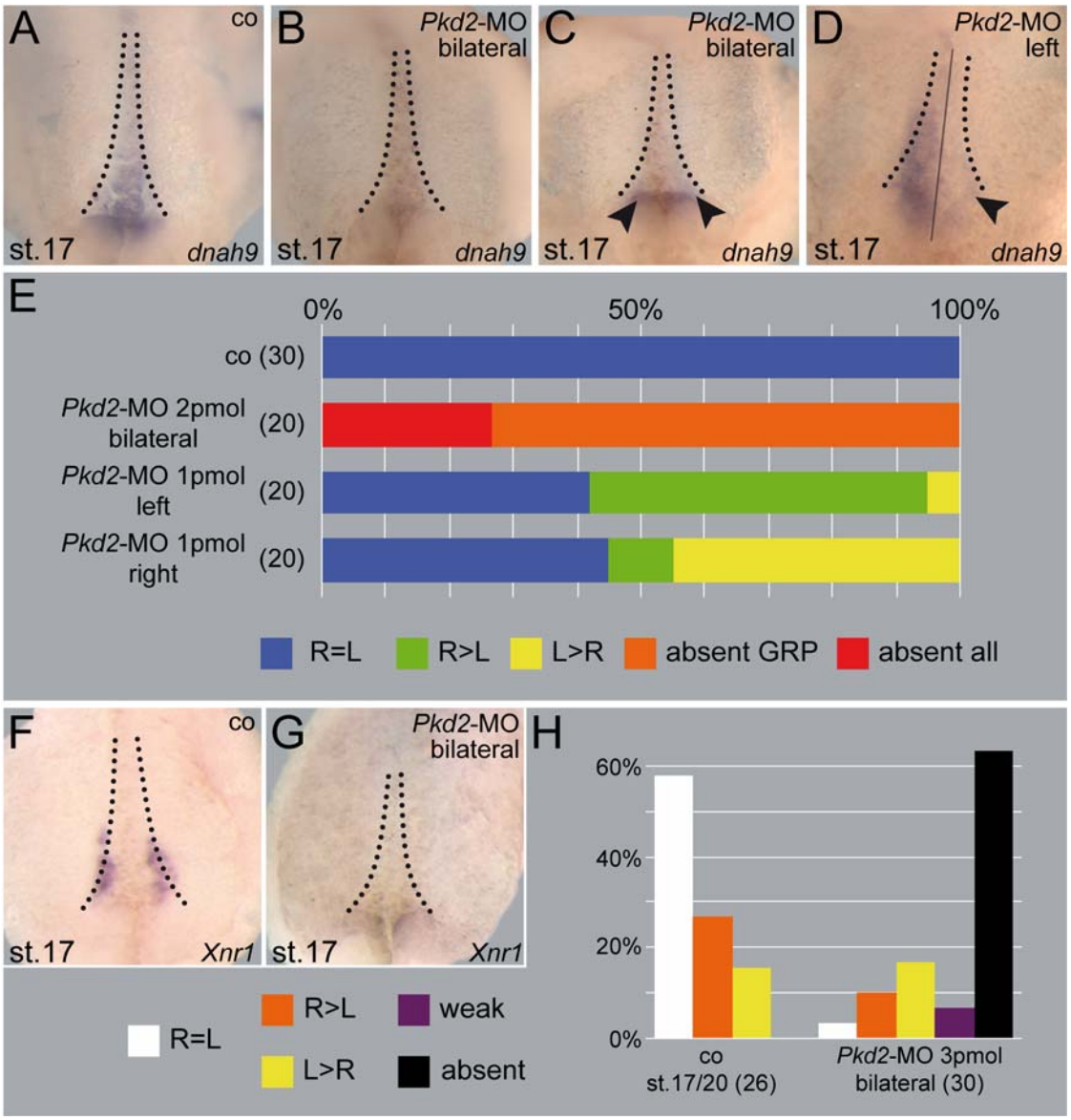

Fig. 27 Loss of *dnah9* and *Xnr1* expression in *Pkd2* morphants
(A-E) WMISH with a *dnah9*-specific antisense probe showed wildtype-like expression in the GRP and dorsal cbc of all stage 17 control embryos (A, E) but reduced expression in the GRP of about 70% (C, E) and total missing of about 30% (B, E) of the embryos bilaterally injected with 2pmol of *Pkd2*-MO. Embryos unilaterally injected with 1pmol displayed reduced expression on the respective side in about 50% of cases (D, E). **(F-H)** WMISH with a *Xnr1*-specific antisense probe showed wildtype-like bilateral expression flanking the GRP in all stage 17 or 20 control embryos (F, H) but loss of expression in over 60% of embryos injected bilaterally with *Pkd2*-MO (G, H).
GRP, gastrocoel roof plate; l, left; r, right

were initiated to reveal its function for flow. The aim was to differentiate if the observed effect on flow was due to a functional or structural interference with the cilia.

3.5.1 Loss of *dnah9* and *Xnr1* expression in *Pkd2* morphants

The first step was to investigate if genes normally expressed within the GRP were still present. Again, the *dnah9* gene was chosen for investigation as it marks ciliated cells. When specimens bilaterally injected with *Pkd2*-MO were analyzed, all of them either showed reduced staining (Fig. 27C, E) at the GRP or no staining at all (Fig. 27B, E), in contrast to 100% expression in controls (Fig. 27A, E). Moreover, unilateral injections confirmed this specific effect as ~50% did not express *dnah9* on the injected side at all (Fig. 27D, E). As another candidate, the bilateral GRP domain of *Xnr1* was tested. Embryos bilaterally injected with *Pkd2*-MO had no *Xnr1* expression in over 60% of cases (Fig. 27G, H) compared to normal wildtype expression in controls (Fig. 27F, H)
These two outcomes raised the question of either ciliary function or, more plausible, that the morphogenesis of the GRP was disturbed.

3.5.2 GRP morphogenesis was massively impaired in *Pkd2* morphants

To clarify if in *Pkd2* morphants ciliation or GRP formation was impaired, embryos were again injected with the Pkd2-MO, dorsal explants were prepared (for descriptions see Blum et al., 2009; Schweickert et al., 2007) for SEM analysis and cells were evaluated for size and ciliation. For each GRP sample a corresponding central part was chosen for higher magnification and thus evaluation of structure (examples in Fig. 28A and B). When co-MO was injected, only very few cells missed a cilium and most of the cilia were correctly positioned at the posterior pole of the cell (Fig. 28A). Strikingly, most of the cells targeted by the *Pkd2*-MO showed no sign of ciliation or posterior polarization was lost (Fig. 28B). Unilateral injections further underlined this effect: As it had been convincingly demonstrated that the left and right part of the GRP stayed clearly separated (see Fig. 16B and Blum et al., 2009), very high magnification pictures from the center of the GRP were taken. An embryo injected only on the left side with *Pkd2*-MO showed normal cells with posteriorly positioned cilia on the uninjected control side but in contrast exhibited larger cells without any cilia on the injected side (Fig. 28C).

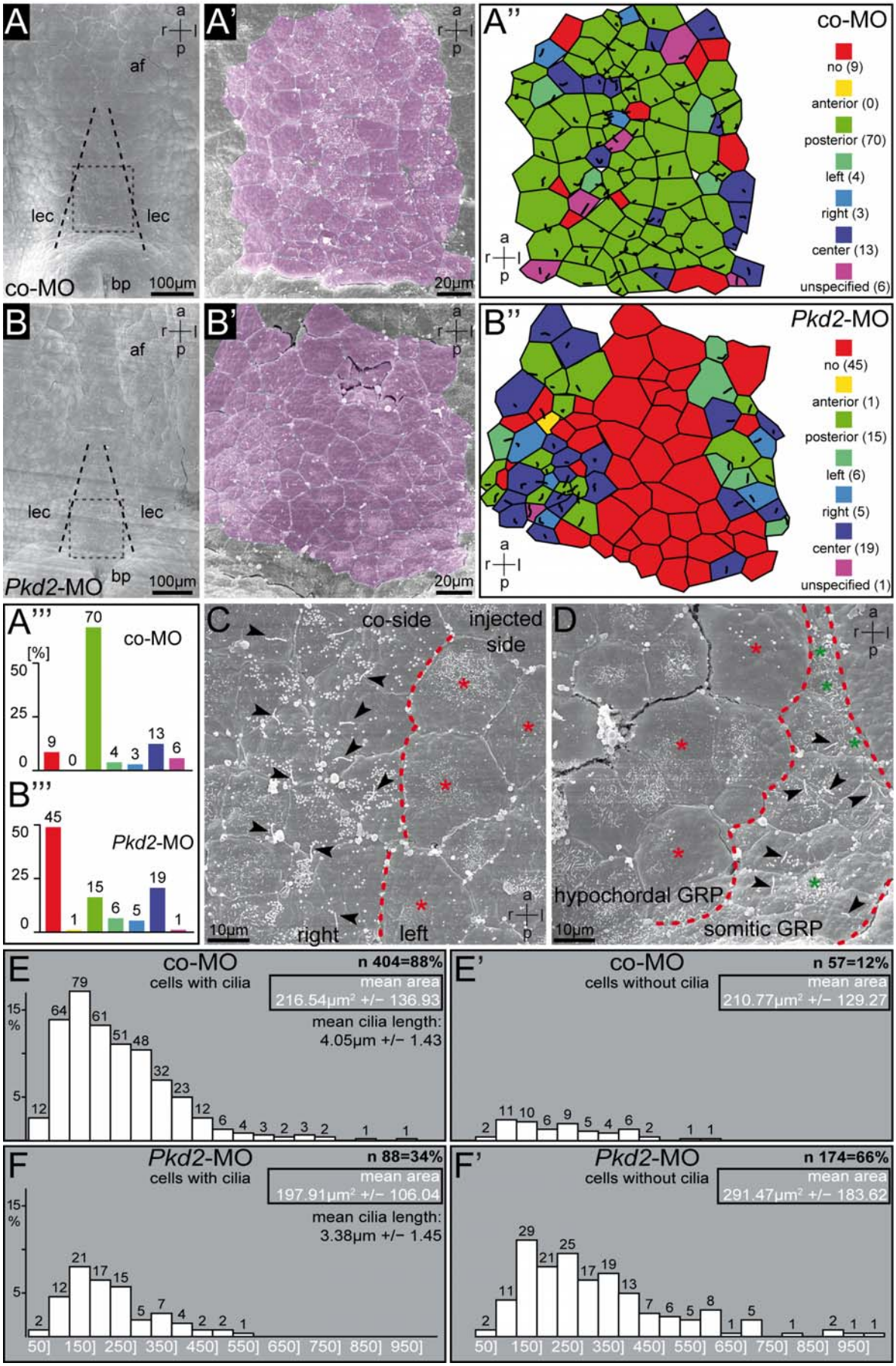
A
A'
A''
co-MO
no (9)
anterior (0)
posterior (70)
left (4)
right (3)
center (13)
unspecified (6)
af
lec
lec
bp
100µm
20µm
B
B'
B''
Pkd2-MO
no (45)
anterior (1)
posterior (15)
left (6)
right (5)
center (19)
unspecified (1)
A'''
B'''
[%]
C
co-side
injected side
right
left
D
hypochordal GRP
somitic GRP
10µm
E
co-MO
cells with cilia
n 404=88%
mean area
216.54µm² +/− 136.93
mean cilia length:
4.05µm +/− 1.43
E'
cells without cilia
n 57=12%
210.77µm² +/− 129.27
F
Pkd2-MO
n 88=34%
197.91µm² +/− 106.04
3.38µm +/− 1.45
F'
291.47µm² +/− 183.62
50] 150] 250] 350] 450] 550] 650] 750] 850] 950]

Fig. 28 GRP morphogenesis is massively impaired in *Pkd2* morphants
(A-B) Results of SEM-based morphological analysis of two representative examples of dorsal explants of embryos injected with 2pmol co-MO (A) or *Pkd2*-MO (B). While overview of the archenteron showed no obvious malformations (B) as compared to the co-MO (A), higher magnification (A', B') and analysis of ciliation revealed loss of ciliation (red cells in B'') and posterior localization of the remaining cilia (B'',B'''; cell numbers indicated) in *Pkd2* morphants but not in co-MO embryos (A'', A'''; cell numbers indicated). **(C)** High magnification of an embryo injected only on the right side with *Pkd2*-MO showed a strict separation of injected and uninjected sides in the midline (C; indicated with dashed line) with smaller, ciliated cells on the former (cilia marked with arrowheads) and larger non-ciliated cells on the later (indicated by red asterisks in C). **(D)** High magnification of another bilaterally injected example demonstrated loss of ciliation in affected larger hypochordal GRP cells (red asterisks in D) but not in more laterally situated smaller somatic GRP cells (cilia indicated by arrowheads in D). Green asterisks highlight very small somatic cells without cilia. **(E-F)** Percental histogram of cell sizes of 461 cells of 6 control embryos (E, E') and 262 cells of 5 *Pkd2*-MO injected embryos (F, F'). Please note no difference in mean cell size and size distribution in co-MO injected embryos (cf. E and E') but an increasing mean size in non-ciliated cells of *Pkd2*-MO injected embryos (cf. F and F'). Cell sizes in μm^2 are indicated at the bottom, cell numbers for size categories above the bars. A-B'', C and D are ventral views of dorsal explants with anterior to the top. a, anterior; af, archenteron roof; l, bp blastopore; GRP, gastrocoel roof plate; left; lec, lateral endodermal crest; n, number of cells; p, posterior; r, right; SEM, scanning electron microscope. SEM procedure was kindly performed by Tina Beyer.

Another noticeable phenomenon was that bilaterally injected specimens which showed larger cells lacking all cilia in most of the GRP cells – i.e. all notochordal and hypochordal cells – often still possessed normal-appearing small somitic GRP cells (i.e. lateral-most cells of the GRP) which possessed a cilium (Fig. 28D).

As for flow measurements above this phenotype was evaluated and quantified for a number of co-MO (n=6) and *Pkd2*-MO (n=5) injected embryos to obtain mean values. As clear separation of left and right parts had been demonstrated, GRPs of those embryos injected unilaterally were assessed separately for the respective sides to obtain morphant halves and internal control halves which could then be grouped to control or morphant GRPs. All of the *Pkd2* morphants showed the same phenotype with more or less severity, whereas none of the control sides or co-MO injected (Fig. 28A, B and data not shown). Evaluation of all cells resulted in a total of 88% ciliated cells, of which 67% showed posteriorly localized cilia with an average length of 4.05µm in controls (Fig. 28E and data not shown), while only 34% of the cells of the *Pkd2* morphants were ciliated with 37.5% posterior localization and an average length of 3.38µm (Fig. 28F and data not shown). Because of the conspicuous fact that cells of morphants appeared larger than wt specimens this feature was assessed as well. While controls showed no difference in cell size between ciliated and non-ciliated cells (cf. 216.54μm^2 vs. 210.77μm^2; Fig. 28E) the sizes of *Pkd2* morphant GRP cells displayed a great range with 197.91μm^2 versus 291.47μm^2 in ciliated or non-ciliated cells (Fig. 28F).

These analyses clearly demonstrated that GRP morphogenesis and ciliation were impaired in *Pkd2*-MO injected specimens, what presented a plausible explanation for the loss of flow.

Taken together, the *Pkd2* experiments revealed a novel and unexpected role of Pkd2 for symmetry breakage in *Xenopus* embryos.

4. Symmetry breakage depends on *xBic-C*

Besides the long-known connection between cilia and LR asymmetry, a similar relationship between LR asymmetry and kidney diseases has began to be established in more detail. The most obvious examples were the *Pkd2* gene, whose mutation or knockdown caused LR axis defects in mice and zebrafish (Bisgrove et al., 2005; Pennekamp et al., 2002; Schottenfeld et al., 2007) and the *Inversin* gene (Morgan et al., 1998; Otto et al., 2003). Another kidney-associated gene which has recently shown to have a connection to LR asymmetry was the mammalian *Bicc1* gene. It was reported to be expressed in the PNC and was shown to be mutated in the *jcpk* and *bpk* mouse mutants which serve as models for polycystic kidney disease (Cogswell et al., 2003; Maisonneuve et al., 2009; Wessely et al., 2001). Interestingly, the *Xenopus laevis* homolog *xBic-C* is expressed in the pronephric system (Wessely and De Robertis, 2000) in a pattern very similar to that described for *Pkd2* in this report (Fig. 21K), indicating a possible overlap of functional requirements.

4.1 Zygotic expression of *xBic-C*

Because of the promising similarity to *Pkd2* we decided to investigate the expression pattern of *xBic-C* to search specifically for expression in the GRP. It had already been reported, that additionally to the pronephros, *xBic-C* transcripts were found maternally at the vegetal pole and zygotically at the dorsal lip in late gastrula stage embryos and at the floorplate and tailbud in tailbud stages (Wessely and De Robertis, 2000). Neurula stage embryos (st.16-18) were fixed and processed for WMISH with a *xBic-C*-specific probe. Concomitantly with the PNC expression in the mouse, expression was indeed found in the GRP, with stronger signals at the lateral parts and weaker in the center (Fig. 29A, B).

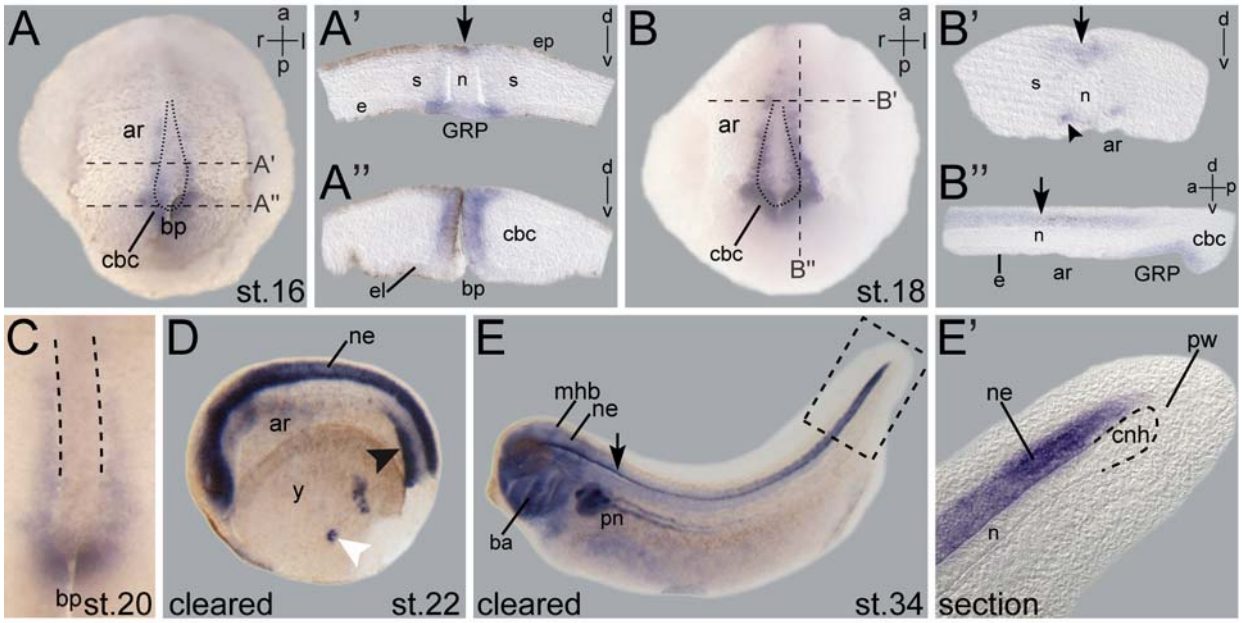

Fig. 29 Zygotic expression of *xBic-C*
WMISH of staged embryos with a *xBic-C*-specific antisense probe. **(A-C)** Expression of *xBic-C* in the posterior part of neurula stage embryos in the floorplate (arrow in A', B', B''), GRP (A, A', B, B''; outlined with dotted lines), ventro-medial part of the presomitic mesoderm anterior to the GRP (arrowhead in B') and in the epithelial lining of the dorsal (A, B'') and lateral part (A'') of the circumblastoporal collar of st.16 (A) and st.18 embryos (B). With disappearance of the GRP expression was strong in the presomitic mesoderm in st.20 (C; axial mesoderm outlined by dashed lines around the notochord) up to st.22 (arrowhead in D). **(D-E)** Later expression also included the neuroectoderm (D, E), floorplate (arrow in E), branchial arches and the pronephric system (E) and sagittal section of the tailbud region demonstrated strong signals in the neuroectoderm dorsal of the notochord and chordoneural hinge (E'). Please note spotty expression in the ventral yolk of stage 22 (white arrowhead in D). Embryos in D and E were cleared by benzyl benzoate/benzyl alcohol treatment. Higher magnificated area of sectioned embryo in E' indicated by dashed box in E. Planes of section in A', A'', B', B'' are indicated in A and B. a, anterior; ar, archenteron; ba, branchial arch; cbc, circumblastoporal collar; cnh, chordoneural hinge; d, dorsal; e, endoderm; el, epithelial layer (of the cbc); ep, epidermis; GRP gastrocoel roof plate; mid-hindbrain boundary; n notochord; ne, neuroectoderm; pn, pronephros; pw, posterior wall; s, somites; v, ventral; y, yolk

Additionally, strong expression could be detected in the epithelial lining of the dorsal and lateral circumblastoporal collar, and in the floorplate (Fig. 29A, B). Notably, sections at the very anterior part of the GRP showed that this part of the expression domain originated from the presomitic mesoderm in the deeper layers (Fig. 29B'). Accordingly, in later stages 20-22 when the GRP had mostly disappeared, the expression became focused into two parallel lines bordering the notochord ventrally (Fig. 29C, D). Further domains were found in the neuroectoderm and, in a spotty pattern, in the ventral, yolky part of early tailbud stages (Fig. 29D). In addition, domains were found in the floorplate, neuroectodermal part of the tailbud, pronephric system, branchial arches, and the mid-hindbrain boundary of late tailbud stages (Fig. 29D, E; and Wessely and De Robertis, 2000).

The detection of *xBic-C* mRNA in the GRP clearly indicated a possible function for this gene in laterality development and thus was chosen to be analyzed functionally.

4.2 *xBic-C* function is required for correct LR development

For knockdown of *xBic-C*, a mixture of two *xBic-C*-specific morpholinos was used which had already been utilized to analyze frog kidney development and whose specificity was shown by Western blot (Tran et al., 2007). Knockdown was expected to yield LR axis defects as it had recently been shown that knockout mice displayed a randomization of LR marker genes (Maisonneuve et al., 2009).

4.2.1 Knockdown of *xBic-C* caused neural tube closure and LR defects

In order to hit the expression region in the GRP, again dorsal-marginal injections were performed as described (cf. Fig. 14A, B; Blum et al., 2009). Bilateral injection of the MO-mixture – but not of the co-MO – resulted in a delay of neural tube closure between early neurula stages and late tailbud stages which was obvious by an open anterior neural tube in early tailbud stage (Fig. 30A). As already shown for *Pkd2* morphants (Fig. 23F), unilateral injection of the MOs together with a red-fluorescent lineage tracer clearly visualized a delay in closure of the neural folds at stage 18. Neural folds stayed open only on the injected side causing this half of the embryo to appear as an early st.14 or 15 embryo, when uninjected control sides resembled st.18 (Fig. 30B). As it had been published that *xBic-C* knockdown caused massive cyst formation very similar to *Pkd2* morphants (Tran et al., 2007), LR experiments were conducted by expression analysis of either *Xnr1* or *Pitx2c* in the left LPM. Bilateral knockdown with the MOs mainly caused loss of left *Xnr1* expression in about 50%, whereas controls and co-MO injections showed less than 5% misexpression (not shown; Maisonneuve et al., 2009). Accordingly, *Pitx2c* evaluation showed that less than 5% of uninjected control embryos or co-MO injected specimens showed laterality defects while bilateral injection of *xBic-C*-MOs caused mostly a loss of induction in the LPM in over 60% of cases (Fig. 30C-E; $p<0.001$). In disagreement with the *Pkd2* knockdown, unilateral injections into the right DMZ had no significant effect on LR development (Fig. 30, bar 4; $p=5.084$).

In order to gain more insight into the spatial requirements of functional xBic-C, lineage-specific, unilateral left injections were performed (cf. Fig. 17A-C). These showed that left DMZ injections with >60% caused nearly exactly the same outcome as bilateral (Fig. 30, bar 5; $p<0.001$).

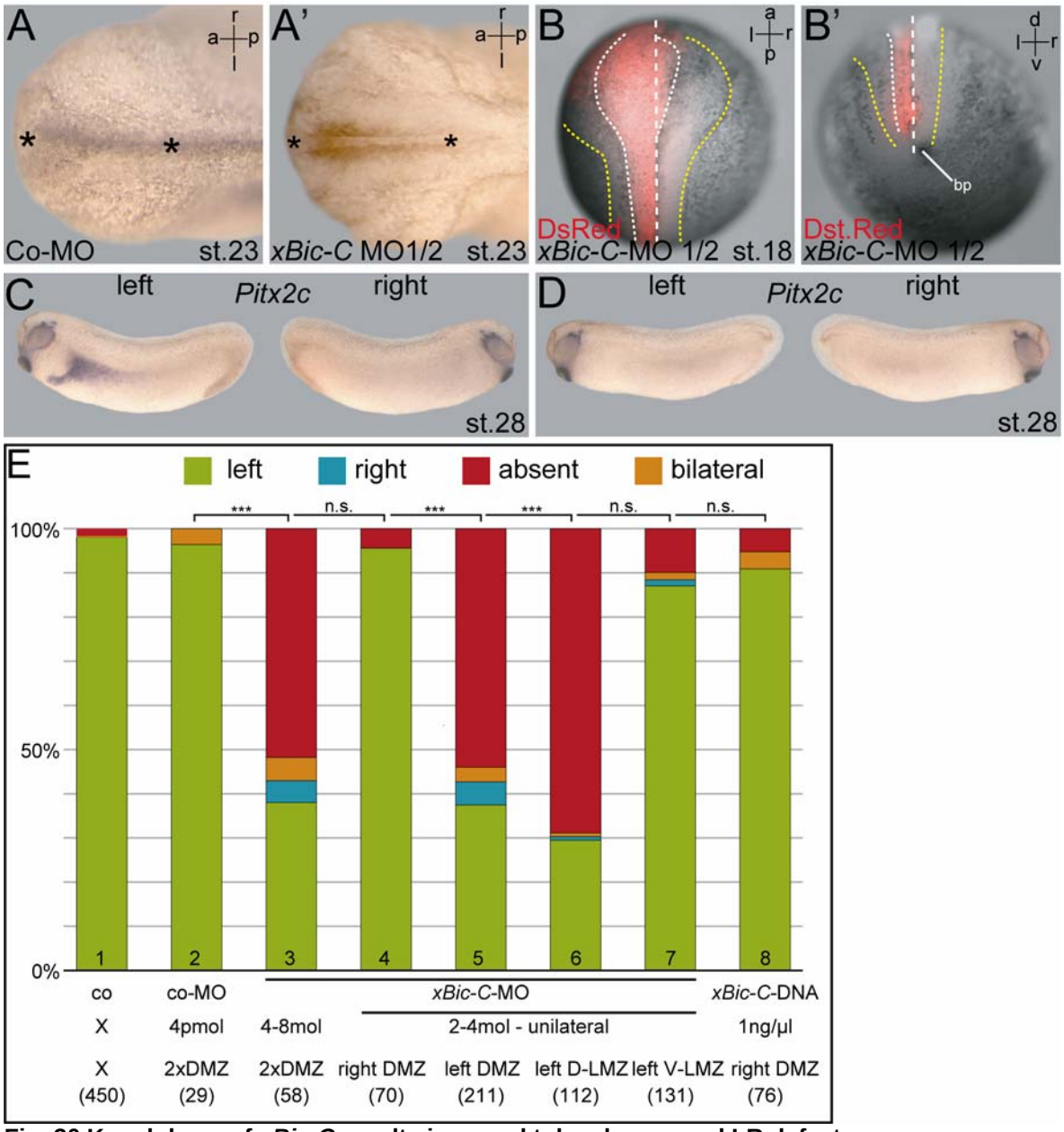

Fig. 30 Knockdown of *xBic-C* results in neural tube closure and LR defects
(A-B) Neural tube closure defects in embryos injected *xBic-C*-MO (A', B, B'). Bilateral injected embryos (A') but not co-MO injected (A) showed anterior neural tube closure defects. Unilaterally left injected embryos (B, B') showed a delay in neural tube closure from anterior (B) to posterior (B') as visualized by coinjection of DsRed lineage tracer. **(C-E)** Knockdown of *xBic-C* results in loss of *Pitx2c*. Bilateral knockdown mostly resulted in missing expression (D, bar 3 in E) in up to 50% in contrast to over 95% normal expression in control and co-MO injected embryos (C, E). Unilateral injections as depicted in Fig. 17 showed no effect when injected into the right DMZ (bar 4) or left ventro-lateral marginal zone (V-LMZ; bar 7) but up to 60% or 70% misexpression when injected in the left DMZ (bar 5) or left dorso-lateral marginal zone (D-LMZ; bar 6), respectively. Gain of function experiments by right-sided injection of 1ng/µl of *xBic-C* DNA resulted in no significant change. anterior; d, dorsal; DMZ, dorsal marginal zone; l, left; p, posterior; r, right; v, ventral

Interestingly, although no significant difference, dorso-lateral injections, targeting slightly more ventral, resulted in even higher percentages (70%) of misexpressed *Pitx2c* (Fig. 30, bar 6; $p<0.001$) while those injected into the ventro-lateral blastomeres had no significant effect (Fig. 30, bar 7; $p=0.850$). As this pointed

towards a left requirement of *xBic-C*, another approach was taken. To test if right-sided gain of function of *xBic-C* would activate the nodal cascade in the embryo, 1ng/µl of DNA was injected into the right DMZ but resulting in no significant effect (Fig. 30, bar 8; p=1.9182).

While these experiments were started, collaboration was initiated with the lab of Daniel Constam at ISREC in Lausanne. Their data, obtained from a *bicc1* knockout mouse, confirmed a conserved role for this protein for LR axis development between mouse and frog and thus convincingly supported our data.
As the knockout-mice showed impaired flow due to incorrect polarization of PNC cilia, some of the *xBic-C*-MO injected embryos from above were also analyzed for leftward flow (see also methods), which was performed together with Thomas Weber. These analyses showed that *xBic-C* morphants, in contrast to controls, showed impaired leftward flow with a range of severity of characteristic phenotypes (for details see Maisonneuve et al., 2009). To better understand the reason for this phenotype, some of the injected embryos were also processed for SEM analysis which was performed by Tina Beyer (University of Hohenheim). These embryos, but not the control specimens, showed a disturbed polarization of the GRP cilia confirming the phenotype of the knockout mice and providing an explanation for the impaired flow (see Maisonneuve et al., 2009).

These analyses revealed a novel role for xBic-C as being a prerequisite for correct cilia polarization, leftward flow, and thus for correct laterality in *Xenopus laevis*. The observed cilia polarization phenotype confirms the planar cell polarity function shown for *Bicc1* in mouse embryos.

4.2.2 *xBic-C*-MO specifically impaired bilateral *Xnr1* expression

After it had been shown that xBic-C is required for a robust flow and thus for correct frog LR development, this raised the question if and how this molecule might be linked to Pkd2. Additionally, it had been shown in parallel in the lab of Oliver Wessely (New Orleans) that Pkd2 function in the frog pronephros was dependent on xBic-C, pointing to a function in the same pathway (Tran et al., 2009). As both partially showed a similar expression pattern and similar phenotypes (cysts, neural tube

closure defects, impaired flow and loss of left marker genes) in *Xenopus*, this issue was to be investigated in more detail.

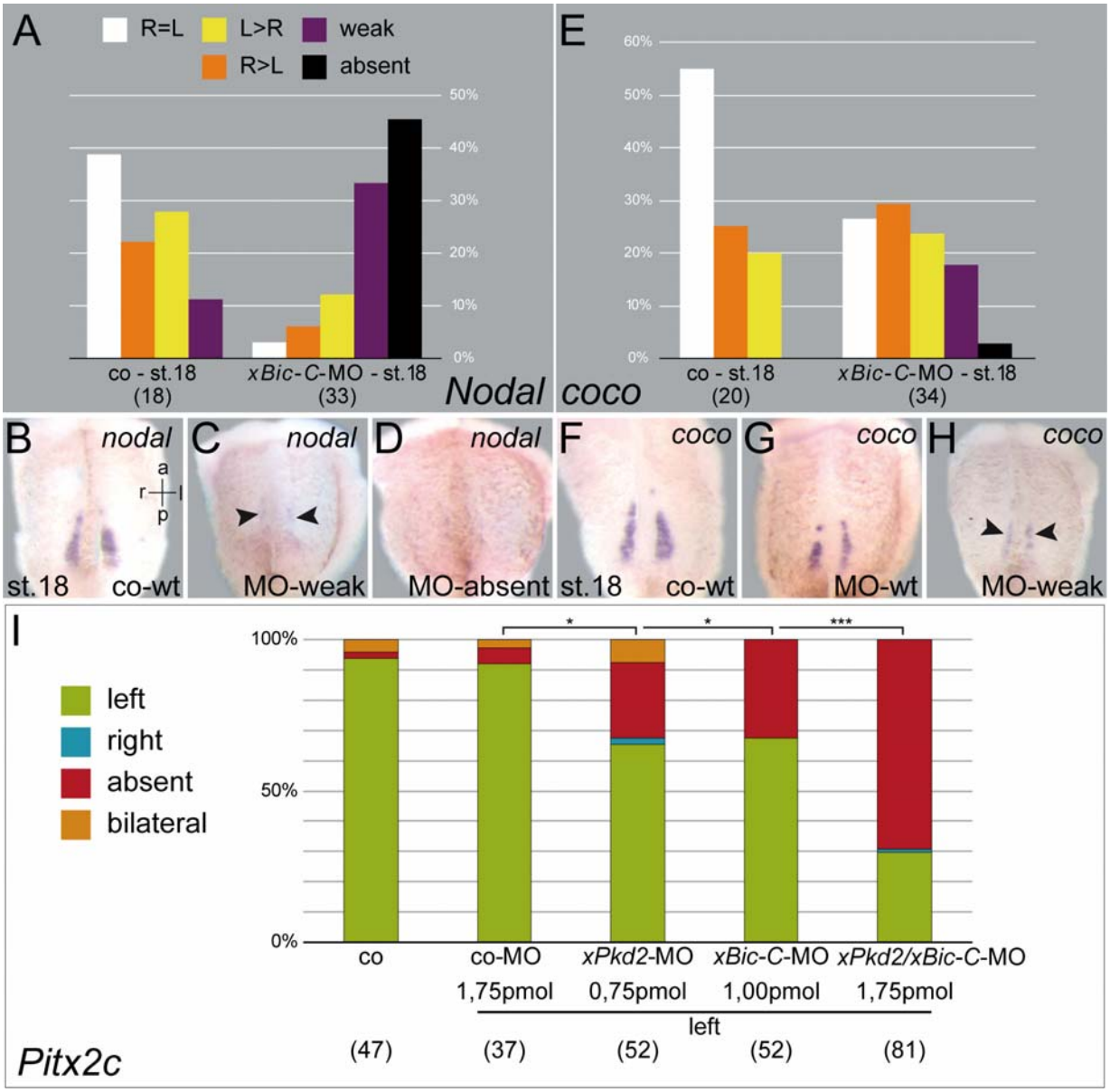

Fig. 31 *xBic-C*-MO impairs bilateral *Xnr1* expression

(A-H) Analyses of dorsal explants at stage 18 after WMISH with a *Xnr1*-specific or *coco*-specific antisense probe. (A-D) Bilateral knockdown of *xBic-C* inhibited *Xnr1* expression in about 45% (A, D) and weakened *Xnr1* in about 30% (A, arrowheads in C) in contrast to wildtype-like expression in control embryos (A, B). (E-H) Bilateral injection of *xBic-C*-MO weakened *coco* expression in about 20% (E, arrowheads in H) in contrast to normal expression in controls (E, F). Please note very rare cases of no *coco* expression in contrast to *nodal* analysis (cf. black bar in A and E). **(I)** Epistatic analysis of Pkd2 and xBic-C function by parallel knockdown and subsequent *Pitx2c* expression analysis. Left-sided injection of 1.75pmol of co-MO caused no changes in left *Pitx2c* expression as compared to wildtype controls. Injection of low doses (0.75pmol and 1.00pmol, respectively) of *Pkd2*- or *xBic-C*-MO caused significant increase in *Pitx2c* misexpression in about 30% of embryos while combination of both morpholinos yielded about 70% misexpression in a very highly significant manner. Please note that most embryos displayed loss of *Pitx2c* activity in the lateral plate mesoderm. l, left; r, right

As a starting point, the effect of *xBic-C* knockdown on the expression patterns of *Xnr1* and of its inhibitor *coco* should be compared at the GRP. Both genes are mainly co-expressed with *xBic-C* at the edge of the GRP in neurula stage embryos (cf. Fig. 29A, B and Fig. 31A, F; Vonica and Brivanlou, 2007). Controls displayed normal wildtype-like *Xnr1* expression with only about 10% of the embryos having weaker expression (Fig. 31A, B). In bilaterally injected *xBic-C* morphants, however, 30% of specimen showed weaker and 40% no expression at all (Fig. 31A, C, D). When *coco* expression was examined in the same morphants, the situation was markedly different. In contrast to controls, less than 20% showed a bilaterally reduced and nearly none showed absent expression (Fig. 31E-H). This outcome clearly hinted at a link of xBic-C with *Xnr1* but not with *coco* transcription.

To further explore the possibility that both, *xBic-C* and *Pkd2* act synergistically in the same pathway, combined knockdown experiments with lower, less efficient doses should be tried. Injections were chosen to be made unilaterally left and as readout for laterality, again *Pitx2c* expression was used. Injection of 1.75pmol of co-MO resulted in less than 10% LR defects (Fig. 31I). When less efficient doses of *Pkd2* or *xBic-C*-MO (0.75 and 1.00pmol, respectively) were injected into the left side, in both cases in about 30% *Pitx2c* was statistically significantly misexpressed, again in most cases with loss of induction (Fig. 31I; $p=0.0111$ and $p=0.0185$, respectively). Combined knockdown of both of these with the same doses increased this to a very highly significant value of ~70% (Fig. 31I; $p<0.001$), strongly portending to an at least partial overlap of function of both.

Overall, these results convincingly showed that *xBic-C* was necessary for the LR pathway on the level of the symmetry breaking event.

5. Hierarchical interplay of flow, nodal, coco, Pkd2 and xBic-C

With the confirmation that all four tested candidates were indeed required for *Xenopus* laterality and the insights into their functional properties, a further approach should be made. All of the obtained results pointed towards a role for all of the four molecules to be required for correct function of leftward flow. But also, there were some hints that they might have more complex or even different roles in the context of LR asymmetry.

To gain more knowledge about interactions or slight differences, and moreover to shed light on the direct consequences of leftward flow, i.e. how it is perceived and a left signal is generated, a number of epistasis experiments were set up. To be able to validate the different knockdowns hierarchically, two more components were used, both of which are known to be involved in frog LR development. The first one, *Xnr1*, is well known to be expressed laterally at the GRP and in the left LPM and both domains have been shown to be important for correct laterality and thus to be a left-sided determinant (Brennan et al., 2002; Saijoh et al., 2003). The second is the Xnr1 antagonist coco, a cerberus/Dan homolog, which had been shown to be co-expressed with *Xnr1* and to be required only on the right side of the frog embryo (Vonica and Brivanlou, 2007).

As both of these were thought to act downstream of the symmetry breaking event and were shown to have reciprocal functions, they offered themselves as ideal candidates for hierarchical calibration of the components of this work.

5.1 Flow-induced transcriptional inhibition of *coco* only on the left side

Before starting with the epistasis experiments, the exact wildtype expression patterns of *Xnr1* and *coco* at the GRP were characterized in detail. For bilateral midline *nodal* expression in the mouse, it had been published that this domain is initiated bilaterally (0-1 somite) and then becomes asymmetrical, with stronger expression on the left side (Lowe et al., 1996). In *Xenopus*, this bilateral domain had only been reported to be symmetrically expressed but no detailed quantifications had been published (Lowe et al., 1996; Mogi et al., 2003; Vonica and Brivanlou, 2007). *Coco* had been shown to be expressed in the posterior paraxial mesoderm flanking the notochord

(and GRP) similar to *Xnr1* and was shown to be expressed in the same cells (Vonica and Brivanlou, 2007).

5.1.1 Wt expression of *nodal* and *coco* during neurulation differently flank the GRP

As mentioned, no detailed stage-dependent analyses with respect to a left or right bias had been published either for *Xnr1* or *coco*. In order to fill this gap and to uncover inconspicuous differences between left and right sides – especially in relation to flow – a detailed stage-specific expression analysis was conducted for both first.

WMISH of dorsal explants with the *Xnr1*-specific probe showed a high number of embryos without expression between stages 12 and 15. Afterwards, *Xnr1* transcripts could be detected between stages 16 and 22 in a very high number of embryos and decreased rapidly from st.23 to 25 (Fig. 32A). At all stages, most of the embryos (~50%) displayed on the left and right side equal domains while the rest was about equally distributed between larger left or right side domains (Fig. 32A, C-E). Absence of domains on either side were only observed in extremely rare cases. To better visualize a possible flow-dependency, embryos were grouped according to pre- and early flow stages, robust flow stages and post-flow stages excluding the ones without expression (Fig. 32B). Although a very slight increase in bilaterally equal and concomitantly a very slight decrease in larger right domains was observed, no significant increase in the number of larger left domains could be detected. This clearly showed that in contrast to the mouse, in frog there was no increase of *Xnr1* transcript on the left side of the GRP.

Next, *coco* expression should be analyzed for asymmetries. Also for *coco*, most of the embryos showed an equal-sized domain during flow stages (~50%; st.14-18), while surprisingly, after flow (st.19-22) a very highly significant increase in domains with larger right halves was found (Fig. 32 F-I; $p<0.001$). This pointed to a possible transcriptional effect of the flow on the left-sided domain of *coco*.

To test the hypothesis that *coco* might be transcriptionally down-regulated on the left side in response to flow whereas *Xnr1* transcription would be independent of flow was tested by Melanie Eberhardt (Eberhardt, 2008). During that work, the

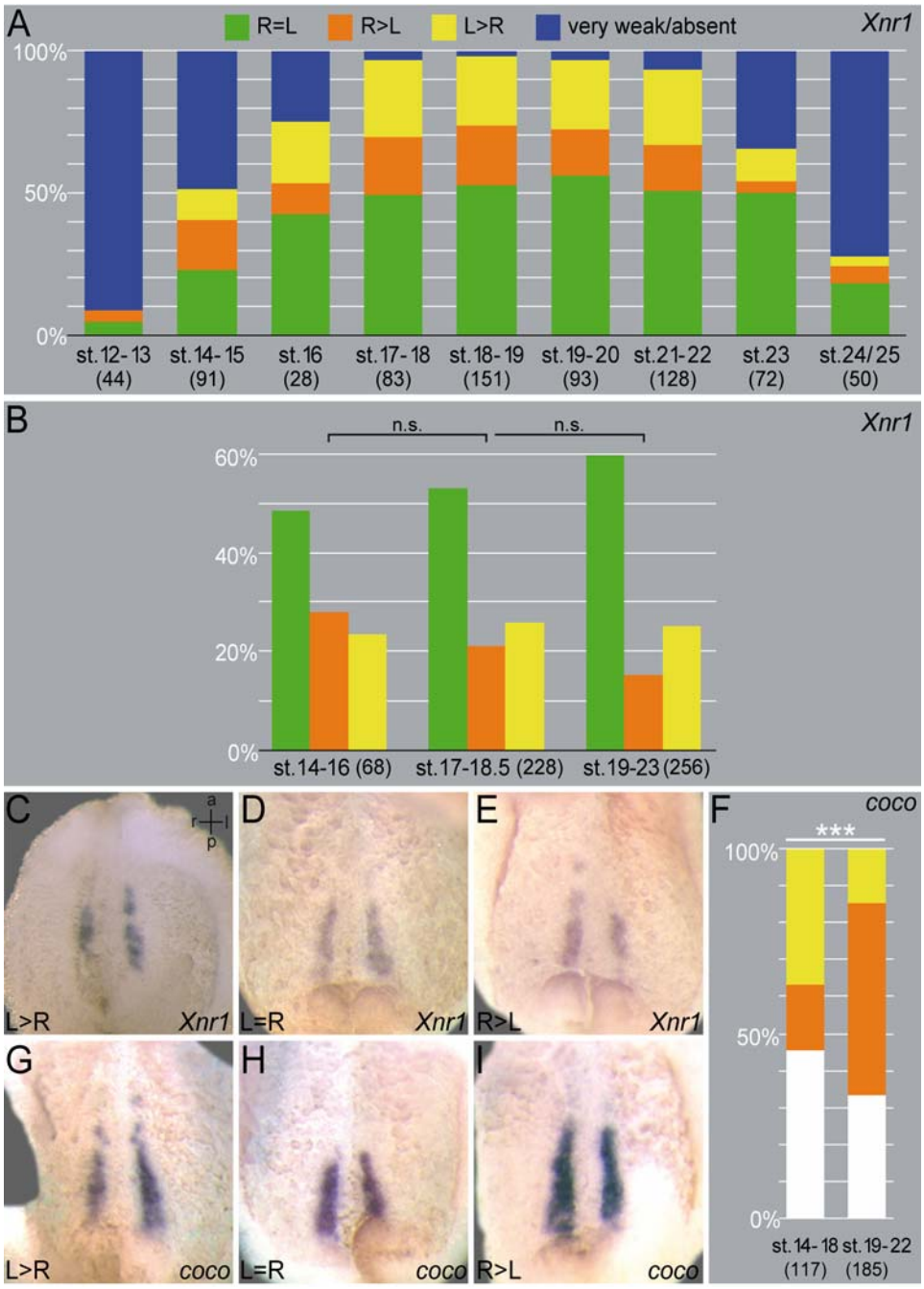

Fig. 32 Wt expression of *nodal* and *coco* during neurulation differently flank the GRP
(A-E) Analysis of dorsal explants with wildtype embryos between stage 12 and 24 after WMISH with a *Xnr1*-specific probe. The bilateral, domain of *Xnr1* started to become detectable between stage 12 and 15 and disappeared between stage 23 and 25 (A). Between stage 16 and 22 about 50% of embryos showed equal-sized left and right domains (A, D), ~20-25% displayed a larger left (A, C) and ~15-20% a larger right part (A, E). Grouping the analyzed embryos in three parts, namely pre- and early flow stages, robust flow stages and post-flow stages, and excluding those with missing expression revealed no significant differences of phenotypic distributions (B). **(F-I)** Analysis of wildtype embryos between stage 14 and 22 after WMISH with a *coco*-specific antisense probe accordingly showed three variants. During flow stages (st.14-18) about 50% of the analyzed embryos had a left and right equal-sized domain (F, H), ~35% a larger left (F, G) and ~15% a larger right part (F, I), whereas after flow (st.19-22) phenotypic distribution switched to 35%, 15%, and 50%, respectively. Please note that the increase in larger right domain parts is statistically very highly significant. C-E and G-I are representative examples of ventral views of dorsal explants with anterior to the top. l, left; r, right. For panel A, see also Pachur, 2007.

independence of the *Xnr1* domain of leftward flow could be proven convincingly by methylcellulose- or *dnah9*-SB-MO-mediated inhibition of the latter. Furthermore, it could be shown, that inhibition of flow by injection of MC or of the *dnah9*-SB-MO resulted in a significant decrease in the number of late neurula stage embryos that show a larger right-sided domain of *coco* (Eberhardt, 2008).

5.1.2 Loss of leftward flow was rescued by loss of coco function

With the insight that *coco* and not *Xnr1* showed a flow-correlative change on the left side and that this dependency was obviously of inhibitory nature, morpholino-mediated rescue experiments were initiated. With the use of a published *coco-MO* (Vonica and Brivanlou, 2007) the hypothesis, that loss of leftward flow would be rescued by an artificial left-sided loss of coco function, was tested.

For these experiments the left marker *Pitx2c* was used to assess the percentage of laterality defect in the injected embryos. Firstly, the *coco-MO* was injected either in the left or in the right DMZ to reproduce the published side-specificity. Indeed, only right injections caused bilateral induction of the nodal cascade in over 60% (Fig. 33A; $p<0.001$) whereas left-sided caused less than 5% ($p= 2.5044$). Then flow was inhibited by injecting methylcellulose in early neurula stages, a treatment that yielded >60% loss of expression ($p<0.001$). Importantly, injection of both, *coco-MO* on the left side and then MC in early neurula stages rescued the loss of *Pitx2c* phenotype in a statistically very highly significant percentage of cases (Fig. 33A; $p<0.001$).

To prove the specificity of this rescue and to investigate the hierarchical relationships with *Xnr1* a further series of experiments was carried out.

In the first part of this series, loss of coco function had only a very highly significant effect (mostly bilateral induction) when injected on the right and not on the left side (Fig. 30F, cf. bar 2 and 3; $p<0.001$ and $p=0.224$). In contrast, injection of *Xnr1*-MO caused a very highly significant rate (>80%) of either loss or right expression of *Pitx2c* after left but no significant rate (<5%) after right injections (Fig. 33F, cf. bar 5 and 4; $p<0.001$ and $p=1.258$; Vonica and Brivanlou, 2007).

With this first part, it could be confirmed that coco is needed on the right and Xnr1 on the left for correct laterality.

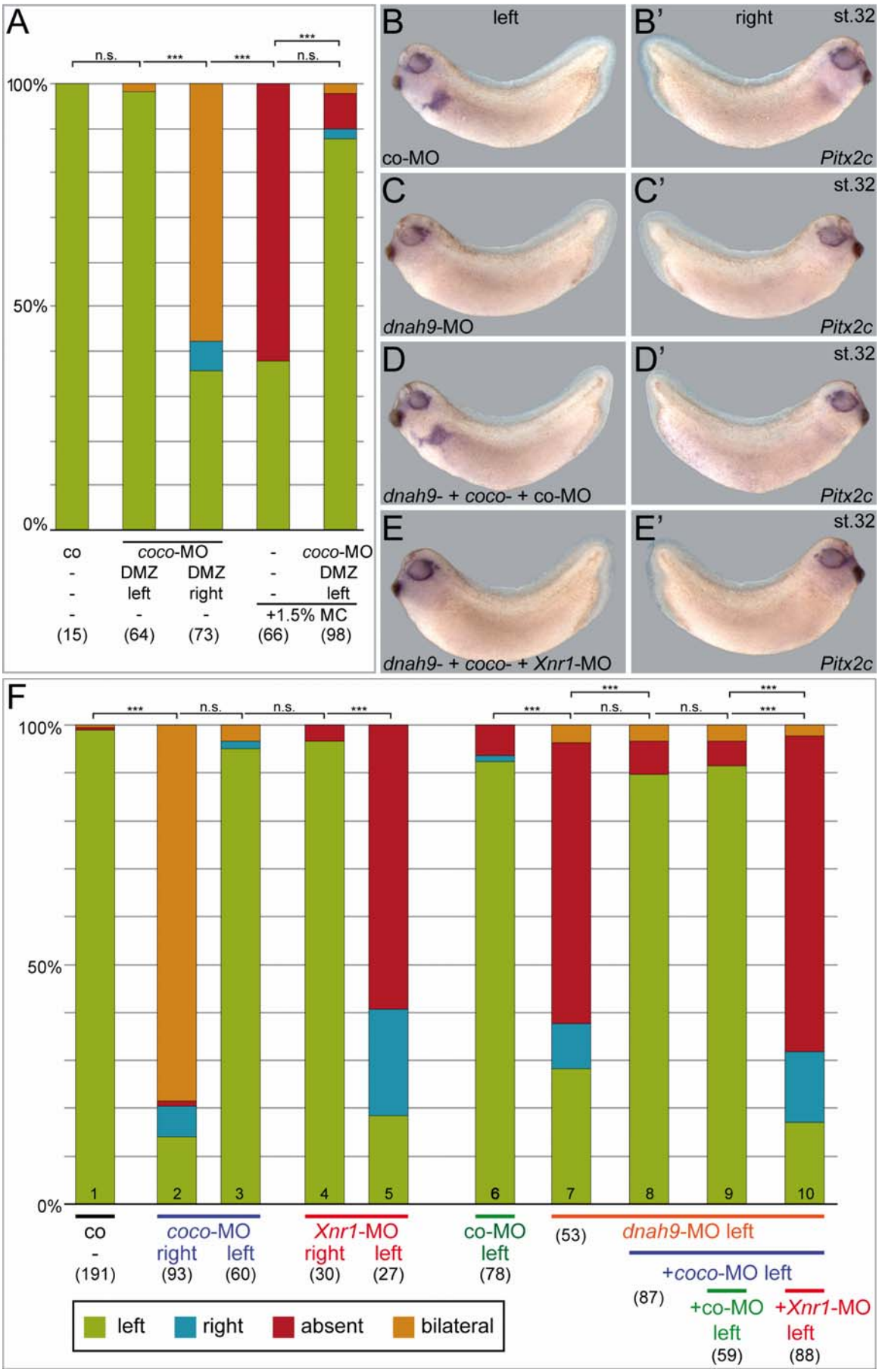
A
n.s.
***
***
n.s.
***
100%
50%
0%
co
-
-
-
(15)
coco-MO
DMZ
left
-
(64)
DMZ
right
-
(73)
-
-
-
(66)
coco-MO
DMZ
left
+1.5% MC
(98)
B
left
co-MO
B'
right
st.32
Pitx2c
C
dnah9-MO
C'
st.32
Pitx2c
D
dnah9- + coco- + co-MO
D'
st.32
Pitx2c
E
dnah9- + coco- + Xnr1-MO
E'
st.32
Pitx2c
F
***
n.s.
n.s.
***
***
n.s.
n.s.
***
***
***
100%
50%
0%
1
2
3
4
5
6
7
8
9
10
co
-
(191)
coco-MO
right
(93)
left
(60)
Xnr1-MO
right
(30)
left
(27)
co-MO
left
(78)
(53)
dnah9-MO left
+coco-MO left
(87)
+co-MO
left
(59)
+Xnr1-MO
left
(88)
left
right
absent
bilateral

Fig. 33 Loss of leftward flow can be rescued by loss of coco function
(A) *Pitx2c* expression analysis after combination of *coco* knockdown and MC-mediated loss of leftward flow. Left-sided knockdown had no effect while right-sided activated *Pitx2c* expression on the right side in about 65%. Early neurula stage archenteron injections of 1.5% MC caused ~60% loss of *Pitx2c* expression. Additional left injection of *coco-MO* rescued this effect with over 85% wildtype-like left expression. **(B-F)** Combination of *dnah9*, *coco*, and *Xnr1* knockdown on the left side of the DMZ. Injection of *coco-MO* activated *Pitx2c* on the right side in >85% when injected on the right but in less than 5% when injected on the left side (cf. bar 2 and 3). Reciprocally, left-sided *Xnr1*-MO injection caused loss of *Pitx2c* or right-sided expression in >80% but in <5% when injected on the right (cf. bar 4 and 5). Left-side co-MO injection had no significant effect on *Pitx2c* (B, bar 6 in F) but left-sided injection of *dnah9*-MO caused >70% misexpression (C, bar 7 in F). Additional coinjection of the *coco-MO* rescued this percentage to ~10% (double knockdown; bar 8) and further adding of a *Xnr1*-MO (triple knockdown; E, bar 10 in F) but not of the co-MO (triple knockdown; D, bar 9 in F) again disturbed correct expression in >80%. DMZ, dorsal marginal zone; MC, methyl cellulose.
MC injections were performed by Axel Schweickert.

In the second part only left DMZ was injected. Control-morpholino alone resulted in less than 10% of altered expression while *dnah9*-MO alone caused over 70% mainly loss of *Pitx2c* (Fig. 33B, C and F, cf. bar 6 and 7; $p<0.001$), very similar to Fig. 16F. When *coco-MO* was added, misexpression dropped to only ~10% (Fig. 33F, bar 8; $p=2.216$), confirming the results obtained by the MC-experiment (Fig. 33A). Finally, when the co-MO was additionally added, no significant change occurred (Fig. 33D, F, bar 9; $p=3.47$) whereas further addition of the *Xnr1*-MO resulted in a very highly significant percentage (>80%) of embryos mostly without expressed *Pitx2c* (Fig. 33E and F, bar 10, $p<0.001$). Nearly all embryos showed normal axial development (cf. Fig. 33B-E).
These wildtype analysis and triple-knockdown experiments revealed a hierarchy where Xnr1 is bilaterally inhibited by coco until the leftward flow caused a left-only release of repression by down regulation of *coco*.

5.2 Loss of xBic-C, but not Pkd2 or Xnr1 were rescued by loss of coco

After these well-documented interactions and arrays, the roles of *Pkd2* and *xBic-C* should be brought in relation to *coco* and *Xnr1* in another series of experiments. Again epistasis tests were performed by combined knockdown of the components.

5.2.1 Loss of Pkd2 could only partially be rescued by loss of coco

Pkd2 had been shown to be required for correct flow and morphogenesis of the GRP (Figs. 26-28). In order to gain a more detailed picture, double-knockdowns were conducted on the left side with either the *Xnr1*- or the *coco-MO*. In this experiment,

left *coco-MO* injection caused again less than 5% altered expression of *Pitx2c* while *Xnr1*-MO resulted in over 90% loss of expression (Fig. 34, bar 2 and 3; p=0.653 and p<0.001).

Very similar to *Xnr1*, *Pkd2*-MO alone mostly inhibited left induction in over 80% (Fig. 34, bar 4; p<0.001). Double-knockdown of both even raised the number to over 95% (Fig. 34, bar 5; p<0.001). More insightful, combination of *Pkd2*- and *coco-MO* resulted in a partial but highly significant rescue of the *Pkd2*-MO phenotype to about 55% misexpression (Fig. 34, bar 6; compared to bar 4, p=0.001).

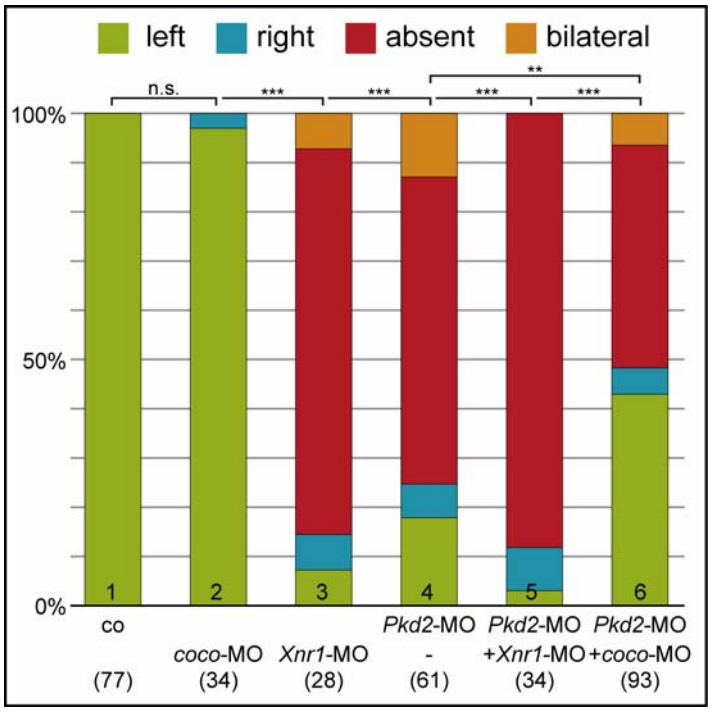

Fig. 34 Loss of Pkd2 can only partially be rescued by loss of coco
Pitx2c expression analysis after left-sided *Pkd2*-MO injections into the DMZ in combination with different morpholinos. *Xnr1* (bar 3) but not *coco* (bar 2) knockdown caused over 90% misexpression of *Pitx2c*. *Pkd2*-MO alone yielded >80% altered expression (bar 4) and in combination with *Xnr1*-MO >95% (bar 5). Combined *Pkd2* and *coco* knockdown rescued the effect to a rate of ~55% misexpression (bar 6). Please note that most cases of misexpression are loss of *Pitx2c* induction.

This final result underlined the massive GRP phenotype obtained for *Pkd2* morphant neurulae.

5.2.2 Loss of xBic-C was rescued by loss of coco

To be also able to make more precise statements about the functional requirements of xBic-C in addition to cilia-polarization, epistasis experiments were performed as well. To compare the disturbed flow phenotype of *xBic-C*-MO injections with the effect of loss of flow by *dnah9* knockdown, the same left-sided triple knockdowns were used as for *dnah9* (Fig. 33F). Again, *Xnr1*-MO yielded ~80% loss of *Pitx2c* while *coco-MO* had no significant effect (Fig. 35, bar 2 and 3; p<0.001 and

p=2.5579). Left injection of *xBic-C*-MO alone inhibited *Pitx2c* expression in 60% of all cases, an effect that could be rescued by coinjection of *coco-MO* in a very highly significant manner down to ~10% (Fig. 35, bars 4 and 5; p<0.001). To explore the effect of an addition of the *Xnr1*-MO, the triple-MO injections were performed. This manipulation again resulted in over 95% of missing or inverted *Pitx2c*, a very highly significant effect as compared to injections where co-MO instead of *Xnr1*-MO was used (Fig.35, bar 7 and 6; p<0.001).

This outcome was very similar to the results obtained for *dnah9* and thus underlined the flow-impairing phenotype of the single knockdown of *xBic-C*.

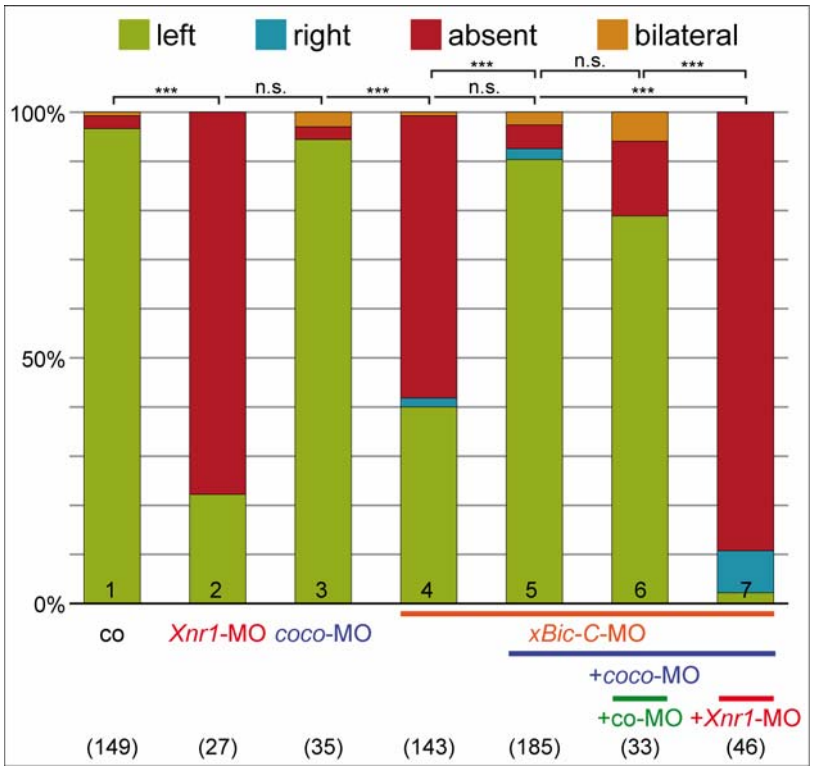

Fig. 35 Loss of xBic-C is rescued by loss of coco
Pitx2c expression analysis after left-sided *xBic-C*-MO injections into the DMZ in combination with different morpholinos. *Xnr1* (bar 2) but not *coco* (bar 3) knockdown caused >75% misexpression of *Pitx2c*. *xBic-C*-MO alone caused 60% altered expression (single knockdown; bar 4) which could be rescued to 10% by adding the *coco-MO* (double knockdown; bar 5). Further adding of the *Xnr1*-MO (triple knockdown; bar 7) resulted again in >95% misexpression, whereas adding of the co-MO only caused ~20% (triple knockdown; bar 6). Please note that most cases of altered expression are loss of *Pitx2c* induction.

5.2.3 *Coco-MO*-induced bilateral *Pitx2c* is only rescued by loss of Xnr1 or Pkd2

The obtained effects were intended to be confirmed independently of leftward flow by unilateral-right injections. In this way, not the ability of the *coco-MO* to rescue the knockdown of the other components but reciprocally the ability of either the *Pkd2*-, *Xnr1*- or *xBic-C*-MO to prevent the right-sided induction of *Pitx2c* as induced by the *coco* knockdown on this half, should be tested.

In these experiments, unilateral-right injection of the *coco-MO* resulted in 100% induction of *Pitx2c* on the right side represented mostly by bilateral expressing embryos (Fig. 36, bar 3). When either *xBic-C*-MO, or *Pkd2*-MO or *Xnr1*-MO were added, right induction occurred in only 65%, 4% or 0%, respectively (Fig. 36, bars 4, 5, 6; each $p<0.001$).

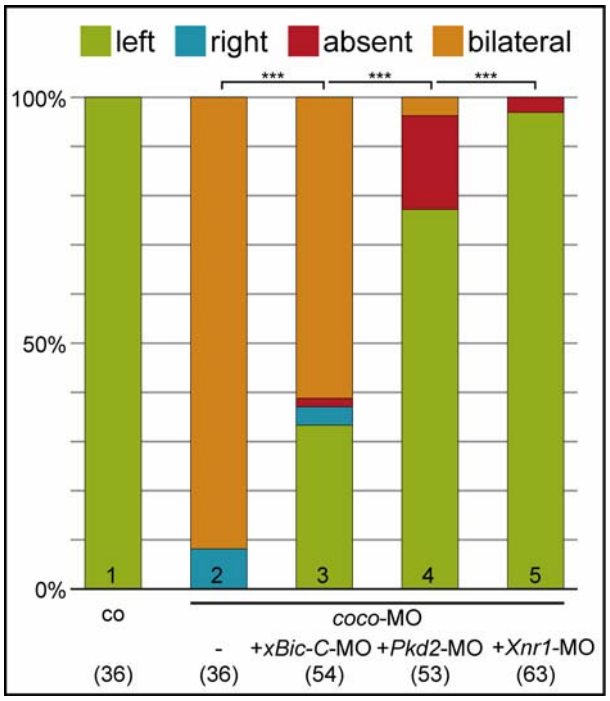

Fig. 36 *Coco-MO* induced bilateral *Pitx2* is rescued by loss of Xnr1 or Pkd2 but not of xBic-C
Pitx2c expression analysis after flow-independent right-sided injections into the DMZ underlined hierarchical situation. Injection of *coco-MO* into the right side resulted in 100% of either bilateral (>90%) or right expression (bar 2). Combination of *coco-MO* with *xBic-C*-MO partly inhibited the right sided induction, yielding about 65% (bar 3) of right activity whereas combination with either *Pkd2*-MO or *Xnr1*-MO could prevent this by resulting in ~5% (bar 4) or 0% (bar 5) of right *Pitx2c* induction in these embryos.

This experimental procedure mostly confirmed the results obtained by the left-sided knockdown. More specifically, *coco* knockdown had no effect when *Pkd2* or *Xnr1* were also knocked down on this right side but - although significant as well - *xBic-C* knockdown could only inhibit *Pitx2c* induction in about 35%.

In summary, the epistasis experiments demonstrated that

1) coco is downstream of the leftward flow,
2) leftward flow causes right inhibition of coco,
3) nodal is downstream of coco,
4) Pkd2 and Xnr1 are both required for nodal induction in the LPM, and
5) xBic-C is upstream of coco.

Discussion

The present work deals with the role of leftward flow for the symmetry breakage in the frog *Xenopus laevis*. The aim was to analyze characteristics and requirements for leftward flow-based symmetry breakage. Therefore, several components were tested for their exact role in this process by loss of function approaches. One main aim was to evaluate the morphogen and the two-cilia models in frog LR axis development. Thereby, general insight into vertebrate LR symmetry breakage and its conservation was to be gained.

1. Morphogen model

It could be convincingly shown that *dynein heavy chain* gene function is conserved in frog ciliary motility, leftward flow and laterality development. Inhibition of dnah5 or 9 function resulted in a high percentage of absent nodal cascade gene expression. Furthermore, specific right-sided loss of leftward flow had no influence on left marker gene induction. This demonstrated that (1) flow on the left side is sufficient to break early symmetry and (2) that no morphogen entering from the right side of the GRP is needed. Therefore, these experiments clearly exclude nodal as the possible transported morphogen at the GRP.

1.1 Conserved function of *dnah* genes for LR asymmetry in *Xenopus*

The bilateral knockdown of the *dnah* genes confirmed the evolutionary conservation of those dyneins for leftward flow in vertebrates and the loss of induction of the nodal cascade after MC injections. As in zebrafish, knockdown of *dnah9* caused laterality defects and *dnah5*-morphants resulted in LR defects like the mouse knockout and PCD in humans (Essner et al., 2005; Ibanez-Tallon et al., 2002; Olbrich et al., 2002; Omran et al., 2000). Surprisingly, *dnah11* could not be detected in the GRP as reported for its mouse homolog *lrd* in the PNC (Fig. 09; Supp et al., 1997). A possibility which cannot be excluded at the moment is a residual expression below the detection level of WMISH. On the other hand, both dyneins could have homologous functions for the generation of flow, compensating for the loss of one

another, as both represent homologs of *Chlamydomonas* beta chain dyneins (Zariwala et al., 2007). In accordance with this assumption, no transcriptional signal could be detected in the mouse PNC after WMISH with a *dnah9*-specific probe or by RT-PCR during preliminary experiments in our lab (our results, unpublished). However, to clarify that dnah9 is necessary for PNC cilia function, a knockout mouse needs to be analyzed for laterality defects.

1.2 Xnr1 is not transported by leftward flow

Unilateral knockdown surprisingly revealed that flow is thus only necessary on the left side of the GRP (Fig. 16). This interesting outcome allows predictions about a putatively transported morphogen and its site of release. If this model applied for *Xenopus*, then any morphogen (or the NVPs) may not be released exclusively at the margins but from the GRP itself; because in such small dimensions (~200µm GRP) leftward flow only on the left side would not suffice to attract particles from the right margin due to the low Reynold's numbers valid for such a system (Purcell, 1977). Thus both sides would receive the same amount of morphogen, which would result in loss of asymmetric gene induction. Therefore, and due to the fact that right-sided knockdown of *Xnr1* (the *Xenopus nodal* gene) shows no LR effects (cf. Fig. 33 and Vonica and Brivanlou, 2007), nodal can be excluded from being transported by the leftward flow in *Xenopus*, as it was considered earlier in mouse (Cartwright et al., 2008; Hamada, 2008; Saijoh et al., 2003; Tabin, 2006).

In such a scenario the inconsistent patterns of asymmetric marker gene expression upon loss of the functionally homologous genes *dnah11* in mouse (*iv* mutant; randomized patterns; Lowe et al., 1996) and *dnah9* in frog (absent expression) may be resolved. In the mouse, the PNC cells are fated to become notochord (Sulik et al., 1994), while in the frog, the ciliated notochord precursors are found only in the central part of the GRP and are flanked by ciliated hypochordal and somitic GRP cells on either side (Fig. 37+ 38B; Schweickert et al., 2007; Shook et al., 2004). If the morphogen arose in the notochordal cells, i.e. the population present in mouse and frog alike, the morphogen would be present in mouse *iv/iv* mutant embryos throughout the pit-like depression of the egg cylinder. A peripherally localized receptor could become randomly activated from the neighboring morphogen-

producing cells, for example by diffusion. In the frog, a morphogen would need to cover a considerably low distance of some 50 µm (Fig. 37), across the hypochordal cells before entering the marginal region where the receptor may reside. In the absence of flow this seems unlikely, resulting in the observed absence of marker expression in *dnah9* and *dnah5* morphants.

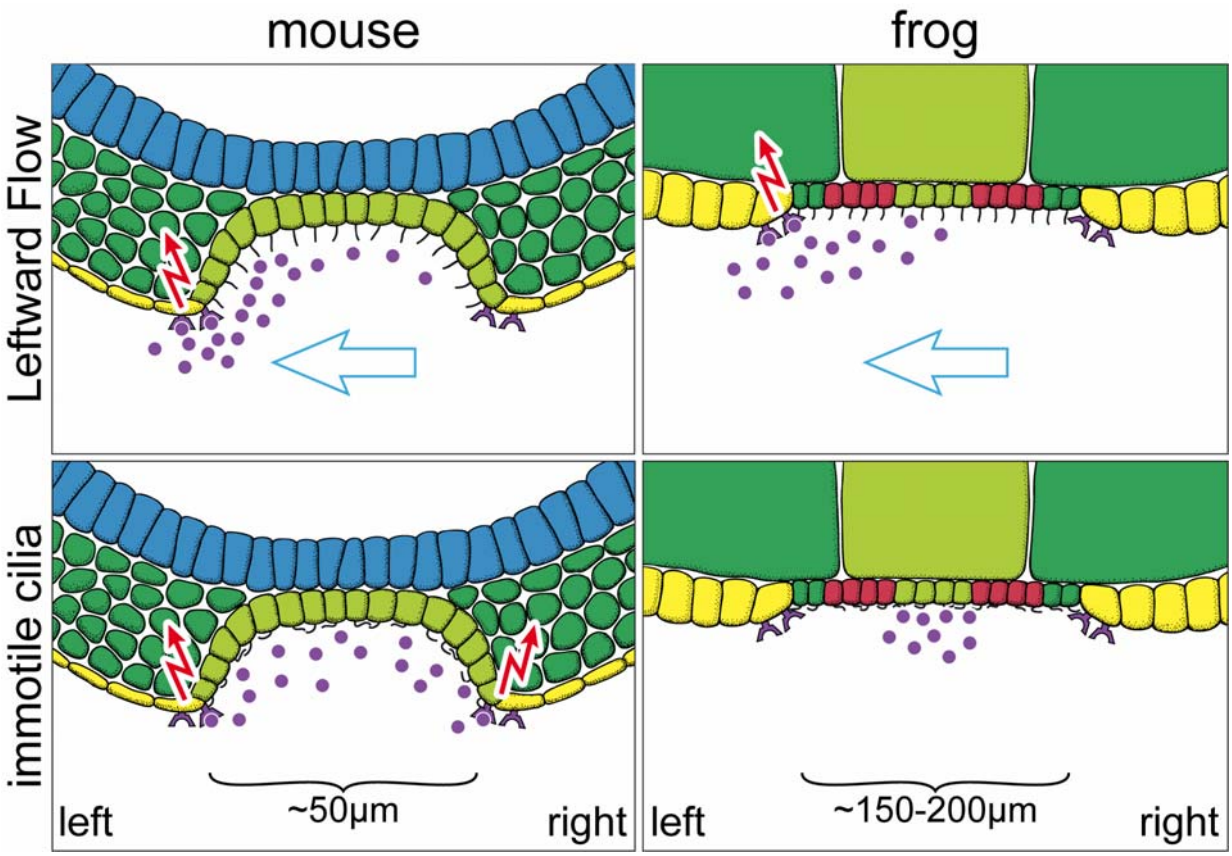

Fig. 37 Model of morphogen-mediated symmetry breakage in mouse and frog.
Leftward flow transports a morphogen (purple circles) across the ciliated epithelia (PNC, GRP). The morphogen emanates from notochordal cells (light green) which are found throughout the PNC and in the center of the GRP. Sensing of the morphogen at the left margin of PNC/GRP triggers transfer of asymmetric cues to the lateral plate mesoderm (red flash). Absence of flow results in short-range diffusion of morphogen, which in mouse can lead to random activation of the Nodal cascade. In frog the distance between site of release and GRP margin is too far for activation by short-range diffusion, precluding induction of LPM *nodal*. Blue, ectoderm; yellow, endoderm; dark green, precursors of somitic mesoderm; light green, notochord and notochordal precursors in the GRP; red, precursor cells of hypochord.

1.3 Maternal *dnah9* is indispensable for gastrulation

In a first approach, injecting a *dnah9* coding morpholino unexpectedly resulted in strong gastrulation defects or even in a stop of gastrulation (Fig.11). Cells did not involute and form a correct AP axis as visualized by WMISH of *Xbra*. *dnah9* was maternally strongly expressed in the animal pole and first zygotically detectable

transcripts on the dorsal lip represented staining of future GRP cells (superficial mesoderm). Also, the *dnah9* splice site morpholino did not result in any gastrulation defect. Therefore, the observed gastrulation defects are most likely due to loss of function of the maternal component. To my knowledge, such phenotypes have not been published in any dynein-related loss of function study in vertebrates so far. However, in zebrafish similar ubiquitous maternal expression of *dnah9* was reported, as well as axial defects after knockdown with high morpholino doses but no gastrulation defects were shown (Essner et al., 2005). Besides, axonemal dynein heavy chain genes have not been reported to be expressed in non-ciliary tissue or having non-axonemal functions (e.g. see Andrews et al., 1996; Maiti et al., 2000).

This raises the question if this early axonemal dnah9 function is specific to lower vertebrates or even amphibians, and moreover, in what cellular processes it is involved. Up to now, no ciliary structures have been reported for the *Xenopus* blastula or gastrula stages or cilia being involved in gastrulation (Monroy et al., 1976; Smith et al., 1976; Tarin, 1971). But promisingly, microtubule-associated processes were shown to be necessary for correct gastrulation movements. More specifically, microtubule depolymerization with Nocodazole but not stabilization with taxol prevented bottle cell invagination, mesoderm involution and convergent extension (CE; Lane and Keller, 1997; Lee and Harland, 2007). Interestingly, the observed phenotype is very reminiscent of the *dnah9* knockdown, as here the bottle cells also seem to form but then do not invaginate and gastrulation is inhibited (Thomas Weber and Ray Keller; personal communication). Although cytoplasmic dynein complexes are well known to migrate along microtubules towards the minus end, the mode of interaction of axonemal dynein complexes is different. An outer arm dynein is fixed to one microtubule doublet and only proceeds a short way on the neighboring doublet to cause sliding (Asai and Koonce, 2001; Bui et al., 2008). The frog dnah9 could in principle be a specialized axonemal heavy chain, which was recruited to serve as a part of a cytoplasmic dynein complex during gastrulation. Another possibility would be that an axonemal dynein complex function was adapted to enable involution movements during gastrulation. Then this complex would be used like in cilia, with the N-terminal part being fixed to one microtubule track and slide alongside with the C-terminal motor domain, to finally displace both of them. This could thus help to reshape invaginating/involuting cells in collaboration with the actin network. To test

such a hypothesis, a specific antibody would be needed to visualize the subcellular localization of dnah9 during gastrula stages. Alternatively, a tagged version (e.g. with GFP or myc) of dnah9 could be used to see cellular localization. However, as the full length of the coding regions is >14.000bp, cloning will be complicated.

1.4 Loss of dynein heavy chain function impairs pronephros development

The second observed phenotype of *dnah9*-MO injected specimens, namely massive edemas, is explained because larval amphibians – in contrast to adult specimens – use an ancient vertebrate pronephros for filtration. This pronephros consists of three tubes, the nephrostomes, which are connected to the coelomic cavity and harbor multiciliated cells inside that resemble epidermal cilia bundles. Accordingly, these cilia move in a wave-like pattern and generate a fluid movement into the pronephric duct (Brandli, 1999; Ryffel, 2003). Consequently, if these cilia are immotile due to loss of dnah9 function in that tissue (where it is expressed; Fig. 08F), body fluid can no longer be removed and cysts arise. The mammalian metanephros in contrast only uses immotile monocilia for sensing (cf. introduction, chapter PKD), thus there is no need for dynein complexes and consequently no cystic phenotype upon loss of function. A similar phenotype was observed in medaka when the dynein pre-assembly complex gene *Ktu*/*PF13* was knocked down. These fish developed edema and mutation in the human gene was likewise identified as a cause for PCD but not for PKD (Omran et al., 2008).

2. The two-cilia model

The easily manipulable leftward flow in *Xenopus* and its fast assessment offered the possibility to dissect the further parts of symmetry breakage – namely what kind of signal is transported and how it is sensed and translocated to the LPM (see also Blum et al., 2009a). In this work, it could be demonstrated, that *XHtr3* and *Pkd2* have an important role for symmetry breakage specifically at the GRP. But very surprisingly, both, inhibition of Pkd2 or serotonin receptor 3 mediated signaling, resulted in a very comparable morphogenesis phenotype of the GRP. These results challenge a conserved role for a *Pkd2*-dependent two-cilia model in frog but point towards an earlier function GRP development during blastula or gastrula stages.

2.1 Loss of Pkd2 results in absent left marker genes and impaired flow

The absent leftward flow and the massive GRP phenotype revealed that the function of Pkd2 obviously is not conserved in *Xenopus*. Furthermore, injections directly targeted at the GRP were very highly significantly more effective than those more laterally, which would target GRP at its margin, the site where a putative Ca^{2+}-signal is supposed to act (Fig. 25). These results strongly support a conserved role for Pkd2 for LR development but also a non-conserved function compared to mice. Nevertheless, the *Pkd2* knockout mouse has never been analyzed for leftward flow and partial ciliation defects can not be excluded, as cilia length was not analyzed in detail and not shown for the whole PNC (McGrath et al., 2003). In principle, the published loss of left Ca^{2+}-signal in the knockout could have also been caused by impaired leftward flow in these mice.
In zebrafish, *Pkd2* morphants, as well as the *Pkd2* "curly up" mutants both showed laterality defects and similar phenotypes (dorsally curled tail and cysts) like the *Xenopus Pkd2* morphants (Fig. 23; Bisgrove et al., 2005; Schottenfeld et al., 2007). Asymmetric marker genes were expressed randomly in both zebrafish studies, with a predominance of bilateral expression patterns. This contradicts the loss of expression in mutant mice (Pennekamp et al., 2002) and *Xenopus* morphants (Fig. 24), which resulted predominantly in an absence of signals. Additionally, Ca^{2+}-signaling was shown to be located in or around the KV in zebrafish and inhibition resulted in bilateral marker gene expression, a condition conflicting with a possible left-sided calcium signal (Sarmah et al., 2005; Schneider et al., 2008).

Of course, a second function for Pkd2 downstream of leftward flow in *Xenopus* cannot be excluded at this time; especially as PC2 did localize to GRP cilia. To address this, stage-dependent imaging and inhibition of Ca^{2+}-signaling during flow stages would be necessary. This could be achieved by adding a calcium inhibitory drug (e.g. thapsigargin; cf. Schneider et al., 2008) during these stages (although tissue penetration into the archenteron might be limited) or alternatively, by injection of a caged *Pkd2*-MO which would again be activated stage-dependently (Ouyang et al., 2009; Shestopalov et al., 2007). Alternatively, an interesting approach would be to use a morpholino against an IFT-component (like a *Polaris*-MO, see Dammermann et al., 2009), which would eliminate all GRP cilia and thus offer the opportunity to

compare loss of motility (by *dnah9*-MO) with loss of cilia directly. This would allow evaluating the probability of the two-cilia model in frog, as exactly these different outcomes (randomized marker genes compared to bilateral or absent) were the basis to propose the model (see Tabin and Vogan, 2003). For this experiment, the frog is particularly useful as it allows inhibiting flow unilaterally. Loss of IFT components was reported to result in additional midline defects, which is known to cause bilateral expression (Bisgrove et al., 1999; Murcia et al., 2000; Ohi and Wright, 2007; Yamamoto et al., 2003). It is thus imaginable that the observed bilateral and absent marker expression in *Polaris* morphant embryos is due to an *iv*-phenotype (left-right-bilateral-absent expression) in combination with midline leaking of the signal – so all left- and right-only inductions would result in bilateral expression patterns. Left-sided IFT-knockdown in frog should thus erase cilia and flow but most likely not cause midline defects. Thereby loss of ciliation would be comparable to loss of motility.
In summary, *Pkd2* seems to be necessary for LR development of all vertebrates; but exact function seems to differ, at least partially.

2.2 *Pkd2*-knockdown severely impairs GRP morphogenesis

SEM analysis of *Pkd2*-morphant GRPs revealed a strong morphogenetic phenotype as represented by altered cell size and mostly a total loss of ciliation in the targeted areas (Fig. 28). This was obviously the cause for the efficient impairment of leftward flow in morphants. Remarkably, unilaterally injected GRPs showed a very strict border between wild type and morphant areas, as seen at the very midline of the specimens (Fig. 28C). This observation nicely confirmed lineage-specific separation of left and right sides as shown in Fig. 16 (cf. also Blum et al., 2009a; Vick et al., 2009), an important experimental approach not feasible in any other model organism.
Another striking effect frequently observed was the nearly complete loss of ciliation in the center – namely the notochordal and hypochordal GRP cells – in parallel to almost wild type-like appearance of the lateral somitic GRP cells (Fig. 28D). This result was supported by the remaining *dnah9* expression in this region in a proportion of specimens after *Pkd2*-knockdown (Fig. 27C, E) and confirmed dorso-lateral marginal zone lineage as shown in Fig. 17B (see also Fig. 38B).
Shorter cilia have not been reported for *Pkd2* knockout mice or for mutant or morphant zebrafish (Bisgrove et al., 2005; Pennekamp et al., 2002; Schottenfeld et

al., 2007). But very similar to this report, thapsigargin-mediated loss of intracellular calcium has been shown to result in disruption of KV formation in two independent studies (Kreiling et al., 2008; Schneider et al., 2008). Remarkably, stably transfected cells inducibly produced a truncated version of the rat PC2 protein displayed shorter cilia, yet linking *Pkd2*-dependent cilia length to mammals (Gallagher et al., 2006).
To summarize, this phenotype suggests a novel role for *Pkd2* in *Xenopus* LR development while it does not exclude a second function in generating a calcium signal downstream of leftward flow.

The Pkd2 morphants, in addition, argue in favor of the morphogen model in *Xenopus*. Knockdown of *Pkd2* only on the right side of the GRP resulted in ~35% of embryos exhibiting altered *Pitx2c* expression, of which most showed absent *Pitx2c* on the left side. As it has been clearly shown that flow on the right side was dispensable for symmetry breakage (Fig. 16), this result would not be in the context of the two-cilia model. If PC2 indeed had – beside GRP morphogenesis – a second function to generate a left-sided Ca^{2+}-signal after bending of mechanosensory cilia, then there should be no difference between knockdown of *dnah9* and *Pkd2* on the right side – in both cases normal left marker gene induction should occur. Interestingly, the high-magnification SEM picture of the GRP of such a unilaterally injected embryo (Fig. 28C) indicated a larger amount of small and large vesicular structures on the surface of the uninjected half. Thus, the right interference with correct morphogenesis might inhibit release of vesicles or molecules and therefore cause a non cell-autonomous effect on the left side. If this was the case, it would favor a morphogen model with signal release inside the GRP for the frog. It would be interesting to perform specific experiments to block vesicle release in the GRP.

2.3 *Pkd2* and *XHtr3* experiments unveil common roles for GRP morphogenesis

Remarkably, the knockdown of the type 3 serotonin receptor caused a very similar phenotype. When *XHtr3* was knocked down specifically at the GRP, this resulted in altered expression of LR markers and in loss of flow (Fig. 18 and data not shown). Importantly, knockdown of serotonin signaling only caused LR defects when targeted dorsally to the GRP and not ventrally (Fig. 18 and Tina Beyer, unpublished). As it has been argued that inhibiting the serotonin pathway – either by gain or loss of function

– would only be effective if injected in the ventral-right blastomere, this is important (Fukumoto et al., 2005). Such an injection scheme does not target the GRP. Another critical part are the pharmacological treatments which have been used to argue for an early function of serotonin for laterality development. As the *Xenopus* embryo has much yolk and a large blastocoele, it is more likely that the drugs used would enrich in the embryonic tissue; thus it was probably impossible to remove them from the rearing medium. If this was the case, the observed laterality defects upon pharmacological inhibition would most probably be caused by interfering with GRP morphogenesis between blastula stage and st. 14 (Schweickert et al., 2007; Shook et al., 2004).

GRP cells injected with either of the serotonin receptor 3 knockdown approaches resulted in loss of ciliation, altered cell sizes and cell shape (Tina Beyer, unpublished). Moreover both loss of XHtr3 and Pkd2 resulted in reduction of *dnah9* and *Xnr1* expressions at the GRP (Fig. 19, 20 and 27). A *serotonin receptor 3a* knockout mouse has not been analyzed for LR defects. The *Pkd2*-knockout was reported to have normal PNC *nodal* expression but as it was not focused on this domain and the published data seems to reveal a slight reduction in transcript (Pennekamp et al., 2002). In order to show that *Pkd2* and *XHtr3* work in a common pathway in *Xenopus*, epistasis experiments might be informative.

For *Xenopus XHtr3*-knockdown, it was further demonstrated by *β-gal* coinjection that cells adopt their correct developmental positions at the dorsal lip during gastrulation and at the GRP during flow stages, excluding apoptotic effects. Additionally, very characteristic changes in the expression of the *hey1* gene, a marker for hypochordal cells, indicated a change of either fate or specification/determination of GRP cells (see Fig. 19).

To unveil the mechanism by which knockdown interferes, analyses needed to be extended to late blastula and early gastrula stages. The determination of the fate to become prospective GRP cells should be manifested during these stages, when the dorsally positioned superficial mesoderm is induced. Concomitantly with this assumption, analysis of *Foxj1* expression on the dorsal lip epithelium of *XHtr3* morphants showed a strong reduction (Axel Schweickert, personal communication). The transcription factor *Foxj1* is known to be expressed in and essential for PNC, KV

and GRP ciliogenesis. Its expression on the dorsal lip during *Xenopus* gastrulation (very similar to *dnah9* during these stages; Fig. 07G) represent the future GRP cells before involution (Aamar and Dawid, 2008; Pohl and Knochel, 2004; Stubbs et al., 2008; Yu et al., 2008; Zhang et al., 2004). In this context, it would be interesting to see if a rescue experiment with a Ca^{2+}-ionophore would be successful in late blastula stages.

Remarkably, the homolog of the serotonin receptor 3 (and other serotonin components) was reported to be found in archenteron cells of the sea urchin *Lytechinus variegatus*, and pharmacological inhibition of Htr3 (or other serotonin signaling components) resulted in impairment of gastrulation (Buznikov et al., 2005).

These analyses revealed that *Pkd2* and *XHtr3* are important factors for the correct morphogenesis of the GRP – most probably during early gastrulation or even earlier. Accordingly, *XHtr3* was shown to be expressed on the dorsal half of gastrula stage embryos by RT-PCR and *Pkd2* could also be detected in the dorsal mesoderm of early gastrula stages by WMISH (Philipp Andre, unpublished and Fig. 21). As the *Pkd2* signal was clearly originating from the deep involuting layer that gives rise to notochord and somites, this indicates a possible non cell-autonomous function. One might speculate that a PC2 generated intracellular Ca^{2+}-signal in the deep layers would either induce an extracellular calcium wave or the activation of secreted molecules (e.g. GFs) that signaled towards the superficial mesoderm (Fig. 38A). Indeed, both dorsal extracellular and intracellular calcium signals were described to be important for gastrulation in *Xenopus* (Leclerc et al., 2003; Wallingford et al., 2001; Webb and Miller, 2006). As large amounts of *Pkd2* transcript were found in the animal half of cleavage stage embryos, another possibility would be that the protein of this maternally derived *Pkd2* is at least partially located in the SM during late blastula/early gastrula stages. Interestingly, a difference in the animal-vegetal border of *Pkd2* expression could be discerned (Fig. 21). Although it was not possible to determine the dorso-ventral axis (as these embryos were albinos), it is imaginable that this indicated an early dorsal but not ventral marginal expression that would be needed for induction of the superficial mesoderm during blastula stages. To clearly separate between maternal and zygotic function of Pkd2, a splice blocking morpholino should be used additionally.

To connect *XHtr3* and *Pkd2* to a signaling pathway, candidate gene expression patterns needed to be analyzed after knockdown. Besides the cilia factor *Foxj1*, interesting genes would be components of the early canonical Wnt or the TGF-β pathways, as those specify the dorsal fate of the deeper mesoderm and most probably also of the superficial mesoderm. Further, β-catenin dependent Wnt-signaling has been shown to indirectly induce convergent extension movements (via *Xnr3* induction), which are important for proper gastrulation movements (Kuhl et al., 2000; Yokota et al., 2003).
As Pkd2 is known to be a Ca^{2+}-channel and Htr3 is also permeable for these ions, the non-canonical Wnt/Ca^{2+} pathway may be also be involved (see also 2.4; Kuhl et al., 2000). Although a ventral mesoderm determination function has been shown during early blastula stages (Kuhl et al., 2001; Kume et al., 1997), later function for the superficial mesoderm might be possible.

2.4 *Pkd2*-knockdown interferes with convergent extension

Besides cyst formation in tadpoles, one intriguing dose-dependent effect of Pkd2 loss of function were blastopore or neural tube closure defects (Fig. 23), as well as axial shortenings (Fig. 24E). Anterior neural tube closure defects (anencephaly) are typically derived from ciliary defects whereas more posterior defects (spina bifida) and axial shortening are often PCP-mediated convergent extension phenotypes (Wallingford, 2006). The non-canonical Wnt (β-catenin independent) or PCP pathway is known to mediate CE movements in *Drosophila*, zebrafish, mouse and *Xenopus* (Keller, 2002; Simons and Mlodzik, 2008).

Pkd2 is zygotically expressed in the neuroectoderm and the involuting axial mesoderm, both of which are known to perform CE movements in *Xenopus* (Wallingford and Harland, 2001; Wallingford and Harland, 2002). Thus it might be necessary for one or both tissues for correct CE during gastrulation and neurulation. In mammalian nephric tubules, defects in PCP signaling were implicated in polycystic kidney disease (Fischer et al., 2006; Simons and Mlodzik, 2008); although no direct link has been made to *Pkd2* up to now.
More informative, *Pkd2* expression in gastrula stages is very similar to that of *Xbra* and *Wnt11* (Ku and Melton, 1993; Smith et al., 1991). *Xbra* is known to be expressed

in mesodermal tissues performing convergent extension movements and induces zygotic transcription of *Wnt11*, which in turn was demonstrated to be a regulator of CE via Dishevelled (Dsh), a main component of the PCP pathway (Tada and Smith, 2000). Inhibition of either of these genes resulted in impaired CE and could be rescued by a truncated Dsh-version, which can only signal through the PCP but not the canonical Wnt pathway. Remarkably, while *Wnt11* transcripts are found in the pre-involuting layers (superficial and deep) of the dorsal lip during mid-gastrula, *Pkd2* was found only in the already involuted layer directly adjacent to *Wnt11* (Fig. 21 and Ku and Melton, 1993).

Furthermore, a direct connection between intracellular Ca^{2+}-signaling during *Xenopus* gastrulation and CE was reported. Calcium waves were detected in the deeper marginal zone of early gastrula DMZ explants – thus in the same tissue where *Pkd2* is expressed. Pharmacological depletion of intracellular calcium stores prevented these calcium waves and inhibited CE in DMZ explants (Wallingford et al., 2001).

Therefore, it would be of great interest (1) to analyze *Xbra* and *Wnt11* expression after *Pkd2* knockdown and vice versa; (2) to analyze if *Pkd2*-knockdown would also inhibit CE in explants; and (3) to test if Dsh or a constitutively active calcium channel were able to rescue the *Pkd2*-MO phenotype.

2.5 xBic-C revealed similar and distinct functions as compared to Pkd2

The loss of function experiments with the *Xenopus* Bicc1 homolog (xBic-C) revealed a novel role for this RNA binding protein for GRP cilia polarization and establishment of LR asymmetry. The GRP phenotype and the resulting impaired flow confirmed the results of the *Bicc1*-knockout mouse described previously (Fig. 30 and Maisonneuve et al., 2009). Interestingly, *xBic-C* and *Pkd2* displayed shared and distinct characteristics. Both are expressed similarly in the *Xenopus* pronephros (Fig. 21, 29; Wessely and De Robertis, 2000) and have recently been demonstrated to interact in this tissue – with xBic-C regulating Pkd2 (Tran et al., 2009). Accordingly, shown in this study, epistasis experiments with lower doses of both morpholinos indicated also a common function for LR symmetry breakage (Fig. 31I). Moreover, both knockdowns resulted in very similar neural tube closure defects (cf. Fig. 23 and 30);

however, *xBic-C*-knockdown did not cause blastopore closure defects and showed axial shortenings at low frequencies (not shown). As *xBic-C* – besides in the GRP – is only expressed neuroectodermally and not in axial mesoderm, this mild phenotype seems to be caused by impaired CE in the neural tube (cf. Wallingford 02). The more drastic phenotype observed for the *Pkd2*-knockdown might therefore perhaps be caused by inhibition of CE in both the neural tube and the mesoderm.

The role of xBic-C for frog CE and GRP cilia polarization is in accordance with the function of its mouse homolog in promoting PCP signaling by inhibiting canonical function of Dishevelled in the PNC. It could be shown in cell cultures that Bicc1 co-localizes with cytoplasmic Dsh in P-bodies, which are known to be centers for RNA processing (Maisonneuve et al., 2009).

However, concerning the functions of Pkd2 and xBic-C for LR axis development, it emerges that both have slightly different roles. While xBic-C should be required during late gastrula and neurula stages for PCP signaling and cilia polarization (approximately between stages 12 and 18), Pkd2 seems to be required earlier.
Consequently, one might imagine that Pkd2 mediates superficial mesoderm specification via Wnt signals (canonical or non-canonical; Fig. 38A, F), afterwards xBic-C mediates GRP cilia polarization via non-canonical Wnt (PCP; Fig. 38D, F).

3. Leftward flow releases nodal of coco repression

After *Xnr1* could be excluded from being transported by the flow, it was analyzed if *Xnr1*, or alternatively its inhibitor *coco*, were dependent on leftward flow – i.e. if they are involved in the read-out of the left-biasing signal (cf. Fig. 38E). As it had been suggested for the mouse that *nodal* gets upregulated with the flow, this was a decisive issue. During these analyses, it could be clearly shown that *coco* but not *Xnr1* was dependent on flow – it is inhibited directly after the most effective period of flow (after stage 18; Fig. 32 and Pachur, 2007). More precisely, during early flow stages, expression of *coco* still slightly increased on both sides (due to an unknown inductive signal), but the left-sided increase was then inhibited by the flow. These results were independently confirmed by Melanie Eberhardt (2008). In her

experiments, she could also demonstrate that this left-sided inhibition was prevented by *dnah9* and MC-mediated loss of leftward flow (Eberhardt, 2008).

The epistasis experiments demonstrated that loss of coco on the left side rescued *dnah9*-MO-mediated loss of flow. Parallel experiments confirmed these results with methyl cellulose and showed that loss of leftward flow in combination with right-sided *coco*-knockdown only induced the nodal cascade in the right LPM (Getwan 09).
These experiments proved that *coco* is the primary target of leftward flow. Because nodal acts downstream of coco, release of nodal protein from coco repression should be the indirect functional consequence of flow.

Stronger right expression domains of *charon* or *Cerl-2* (the *coco* homologs) were published for medaka and mouse, respectively, and loss of function resulted in bilateral *nodal* induction in the LPM. The right-sided nodal inhibition thus seems to constitute the conserved function for these genes. It would therefore be interesting to perform similar loss of fluid-flow and Cerl-2 function (or charon in fish) experiments in mouse and the fish species. Indeed, although not shown in detail, flow inhibition in medaka apparently resulted in prevention of stronger right-sided expression of *charon* (Hojo et al., 2007).
Most of the mouse embryos of the *Cerl-2* knockout displayed bilateral expression of *nodal* in the LPM, but suprisingly, 40% showed normal left expression (Marques et al., 2004). Nevertheless, crossing the *iv*-mutant mouse with the *Cerl-2*-knockout should result in a random activation of LPM marker genes as well as in a random inhibition of *Cerl-2* at the PNC – namely left, right, bilaterally or without inhibition.
This finally predicts that repression of a nodal inhibitor is a conserved feature for leftward flow-mediated symmetry breakage in vertebrates – and moreover, also valid downstream of asymmetric cell migration-based symmetry breakage in the chicken embryo (Gros et al., 2009).

Although with these results the consequences directly downstream of leftward flow seem well-defined, the mechanism how coco is inhibited remains unclear. Only about 50% of wild type embryos show a clear right-elevated expression of *coco* at the GRP (Fig. 32). This is in contradiction to over 95% of wild type *Xenopus* embryos that normally express LR marker genes only in the left LPM (e.g. Fig. 33-36). Thus

transcriptional regulation seems not to be the sole mechanism. A second possibility would be a post-translational control of the coco protein. But as such a process in turn could not explain the observed right bias on the mRNA level, this also appears unlikely. A third possibility would be that left-sided *coco* is controlled by a post-transcriptional mechanism, which could lead to both mRNA and protein reduction.
These results strongly indicate a flow-induced process of inhibition or active degradation of *coco* mRNA on the left side (Fig. 38F).

Promising candidates for such a process would be microRNAs (miRNAs), small (~22bp) non-coding mRNAs that are well known to be post-transcriptional gene regulators. They influence mRNA translation by binding the 3'UTR-sequence of their target mRNA and thereby induce either translational inhibition or destabilization (Bushati and Cohen, 2007; Filipowicz et al., 2008). In *Xenopus*, some approaches to identify miRNAs have already been conducted and candidate expression patterns were analyzed (Walker and Harland, 2008; Watanabe et al., 2005). Such expression analyses could be screened for promising signals in or near the GRP. If a miRNA specifically inhibited *coco* on the left side, then it could be expressed bilaterally and subsequently be flow-activated on the left (e.g. due to induction by or co-function of another factor). Alternatively, its expression might be induced or increased on the left side by leftward flow. If this was indeed the case, then LR asymmetries in expression patterns of candidate miRNAs would be expected in a relative small time window during and shortly after flow stages.
Once a possible miRNA is identified, loss and gain of function studies could be performed very similar to those shown here. Left miRNA knockdown or sequestering should prevent *coco* inhibition, and loss of flow might be rescued by injection of the miRNA, as putatively seen by decrease in *coco* expression and induction of marker genes on the left side. Two of such detailed analyses were, for example, performed with miRNAs specifically regulating nodal signaling and thus the formation of the Spemann organizer (Martello et al., 2007; Rosa et al., 2009).

4. Hierarchical integration of LR components

The present data of a clear hierarchy for several components represents a starting point to analyze other less clear components. For example, together with structural analyses (e.g. SEM or IHC), such testable components may thereby be categorized as necessary for GRP morphogenesis, for GRP function, for *coco* inhibition, for Xnr1 stabilization at the GRP or finally for activation and maintenance of the nodal cascade in the LPM.

4.1 Pkd2 additionally impaired *Xnr1* expression

If *Pkd2*-knockdown only interfered with leftward flow due to incorrect GRP morphogenesis, then a combined injection with the *coco*-MO should have rescued the obtained phenotype and activation of *Pitx2c* in the LPM should occur. In contrast to the clear rescue obtained in a similar setup with *dnah9*-MO or MC in combination with the *coco*-MO (Fig. 31), the knockdown with *Pkd2*-MO could only partially be rescued (Fig. 34). These results indicate a broader function, which is in agreement with the efficient inhibition of *Xnr1* expression at the GRP in *Pkd2*-MO injected specimens (Fig. 27). As it could recently be shown by detailed comparative expression analysis of *Xnr1* followed by SEM analysis that the *Xnr1* expressing cells are the ciliated somitic GRP cells (Isabelle Schneider and Tina Beyer, University of Hohenheim, personal communication), the observed loss of *Xnr1* expression seems to be part of the morphogenesis defect caused by loss of Pkd2. Thus, artificial inhibition of coco seems not to be sufficient to release enough Xnr1 protein for activation of the cascade in the LPM in this case. In this context it would also be of interest to analyze *coco* expression in *Pkd2* morphants to reveal if the knockdown affects *Xnr1* specifically, if the cells change their transcriptional pool more broadly or if they disappeared altogether. Additionally, *Pkd2*-knockdown could also inhibit *xBic-C* and consequently indirectly *Xnr1*. Alternatively, it might still be possible that Pkd2 has a second function to generate a calcium-signal in the somitic GRP cells or the presomitic mesoderm to activate nodal signaling in the LPM (see also below).
Due to the comparable phenotypic outcome of the *XHtr3*-knockdown, it would be also interesting to perform combinatorial knockdown experiments with *coco*.

4.2 xBic-C reveals a complex role for LR development

Unilateral *xBic-C* morphants clearly showed that xBic-C was only necessary on the left side of the GRP and not on the right or in the left LPM for nodal signaling (Fig. 30). Remarkably (although not significant), dorso-lateral marginal injections were slightly more effective than dorsal-marginal injections. The lateral lineage targets the lateral part of the GRP (somitic and perhaps hypochordal GRP) and the presomitic

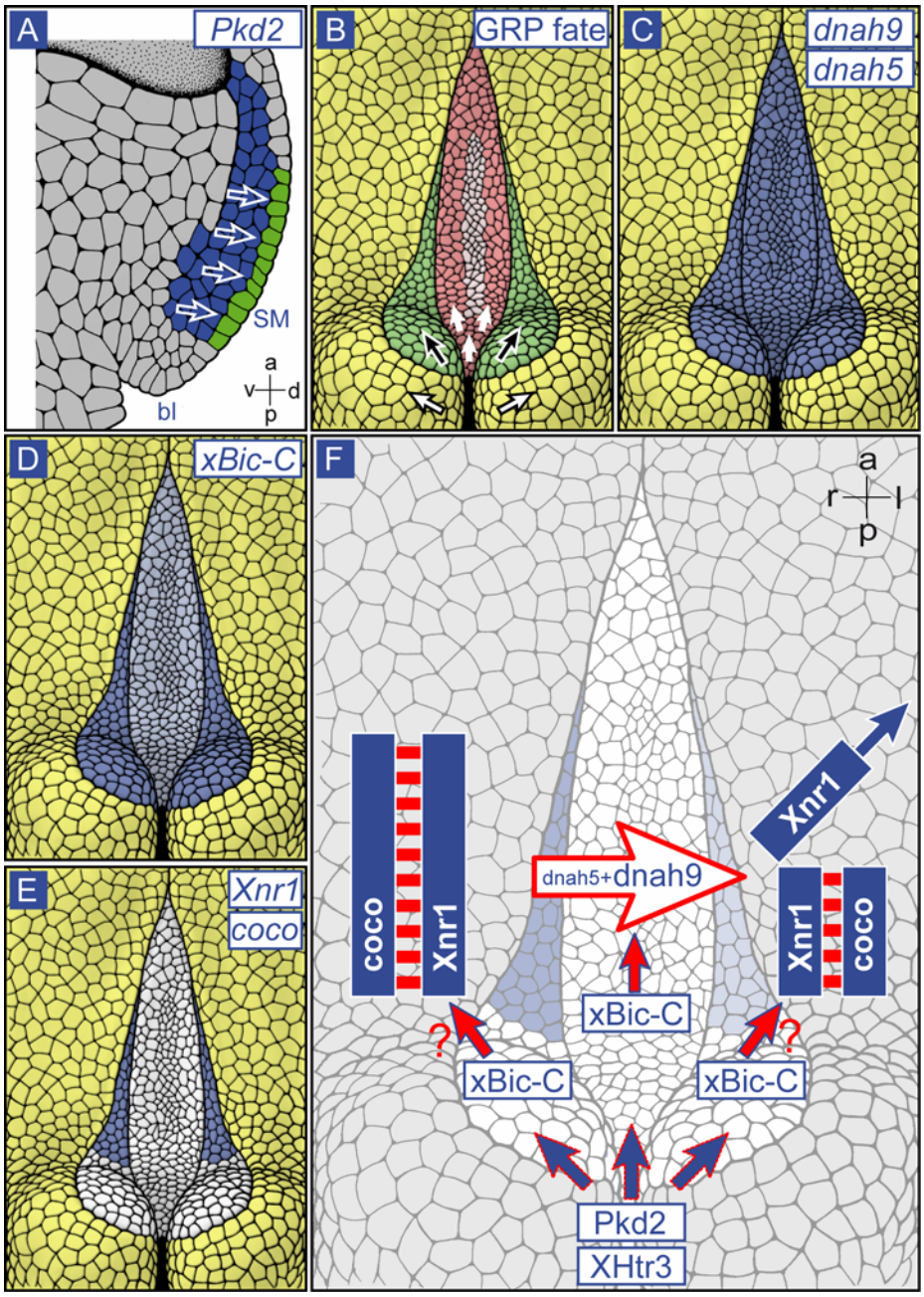

Fig. 38 Proposed temporal and spatial functions of the analyzed LR pathway components.
(A) Pre-/early gastrula expression of *Pkd2* in the deep marginal zone might be involved in correct induction of the superficial mesoderm (green) and thus GRP morphogenesis. Sagittally bisected gastrula at ~st.10. **(B)** Fates of the GRP sub-regions and injection scheme used in this study. Dorsal-marginal injections (white arrows) targeted the center of the GRP with the hypochordal precursor cells (dark red) encompassing the notochordal precursors (light red). Dorso-lateral injections (white-framed

black arrows) targeted the somitic precursors (green) and ventral injections (black-framed white arrows) the endoderm outside the GRP. **(C-F)** Expression patterns and proposed spatial function of the components during neurula stages. *dnah5* and *9* are expressed in the whole GRP (C), *xBic-C* strong in the somitic and weaker in the notochordal and hypochordal lineage (D) and *coco* and *Xnr1* are co-expressed in the anterior part of the somitic GRP cells (E). Please note divergent expression in the posterior part of the somitic GRP. (F) Spatial interaction network of the LR components in the final phase of flow-based symmetry breakage (~st.18). XHtr3 and Pkd2 are involved in GRP morphogenesis pre-neurulation. xBic-C is required (1) for cilia polarization, flow and (2) possibly for *Xnr1* stabilization. dnah5 and 9 are needed for cilia motility and flow. Coco binds Xnr1 to prevent bilateral marker gene induction; both are balanced before flow. Leftward flow releases Xnr1 from coco repression, probably by post-transcriptional inhibition of *coco* RNA. Xnr1, in turn, might then activate left marker genes directly or indirectly by an unknown mechanism. Weaker left *coco* expression is indicated in blue in the background. Arrows indicate biased positive or inductive signals.
All figures were prepared with drawings adapted from a SEM picture of a perfectly zoned GRP (SEM provided by Tina Beyer). Note that only superficial tissues are shown. Orientation for GRPs in (B)-(F) indicated in (F). Blue, expression patterns; yellow, endoderm. a, anterior; bl, blastopore lip; d, dorsal; l, left; p, posterior; r, right; SM, superficial mesoderm; v, ventral

mesoderm (cf. Fig. 17). In contrast, when the *dnah9*-MO was injected accordingly – it only influences ciliary motility and not cell fate or morphology – a significantly smaller amount of specimens displayed LR defects than those dorsal-marginally injected (Fig.17). These differing outcomes may thus not be explained just by impaired leftward flow due to cilia polarization defects but by a more complex role of xBic-C during symmetry breakage.

xBic-C is expressed weaker in the middle of the GRP (notochordal and hypochordal regions) and very strong laterally (somitic region) and in the deeper presomitic paraxial mesoderm (cf. Fig. 38D). This paraxial expression extends significantly more anteriorly than the GRP and stays strongly activated at least until stage 22 – considerably after disappearing of the GRP and activation of nodal signaling in the LPM (Fig. 29).

As *xBic-C* showed no sign of left or right bias in its expression domain (Pachur, 2007) but was clearly necessary on the left side, several possibilities remain, which are discussed below.

One option is that xBic-C repressor function would either be activated or that it was itself involved in activation of a miRNA repressor, both only on the left to suppress *coco* flow-dependently. In each case, a second candidate is needed, either as an activator or as a co-factor, because xBic-C acts cell-autonomously and may therefore itself not be transported by the flow. A missing co-factor would be in accordance with the right-sided gain of function of xBic-C that did not result in right induction of the LR

cascade (Fig. 30). In *Drosophila*, the Bicc1 homolog was shown to directly repress *oskar* mRNA during AP axis development, an observation that would favor a repressive function (Mahone et al., 1995; Saffman et al., 1998).
Furthermore, xBic-C could also be a flow-independent stabilizing or competence factor for *Xnr1* and/or *coco*. It could be shown that *Xnr1* expression in *xBic-C*-morphants is markedly reduced or absent at the GRP but that of *coco* is only weakly influenced (Fig. 31). Therefore, this would favor a stabilizing regulation of *Xnr1* mRNA (or perhaps its transcriptional Smad activators), which would again be in conformance with the ineffective right-sided gain of function.
In early development, *coco* is expressed more animally, and reciprocally, *xBic-C* and *Xnr1* are found more vegetally in cleavage and blastula stages; in addition Xnr1 and xBic-C are both involved in endoderm induction (Bell et al., 2003; Osada and Wright, 1999; Wessely and De Robertis, 2000). Interestingly, the authors of this study already suggested xBic-C to function either as a repressor of an ectodermal determinant (like *coco*) or as an activator of an endodermal determinant (like *Xnr1*).

As all three factors, *xBic-C*, *coco*, *Xnr1* are co-expressed at the GRP, the actual xBic-C interacting part is difficult to discern. Therefore, epistasis experiments were performed. Remarkably, although *xBic-C* morphants were shown to have reduced *Xnr1* expression at the GRP (Fig. 31), left-sided inhibition of *xBic-C* could nearly fully be rescued by coinjection of the *coco*-MO. This indicated that *coco*-knockdown is very efficient and thus there should be enough Xnr1 protein left to induce the left cascade. Further, the triple knockdown with additional inhibition of *Xnr1* again led to nearly 100% loss of *Pitx2c* induction (Fig. 35). In a next step, right-sided, flow-independent knockdowns were chosen. In this approach, the coinjection of *xBic-C*-MO prevented *coco*-MO-induced right induction of *Pitx2c* in about 35% of the embryos. This result confirmed a second function for xBic-C – independent of flow. Furthermore, it seems unlikely that xBic-C is involved in flow-induced repression of *coco* on the left.
Finally, this leaves open only one possibility, namely the destabilization of *Xnr1* due to loss of xBic-C function. This should account for the 35% of the embryos that did not activate nodal signaling in the right LPM. Although this seems to be the most-likely explanation, more detailed analyses are needed for verification.

Conspicuously, a large amount of *xBic-C* transcript is detected in the paraxial mesoderm long after the first activation of nodal signaling in the LPM (see also above). This then raises the question if it is needed to stabilize *Xnr1* for longer – to ensure correct induction of the LPM expression. Then, xBic-C could represent a Xnr1 co-mediator for the direct connection of (*coco*-repressive) leftward flow sensing and transfer of the signal to the LPM. In the light of this reasoning, it is also of interest that *Drosophila* Bicc1 was shown to coimmunoprecipitate with several mRNAs that are associated with cytoskeletal regulation processes of the actin and microtubule cytoskeleton (Chicoine et al., 2007). As somitic GRP cells need to undergo cytoskeletal rearrangements to be able to enter the presomitic mesoderm – and may thereby help to promote the left signal – this could also offer an interesting link.

4.3 Paraxial Xnr1 is released of coco repression on the left side

The different epistasis experiments all showed that Xnr1 acts downstream of the other components (Figs. 33-36). Together with the fact that Xnr1 is not transported by the leftward flow, this results in the conclusion that the release of Xnr1 from coco-mediated repression represents the final interpretation of the flow (Fig. 38F). Xnr1 should therefore be the direct or indirect activator of nodal signaling in the LPM. If it does not simply diffuse into the LPM, then there needs to be a mechanism to bridge the tissue of the presomitic and intermediate mesoderm. There are several transfer routes a molecule might take to reach the LPM, intracellular through the mesoderm or endoderm, or extracellular through the archenteron or between the germ layers (Blum et al., 2009a). The external route has been recently excluded in the mouse embryo. A further possible mechanism would be a GAG-mediated transfer of Xnr1 itself along the extracellular matrix between mesoderm and endoderm. But this has only been shown for mouse and awaits to be tested in frog (Oki et al., 2007).
As already mentioned, the calcium signal published for several species at the margin of the PNC or KV might also be important in the presomitic mesoderm as a relay mechanism to bypass the presomitic mesoderm. In the mouse, the published calcium-signals on the left side do not appear to be at the margin of the PNC but rather more laterally in the mesoderm or endoderm; perhaps even omitting the nodal expressing cells at the edge of the PNC (Hadjantonakis et al., 2008; McGrath et al., 2003).

It would be interesting to test if there was a calcium signal in frog after flow stages – and if so, whether it was in the presomitic mesoderm as postulated. In support of this notion, *Pkd2* was expressed in the very posterior presomitic mesoderm and the lateral circumblastoporal collar (Fig. 21). However, the actual mechanism of nodal activation in the LPM needs to be addressed.

5. Evolutionary considerations about leftward flow

5.1 Basal vertebrates: facts about sturgeons

With the LR framework gained by the presented results and the now available knowledge about the homologous epithelial structures that generate a leftward flow in different species, I like to enclose some evolutionary considerations. Recently – since we have known that leftward flow is widespread among vertebrates – we have extended our efforts to explore the phylogenetic origins of a leftward flow-based symmetry-breaking mechanism (Blum et al., 2009b).

The first remarkable finding was that it had been published already in 1993, that sturgeons possess a GRP at the archenteron roof during neurula stages, very similar to amphibians (Bolker, 1993). Though originally not searched for, one can indeed recognize single cilia on the sturgeon's GRP cells (Blum et al., 2009b). This is an inconspicuous finding that implicates a strong statement. Sturgeons belong to the chondrostean fish, very basal ray-finned fish and thus very basal vertebrates, and display a mode of development – especially of gastrulation – that is very similar to that of amphibians (Bolker, 1994; Collazo et al., 1994; Cooper and Virta, 2007).
Therefore, with this mode of early development and a conserved GRP, we may conclude that the ciliated epithelium represents the ancestral form of symmetry breaking mechanism in vertebrates. Though no established model organism, it would be worth to explore a leftward flow in sturgeons and the conserved left nodal cascade. Thus, in the following, some theoretical considerations about the origin of leftward flow in deuterostomes will be presented.

5.2 Primitive chordates: predictions for Amphioxus

An asymmetric nodal cascade was described in the tunicates *Ciona intestinalis*, *Botryllus schlosseri* and *Halocynthia roretzi* (Morokuma et al., 2002; Tiozzo et al., 2005) and the cephalochordate *Branchiostoma* (Amphioxus; Boorman and Shimeld, 2002; Yu et al., 2002). Here I like to discuss amphioxus, as it is considered to represent an ancestral state of chordate evolution, while the more derived tunicates have recently been grouped together with the vertebrates (Bourlat et al., 2006; Delsuc et al., 2006). As in vertebrates, *nodal* is first expressed in the amphioxus organizer (dorsal lip; Yu et al., 2002; Yu et al., 2007). During gastrulation, this domain invaginates and simultaneously splits, so that in the 10 hr neurula a left and right domain is observed, separated by notochordal mesoderm (Yu et al., 2002). The *nodal* domain represents the paraxial mesoderm, derived from superficial cells like in vertebrates (Fig. 39; cf. Fig. 02). This setting thus is quite reminiscent of a vertebrate laterality coordinator, i.e. a bilateral *nodal* domain within the archenteron, encasing notochordal mesoderm laterally and bordered by endodermal cells (Figure 39A). Therefore, I like to predict that the notochordal cells harbor the laterality coordinator and possess polarized cilia which produce a leftward flow. Cilia have been described on the dorsal lip as well as on archenteral cells at late gastrula (Hirakow and Kajita, 1991). About 90 minutes after bilateral induction of *nodal*, the right-sided domain diminishes and eventually disappears (Yu et al., 2002). This should be the result of a leftward flow. As a BLAST search in the database revealed the existence of a *Cerberus* homolog gene in Amphioxus (accession: ACF94996), I like to suggest that this might be expressed (temporarily and spatially) very similarly to the bilateral *nodal* domain. Further it should be reduced on the left side – simultaneously or just before *nodal* gets asymmetrically indeed. Afterwards, the left-sided domain spreads in due course into all three germ layers as well as along the anterior-posterior axis, providing cues for later asymmetric morphogenesis.

5.3 Deuterostomes: speculations about sea urchins

Echinoderms and hemichordates are considered to constitute the monophyletic group of the Ambulacraria, based on molecular and morphological criteria (Bourlat et al., 2006; Delsuc et al., 2006; Smith, 2008; Swalla, 2006). A nodal cascade has been

described in sea urchins (Duboc and Lepage, 2008; Duboc et al., 2005) and thus should also be present in hemichordates.

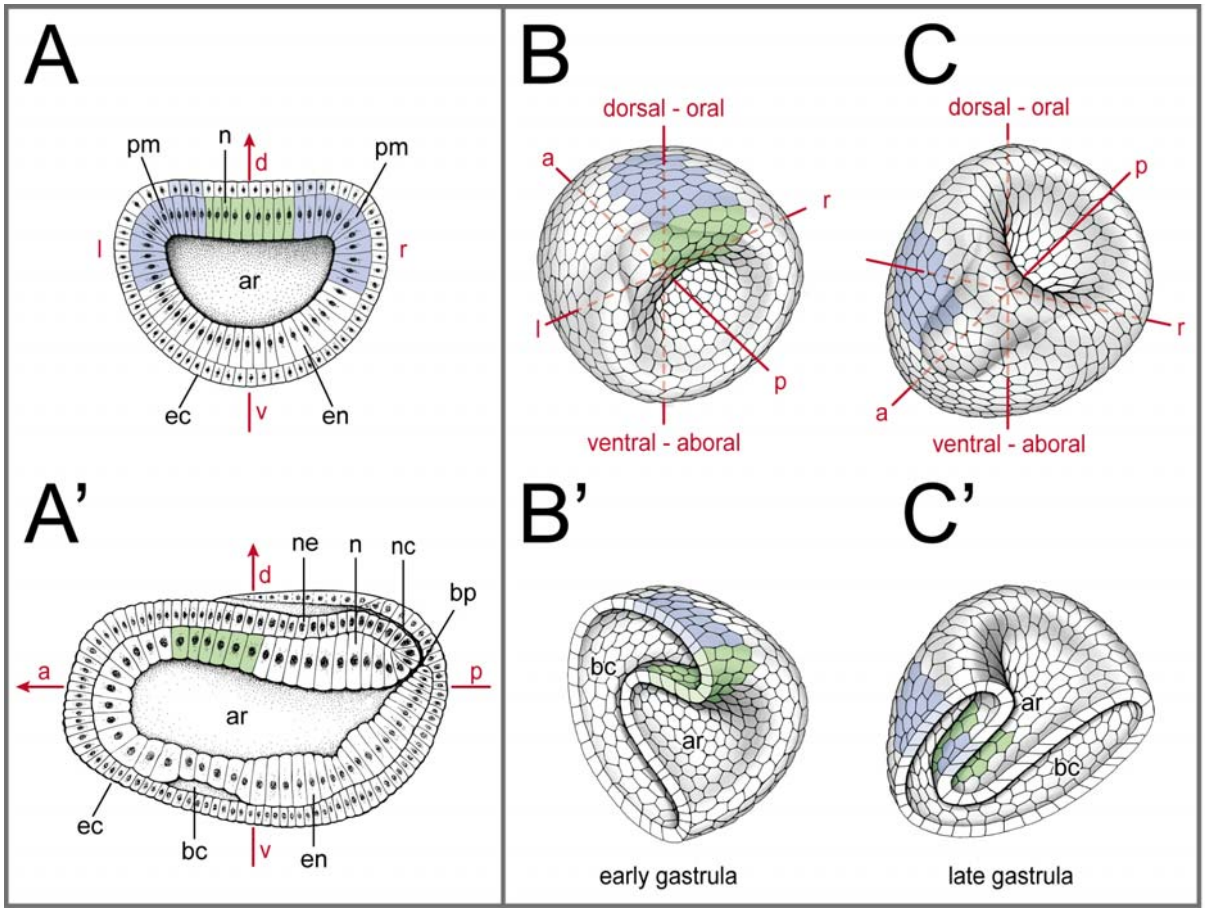

Fig. 39 Amphioxus and sea urchin
(A) Amphioxus. Schematic drawing of a neurula stage amphioxus embryo cut transversely (A) and mid-sagitally (A'). The bilateral *Nodal* expression indicated in blue (A) predicts an in-between GRP in the archenteron (green in A, A'). **(B, C)** Sea urchin. 3D schematic drawings of early (B, B') and late (C, C') gastrula sea urchin embryos in whole-mount (B, C) and bisected along the dorso-ventral (B') and LR (C') axis, respectively. Proposed right half shown in (B'), and oral half shown in (C'). Early (dorsal / aboral) symmetric *Nodal* organizer domain in (B) and (B') and late asymmetric expression domains in ectoderm and archenteron in (C) and (C') are indicated in blue. The supposed position of a field of polarized ciliated cells is indicated in green. The conventional echinoderm body plan is inverted to account for (a) conserved left asymmetry of *Nodal* expression; and (b) organizer gene expression on the dorsal side. Expression domains are indicated according to (Yu et al., 2002 - A), (Duboc et al., 2004 - B, B') and (Duboc et al., 2005 - C, C'). Schemes were redrawn from (Yu et al., 2002 - A) and (Conklin, 1932 - A'). a, anterior; ar, archenteron; bc, blastocoel; bp, blastopore; d, dorsal; ec, ectoderm; en, endoderm; l, left; n, notochord; nc, neuroenteric canal; ne, neuroectoderm; pm, paraxial mesoderm; r, right; v, ventral.

Nodal expression in sea urchins is seen in the oral ectoderm of the blastula/gastrula. At late gastrula, an asymmetric domain appears at the tip of the archenteron in a few cells, mostly (i.e. in about 70 % of cases) displaced to the right side (Fig. 39C, C'). Shortly thereafter, the ectodermal domain gets displaced to the right as well (Duboc et al., 2005). But in contrast to Amphioxus, no *Cerberus* homolog could be found by a BLAST search. As echinoderms never show a bilateral *nodal* domain (and have

never developed a true head), this might not be necessary. The archenteral tip cells should be mesodermal in character, as they give rise to the coelomic sac which splits into the two pouches. If there was a flow, which we like to speculate, it should precede the asymmetric induction of *nodal* in the archenteron and be directed towards this domain. Another reason for this speculation, besides the mesodermal nature of surface-derived archenteron tip cells, is the fact that monocilia have been found on archenteral cells in a crinoid, the feather star *Comanthus japonica* (Holland, 1976). Additionally, very recently we could clearly confirm archenteral cilia for *Paracentrotus lividus*, the common sea urchin, which was used for the main LR studies (our unpublished data; cf. Duboc et al., 2005).

The right-sided nature of *nodal* expression might be considered a non-conserved aspect of LR asymmetry. If, however, asymmetric *nodal* expression was conserved and left-sided like in chordates (as depicted in Fig. 39C and C'), the sole complication to the sea urchin body plan would be that the mouth in the larva would open on the dorsal instead of the ventral side (cf. Duboc and Lepage, 2008). This possibility seems attractive, as dorsal/organizer markers consistently are expressed in the oral ectoderm, i.e. *nodal*, *lefty*, *Brachyury* and *Goosecoid* (Duboc and Lepage, 2008; Duboc et al., 2005). Therefore, the archenteral cells on the oral side, derived from oral/dorsal blastula cells, could be the cells which become polarized and produce a vectorial flow. Alternatively, if all archenteral cells were ciliated and polarized, these cells could be secreting a morphogen. This would correspond perfectly well with the situation in the vertebrates, where the superficial mesoderm cells, derived from the dorsal side, polarize posteriorly following their invagination onto the dorsal side of the archenteron (Shook et al., 2004).

As new model organisms are being established, and more sophisticated techniques become available for live imaging of tiny embryos and fragments thereof, these proposals may soon become accessible to experimental examination. For protostomes, asymmetries have been described and new ones continue to be found until today but no sign of a flow-based symmetry breakage was reported (Okumura et al., 2008; Speder et al., 2007). Surprisingly, in contrast to what was suggested before, a first non-deuterostome *nodal* homolog has been detected in snails – i.e. in lophotrochozoans (Grande and Patel, 2009).

This finding suggests that flow arose in the deuterostomes and raises the question, why and how polarized ciliation and leftward flow where recruited to the symmetry breaking mechanism. It will be instrumental to identify further components of flow-mediated symmetry breakage in lophotrochozoans and ecdysozoans like snails, annelids or arthropods.

Material and Methods

Xenopus laevis embryological procedures

Obtaining of *Xenopus* embryos

For embryonic experiments, *Xenopus laevis* females were stimulated for ovulation by subcutaneous injection with 50µl of human chorionic gonadotropin (hcg) one week prior to oviposition. About 10-12h before desired time point, females were injected again subcutaneous with 400-700µl of hcg. The following day the spawning was supported by manual massage.

In vitro fertilization

In vitro fertilization was done with sperm extracted from *Xenopus* testes isolated from adult males and kept in 1xMBSH at 4°C. For fertilization about 1-2mm^3 of the testis was placed in 1ml 1xMBSH, macerated and subsequently added to the eggs. After 1-5min waiting and subsequent addition of DDW, the fertilization began and about 40min later eggs were incubated for max. 7min in 2% cystein (pH 7.99) to be dejellied. The cystein solution was then removed by several washing steps in 0.1xMBSH. If injection should follow, eggs were again washed and further kept in 1xMBSH in Petri dishes.

Microinjections

For the injection the embryos were transferred to 2% Ficoll solution in a Petri dish coated with agarose. Embryos were injected at the 4-8 cell stage using a Harvard Apparatus setup with a thin glass-needle (5-10µm diameter). Drop size was calibrated to about 7-8 nl / injection. Lineage tracer RNAs were prepared using the Ambion message machine kit and diluted to a concentration of about 50-100 ng/µl. In all experiments only 4-8 cell embryos with a clear dorso-ventral segregation of pigment were used for injections (Danilchik and Black, 1988; Klein, 1987) and only correctly targeted specimens (controlled by co-injected lineage tracer GFP, RFP, or rhodamine dextran: 0.5-1.0µg/µl) were processed for further analysis (cf. Fig. 14+17).

Fixation

For WMISH:
Embryos were cultivated to the stage of interest and then transferred into 4ml of freshly prepared 1xMEMFA for fixation. After incubation for 1-2h at room temperature or overnight at 4°C embryos were washed with ethanol. 30min later the embryos were washed again in ethanol and stored at -20°C
For WMIHC:
Embryos were cultivated to the stage of interest and then transferred into 4ml of freshly prepared 4% PFA for fixation. After incubation for 1h at room temperature embryos were washed with several times with PBS-.

Knockdowns using specific morpholinos

Morpholinos are gene-specific, synthetic, stable, single-stranded antisense-oligonucleotides that bind the complementary mRNA of the gene of desire to prevent translation or splicing of the latter (Gene Tools, LLC, Philomath, USA). After delivery

into the cell, they bind to the mRNA and specifically inhibit translation of the mRNA. This causes a gene knockdown. As knockdown efficiency and endogenous gene activities differ, concentration for every MO was determined individually. Morpholinos were used at 0.25-8 pmol/embryo (i.e. injected at a concentration between ~30 and ~500µM) as indicated.
Specific morpholinos used in this work are:

dnah5-SB-MO:	5'-TGTACAGACCTGATTACCCTCTAGA-3'
dnah9-SB-MO:	5'-CATAGGAATCAACTCACTTTTTCTC-3'
dnah9-AUG-MO:	5'-GGTCACGTTTTGGAGGTGCAGTGGC-3'
Pkd2-MO:	5'-GGTTTGATTCTGCTGGGATTCATCG-3'
xBic-C-MO1:	5'-TAGACTCGCACTGAGCCGCCATTCT-3'
xBic-C-MO2:	5'-CCATTGTGCTACTGCCGCCGCTAAC-3'
Htr3a-MO:	5'-GTGTTGGGAACATTTTCCTTAGATC-3'
Htr3c1-MO:	5'-GATGTTAAGTGTAGAGTCATTCTGG-3'
Htr3c2-MO:	5'-ACAGATCAGAGTGTTTGCTTTGTCA-3'
coco-MO:	5'-CTGGTGGCCTGGAACAACAGCATGT-3'
Xnr1-MO:	5'- GCTGTCAGAAATGCCATGCTTGCAC-3'

For control-injections to exclude injection artifacts either the standard control- or the random control-morpholino were used.

Video-tracking of tadpoles

Embryos were unilaterally injected into the left or right ventral animal blastomere at the 4-8 cell stage with 1 pmol *dnah9*-MO and lineage tracer DsRed (100 ng/µl) to target the epidermis. Specimens were raised to stage 32 on 1% agarose dishes in 0.1 x MBSH. At this stage, the ciliary based motion of the embryos was fast and robust in wildtype tadpoles (data not shown). As embryos at this stage lie on their sides, it was possible to test the motion of either side individually. To circumvent muscle contractions (active swimming), which would compromise cilia-based motion; embryos were anesthetized with benzocaine (Sigma). After validation of unilateral lineage tracer expression, embryos were placed individually in agarose-coated Petri dishes with 0.1 x MBSH + benzocaine. Six Petri dishes were analyzed in parallel (cf. Fig. 13B) and embryo motion was recorded for 10 min at 25 fps using a Sony DCR-HC23E CCD camcorder and VirtualDub (http://www.virtualdub.org). Subsequently, each embryo was flipped over to the other side and motion was recorded likewise. Movies were automatically analyzed by a custom-made video tracking software written in C# (developed by D. Shcherbakov, Institute of Zoology, University of Hohenheim). The procedure comprised the following steps: (1) the positioning of the embryo was analyzed via contour detection in each frame; (2) the center of the embryo (center of mass) was calculated and its trajectory over the experimental time was computed; (3) raw data were imported into MS Access database (Microsoft Corporation) allowing for the calculation of mean velocity of embryo sides. Embryos which showed no movements or movements which were interrupted artificially (e.g. caused by unevenness of the agarose) were excluded from the analysis. The uninjected side served as internal control. Therefore determination of statistical significance was performed by Wilcoxon matched pairs test (Statistica 6.1 – StatSoft Inc.). Protocol as described in Vick et al. 2009.

Flow analysis

Frog embryos were raised to stage 16–18 in 0.1xMBSH, dorsal explants were prepared, mounted ventral side up in a Vaseline ring drawn onto a glass slide that served as adjustable spacer. The coverslip was fit to the height of the explant to hold it in place. The extracellular flow at the GRP was recorded following addition of fluorescent latex beads (500nm FluoSphere®, Molecular Probes (Blum et al., 2009)) in dilution of 1:2500 in 1xMBSH as described (Schweickert et al., 2007). Movies were acquired on a Zeiss AxioMot2 mounted with the CCD AxioCam Hsc (Zeiss) via AxioVision 4.6 under the green fluorescent channel at 2 fps.
For the analysis, particles were tracked by the ImageJ plugin ParticleTracker (Abramoff et al., 2004; Sbalzarini and Koumoutsakos, 2005) and qualitative and quantitative measurements were calculated with a custom-made program (Thomas Weber, University of Hohenheim) written in statistical-R (R-Development-Core-Team, 2008).
Flow was analyzed as follows: trajectories with less than 10 frames duration were excluded because necessary information was not gained on short tracks. Masks covering the GRP or GRP halves were introduced to calculate the flow parameters of trajectories above these areas exclusively. To exclude particles not driven by flow (Brownian motion), a Rayleigh's test of uniformity was performed on each trajectory to tell particles with directed movement from random particle motion. Particles were considered ‘directed’ when they reached a mean-resultant-length (rho) of >0.6. To determine the general direction of flow, a second Rayleigh's test of uniformity was performed comprising the mean angles of ‘directed’ particles above the GRP.
To visualize particle movement, gradient-time-trails (GTT) for each trajectory meeting the above criteria were produced. GTTs represent a span of 25sec of particle coordinates that is colored time-dependently according to the color-gradient green (start of time span, 0sec), yellow (mid of time span, 12.5sec), red (end of time span, 25sec). The time span is visualized by the color gradient for each analysis respectively (cf. figure legends). Flow analysis and visualization software was developed by Thomas Weber (University of Hohenheim).

Videographic cilia imaging
Procedure was as described in (Vick et al., 2009): Fluorescent in vivo imaging of epidermal and GRP cilia motility was performed following PACRG::eGFP (TW and MB, unpublished) injection. Time-lapse sequences were recorded on a Zeiss Axioskop equipped with a CCD camera (AxioCam Hsm, Zeiss) with AxioVision 4.6 (Zeiss) at 62 frames per sec (fps).

Reverse Transcriptase Polymerase Chain Reaction (RT-PCR)

Isolation of RNA
Total RNA of desired stages or injected embryos was extracted by phenol-chloroform extraction and ethanol precipitation with Peqlab peqGold Trifast solution following the peqGold Trifast protocol. 1ml of the solution was used for the isolation of RNA of about 3 embryos. RNA was eluted in 25µl sterile DDW, measured photometrically and stored at -80°C.

First strand cDNA synthesis
cDNA was synthesized from total RNA preparations by reverse transcription using MMLV Reverse Transcriptase. A standard protocol started with 1µg of total RNA to which 0.5µl of random hexamers was added and filled up with sterile water to a total volume of 14µl. The solution was heated to 70°C for 5min melting secondary structures within the template. Further snap cooling on ice prevented these structures from reforming. The reagents were then supplemented with 5µl 5x M-MLV Reaction Buffer, 1.25µl 10mM dNTPs, 1µl (200units) of M-MLV RT and filled up to a volume of 25µl. After an initial incubation for 10min at room temperature, the reaction was put to 50°C for another 50min to complete first strand synthesis. The reaction was stopped by a final step at 60°C. The cDNA was stored at -20°C.

Standard PCR protocol
For a 25µl PCR reaction 1µl of previously prepared template cDNA was mixed with 2mM dNTPs, 1U of Taq DNA polymerase, 5µl 5x Buffer, 1µl of each forward and reverse primer at a concentration of 10µM and filled up to 25µl with sterile double distilled water (DDW). A standard PCR cycling program started with (1) 1' at 95°C, followed by (2) 30'' at 95°C, (3) 30'' or 1' at a primer pair specific annealing temperature and (4) 1' at 72°C. Steps (2) to (4) were repeated for 35 times before the reaction was (5) stopped and kept in the cycler at 8°C. Step (1) and (2) yield a denaturation of the double-stranded template DNA, step (3) allows hybridization of the primers to the single-stranded DNA and during step (4) the Taq polymerase elongates the sequences at the primer's 3' end. For the detection of gene expression using Reverse Transcriptase-PCR (RT-PCR) the steps (2) to (4) were repeated between 28 and 33 times, as indicated.
If the product was intended to be further amplified in bacteria (for cloning), an extra 10min at 72°C were added after 35-40 cycles to make use of the Taq Polymerase's Terminal Transferase activity, that adds an extra deoxyadenosine onto each 3' end of already existing double-stranded PCR product. This creates a single 3'-A overhang that can be utilized for ligation into a cloning vector.

Oligonucleotides and PCR conditions
For the design of primers, sequences were obtained either from NCBI EST database or by BLAST search of the *Xenopus tropicalis* genome (http://www.jgi.doe.gov) with a corresponding published mouse sequence. The following primer combinations and PCR conditions were used:

Primers used for RT-PCR and morpholino synthesis

dnah5 (175bp; genomic about 600bp)

forward:	5e2	5' GGA GGA GAA GGA AGC AAA ACG GG 3'
reverse:	5i2	5' CAC TGG CAC AAG ATT TCT TGT G 3'
reverse:	5e3	5' CAT AAT GTG CCG AAG TCC TCC AAC TG 3'

dnah9 (5UTR_F1/9e3 : 845bp; 9e2/9e3: 225 bp; genomic ~1500bp/~1400bp)

forward	5UTR_F1	5'TGC AAA CAC TGT TGC CAT GGC3'
forward:	9e2	5' GGA CGT TTG TGA TGG TCG G 3'
forward:	9i2	5' CAA CAA GGC AGA GGT TAG TC 3'
reverse:	9e3	5' TGG GGT TTT TTC CTT GCA GAA G 3'

Primers used for the synthesis of in-situ hybridization (ISH) probes

dnah5 (551 bp)

forward:	for1	5' CTT TGG TGT CAT TGG AAT AGG GC 3'
reverse:	rev1	5' AGT ATC CCA GCC ATG TGA GG 3'

dnah9 (845bp)

forward	5UTR_F1	5'TGC AAA CAC TGT TGC CAT GGC3'
reverse:	9e3	5' TGG GGT TTT TTC CTT GCA GAA G 3'

dnah11 (1131 bp)

forward:	for1	5' GAA CAC CTT GTT AGA TTT GTC ATT G 3'
reverse:	rev1	5' GCT CTG CAT AAT TAC TTG TAA C 3'

Ligation of PCR products into cloning vectors

PCR-products were ligated into the linearized pGEM-T Easy (Promega) vector with the T4 ligase. In a standard reaction, 2.5µl of ligation buffer, 0.5µl of vector and 0.5µl of T4 ligase were combined with 1.5µl of fresh PCR product. The reaction was incubated for 1h at RT or overnight at 4°C and then transformed into bacteria.

Bacterial transformation and clonal selection

The ligated vectors were transformed into chemically competent XL1-blue cells using the heat shock method. Different volumes (typically 100, 150) of bacteria-solution were plated on LB-agar selective plates (100µg/ml ampicillin / 0.5mM IPTG / 80µg/ml X-Gal) and incubated overnight. The missing blue color of the clones indicated insertion of a PCR product into the multiple cloning site. Such clones were selected for amplification and analysis using a mini-prep procedure.

Amplification of gene sequences

Plasmid-DNA preparation

Preparation of small amounts of plasmid DNA (mini-prep)

Plasmid DNA from *E. coli* cultures was isolated using a modified alkaline lysis protocol. All centrifugation steps were done at RT. 3ml of selective LB medium (100µg/ml Ampicillin) were inoculated with a single white bacteria colony from a selective plate and grown overnight with shaking at 37°C. 1.5ml of the culture was poured into a micro centrifuge tube and bacteria were pelleted in a micro centrifuge at 5000rpm for 5min. Supernatant was discarded and the pellet resuspended by heavy vortexing in 100µl P1 buffer. When the bacteria suspension appeared uniform, 200µl of P2 buffer were added for alkaline lysis and the tube was inverted several times to thoroughly mix the reagents, after 5min reaction was stopped by neutralizing with 150µl of P3, again inverting the tube several times. After 20min of incubation on ice, the lysate was cleared from precipitate containing genomic DNA, cell debris, proteins and potassium dodecyl sulphate by centrifugation in a micro centrifuge at 13 000 rpm for 10min. Supernatant was transferred to a fresh tube and mixed well with 1ml of 100% Ethanol to precipitate DNA. After precipitation for 30min at -20°C the plasmid DNA was pelleted by centrifuging at 13 000 rpm for 10min. The pellet was washed in 70% ethanol, centrifuged briefly, dried and resuspended in 50µl sterile DDW.

Preparation of medium amounts of plasmid DNA (midi-prep)
100ml of selective LB medium (100µg/ml ampicillin) were inoculated with 1ml of a solution of a positively tested bacteria clone and grown overnight in a 1000ml conical flask with vigorous shaking at 37°C. Bacteria were harvested by centrifugation, lysed and DNA was purified following the Promega "PureYield Plasmid Midiprep System" using the vacuum method.

Measuring the concentration of nucleic acids
The concentration of nucleic acids in aqueous solutions was determined via spectrophotometry. The ratio of absorption (A) at 260nm and 280nm wavelength indicated the purity of the solution (pure nucleic acid solution: 1.8 for DNA, 2.0 for RNA). The content of either DNA or RNA was inferred from the A260 value with 1 unit corresponding to 50µg/µl DNA and 40µg/µl RNA.

Restriction enzyme digests of DNA
To check for insertion of the correct PCR product after mini-prep, inserts were released from the plasmids by digestion with a restriction enzyme cutting on both sides of the multiple cloning site. Typically to 5µl of plasmid-DNA, 2µl 10x buffer, 0.2 µl BSA and 0.5µl enzyme were added, the mixture was filled up with 12.3µl sterile DDW to a final volume of 20µl and incubated at 37°C for 2hrs. After digestion the whole volume of the reaction was analyzed on an agarose gel. For linearization digests typically 20µg of plasmid-DNA was used in a 100µl reaction. 4µl of restriction enzyme were used and the digestion was incubated overnight at 37°C. Approximately 600ng of the digestion were controlled on a 1% agarose gel.

Agarose gel analysis
The products of each reaction were checked on a standard 1.0-1.5% agarose gel with a concentration of 0,4µl/ml ethidium bromide solution.

Synthesis of capped RNA
For capped RNA synthesis the Ambion kit mMESSAGE mMACHINE (High yield capped RNA Transcription kit) was used. For the reaction 4µl nuclease free H_2O, 10µl 2xNTP/CAP (ATP, 10mM; CTP, 10mM; UTP, 10mM; GTP, 2mM, cap analog, 8mM), 2µl 10xbuffer, 2µl linearized CS^{2+} (~2 µg) and 2µl enzyme mixture (containing SP6 RNA polymerase) were mixed. After incubation for 2h at 37°C, 1µl DNase was added with a subsequent incubation of 15min. Then mRNA was twice phenol-chloroform extracted and precipitated in isopropyl alcohol. Concentration of the mRNA was then determined by spectrophotometry and the quality by running on an agarose gel.

Whole mount in situ hybridization

In vitro transcription of RNA probes
200ng linearized plasmid with the insert of interest was used as a template. 20u of either Sp6 or T7 polymerase were added to a mixture of template, 4µl Transcription Buffer, 0.5µl (= 20units) RNasin, 2µl DTT and 2µl 10x Dig-Mix. After adding sterile DDW to a final volume of 20µl the mixture was incubated at 37°C for 2hrs. After gel check with 2µl in 10µl DDW on a 1% agarose gel, 115µl 100% EtOH and 3.75µl 4M LiCl were added to the mixture and RNA was precipitated at -20°C for at least 30min. After centrifuging 13 000rpm at 4°C for 20min; the resulting pellet was rinsed in 70%

EtOH and centrifuged again for 5min. The pellet was air-dried and resuspended in 50µl of a 1:1 mixture of sterile DDW and formamide. The RNA was stored at -80°C.

In situ hybridization

Whole mount in situ hybridization used to detect the expression pattern of specific genes in *Xenopus* embryos. Protocol originally adapted from the De Robertis lab (Belo et al., 1997).

Day 1: All steps (except Proteinase K) until pre-hybridization were performed on ice. On the first day of the procedure, tissue was prepared for taking up the antisense RNA probe, which hybridizes to the endogenous target RNA. Embryos were rehydrated from storage in 100% ethanol through a graded series of 75%, 50% and 25% ethanol in PBS$^-$. Embryos were washed three times for at least 5min in PBS$^-$w and then the tissue was permeabilized for ~15-20min in 10µg/µl Proteinase K in PBS$^-$w at RT. Digestion was stopped in 2mg/ml glycine followed by three washing steps in PBS$^-$w for 5min each. The tissue was then refixed for 15min at RT in 4% PFA supplemented with 0.2% glutaraldehyde. After washing three times in PBS$^-$w for 5min the embryos were transferred into a 1:1 mixture of hybridization solution and PBS$^-$w. After equilibration in 100% hybridization solution, a pre-hybridization period in 900µl hybridization solution at 65°C for 2-3hrs eliminated endogenous phosphatases. Depending on the concentration of the RNA, about 1µl of antisense probe (~20ng) diluted in 100µl hybridization solution was added to the vial and the embryo was incubated with the probe overnight at 70°C.

Day 2: On the second day excess antisense probe was removed in high stringency washing steps and the tissue was prepared for incubation with the anti-digoxygenin antibody. In a first step, 1 to 3 washing steps (30min each) in 100% hybridization mix at 70°C were used to reduce background staining depending on the probe. Then the solution was again replaced with 800µl hybridization solution. In three steps (5 min each) each 400µl of 2xSSC (pH 4.5) were added and the embryo was washed twice in 2xSSC (pH 7) at 70°C afterwards. The washing steps in SSC were followed by four washing intervals in MABw, twice at RT for 10min and another two times at 70°C for 30min. Afterwards, embryos were washed three times in PBS$^-$w at RT for 10min each and were then pre-incubated in antibody-blocking buffer at 4°C for 2hrs. In a second tube, the anti-digoxygenin antibody coupled to alkaline phosphatase was diluted 1/10,000 and pre-blocked for the same time. After the 2hrs of pre-incubation, the blocking buffer was replaced with the antibody-solution and the embryos were incubated with the antibody overnight at 4°C on a laboratory shaker.

Day 3: On the third day, unbound antibody was removed in extensive washing steps and the staining reaction was started. Embryos were rinsed and then washed six times for 45min each in PBS$^-$w containing 0.1% BSA. The washing in BSA was followed by two washing steps with PBS$^-$w for 30min each and embryos were then transferred into AP1 buffer, which adjusts the pH of the tissue for the optimal reaction of the alkaline phosphatase. AP1 buffer was changed 1-4 times according to probe type and then replaced by a 1:1 mixture of AP1 buffer and BMPurple, the substrate for the alkaline phosphatase. The staining process was controlled and stopped by washing in PBS$^-$w, when the expected signal had reached a dark blue to violet color. A gradual methanol series intensified the signal and the embryos were afterwards stored in 100% methanol at -20°C.

Histological analysis of embryos after in situ hybridization
After rehydration embryos were equilibrated in a small volume of embedding medium (~1ml). 2ml of embedding medium were mixed shortly but vigorously with 140µl of glutaraldehyde and poured into a square mold formed of two glass brackets. The mixture was allowed to harden and the equilibrated embryo was transferred upon the surface of the block, excess embedding medium was carefully removed. Another 2ml of embedding medium mixed with glutaraldehyde were poured into the mold so that the embryo was now sandwiched between two layers of embedding mix. The hardened block was trimmed with a razor blade and glued onto a plate. The plate was mounted into the holder of the vibratome and 30µm thick sections were prepared. The sections were arranged onto glass slides, embedded with mowiol and protected with glass cover slips.

Statistical analysis
Statistical calculations of marker gene expression patterns were performed using Pearson's chi-square test (Bonferroni corrected; Statistica 6.1 – StatSoft Inc.) unless indicated otherwise.

Photo documentation
Documentation of living or fixed embryos was performed after stepwise rehydration in PBS- with a Zeiss dissecting microscope STEREO Discovery.V12 or a LEICA MZFLIII with a digital camera (AxioCam HRc, Zeiss). Analyses of vibratome sections were performed with a Zeiss microscope Axioskop 2 with a digital camera (AxioCam HRc, Zeiss). For image processing (contrast, background, arrangement, layout, etcetera) Photoshop CS3 and Illustrator CS3 (both Adobe Systems) was used – in most cases with the very very kind and professional help of Thomas Weber (University of Hohenheim). All raw drawings were made by Bernd Schmid after instruction and then further processed with Photoshop and Illustrator.

Buffers, Solutions and Media

For in situ hybridization:

Phosphate Buffered Saline 10x (PBS, 1l)
80g NaCl
2g KCl
14.4g Na_2HPO_4
2.4g KH_2PO_4
800ml DDW
adjust pH to 7.4, add DDW to 1L, autoclave.

PBSw (500ml)
500ml PBS^-
500µl Tween20.

Alkaline Phosphatase Buffer (AP1, 1l)
100ml 1M TRIS pH 9.5
20ml 5M NaCl
50ml 1M MgCl
add DDW to 1l.
Maleic Acid Buffer 5x (MAB, 1l)

58.05g (100mM) Maleic Acid
43.83g (150mM) NaCl
800ml DDW
adjust pH to 7.5 with 10N NaOH, add DDW to 1l, autoclave.

Sodium Citrate Buffer 20x (SSC, 1l)
175.3g NaCl
88.2g Sodium citrate
800ml DDW
adjust pH to 7.0, add DDW to 1l, autoclave.

Hybridization solution (1l)
10g Boehringer Block
500ml Formamide
250ml SSC 20x
Heat to 65°C for 1 hour
120ml DDW
100ml Torula RNA (10mg/ml in DDW; filtered)
2ml Heparin (50mg/ml in 1x SSC pH 7)
5ml 20% Tween-20
10ml 10% CHAPS
10ml 0.5M EDTA

Antibody Blocking Buffer
10% Heat Inactivated Goat Serum
1% Boehringer Block
0.1% Tween-20
dissolve in PBS at 70°C, vortexing frequently, then filter (0.45µm).

For frog experiments:

5xMBSH (1l)
25.7g NaCl
0.375g KCl
1g $NaHCO_3$
1g $MgSO_4/7H_2O$
0.39g $(CaNO_3)^2/4H_2O$
0.3g $CaCl_2/2H_2O$
11.9g Hepes
5 ml Penicillin/Streptomycin

10xMEMFA (500ml)
2M MOPS (pH 7.4)
200ml 100mM EGTA
10ml 1M $MgSO_4$
add DDW to 1l, autoclave.

1xMEMFA
10 % 10xMEMFA
10 % Formaldehyde 37%
80 % H_2O.

Gurdon's buffer
88mM NaCl
15mM HEPES
1mM KCl
15mM Tris-HCl, pH 7.6

Ficoll
2% Ficoll diluted in 1xMBSH

Cystein
2% Cystein diluted in DDW. Adjust pH to 7.99.

For bacteria culture:

Super Optimal Catabolite repression medium (S.O.C.)
0.5% Yeast extract
2.0% Tryptone
10mM NaCl
2.5mM KCl
10mM $MgCl_2$
10mM $MgSO_4$
20mM Glucose
autoclave

Lysogeny Broth (LB) medium
1% Tryptone
1% NaCl
0.5% Yeast extract
adjust pH to 7.0, autoclave.

LB agar
1% Tryptone
1% NaCl
0.5% Yeast extract
adjust pH to 7.0, add 15g/l agar before autoclaving.

For DNA preparation:

P1
50mM TRIS HCl
10mM EDTA pH 8
add RNaseA (DNase free) to a final concentration of 100µg/ml

P2
0,2M NaOH
1% SDS

P3
3M Potassium acetate, pH 5.5

For other applications:

Embedding medium for vibratome sections
2.2g Gelatine
135g Bovine Serum Albumin
90g Sucrose
dissolve in 450ml PBS.

Mowiol (Mounting medium)
96g Mowiol 488
24g Glycerol
24ml DDW
stir for 2h, then add
48ml TRIS 0.2M pH 8.5
stir for 20min at 50°C
centrifuge for 15min at 5000rpm, keep supernatant
and store at -20°C.

Tris Acetate EDTA Buffer (TAE)
40mM Tris-acetate
2mM EDTA
adjust pH to 8.0.

Sources of supply

Chemicals and lab-ware

Acetic acid	AppliChem, Darmstadt
Agarose	Roth, Karlsruhe
Albumin fraction V	AppliChem, Darmstadt
Ampicillin	AppliChem, Darmstadt
Anti-Digoxigenin-AP	Roche, Mannheim
BM Purple	Roche, Mannheim
Boehringer Block	Roche, Mannheim
Bovine serum albumin	AppliChem, Darmstadt
BSA	AppliChem
CAS-Block	Zymed (Invitrogen) Karlsruhe
CHAPS	Sigma, Schnelldorf
Chloroform	Merck, Darmstadt
Cystein	Roth, Karlsruhe
Desoxynucleosidtriphosphate (dNTPs)	Promega, Mannheim
Dig-Mix	Roche, Mannheim
Dimethylsulfoxid (DMSO)	Roth, Karlsruhe
Disodium hydrogen phosphate	AppliChem, Darmstadt
Dithioreitol (DTT)	Promega, Mannheim
Glass slides	Roth, Karlsruhe
Glass cover slips	Roth, Karlsruhe
DigMix	Roche, Mannheim
DTT	Promega, Mannheim
DMSO	Roth, Karlsruhe
EDTA	Roth, Karlsruhe

Ethanol	Roth, Karlsruhe
Ethidiumbromide	Roth, Karlsruhe
Ethyl-p-Aminobenzoat (Benzocain)	Sigma, Schnelldorf
ethylenediaminetetraacetic acid EDTA	Roth, Karlsruhe
ethylene glycol tetraacetic acid EGTA	Roth, Karlsruhe
Ficoll	AppliChem, Darmstadt
FluoSphere Fluorescent beads 500nm	Invitrogen, (Molecular Probes), Karlsruhe,
Formaldehyd	AppliChem, Darmstadt
Forceps (#3, #5)	Fine Science Tools, Heidelberg
Formamide	Roth, Karlsruhe
Gelatine	Roth, Karlsruhe
Glucose	AppliChem, Darmstadt
Glutaraldehyde	AppliChem, Darmstadt
Glycerol	Roth, Karlsruhe
Glycin	AppliChem, Darmstadt
Goat serum	Sigma, Schnelldorf
HCG (human chorionic gonadotropin)	Sigma, Schnelldorf
HCl (37%)	Merck, Darmstadt
Hepes	AppliChem, Darmstadt
Heparin	Sigma, Schnelldorf
Injection-needle Sterican (0,4x20 mm)	B. Braun, Melsungen
Injection syringe F1, 1ml	B. Braun, Melsungen
Lambda-DNA	Promega, Mannheim
Ligase (T4-Ligase)	Promega, Mannheim
Lithium chloride	Serva, Heidelberg
Loading Buffer	AppliChem, Darmstadt
Magnesium chloride	Roth, Karlsruhe
Magnesium sulfate	AppliChem, Darmstadt
Maleic acid	Roth, Karlsruhe
Methanol	Roth, Karlsruhe
Micro centrifuge tubes	Sarstedt, Nümbrecht
Objective slides	Roth, Karlsruhe
Oligonucleotides	Operon, Cologne
Parafilm	Roth, Karlsruhe
Paraformaldehyde	AppliChem, Darmstadt
PBS+ (10x)	Gibco (Invitrogen) Karlsruhe
Penicillin/Streptomycin	Gibco (Invitrogen) Karlsruhe
pGEM-T-Easy-Vektor	Promega, Mannheim
Phenol/chloroform (Rotiphenol)	Roth, Karlsruhe
Plastic pipettes	Sarstedt, Nümbrecht
2-Propanol	Roth, Karlsruhe
Proteinase K	Roth, Karlsruhe
Rhodamine dextran	Molecular Probes (Invitrogen), Karlsruhe
RNAse A	Roth, Karlsruhe
RNAsin	Promega, Mannheim
Rose-Gal	Roth, Karlsruhe
Sucrose	AppliChem, Darmstadt
Sodium acetate	Roth, Karlsruhe
Sodium chloride	Roth, Karlsruhe
Sodium citrate	Roth, Karlsruhe
Sodium dihydrogen phosphate	AppliChem, Darmstadt

Sodium hydroxide	AppliChem, Darmstadt
Sp6-RNA-Polymerase	Promega, Mannheim
Syringe filters	Whatman, Dassel
T7-RNA-Polymerase	Promega, Mannheim
Taq-DNA-Polymerase (Go-Taq)	Promega, Mannheim
Torula RNA	Sigma, Schnelldorf
TRIS base	AppliChem, Darmstadt
TRIS HCl	AppliChem, Darmstadt
Triton-X100	Serva, Heidelberg
Tryptone	AppliChem, Darmstadt
Tween-20	AppliChem, Darmstadt
X-Gal	Roth, Karlsruhe

Kits:

DNA-Purification-Kit (Easy-Pure)	Biozym, Hessisch Oldendorf
mMESSAGE mMACHINE SP6	Ambion, Darmstadt
pGEM-T Easy Vector System	Promega, Mannheim
PureYield Plasmid Midiprep System	Promega, Mannheim
PeqGOLD TriFast	Peqlab, Erlangen

Proteins and Antibodies:

Restriction enzymes and buffers	Promega, Mannheim
Modifying enzymes and buffers	Promega, Mannheim
Mouse anti-acetylated α-tubulin	Sigma, Schnelldorf
Rabbit anti-serotonin	Chemicon
Rabbit anti-PC2	US Biological
Mouse anti-PC2	gift of Dr. Ralph Witzgall, Regensburg
Anti-digoxigenin	AP Roche, Mannheim

Special Hardware:

Peltier Thermal Cycler PTC-200	Biozym, Hessisch Oldendorf
Vibratome	Leica, Bensheim
Stereo microscope	Zeiss, Oberkochen
Zeiss DSM 940A	Zeiss, Oberkochen
LSM 5 Pascal	Zeiss, Oberkochen
Axioplan 2	Zeiss, Oberkochen

Animals

Frogs

Adult African clawed frogs (*Xenopus laevis*) were obtained from Guy Pluck, Xenopus express, Ancienne Ecole de Vernassal, Le Bourg 43270, Vernassal, Haute-Loire, France. They were and kept species-appropriate at a 12h light-cycle in the animal facility of the Institute of Zoology, University of Hohenheim.

Some parts of the Materials and Methods sections have been adapted from Andre 2009.

References

Aamar, E., and Dawid, I. B. (2008). Isolation and expression analysis of foxj1 and foxj1.2 in zebrafish embryos. *Int J Dev Biol* **52,** 985-91.

Abramoff, M. D., Magelhaes, P. J., and Ram, S. J. (2004). Image Processing with ImageJ. *Biophotonics International* **11,** 36-42.

Afzelius, B. A. (1976). A human syndrome caused by immotile cilia. *Science* **193,** 317-9.

Afzelius, B. A. (2004). Cilia-related diseases. *J Pathol* **204,** 470-7.

Agius, E., Oelgeschlager, M., Wessely, O., Kemp, C., and De Robertis, E. M. (2000). Endodermal Nodal-related signals and mesoderm induction in *Xenopus*. *Development* **127,** 1173-83.

Andrews, K. L., Nettesheim, P., Asai, D. J., and Ostrowski, L. E. (1996). Identification of seven rat axonemal dynein heavy chain genes: expression during ciliated cell differentiation. *Mol Biol Cell* **7,** 71-9.

Asai, D. J., and Koonce, M. P. (2001). The dynein heavy chain: structure, mechanics and evolution. *Trends Cell Biol* **11,** 196-202.

Asai, D. J., and Wilkes, D. E. (2004). The dynein heavy chain family. *J Eukaryot Microbiol* **51,** 23-9.

Bae, Y. K., Qin, H., Knobel, K. M., Hu, J., Rosenbaum, J. L., et al. (2006). General and cell-type specific mechanisms target TRPP2/PKD-2 to cilia. *Development* **133,** 3859-70.

Barr, M. M., and Sternberg, P. W. (1999). A polycystic kidney-disease gene homologue required for male mating behaviour in C. elegans. *Nature* **401,** 386-9.

Bartoloni, L., Blouin, J. L., Pan, Y., Gehrig, C., Maiti, A. K., et al. (2002). Mutations in the DNAH11 (axonemal heavy chain dynein type 11) gene cause one form of situs inversus totalis and most likely primary ciliary dyskinesia. *Proc Natl Acad Sci U S A* **99,** 10282-6.

Beck, C. W., and Slack, J. M. (1999). A developmental pathway controlling outgrowth of the *Xenopus* tail bud. *Development* **126,** 1611-20.

Beckers, A., Alten, L., Viebahn, C., Andre, P., and Gossler, A. (2007). The mouse homeobox gene Noto regulates node morphogenesis, notochordal ciliogenesis, and left right patterning. *Proc Natl Acad Sci U S A* **104,** 15765-70.

Beddington, R. S., Jaenisch, R., Smith, A. B., McLaren, A. L., Lawson, K. A., et al. (1992). Three-dimensional representation of gastrulation in the mouse. *Ciba Found Symp* **165,** 55-60.

Bell, E., Munoz-Sanjuan, I., Altmann, C. R., Vonica, A., and Brivanlou, A. H. (2003). Cell fate specification and competence by Coco, a maternal BMP, TGFbeta and Wnt inhibitor. *Development* **130,** 1381-9.

Belo, J. A., Bachiller, D., Agius, E., Kemp, C., Borges, A. C., et al. (2000). Cerberus-like is a secreted BMP and nodal antagonist not essential for mouse development. *Genesis* **26,** 265-70.

Belo, J. A., Bouwmeester, T., Leyns, L., Kertesz, N., Gallo, M., et al. (1997). Cerberus-like is a secreted factor with neutralizing activity expressed in the anterior primitive endoderm of the mouse gastrula. *Mech Dev* **68,** 45-57.

Belo, J. A., Silva, A. C., Borges, A. C., Filipe, M., Bento, M., et al. (2008). Generating asymmetries in the early vertebrate embryo: the role of the Cerberus-like family. *Int J Dev Biol*.

Bisgrove, B. W., Essner, J. J., and Yost, H. J. (1999). Regulation of midline development by antagonism of lefty and nodal signaling. *Development* **126,** 3253-62.

Bisgrove, B. W., Snarr, B. S., Emrazian, A., and Yost, H. J. (2005). Polaris and Polycystin-2 in dorsal forerunner cells and Kupffer's vesicle are required for specification of the zebrafish left-right axis. *Dev Biol* **287,** 274-88.

Bisgrove, B. W., and Yost, H. J. (2006). The roles of cilia in developmental disorders and disease. *Development* **133,** 4131-43.

Blum, M., Andre, P., Muders, K., Schweickert, A., Fischer, A., et al. (2007). Ciliation and gene expression distinguish between node and posterior notochord in the mammalian embryo. *Differentiation* **75,** 133-46.

Blum, M., Beyer, T., Weber, T., Vick, P., Andre, P., et al. (2009a). *Xenopus*, an ideal model system to study vertebrate left-right asymmetry. *Dev Dyn* **238,** 1215-1225.

Blum, M., Weber, T., Beyer, T., and Vick, P. (2009b). Evolution of leftward flow. *Semin Cell Dev Biol* **20,** 464-71.

Bolker, J. A. (1993). Gastrulation and mesoderm morphogenesis in the white sturgeon. *J Exp Zool* **266,** 116-31.

Bolker, J. A. (1994). Comparison of Gastrulation in Frogs and Fish. *Amer. Zool.* **34,** 313-322.
Boorman, C. J., and Shimeld, S. M. (2002a). The evolution of left-right asymmetry in chordates. *Bioessays* **24,** 1004-11.
Boorman, C. J., and Shimeld, S. M. (2002b). Pitx homeobox genes in Ciona and amphioxus show left-right asymmetry is a conserved chordate character and define the ascidian adenohypophysis. *Evol Dev* **4,** 354-65.
Bourlat, S. J., Juliusdottir, T., Lowe, C. J., Freeman, R., Aronowicz, J., et al. (2006). Deuterostome phylogeny reveals monophyletic chordates and the new phylum Xenoturbellida. *Nature* **444,** 85-8.
Bouwmeester, T., Kim, S., Sasai, Y., Lu, B., and De Robertis, E. M. (1996). Cerberus is a head-inducing secreted factor expressed in the anterior endoderm of Spemann's organizer. *Nature* **382,** 595-601.
Brandli, A. W. (1999). Towards a molecular anatomy of the *Xenopus* pronephric kidney. *Int J Dev Biol* **43,** 381-95.
Brennan, J., Norris, D. P., and Robertson, E. J. (2002). Nodal activity in the node governs left-right asymmetry. *Genes Dev* **16,** 2339-44.
Brown, N. A., and Wolpert, L. (1990). The development of handedness in left/right asymmetry. *Development* **109,** 1-9.
Brusca, G., and Brusca, R. (2003). "Invertebrates." Palgrave Macmillan,
Bruss, M., Barann, M., Hayer-Zillgen, M., Eucker, T., Gothert, M., et al. (2000). Modified 5-HT3A receptor function by co-expression of alternatively spliced human 5-HT3A receptor isoforms. *Naunyn Schmiedebergs Arch Pharmacol* **362,** 392-401.
Bui, K. H., Sakakibara, H., Movassagh, T., Oiwa, K., and Ishikawa, T. (2008). Molecular architecture of inner dynein arms in situ in Chlamydomonas reinhardtii flagella. *J Cell Biol* **183,** 923-32.
Bushati, N., and Cohen, S. M. (2007). microRNA functions. *Annu Rev Cell Dev Biol* **23,** 175-205.
Buznikov, G. A., Peterson, R. E., Nikitina, L. A., Bezuglov, V. V., and Lauder, J. M. (2005). The pre-nervous serotonergic system of developing sea urchin embryos and larvae: pharmacologic and immunocytochemical evidence. *Neurochem Res* **30,** 825-37.
Campione, M., Steinbeisser, H., Schweickert, A., Deissler, K., van Bebber, F., et al. (1999). The homeobox gene Pitx2: mediator of asymmetric left-right signaling in vertebrate heart and gut looping. *Development* **126,** 1225-34.
Cartwright, J. H., Piro, N., Piro, O., and Tuval, I. (2008). Fluid dynamics of nodal flow and left-right patterning in development. *Dev Dyn*.
Caspary, T., Larkins, C. E., and Anderson, K. V. (2007). The graded response to Sonic Hedgehog depends on cilia architecture. *Dev Cell* **12,** 767-78.
Chen, C., and Shen, M. M. (2004). Two modes by which Lefty proteins inhibit nodal signaling. *Curr Biol* **14,** 618-24.
Chen, Y., and Schier, A. F. (2001). The zebrafish Nodal signal Squint functions as a morphogen. *Nature* **411,** 607-10.
Cheng, A. M., Thisse, B., Thisse, C., and Wright, C. V. (2000). The lefty-related factor Xatv acts as a feedback inhibitor of nodal signaling in mesoderm induction and L-R axis development in *Xenopus*. *Development* **127,** 1049-61.
Cheng, S. K., Olale, F., Brivanlou, A. H., and Schier, A. F. (2004). Lefty blocks a subset of TGFbeta signals by antagonizing EGF-CFC coreceptors. *PLoS Biol* **2,** E30.
Chicoine, J., Benoit, P., Gamberi, C., Paliouras, M., Simonelig, M., et al. (2007). Bicaudal-C recruits CCR4-NOT deadenylase to target mRNAs and regulates oogenesis, cytoskeletal organization, and its own expression. *Dev Cell* **13,** 691-704.
Christopher, K., Chang, J., and Goldberg, J. (1996). Stimulation of cilia beat frequency by serotonin is mediated by a Ca2+ influx in ciliated cells of Helisoma trivolvis embryos. *J Exp Biol* **199,** 1105-13.
Christopher, K. J., Young, K. G., Chang, J. P., and Goldberg, J. I. (1999). Involvement of protein kinase C in 5-HT-stimulated ciliary activity in Helisoma trivolvis embryos. *J Physiol* **515 (Pt 2),** 511-22.
Chu, D. T., and Klymkowsky, M. W. (1989). The appearance of acetylated alpha-tubulin during early development and cellular differentiation in *Xenopus*. *Dev Biol* **136,** 104-17.
Cogswell, C., Price, S. J., Hou, X., Guay-Woodford, L. M., Flaherty, L., et al. (2003). Positional cloning of jcpk/bpk locus of the mouse. *Mamm Genome* **14,** 242-9.
Collazo, A., Bolker, J., and Keller, R. (1994). A phylogenetic perspective on teleost gastrulation. *Am Nat* **144,** 133-152.
Conklin, E. G. (1932). The embryology of Amphioxus. *J Morph* **54,** 69-151.

Constam, D. B. (2009). Running the gauntlet: an overview of the modalities of travel employed by the putative morphogen Nodal. *Curr Opin Genet Dev* **19,** 302-7.
Cooke, J. (2004). Developmental mechanism and evolutionary origin of vertebrate left/right asymmetries. *Biol Rev Camb Philos Soc* **79,** 377-407.
Cooper, M. S., and Virta, V. C. (2007). Evolution of gastrulation in the ray-finned (actinopterygian) fishes. *J Exp Zool B Mol Dev Evol* **308,** 591-608.
Corpet, F. (1988). Multiple sequence alignment with hierarchical clustering. *Nucl. Acids Res.* **16,** 10881-10890.
Crease, D. J., Dyson, S., and Gurdon, J. B. (1998). Cooperation between the activin and Wnt pathways in the spatial control of organizer gene expression. *Proc Natl Acad Sci U S A* **95,** 4398-403.
Croce, J. C., and McClay, D. R. (2006). The canonical Wnt pathway in embryonic axis polarity. *Semin Cell Dev Biol* **17,** 168-74.
Dale, L., and Slack, J. M. (1987). Fate map for the 32-cell stage of *Xenopus* laevis. *Development* **99,** 527-51.
Dammermann, A., Pemble, H., Mitchell, B. J., McLeod, I., Yates, J. R., 3rd, et al. (2009). The hydrolethalus syndrome protein HYLS-1 links core centriole structure to cilia formation. *Genes Dev* **23,** 2046-59.
Danilchik, M. V., and Black, S. D. (1988). The first cleavage plane and the embryonic axis are determined by separate mechanisms in *Xenopus* laevis. I. Independence in undisturbed embryos. *Dev Biol* **128,** 58-64.
Davis, N. M., Kurpios, N. A., Sun, X., Gros, J., Martin, J. F., et al. (2008). The chirality of gut rotation derives from left-right asymmetric changes in the architecture of the dorsal mesentery. *Dev Cell* **15,** 134-45.
Dawe, H. R., Farr, H., Portman, N., Shaw, M. K., and Gull, K. (2005). The Parkin co-regulated gene product, PACRG, is an evolutionarily conserved axonemal protein that functions in outer-doublet microtubule morphogenesis. *J Cell Sci* **118,** 5421-30.
De Robertis, E. M. (2006). Spemann's organizer and self-regulation in amphibian embryos. *Nat Rev Mol Cell Biol* **7,** 296-302.
De Robertis, E. M. (2009). Spemann's organizer and the self-regulation of embryonic fields. *Mech Dev*.
De Robertis, E. M., Larrain, J., Oelgeschlager, M., and Wessely, O. (2000). The establishment of Spemann's organizer and patterning of the vertebrate embryo. *Nat Rev Genet* **1,** 171-81.
Delsuc, F., Brinkmann, H., Chourrout, D., and Philippe, H. (2006). Tunicates and not cephalochordates are the closest living relatives of vertebrates. *Nature* **439,** 965-8.
Doran, S. A., Koss, R., Tran, C. H., Christopher, K. J., Gallin, W. J., et al. (2004). Effect of serotonin on ciliary beating and intracellular calcium concentration in identified populations of embryonic ciliary cells. *J Exp Biol* **207,** 1415-29.
Duboc, V., and Lepage, T. (2008). A conserved role for the nodal signaling pathway in the establishment of dorso-ventral and left-right axes in deuterostomes. *J Exp Zoolog B Mol Dev Evol* **310,** 41-53.
Duboc, V., Rottinger, E., Besnardeau, L., and Lepage, T. (2004). Nodal and BMP2/4 signaling organizes the oral-aboral axis of the sea urchin embryo. *Dev Cell* **6,** 397-410.
Duboc, V., Rottinger, E., Lapraz, F., Besnardeau, L., and Lepage, T. (2005). Left-right asymmetry in the sea urchin embryo is regulated by nodal signaling on the right side. *Dev Cell* **9,** 147-58.
Eberhardt, M. (2008). Link-Rechts Achsenentwicklung in *Xenopus laevis*: Manipulation des asymmetrischen, cilienbasierenden Flüssigkeitsstromes und dessen Auswirkung auf die Genexpression der Wachstumsfaktoren *Xnr1* und *Coco* in der embryonalen Mittellinie. Diploma-Thesis, University of Hohenheim.
Ekker, S. C., McGrew, L. L., Lai, C. J., Lee, J. J., von Kessler, D. P., et al. (1995). Distinct expression and shared activities of members of the hedgehog gene family of *Xenopus* laevis. *Development* **121,** 2337-47.
Essner, J. J., Amack, J. D., Nyholm, M. K., Harris, E. B., and Yost, H. J. (2005). Kupffer's vesicle is a ciliated organ of asymmetry in the zebrafish embryo that initiates left-right development of the brain, heart and gut. *Development* **132,** 1247-60.
Essner, J. J., Vogan, K. J., Wagner, M. K., Tabin, C. J., Yost, H. J., et al. (2002). Conserved function for embryonic nodal cilia. *Nature* **418,** 37-8.
Feistel, K., and Blum, M. (2006). Three types of cilia including a novel 9+4 axoneme on the notochordal plate of the rabbit embryo. *Dev Dyn* **235,** 3348-58.

Filipowicz, W., Bhattacharyya, S. N., and Sonenberg, N. (2008). Mechanisms of post-transcriptional regulation by microRNAs: are the answers in sight? *Nat Rev Genet* **9,** 102-14.
Fischer, E., Legue, E., Doyen, A., Nato, F., Nicolas, J. F., et al. (2006). Defective planar cell polarity in polycystic kidney disease. *Nat Genet* **38,** 21-3.
Fliegauf, M., Benzing, T., and Omran, H. (2007). When cilia go bad: cilia defects and ciliopathies. *Nat Rev Mol Cell Biol* **8,** 880-93.
Fliegauf, M., Olbrich, H., Horvath, J., Wildhaber, J. H., Zariwala, M. A., et al. (2005). Mislocalization of DNAH5 and DNAH9 in respiratory cells from patients with primary ciliary dyskinesia. *Am J Respir Crit Care Med* **171,** 1343-9.
Fukumoto, T., Blakely, R., and Levin, M. (2005a). Serotonin transporter function is an early step in left-right patterning in chick and frog embryos. *Dev Neurosci* **27,** 349-63.
Fukumoto, T., Kema, I. P., and Levin, M. (2005b). Serotonin signaling is a very early step in patterning of the left-right axis in chick and frog embryos. *Curr Biol* **15,** 794-803.
Gallagher, A. R., Hoffmann, S., Brown, N., Cedzich, A., Meruvu, S., et al. (2006). A truncated polycystin-2 protein causes polycystic kidney disease and retinal degeneration in transgenic rats. *J Am Soc Nephrol* **17,** 2719-30.
Getwan, M. (2009). Die embryonale Funktion des sekretierten Wachstumsfaktors Coco bei der Festlegung der Organlateralität von *Xenopus laevis*. Diploma-Thesis, University of Hohenheim.
Gilbert, S. (2006). "Developmental Biology." Palgrave Macmillan,
Ginger, M. L., Portman, N., and McKean, P. G. (2008). Swimming with protists: perception, motility and flagellum assembly. *Nat Rev Microbiol* **6,** 838-50.
Gont, L. K., Steinbeisser, H., Blumberg, B., and de Robertis, E. M. (1993). Tail formation as a continuation of gastrulation: the multiple cell populations of the *Xenopus* tailbud derive from the late blastopore lip. *Development* **119,** 991-1004.
Grande, C., and Patel, N. H. (2009). Nodal signalling is involved in left-right asymmetry in snails. *Nature* **457,** 1007-11.
Gros, J., Feistel, K., Viebahn, C., Blum, M., and Tabin, C. J. (2009). Cell movements at Hensen's node establish left/right asymmetric gene expression in the chick. *Science* **324,** 941-4.
Guichard, C., Harricane, M. C., Lafitte, J. J., Godard, P., Zaegel, M., et al. (2001). Axonemal dynein intermediate-chain gene (DNAI1) mutations result in situs inversus and primary ciliary dyskinesia (Kartagener syndrome). *Am J Hum Genet* **68,** 1030-5.
Hadjantonakis, A. K., Pisano, E., and Papaioannou, V. E. (2008). Tbx6 regulates left/right patterning in mouse embryos through effects on nodal cilia and perinodal signaling. *PLoS ONE* **3,** e2511.
Hamada, H. (2008). Breakthroughs and future challenges in left-right patterning. *Dev Growth Differ* **50 Suppl 1,** S71-8.
Hamburger, V., and Hamilton, H. L. (1992). A series of normal stages in the development of the chick embryo. 1951. *Dev Dyn* **195,** 231-72.
Harris, P. C., and Torres, V. E. (2009). Polycystic kidney disease. *Annu Rev Med* **60,** 321-37.
Hashimoto, H., Aritaki, M., Uozumi, K., Uji, S., Kurokawa, T., et al. (2007). Embryogenesis and expression profiles of charon and nodal-pathway genes in sinistral (Paralichthys olivaceus) and dextral (Verasper variegatus) flounders. *Zoolog Sci* **24,** 137-46.
Hashimoto, H., Rebagliati, M., Ahmad, N., Muraoka, O., Kurokawa, T., et al. (2004). The Cerberus/Dan-family protein Charon is a negative regulator of Nodal signaling during left-right patterning in zebrafish. *Development* **131,** 1741-53.
Hassoun, R., Schwartz, P., Feistel, K., Blum, M., and Viebahn, C. (2009). Axial differentiation and early gastrulation stages of the pig embryo. *Differentiation*.
Hausen, P., and Riebesell, M. (1991). "The Early Development of *Xenopus* Laevis. An Atlas of the Histology." Springer-Verlag GmbH,
Heasman, J., Wessely, O., Langland, R., Craig, E. J., and Kessler, D. S. (2001). Vegetal localization of maternal mRNAs is disrupted by VegT depletion. *Dev Biol* **240,** 377-86.
Hensen, V. (1876). Beobachtungen ueber die Befruchtung und Entwicklung des Kaninchens and Meerschweinchens. *Z Anat Entwicklungsgesch* **1,** 213-273 + 353-423.
Hirakow, R., and Kajita, N. (1991). Electron microscopic study of the development of amphioxus, Branchiostoma belcheri tsingtauense: the gastrula. *Journal of Morphology* **207,** 37-52.
Hirokawa, N., Tanaka, Y., Okada, Y., and Takeda, S. (2006). Nodal flow and the generation of left-right asymmetry. *Cell* **125,** 33-45.
Hojo, M., Takashima, S., Kobayashi, D., Sumeragi, A., Shimada, A., et al. (2007). Right-elevated expression of charon is regulated by fluid flow in medaka Kupffer's vesicle. *Dev Growth Differ* **49,** 395-405.

Holland, N. D. (1976). The fine structure of the embryo during the gastrula stage of Comanthus japonica (Echinodermata: Crinoidea). *Tissue Cell* **8,** 491-510.
Hook, P., and Vallee, R. B. (2006). The dynein family at a glance. *J Cell Sci* **119,** 4369-71.
Hornef, N., Olbrich, H., Horvath, J., Zariwala, M. A., Fliegauf, M., et al. (2006). DNAH5 mutations are a common cause of primary ciliary dyskinesia with outer dynein arm defects. *Am J Respir Crit Care Med* **174,** 120-6.
Hummel, K. P., and Chapman, D. B. (1959). Visceral inversion and associated anomalies in the mouse. *J. Hered.* **50,** 9-13.
Ibanez-Tallon, I., Gorokhova, S., and Heintz, N. (2002). Loss of function of axonemal dynein Mdnah5 causes primary ciliary dyskinesia and hydrocephalus. *Hum Mol Genet* **11,** 715-21.
Ikeda, K., Ikeda, T., Morikawa, K., and Kamiya, R. (2007). Axonemal localization of Chlamydomonas PACRG, a homologue of the human Parkin-coregulated gene product. *Cell Motil Cytoskeleton* **64,** 814-21.
Karcher, C., Fischer, A., Schweickert, A., Bitzer, E., Horie, S., et al. (2005). Lack of a laterality phenotype in Pkd1 knock-out embryos correlates with absence of polycystin-1 in nodal cilia. *Differentiation* **73,** 425-32.
Karthagener, M. (1933). Zur Pathogenese der Bronchiektasien: Bronchiektasien bei Situs viscerum inversus. *Beiträge zum Klinik der Tuberkulose* **83,** 489-501.
Keller, R. (2002). Shaping the vertebrate body plan by polarized embryonic cell movements. *Science* **298,** 1950-4.
Keller, R., and Danilchik, M. (1988). Regional expression, pattern and timing of convergence and extension during gastrulation of *Xenopus* laevis. *Development* **103,** 193-209.
Keller, R. E., Danilchik, M., Gimlich, R., and Shih, J. (1985). The function and mechanism of convergent extension during gastrulation of *Xenopus* laevis. *J Embryol Exp Morphol* **89 Suppl,** 185-209.
Klein, S. L. (1987). The first cleavage furrow demarcates the dorsal-ventral axis in *Xenopus* embryos. *Dev Biol* **120,** 299-304.
Konig, P., Krain, B., Krasteva, G., and Kummer, W. (2009). Serotonin increases cilia-driven particle transport via an acetylcholine-independent pathway in the mouse trachea. *PLoS One* **4,** e4938.
Kramer-Zucker, A. G., Olale, F., Haycraft, C. J., Yoder, B. K., Schier, A. F., et al. (2005). Cilia-driven fluid flow in the zebrafish pronephros, brain and Kupffer's vesicle is required for normal organogenesis. *Development* **132,** 1907-21.
Kreiling, J. A., Balantac, Z. L., Crawford, A. R., Ren, Y., Toure, J., et al. (2008). Suppression of the endoplasmic reticulum calcium pump during zebrafish gastrulation affects left-right asymmetry of the heart and brain. *Mech Dev* **125,** 396-410.
Ku, M., and Melton, D. A. (1993). Xwnt-11: a maternally expressed *Xenopus* wnt gene. *Development* **119,** 1161-73.
Kuhl, M., Geis, K., Sheldahl, L. C., Pukrop, T., Moon, R. T., et al. (2001). Antagonistic regulation of convergent extension movements in *Xenopus* by Wnt/beta-catenin and Wnt/Ca2+ signaling. *Mech Dev* **106,** 61-76.
Kuhl, M., Sheldahl, L. C., Park, M., Miller, J. R., and Moon, R. T. (2000). The Wnt/Ca2+ pathway: a new vertebrate Wnt signaling pathway takes shape. *Trends Genet* **16,** 279-83.
Kume, S., Muto, A., Inoue, T., Suga, K., Okano, H., et al. (1997). Role of inositol 1,4,5-trisphosphate receptor in ventral signaling in *Xenopus* embryos. *Science* **278,** 1940-3.
Kupffer, C. (1868). Beobachtungen über die Entwicklung der Knochenfische. *Archiv für Mikroskopische Anatomie* **4,** 209-272.
Lane, M. C., and Keller, R. (1997). Microtubule disruption reveals that Spemann's organizer is subdivided into two domains by the vegetal alignment zone. *Development* **124,** 895-906.
Leclerc, C., Lee, M., Webb, S. E., Moreau, M., and Miller, A. L. (2003). Calcium transients triggered by planar signals induce the expression of ZIC3 gene during neural induction in *Xenopus*. *Dev Biol* **261,** 381-90.
Lee, J. Y., and Harland, R. M. (2007). Actomyosin contractility and microtubules drive apical constriction in *Xenopus* bottle cells. *Dev Biol* **311,** 40-52.
Levin, M. (2003). Motor protein control of ion flux is an early step in embryonic left-right asymmetry. *Bioessays* **25,** 1002-10.
Levin, M., Johnson, R. L., Stern, C. D., Kuehn, M., and Tabin, C. (1995). A molecular pathway determining left-right asymmetry in chick embryogenesis. *Cell* **82,** 803-14.
Levin, M., and Mercola, M. (1998). Gap junctions are involved in the early generation of left-right asymmetry. *Dev Biol* **203,** 90-105.

Levin, M., Thorlin, T., Robinson, K. R., Nogi, T., and Mercola, M. (2002). Asymmetries in H+/K+-ATPase and cell membrane potentials comprise a very early step in left-right patterning. *Cell* **111,** 77-89.

Long, S., Ahmad, N., and Rebagliati, M. (2003). The zebrafish nodal-related gene southpaw is required for visceral and diencephalic left-right asymmetry. *Development* **130,** 2303-16.

Lowe, L. A., Supp, D. M., Sampath, K., Yokoyama, T., Wright, C. V., et al. (1996). Conserved left-right asymmetry of nodal expression and alterations in murine situs inversus. *Nature* **381,** 158-61.

MacDonald, B. T., Tamai, K., and He, X. (2009). Wnt/beta-catenin signaling: components, mechanisms, and diseases. *Dev Cell* **17,** 9-26.

Mahone, M., Saffman, E. E., and Lasko, P. F. (1995). Localized Bicaudal-C RNA encodes a protein containing a KH domain, the RNA binding motif of FMR1. *Embo J* **14,** 2043-55.

Maisonneuve, C., Guilleret, I., Vick, P., Weber, T., Andre, P., et al. (2009). Bicaudal C, a novel regulator of Dvl signaling abutting RNA-processing bodies, controls cilia orientation and leftward flow. *Development* **136,** 3019-30.

Maiti, A. K., Mattei, M. G., Jorissen, M., Volz, A., Zeigler, A., et al. (2000). Identification, tissue specific expression, and chromosomal localisation of several human dynein heavy chain genes. *Eur J Hum Genet* **8,** 923-32.

Manner, J. (2001). Does an equivalent of the "ventral node" exist in chick embryos? A scanning electron microscopic study. *Anat Embryol (Berl)* **203,** 481-90.

Marques, S., Borges, A. C., Silva, A. C., Freitas, S., Cordenonsi, M., et al. (2004). The activity of the Nodal antagonist Cerl-2 in the mouse node is required for correct L/R body axis. *Genes Dev* **18,** 2342-7.

Martello, G., Zacchigna, L., Inui, M., Montagner, M., Adorno, M., et al. (2007). MicroRNA control of Nodal signalling. *Nature* **449,** 183-8.

McGrath, J., Somlo, S., Makova, S., Tian, X., and Brueckner, M. (2003). Two populations of node monocilia initiate left-right asymmetry in the mouse. *Cell* **114,** 61-73.

Meinhardt, H., and Gierer, A. (2000). Pattern formation by local self-activation and lateral inhibition. *Bioessays* **22,** 753-60.

Mencl, S. (2008). Epidermale Cilien in der *Xenopus laevis* Kaulquappe als Modellsystem zur Untersuchung pharmakologischer Effektoren der Cilienschlagfrequenz. Diploma-Thesis, University of Hohenheim.

Meno, C., Saijoh, Y., Fujii, H., Ikeda, M., Yokoyama, T., et al. (1996). Left-right asymmetric expression of the TGF beta-family member lefty in mouse embryos. *Nature* **381,** 151-5.

Mogi, K., Goto, M., Ohno, E., Azumi, Y., Takeuchi, S., et al. (2003). *Xenopus* neurula left-right asymmetry is respeficied by microinjecting TGF-beta5 protein. *Int J Dev Biol* **47,** 15-29.

Monroy, A., Baccetti, B., and Denis-Donini, S. (1976). Morphological changes of the surface of the egg of *Xenopus* laevis in the course of development. III. Scanning electron microscopy of gastrulation. *Dev Biol* **49,** 250-9.

Moody, S. A. (1987). Fates of the blastomeres of the 32-cell-stage *Xenopus* embryo. *Dev Biol* **122,** 300-19.

Morgan, D., Turnpenny, L., Goodship, J., Dai, W., Majumder, K., et al. (1998). Inversin, a novel gene in the vertebrate left-right axis pathway, is partially deleted in the inv mouse. *Nat Genet* **20,** 149-56.

Morokuma, J., Ueno, M., Kawanishi, H., Saiga, H., and Nishida, H. (2002). HrNodal, the ascidian nodal-related gene, is expressed in the left side of the epidermis, and lies upstream of HrPitx. *Dev Genes Evol* **212,** 439-46.

Murcia, N. S., Richards, W. G., Yoder, B. K., Mucenski, M. L., Dunlap, J. R., et al. (2000). The Oak Ridge Polycystic Kidney (orpk) disease gene is required for left-right axis determination. *Development* **127,** 2347-55.

Nakamura, T., Mine, N., Nakaguchi, E., Mochizuki, A., Yamamoto, M., et al. (2006). Generation of robust left-right asymmetry in the mouse embryo requires a self-enhancement and lateral-inhibition system. *Dev Cell* **11,** 495-504.

Nguyen, T., Chin, W. C., O'Brien, J. A., Verdugo, P., and Berger, A. J. (2001). Intracellular pathways regulating ciliary beating of rat brain ependymal cells. *J Physiol* **531,** 131-40.

Nieuwkoop, P., and Faber, J. (1994). "Normal Table of *Xenopus laevis* (Daudin)." Garland Pub,

Nieuwkoop, P. D. (1973). The organization center of the amphibian embryo: its origin, spatial organization, and morphogenetic action. *Adv Morphog* **10,** 1-39.

Nonaka, S., Shiratori, H., Saijoh, Y., and Hamada, H. (2002). Determination of left-right patterning of the mouse embryo by artificial nodal flow. *Nature* **418,** 96-9.

Nonaka, S., Tanaka, Y., Okada, Y., Takeda, S., Harada, A., et al. (1998). Randomization of left-right asymmetry due to loss of nodal cilia generating leftward flow of extraembryonic fluid in mice lacking KIF3B motor protein. *Cell* **95,** 829-37.
Nonaka, S., Yoshiba, S., Watanabe, D., Ikeuchi, S., Goto, T., et al. (2005). De novo formation of left-right asymmetry by posterior tilt of nodal cilia. *PLoS Biol* **3,** e268.
Ohi, Y., and Wright, C. V. (2007). Anteriorward shifting of asymmetric Xnr1 expression and contralateral communication in left-right specification in *Xenopus*. *Dev Biol* **301,** 447-63.
Okada, Y., Nonaka, S., Tanaka, Y., Saijoh, Y., Hamada, H., et al. (1999). Abnormal nodal flow precedes situs inversus in iv and inv mice. *Mol Cell* **4,** 459-68.
Okada, Y., Takeda, S., Tanaka, Y., Belmonte, J. C., and Hirokawa, N. (2005). Mechanism of nodal flow: a conserved symmetry breaking event in left-right axis determination. *Cell* **121,** 633-44.
Oki, S., Hashimoto, R., Okui, Y., Shen, M. M., Mekada, E., et al. (2007). Sulfated glycosaminoglycans are necessary for Nodal signal transmission from the node to the left lateral plate in the mouse embryo. *Development* **134,** 3893-904.
Okumura, T., Utsuno, H., Kuroda, J., Gittenberger, E., Asami, T., et al. (2008). The development and evolution of left-right asymmetry in invertebrates: lessons from Drosophila and snails. *Dev Dyn* **237,** 3497-515.
Olbrich, H., Haffner, K., Kispert, A., Volkel, A., Volz, A., et al. (2002). Mutations in DNAH5 cause primary ciliary dyskinesia and randomization of left-right asymmetry. *Nat Genet* **30,** 143-4.
Omran, H., Haffner, K., Volkel, A., Kuehr, J., Ketelsen, U. P., et al. (2000). Homozygosity mapping of a gene locus for primary ciliary dyskinesia on chromosome 5p and identification of the heavy dynein chain DNAH5 as a candidate gene. *Am J Respir Cell Mol Biol* **23,** 696-702.
Omran, H., Kobayashi, D., Olbrich, H., Tsukahara, T., Loges, N. T., et al. (2008). Ktu/PF13 is required for cytoplasmic pre-assembly of axonemal dyneins. *Nature* **456,** 611-6.
Osada, S. I., and Wright, C. V. (1999). *Xenopus* nodal-related signaling is essential for mesendodermal patterning during early embryogenesis. *Development* **126,** 3229-40.
Otto, E. A., Schermer, B., Obara, T., O'Toole, J. F., Hiller, K. S., et al. (2003). Mutations in INVS encoding inversin cause nephronophthisis type 2, linking renal cystic disease to the function of primary cilia and left-right axis determination. *Nat Genet* **34,** 413-20.
Ouyang, X., Shestopalov, I. A., Sinha, S., Zheng, G., Pitt, C. L., et al. (2009). Versatile synthesis and rational design of caged morpholinos. *J Am Chem Soc* **131,** 13255-69.
Pachur, A. (2007). Klonierung und Charakterisierung der Gene Xnr 1, BicC und Ablim -1/ -2 in Neurulaembryonen des Krallenfrosches *Xenopus* laevis. Thesis, University of Hohenheim.
Palmer, A. R. (2004). Symmetry breaking and the evolution of development. *Science* **306,** 828-33.
Pazour, G. J., San Agustin, J. T., Follit, J. A., Rosenbaum, J. L., and Witman, G. B. (2002). Polycystin-2 localizes to kidney cilia and the ciliary level is elevated in orpk mice with polycystic kidney disease. *Curr Biol* **12,** R378-80.
Pedersen, L. B., Veland, I. R., Schroder, J. M., and Christensen, S. T. (2008). Assembly of primary cilia. *Dev Dyn* **237,** 1993-2006.
Pennekamp, P., Karcher, C., Fischer, A., Schweickert, A., Skryabin, B., et al. (2002). The ion channel polycystin-2 is required for left-right axis determination in mice. *Curr Biol* **12,** 938-43.
Pflugfelder, O. (1970). "Lehrbuch der Entwicklungsgeschichte und Entwicklungsphysiologie der Tiere." G. Fischer VEB,
Piccolo, S., Agius, E., Leyns, L., Bhattacharyya, S., Grunz, H., et al. (1999). The head inducer Cerberus is a multifunctional antagonist of Nodal, BMP and Wnt signals. *Nature* **397,** 707-10.
Pichon, B., Taelman, V., Kricha, S., Christophe, D., and Bellefroid, E. J. (2002). XHRT-1, a hairy and Enhancer of split related gene with expression in floor plate and hypochord during early *Xenopus* embryogenesis. *Dev Genes Evol* **212,** 491-5.
Pohl, B. S., and Knochel, W. (2004). Isolation and developmental expression of *Xenopus* FoxJ1 and FoxK1. *Dev Genes Evol* **214,** 200-5.
Praetorius, H. A., and Spring, K. R. (2003). The renal cell primary cilium functions as a flow sensor. *Curr Opin Nephrol Hypertens* **12,** 517-20.
Purcell, E. M. (1977). Life at Low Reynolds Number. *American Journal of Physics* **45,** 3-11.
Rankin, C. T., Bunton, T., Lawler, A. M., and Lee, S. J. (2000). Regulation of left-right patterning in mice by growth/differentiation factor-1. *Nat Genet* **24,** 262-5.
Raya, A., Kawakami, Y., Rodriguez-Esteban, C., Ibanes, M., Rasskin-Gutman, D., et al. (2004). Notch activity acts as a sensor for extracellular calcium during vertebrate left-right determination. *Nature* **427,** 121-8.
R-Development-Core-Team. (2008). "R: A language and environment for statistical computing." R Foundation for Statistical Computing, Vienna, Austria.

Rodriguez Esteban, C., Capdevila, J., Economides, A. N., Pascual, J., Ortiz, A., et al. (1999). The novel Cer-like protein Caronte mediates the establishment of embryonic left-right asymmetry. *Nature* **401,** 243-51.
Rosa, A., Spagnoli, F. M., and Brivanlou, A. H. (2009). The miR-430/427/302 family controls mesendodermal fate specification via species-specific target selection. *Dev Cell* **16,** 517-27.
Ryan, A. K., Blumberg, B., Rodriguez-Esteban, C., Yonei-Tamura, S., Tamura, K., et al. (1998). Pitx2 determines left-right asymmetry of internal organs in vertebrates. *Nature* **394,** 545-51.
Ryffel, G. U. (2003). What can a frog tell us about human kidney development. *Nephron Exp Nephrol* **94,** e35-43.
Saffman, E. E., Styhler, S., Rother, K., Li, W., Richard, S., et al. (1998). Premature translation of oskar in oocytes lacking the RNA-binding protein bicaudal-C. *Mol Cell Biol* **18,** 4855-62.
Saijoh, Y., Oki, S., Ohishi, S., and Hamada, H. (2003). Left-right patterning of the mouse lateral plate requires nodal produced in the node. *Dev Biol* **256,** 160-72.
Sakuma, R., Ohnishi Yi, Y., Meno, C., Fujii, H., Juan, H., et al. (2002). Inhibition of Nodal signalling by Lefty mediated through interaction with common receptors and efficient diffusion. *Genes Cells* **7,** 401-12.
Sanderson, M. J., Dirksen, E. R., and Satir, P. (1985). The antagonistic effects of 5-hydroxytryptamine and methylxanthine on the gill cilia of Mytilus edulis. *Cell Motil* **5,** 293-309.
Sarmah, B., Latimer, A. J., Appel, B., and Wente, S. R. (2005). Inositol polyphosphates regulate zebrafish left-right asymmetry. *Dev Cell* **9,** 133-45.
Satir, P., and Christensen, S. T. (2007). Overview of structure and function of mammalian cilia. *Annu Rev Physiol* **69,** 377-400.
Sbalzarini, I. F., and Koumoutsakos, P. (2005). Feature point tracking and trajectory analysis for video imaging in cell biology. *J Struct Biol* **151,** 182-95.
Schneider, I., Houston, D. W., Rebagliati, M. R., and Slusarski, D. C. (2008). Calcium fluxes in dorsal forerunner cells antagonize beta-catenin and alter left-right patterning. *Development* **135,** 75-84.
Scholey, J. M., and Anderson, K. V. (2006). Intraflagellar transport and cilium-based signaling. *Cell* **125,** 439-42.
Schor, S. L. (1965). Serotonin and Adenosine Triphosphate: Synergistic Effect on the Beat Frequency of Cilia of Mussel Gills. *Science* **148,** 500-1.
Schottenfeld, J., Sullivan-Brown, J., and Burdine, R. D. (2007). Zebrafish curly up encodes a Pkd2 ortholog that restricts left-side-specific expression of southpaw. *Development* **134,** 1605-15.
Schwabe, G. C., Hoffmann, K., Loges, N. T., Birker, D., Rossier, C., et al. (2008). Primary ciliary dyskinesia associated with normal axoneme ultrastructure is caused by DNAH11 mutations. *Hum Mutat* **29,** 289-98.
Schweickert, A., Weber, T., Beyer, T., Vick, P., Bogusch, S., et al. (2007). Cilia-driven leftward flow determines laterality in *Xenopus*. *Curr Biol* **17,** 60-6.
Shen, M. M. (2007). Nodal signaling: developmental roles and regulation. *Development* **134,** 1023-34.
Shestopalov, I. A., Sinha, S., and Chen, J. K. (2007). Light-controlled gene silencing in zebrafish embryos. *Nat Chem Biol* **3,** 650-1.
Shook, D. R., Majer, C., and Keller, R. (2004). Pattern and morphogenesis of presumptive superficial mesoderm in two closely related species, *Xenopus* laevis and *Xenopus* tropicalis. *Dev Biol* **270,** 163-85.
Simard, A., Di Giorgio, L., Amen, M., Westwood, A., Amendt, B. A., et al. (2009). The Pitx2c N-terminal domain is a critical interaction domain required for asymmetric morphogenesis. *Dev Dyn* **238,** 2459-70.
Simons, M., and Mlodzik, M. (2008). Planar cell polarity signaling: from fly development to human disease. *Annu Rev Genet* **42,** 517-40.
Sive, H., Grainger, R., and Harland, R. (2000). "Early Development of *Xenopus laevis*: A Laboratory Manual." Cold Spring Harbor Laboratory Press, Cold Spring Harbor, New York.
Slack, J. M., Holland, P. W., and Graham, C. F. (1993). The zootype and the phylotypic stage. *Nature* **361,** 490-2.
Smith, A. B. (2008). Deuterostomes in a twist: the origins of a radical new body plan. *Evol Dev* **10,** 493-503.
Smith, J. C., Price, B. M., Green, J. B., Weigel, D., and Herrmann, B. G. (1991). Expression of a *Xenopus* homolog of Brachyury (T) is an immediate-early response to mesoderm induction. *Cell* **67,** 79-87.

Smith, J. L., Osborn, J. C., and Stanisstreet, M. (1976). Scanning electron microscopy of lithium-induced exogastrulae of *Xenopus* laevis. *J Embryol Exp Morphol* **36,** 513-22.
Smith, W. C., and Harland, R. M. (1991). Injected Xwnt-8 RNA acts early in *Xenopus* embryos to promote formation of a vegetal dorsalizing center. *Cell* **67,** 753-65.
Speder, P., Petzoldt, A., Suzanne, M., and Noselli, S. (2007). Strategies to establish left/right asymmetry in vertebrates and invertebrates. *Curr Opin Genet Dev* **17,** 351-8.
Spemann, H., and Mangold, H. (1924). Über Induktion von Embryonalanlagen durch Implantation artfremder Organisatoren. *Arch Mikrosk Anat Entwicklungsmech* **100,** 599-638.
Stanley, E., Biben, C., Kotecha, S., Fabri, L., Tajbakhsh, S., et al. (1998). DAN is a secreted glycoprotein related to *Xenopus* cerberus. *Mech Dev* **77,** 173-84.
Stern, C. (2004). "Gastrulation: From Cells to Embryo." Cold Spring Harbor Laboratory,
Storm van's Gravesande, K., and Omran, H. (2005). Primary ciliary dyskinesia: clinical presentation, diagnosis and genetics. *Ann Med* **37,** 439-49.
Stubbs, J. L., Oishi, I., Izpisua Belmonte, J. C., and Kintner, C. (2008). The forkhead protein Foxj1 specifies node-like cilia in *Xenopus* and zebrafish embryos. *Nat Genet*.
Sulik, K., Dehart, D. B., Iangaki, T., Carson, J. L., Vrablic, T., et al. (1994). Morphogenesis of the murine node and notochordal plate. *Dev Dyn* **201,** 260-78.
Sun, Z., Amsterdam, A., Pazour, G. J., Cole, D. G., Miller, M. S., et al. (2004). A genetic screen in zebrafish identifies cilia genes as a principal cause of cystic kidney. *Development* **131,** 4085-93.
Supp, D. M., Brueckner, M., Kuehn, M. R., Witte, D. P., Lowe, L. A., et al. (1999). Targeted deletion of the ATP binding domain of left-right dynein confirms its role in specifying development of left-right asymmetries. *Development* **126,** 5495-504.
Supp, D. M., Witte, D. P., Potter, S. S., and Brueckner, M. (1997). Mutation of an axonemal dynein affects left-right asymmetry in inversus viscerum mice. *Nature* **389,** 963-6.
Swalla, B. J. (2006). Building divergent body plans with similar genetic pathways. *Heredity* **97,** 235-43.
Tabin, C. (2005). Do we know anything about how left-right asymmetry is first established in the vertebrate embryo? *J Mol Histol* **36,** 317-23.
Tabin, C. J. (2006). The key to left-right asymmetry. *Cell* **127,** 27-32.
Tabin, C. J., and Vogan, K. J. (2003). A two-cilia model for vertebrate left-right axis specification. *Genes Dev* **17,** 1-6.
Tada, M., and Smith, J. C. (2000). Xwnt11 is a target of *Xenopus* Brachyury: regulation of gastrulation movements via Dishevelled, but not through the canonical Wnt pathway. *Development* **127,** 2227-38.
Tanaka, C., Sakuma, R., Nakamura, T., Hamada, H., and Saijoh, Y. (2007). Long-range action of Nodal requires interaction with GDF1. *Genes Dev* **21,** 3272-82.
Tanaka, Y., Okada, Y., and Hirokawa, N. (2005). FGF-induced vesicular release of Sonic hedgehog and retinoic acid in leftward nodal flow is critical for left-right determination. *Nature* **435,** 172-7.
Tao, Q., Yokota, C., Puck, H., Kofron, M., Birsoy, B., et al. (2005). Maternal wnt11 activates the canonical wnt signaling pathway required for axis formation in *Xenopus* embryos. *Cell* **120,** 857-71.
Tarin, D. (1971). Scanning electron microscopical studies of the embryonic surface during gastrulation and neurulation in *Xenopus* laevis. *J Anat* **109,** 535-47.
Tatusova, T. A., and Madden, T. L. (1999). BLAST 2 Sequences, a new tool for comparing protein and nucleotide sequences. *FEMS Microbiol Lett* **174,** 247-50.
Thisse, C., and Thisse, B. (1999). Antivin, a novel and divergent member of the TGFbeta superfamily, negatively regulates mesoderm induction. *Development* **126,** 229-40.
Tiozzo, S., Christiaen, L., Deyts, C., Manni, L., Joly, J. S., et al. (2005). Embryonic versus blastogenetic development in the compound ascidian Botryllus schlosseri: insights from Pitx expression patterns. *Dev Dyn* **232,** 468-78.
Tran, U., Pickney, L. M., Ozpolat, B. D., and Wessely, O. (2007). *Xenopus* Bicaudal-C is required for the differentiation of the amphibian pronephros. *Dev Biol* **307,** 152-64.
Tran, U., Zakin, L., Schweickert, A., Agrawal, R., Döger, R., et al. (2009). The RNA-binding molecule Bicaudal-C is required for post-transcriptional regulation of Polycystin-2 in the kidney by antagonizing miR-17 activity. *Development*, **submitted**.
Turing, A. M. (1952). The chemical basis of morphogenesis. *Philosophical Transactions of the Royal Society of London. Series B* **237,** 37-72.
Vassilev, P. M., Guo, L., Chen, X. Z., Segal, Y., Peng, J. B., et al. (2001). Polycystin-2 is a novel cation channel implicated in defective intracellular Ca(2+) homeostasis in polycystic kidney disease. *Biochem Biophys Res Commun* **282,** 341-50.

Venglarik, C. J., Gao, Z., and Lu, X. (2004). Evolutionary conservation of Drosophila polycystin-2 as a calcium-activated cation channel. *J Am Soc Nephrol* **15,** 1168-77.
Vick, P., Schweickert, A., Weber, T., Eberhardt, M., Mencl, S., et al. (2009). Flow on the right side of the gastrocoel roof plate is dispensable for symmetry breakage in the frog *Xenopus* laevis. *Dev Biol* **331,** 281-91.
Vonica, A., and Brivanlou, A. H. (2007). The left-right axis is regulated by the interplay of Coco, Xnr1 and derriere in *Xenopus* embryos. *Dev Biol* **303,** 281-94.
Wada, Y., Mogami, Y., and Baba, S. (1997). Modification of ciliary beating in sea urchin larvae induced by neurotransmitters: beat-plane rotation and control of frequency fluctuation. *J Exp Biol* **200,** 9-18.
Walker, J. C., and Harland, R. M. (2008). Expression of microRNAs during embryonic development of *Xenopus* tropicalis. *Gene Expr Patterns* **8,** 452-6.
Wallingford, J. B. (2006). Planar cell polarity, ciliogenesis and neural tube defects. *Hum Mol Genet* **15 Spec No 2,** R227-34.
Wallingford, J. B., Ewald, A. J., Harland, R. M., and Fraser, S. E. (2001). Calcium signaling during convergent extension in *Xenopus*. *Curr Biol* **11,** 652-61.
Wallingford, J. B., Fraser, S. E., and Harland, R. M. (2002). Convergent extension: the molecular control of polarized cell movement during embryonic development. *Dev Cell* **2,** 695-706.
Wallingford, J. B., and Harland, R. M. (2001). *Xenopus* Dishevelled signaling regulates both neural and mesodermal convergent extension: parallel forces elongating the body axis. *Development* **128,** 2581-92.
Wallingford, J. B., and Harland, R. M. (2002). Neural tube closure requires Dishevelled-dependent convergent extension of the midline. *Development* **129,** 5815-25.
Watanabe, T., Takeda, A., Mise, K., Okuno, T., Suzuki, T., et al. (2005). Stage-specific expression of microRNAs during *Xenopus* development. *FEBS Lett* **579,** 318-24.
Webb, S. E., and Miller, A. L. (2006). Ca2+ signaling and early embryonic patterning during the blastula and gastrula periods of zebrafish and *Xenopus* development. *Biochim Biophys Acta* **1763,** 1192-208.
Wessely, O., and De Robertis, E. M. (2000). The *Xenopus* homologue of Bicaudal-C is a localized maternal mRNA that can induce endoderm formation. *Development* **127,** 2053-62.
Wessely, O., Tran, U., Zakin, L., and De Robertis, E. M. (2001). Identification and expression of the mammalian homologue of Bicaudal-C. *Mech Dev* **101,** 267-70.
Wilson, P. D. (2004). Polycystic kidney disease. *N Engl J Med* **350,** 151-64.
Witzgall, R. (2005). New developments in the field of cystic kidney diseases. *Curr Mol Med* **5,** 455-65.
Wolpert, L., Beddington, R., Brockes, J., Jessell, T., Lawrence, P., et al. (1997). "Principles of Development." Oxford University Press,
Yamamoto, M., Mine, N., Mochida, K., Sakai, Y., Saijoh, Y., et al. (2003). Nodal signaling induces the midline barrier by activating Nodal expression in the lateral plate. *Development* **130,** 1795-804.
Yokota, C., Kofron, M., Zuck, M., Houston, D. W., Isaacs, H., et al. (2003). A novel role for a nodal-related protein; Xnr3 regulates convergent extension movements via the FGF receptor. *Development* **130,** 2199-212.
Yu, J. K., Holland, L. Z., and Holland, N. D. (2002). An amphioxus nodal gene (AmphiNodal) with early symmetrical expression in the organizer and mesoderm and later asymmetrical expression associated with left-right axis formation. *Evol Dev* **4,** 418-25.
Yu, J. K., Satou, Y., Holland, N. D., Shin, I. T., Kohara, Y., et al. (2007). Axial patterning in cephalochordates and the evolution of the organizer. *Nature* **445,** 613-7.
Yu, X., Ng, C. P., Habacher, H., and Roy, S. (2008). Foxj1 transcription factors are master regulators of the motile ciliogenic program. *Nat Genet*.
Zariwala, M. A., Knowles, M. R., and Omran, H. (2007). Genetic defects in ciliary structure and function. *Annu Rev Physiol* **69,** 423-50.
Zhang, M., Bolfing, M. F., Knowles, H. J., Karnes, H., and Hackett, B. P. (2004). Foxj1 regulates asymmetric gene expression during left-right axis patterning in mice. *Biochem Biophys Res Commun* **324,** 1413-20.
Zhang, Y., and Levin, M. (2009). Particle tracking model of electrophoretic morphogen movement reveals stochastic dynamics of embryonic gradient. *Dev Dyn* **238,** 1923-35.
Zivert, A. K. (1904). Über einen Fall von Bronchiectasie bei einem Patienten mit situs inversus viscerum. *Berliner klinische Wochenschrift* **41,** 139-141.